Performance of a Solar Air Heater Incorporating Thermal Storage

Francois Lombaard

Thesis presented in partial fulfilment of the requirements for the degree of Master of Science in Mechanical Engineering at the University of Stellenbosch

Thesis supervisor: Prof. D.G. Kröger

December 2002

Declaration

I, the undersigned, hereby declare that the work contained in this thesis is my own original work and that I have not previously in its entirety or part submitted it at any university for a degree.

Signature:

Date:

Abstract

In the present study, research was conducted to determine the feasibility of water energy storage through which the output of heated air by an upward facing solar air heater could be prolonged. Following a systematic approach, a number of experimental test swere initially performed on an upward facing solar air heater in order to obtain a benchmark that could be used to evaluate the influence of water storage during the day-time performance of a solar air heater. As expected, an increase in the air mass flow rate not only led to an increase in the collector efficiency but also to a decrease in the temperature gain across the collector. In addition, a number of day- and night-time experiments were executed on a plastic covered water tank in order to evaluate it's ability to store and discharge thermal energy. Results clearly indicated that the plastic covered water tank was both an ideal collector and storage medium of solar energy. Experimental results also revealed that the plastic covered water tank was an ideal source of thermal energy for a solar air heater during night-time operation. Subsequently, both day- and night-time experiments were performed on an upward facing solar air heater in which plastic covered water tanks were installed. Day-time experimental results revealed that the modified solar air heater still had the same collector efficiency tendency, as observed in the initial solar air heater experiments, but that the water energy storage led to a dramatic decrease in the absorber plate temperature and in the corresponding temperature gain experienced across the collector. In contrast, the night-time operation results clearly indicated that the water energy storage was not only able to prolong the output of heated air by the solar air heater, but was further able to increase the air temperature by between 7.5 and 1.5 °C, depending on the air mass flow rate. It was furthermore shown in the study that available theory is able to accurately predict the performance of an upward facing solar air heater, either with or without water energy storage, as long as the equations are employed within their range of validity.

Opsomming

In die hierdie studie is daar ondersoek ingestel na die lewensvatbaarhied van son-energiestoring in water ten einde die tydperk van lugverhitting deur 'n son-lugverwarmer te verleng. 'n Sistematiese prosedure is gevolg waardeur daar aanvanklik 'n aantal eksperimente op 'n son-lugverwarmer uitgevoer is om sodoende die eienskappe van so 'n lugverhittingstelsel, sonder energie storing, te vekry. Die resultate het getoon dat 'n toename in die massavloei tempo van die lug lei tot 'n toename in die kollektor effektiwiteit van die stelsel, maar terselfdetyd lei tot 'n afname in die temperatuur styging in die kollektor. Met die eienskappe van die lugverwarmingstelsel bekend, is daar voorts 'n aantal dag- en nag-eksperimente uitgevoer op 'n plastiek bedekte watertenk om die storing en vryselling van termiese energie deur die watertenk te kwantifiseer. Die resultate het daarop gedui dat die plastiek bedekte watertenk nie net beide 'n goeie kollektor en stoor medium vir son-energie is nie, maar ook dat dit 'n ideale bron van termiese energie vir 'n lugverwarmingstelsel tydens die nag is. Met inagname van die vorige resultate, is daar dan 'n aantal plastiek bedekte watertenks in die apparaat geinstalleer, en 'n aantal dag- en nag-eksperimente is uitgevoer. Die dag-eksperimente het getoon dat die die nuwe lugverwarmer met water energie storing dieselfde eienskappe toon ten opsigte van die kollektor effektiwiteit as die oorspronkilke son-lugverwarmer. Tog, as gevolg van die laer absoberende plaat temperature was die temperatuur toename in die kollektor heelwat laer. In kontras hiermee dui die nagresultate aan dat die plastiek bedekte watertenks nie net die vermoë het om die tydperk van lugverwarming te verleng nie, maar ook dat die lug tempertuur, afhangende van die massavloei tempo van die lug, met tussen 1.5 en 7.5 °C verhoog kan word. Die studie het laastens ook getoon dat dit moontlik is om met behulp van beskikbare teorie die temperatuur toename in die kollektor van 'n son-lugverwarmer met of sonder water energie storing, akkuraat te voorspel, mits die vergelykings binne hul geldige gebiede gebruik word.

Dedication

This thesis is dedicated towards all the people who have encouraged me throughout both my undergraduate as well as postgraduate studies, but also to Prof. Kröger and his enthusiasm for his subject.

Acknowledgements

The financial assistance of the National Research Foundation (NRF) towards this research is hereby acknowledged. Opinions expressed and conclusions arrived are those of the author and are not necessarily to be attributed to the National Research Foundation.

Table of Contents

List of Tables

List of Figures

List of Symbols

Duct cross-sectional area, m^2	A_d
Nozzle area, m^2	A_n
Upstream cross-sectional area, m^2	A_{tus}
Constant	a
Constant	b
Coefficient of extinction, m^{-1}	C_e
Nozzle discharge coefficient	C_n
Constant	c
Specific heat capacity, J/kgK	c_p
Nozzle diameter, m	D
Rectangular duct hydraulic diameter, m	Dh
Constant	d
Pressure difference between atmosphere and pressure upstream of nozzles, Pa	dp_d
Pressure drop across nozzle, Pa	dp_n
Day of Year, days	DOY
Equation of time, minutes	EOT
Collector efficiency factor	F'
Height of rectangular duct, m	H
Length weighted averaged heat transfer coefficient between point "a" and "b", W/m^2K	$\bar{h}_{b-a}$
Length weighted averaged heat transfer coefficient for cover, W/m^2K	$\bar{h}_c$
Length weighted averaged heat transfer coefficient for absorber plate, W/m^2K	$\bar{h}_p$
Cover – air convective heat transfer coefficient, W/m^2K	h_c
Plate – air convective heat transfer coefficient, W/m^2K	h_p
Plate – air linearized radiative heat transfer coefficient, W/m^2K	h_{pc}
Cover – sky linearized radiative heat transfer coefficient, W/m^2K	h_{rs}
Wind-induced convective heat transfer coefficient, W/m^2K	h_w
Incident horizontal solar radiation, W/m^2	Ih
Colburn heat transfer analogy	j
Rectangular duct loss coefficient	K_d
Thermal conductivity, W/mK	k
Length, m	L
Effective length, m	L_e
Mass flow rate, kg/s	m
Refractive index	n

Annual phase angle, radians	P
Atmospheric pressure, Pa	p_a
Upstream nozzle pressure, Pa	p_{up}
Vapour pressure, Pa	p_v
Convective heat exchange between solar air heater cover and air, W/m^2	q_c
Convective heat exchange between cover and ambient, W/m^2	q_{ca}
Convective heat exchange between solar air heater absorber plate and air, W/m^2	q_p
Radiative heat exchange between cover and absorber plate, W/m^2	q_{pc}
Net long-wave radiation heat exchange between absorber plate and sky, W/m^2	q_{ps}
Radiative heat exchange between cover and sky, W/m^2	q_{rs}
Total heat loss from cover to environment due to convection and sky radiation, W/m^2K	q_t
Useful energy per unit area, W/m^2	q_u
Solar energy absorbed by the absorber plate per unit area, W/m^2	S
Air temperature, °C or K	T
Mean air temperature, °C or K	$\overline{T}$
Ambient temperature, °C or K	T_a
Cover temperature, °C or K	T_c
Dry-bulb outlet air temperature, °C or K	T_{db}
Film temperature, °C or K	T_f
Air inlet temperature, °C or K	T_{in}
Plate temperature, °C or K	T_p
Equivalent blackbody sky temperature, K	T_{sky}
Water temperature, °C or K	T_w
Wet-bulb outlet air temperature, °C or K	T_{wb}
Thickness, m or time, s	t
Back loss coefficient, W/m^2K	U_b
Overall heat loss coefficient, W/m^2K	U_L
Top loss coefficient, W/m^2K	U_t
Wind speed, m/s	v_w
Width of rectangular duct, m	W
Position along flow direction, m	x
Year	Y
Leap year adjustment to the day, days	YADJ
Nozzle approach velocity factor for a compressible fluid	Y_n

Dimensionless numbers

Grashof number	Gr
Nusselt number	Nu

Prandtl number	Pr
Rayleigh number	Ra
Reynolds number	Re

Greek symbols

Effective absorbtivity of surface	α'
Absorbtivity of surface	α
Absorber plate long-wave absorptivity	α_p
Slope angle, °	β
Declination angle	δ
Latitude of location, °	ϕ
Longitude of location, °.	ϕ_l
Gas expansion factor	ϕ_g
Standard meridian for location, °	ϕ_m
Cover emissivity	ε_c
Film emissivity	ε_f
Plate emissivity	ε_p
Collector efficiency, %	η_c
Dynamic viscosity, kg/ms	μ
Incidence angle, °	θ_1
Refractive index angle, °	θ_2
Density, kg/m^3 or reflectivity of surface	ρ
Effective reflectivity of surface	ρ'
Stephan-Boltzman constant, 5.67 x 10^{-8} W/m^{2}K^4	σ
Effective transmissivity of surface	τ'
Transmissivity of surface	τ
Transmissivity due to absorbtance of surface	τ_α
Hour angle, °	ω
Experimental time in hours after midnight, hours	ψ

Subscripts

Ambient	a
Air film	af
Air-vapour	av
Beam	b
Cover	c
Cover-air / convection-air	ca

Cover-film	cf
Diffuse	d
Film	f
Film-water	fw
Nozzle	n
Plate	p
Plate-cover	pc
Radiation-sky	rs
Sky	sky
Total	T
Wind	v
Water	w

Chapter 1: Introduction

With coal and other fossil fuels still being our primary source of energy, and people becoming more concerned with the pollution of the environment, the question arises whether or not renewable energy could not be used to fill this void left in the energy market? However, these same public concerns surrounding pollution of the environment and energy shortages were already being raised during the 1970's oil crisis. Now, nearly three decades later, it seems as though the initiatives and attempts of the 1970's to utilise renewable energy have failed, with renewable energy sources only supplying somewhere between 15% and 20% of the total world energy demand [01PA1].

McVeigh et al. [00MV1] conducted a study in order to verify whether the public opinion surrounding the failure of renewable energy in the past three decades is valid. Their study's results indicated that although the penetration of renewable energy into the energy market has fallen short of projections, the cost associated with renewable energy has fallen in accordance with past projections. However, if the cost associated with renewable energy has fallen in accordance with past projections why has renewable energy not penetrated the energy market as expected?

The reason for the lack of renewable energy penetration into the world energy market is due to two reasons according to McVeigh et al. [00MV1]. Firstly, technological developments led to both a decline in the technical costs as well as in the price of fossil-fuelled electricity. Secondly, technological changes led to a dramatic improvement in the environmental performance of these technologies; consequently leading to cleaner fossil-fuelled energy.

Nevertheless, in the past decade renewable energy has been earmarked as a strong contender to improve the plight of people in rural areas, with the World Bank accelerating the lending of funds for renewable energy projects. For instance in the past decade the World Bank Group and Global Environmental Facility approved seventeen renewable energy projects with a total cost of $3.2 billion [01MA1].

In the past two years the University of Stellenbosch joined the renewable energy research and development world, by undertaking an ambitious project to evaluate the performance of a solar chimney power plant. The primary objective of this project is to access whether or not it is possible to convert available solar radiation into a consistent source of electricity, through the use of a solar chimney. In this instance, a hypothetical 200 MW solar chimney power plant located near Sishen in South Africa is being studied.

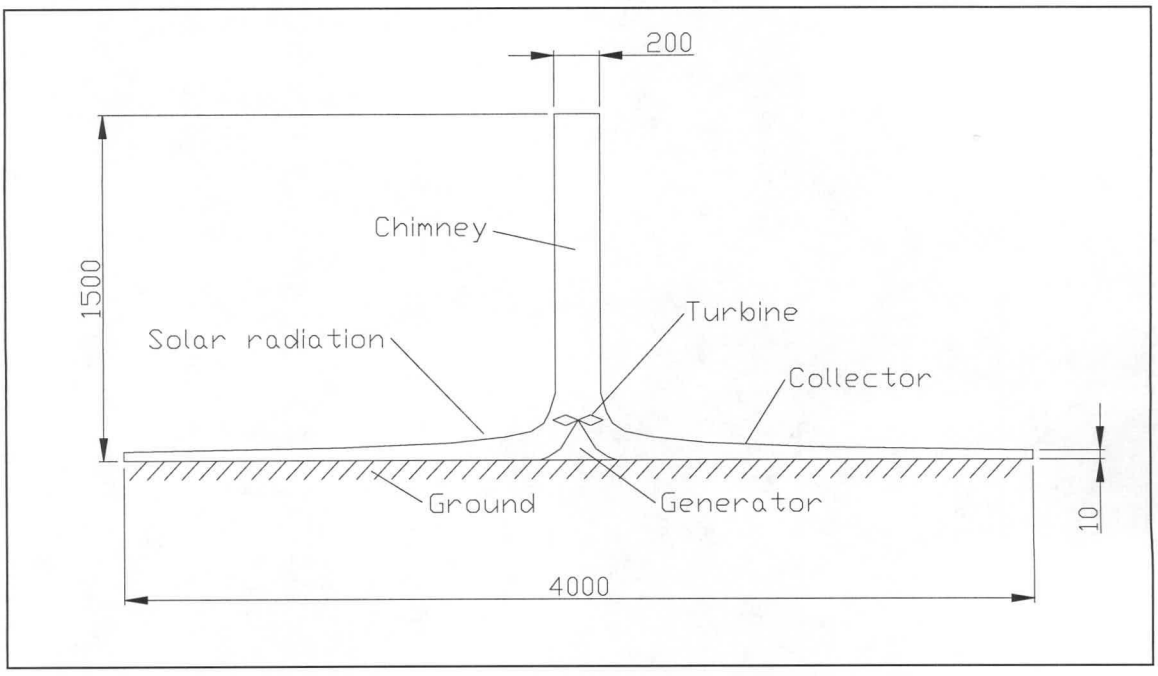

Figure 1.1: Schematic presentation of a solar chimney power plant

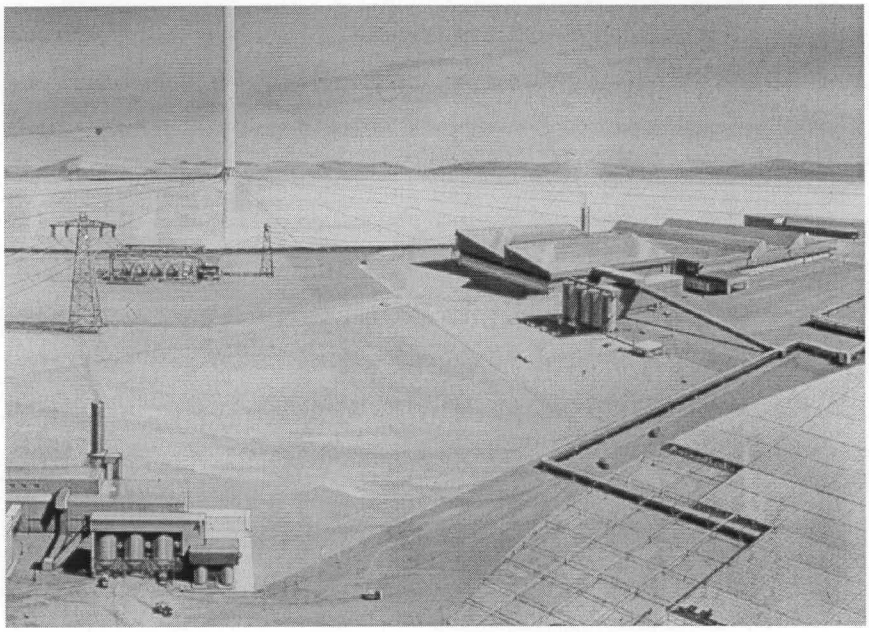

Figure 1.2: Artist impression of solar power plant with surrounding industry

A semi-desert climate prevails in the Sishen region and as such is ideal for a solar chimney power plant. A schematic presentation and artist impression of such a solar chimney power plant are shown in Figure 1.1 and Figure 1.2 respectively.

From Figure 1.1 it is apparent that a 200 MW solar chimney power plant would consist of three main components, namely a glass collector, located approximately 10 m above the ground and having a diameter of 4000 m and a chimney with a height of 1500m. The turbine and electrical generator are located at the base of the chimney (see Figure 1.1).

During the day incident solar radiation is transmitted through the glass collector and is absorbed by the ground. Of this absorbed energy, a certain percentage will be conducted into the ground, while the rest of the absorbed energy is transferred to either the air between the ground and cover or the glass cover through convection and long-wave radiation respectively. As a result a condition will prevail whereby the column of air within the chimney will be less dense than an equivalent column of air on the outside of the chimney, with the results that a draft is induced within the chimney, which ultimately drives the turbine.

During the night-time the same process occurs as described above, but in this instance the output of the power plant is determined by the amount of solar energy stored in the ground during the day, as well as the rate at which this stored energy is released from the ground to the air and collector respectively.

Conducting a numerical simulation, Hedderwick [01HE1], determined the output of the solar chimney power plant shown in Figure 1.1 over a period of one year. From the results of the simulation, it was evident that sufficient energy is not stored in the ground during the daytime, in order to obtain a consistent output of electricity throughout a 24 hour period for 365 days a year. For instance, the maximum output during midsummer (21st of December) was 118 MW, in comparison to 53 MW for midwinter (21st of June). Therefore, to obtain a more constant output of electricity from the power plant, a more effective storage system needs to be implemented within the solar chimney power plant.

Water is the most widely used energy storage medium in the solar energy world. It is further more also inexpensive and environmental friendly. Therefore, a possible solution to the solar chimney storage problem is to place plastic containers, filled with water, on the ground in a section of the collector, thereby possibly creating a more effective solar energy storage system.

Therefore, the aim of the present study is to investigate the characteristics and performance of a water storage system, in this instance plastic covered water tanks, as well as the influence of such an energy storage system on the performance of an upward facing solar air heater (see Figure 1.3) during both day-and night-time. This will be achieved through a systematic approach that will include experimental research, as well as an investigation into the validity of available theory used to predict the performance of solar air heaters; more particular the performance of an upward facing solar air heater.

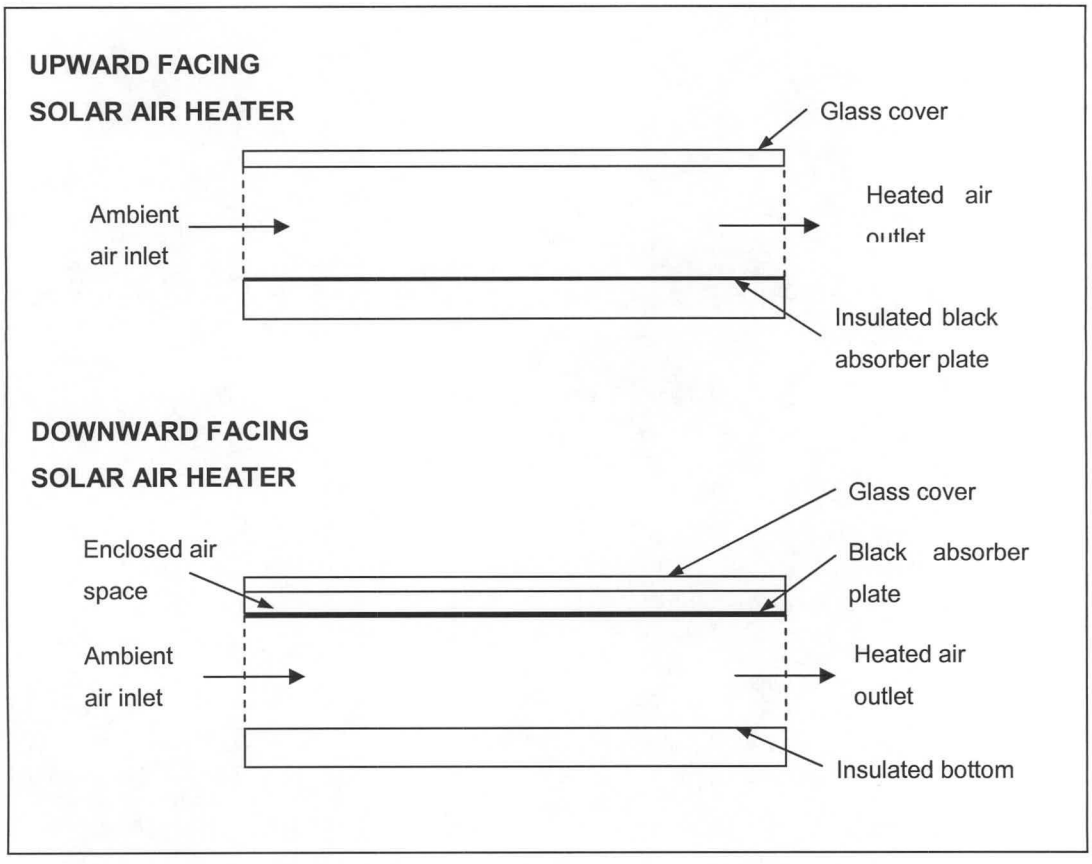

Figure 1.3: Schematic presentation of an upward and downward facing solar air heater

In Chapter 2 the main concern will be to determine experimentally the performance of an upward facing solar air heater and to compare this results to theoretical predictions. These results will also be used in later chapters to evaluate the influence of water energy storage.

Thereafter, in Chapter 3, the focus will shift towards the experimental and theoretical investigation of a plastic covered water tank; in particular in its ability to store and release its stored energy.

Finally, in Chapter 4, the theory obtained in the previous chapters will be combined to predict the influence of a plastic covered water tank system on an upward facing solar air heater system for both day- and night-time operation. These results will also be confirmed by experimental investigations.

Chapter 2: Performance evaluation of an upward facing solar air heater

Solar air heaters occupy an important place among solar heating systems, as they are comparatively inexpensive and both easy to construct and to maintain. Solar air heaters are, consequently, ideal for living space heating or even the drying of agricultural products [99BA1].

In this study, a number of experiments are conducted on an 8m long upward facing solar air heater, with the primary objective being the determination of the performance characteristics thereof. The experimental results are then compared with theoretical predictions, and the results will be used to predict the performance of a solar air heater incorporating plastic covered water tanks.

2.1 Theoretical performance evaluation

From the literature, it is evident that extensive research has been conducted into both the design procedure and optimisation of solar air heaters [84GA1, 85FR1, 94SA1, 96HE1, 96YE1, 97HA1, 98AL1, 98KA1, 98YE1, 99HA1, 99HA2, 00GA1, 00NJ1]. It is also evident that most of the research is based on the earlier work of Duffie and Beckman [91DU1]; in particular with regard to the following equation

$$q_u = F'\left[S - U_L\left(T - T_a\right)\right] \tag{2.1}$$

which defines the available useful heating energy per unit area, q_u, at any position along the flow direction of a solar air heater, for given air and ambient temperature's of T and T_a respectively. S refers to the solar energy that is absorbed by the absorber plate of the solar air heater (see Figure 2.1). U_L in turn is the overall heat loss coefficient and F' is the collector efficiency factor.

With the available energy per unit area known, the instantaneous collector efficiency of the solar air heater, as defined by equation (2.2), can be evaluated for either a section of the solar air heater or the entire solar air heater.

$$\eta_c = \frac{q_u}{Ih_T} \tag{2.2}$$

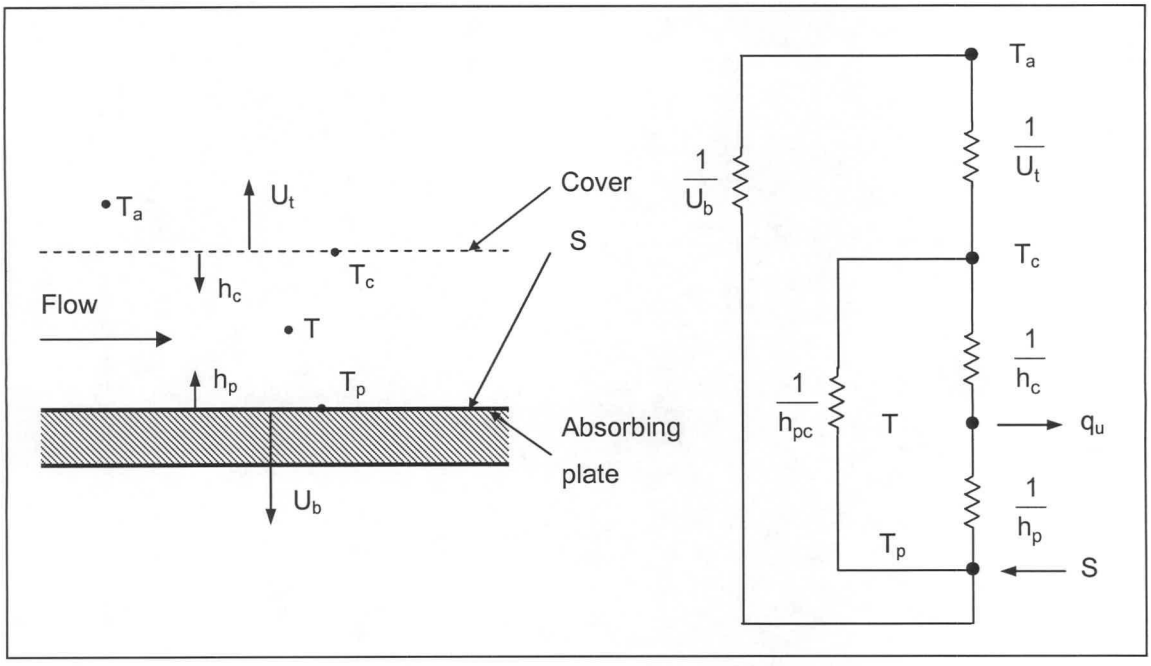

Figure 2.1: Upward facing solar air heater and associated thermal network

Duffie and Beckman [91DU1], referring to a single-cover upward facing solar air heater as shown in Figure 2.1, state that equation (2.3) should be used for the determination of the overall heat loss coefficient

$$U_L = \frac{(U_b + U_t)(h_{pc}\,h_c + h_{pc}\,h_p + h_p\,h_c) + U_b\,U_t\,(h_c + h_p)}{h_{pc}\,h_c + U_t\,h_p + h_{pc}\,h_p + h_c\,h_p} \tag{2.3}$$

while the collector efficiency factor is to be evaluated according to the following relation:

$$F' = \frac{h_{pc}\,h_c + U_t\,h_p + h_{pc}\,h_p + h_c\,h_p}{(U_t + h_{pc} + h_c)(U_b + h_{pc} + h_p) - h_{pc}^2} \tag{2.4}$$

In the previous two equations, h_p refers to the convective heat transfer coefficient between the absorber plate and the air, while h_c refers to the convective heat transfer coefficient between the cover of the solar air heater and the air underneath it. h_{pc}, is the linearized radiation heat transfer coefficient for the long-wave radiation heat exchange between the cover and the absorber plate (equation (2.5)).

$$h_{pc} = \sigma\left[\frac{1}{\varepsilon_c} + \frac{1}{\varepsilon_p} - 1\right]^{-1}\left(T_p^2 + T_c^2\right)\left(T_p + T_c\right) \tag{2.5}$$

The back loss coefficient, U_b, for the absorber plate which has a thermal conductivity of k_p and thickness t_p, is

$$\frac{1}{U_b} = \frac{t_p}{k_p} \tag{2.6}$$

while the top loss coefficient, U_t (equation (2.7)), accounts for both the wind-induced convective heat loss from the upper surface of the cover to the environment, for a wind-induced convective heat transfer coefficient h_w, as well as for the long-wave radiation heat exchange between the cover and the sky, with h_{rs} defining a sky radiation heat transfer coefficient.

$$\frac{1}{U_t} = \frac{1}{h_w} + \frac{1}{h_{rs}} \tag{2.7}$$

An intensive literature search into the evaluation of the wind-induced convective heat transfer coefficient h_w, revealed that although extensive research has been done, much uncertainty and ambiguity surrounds reliable equations for the evaluation of this heat transfer coefficient.

For instance, Duffie and Beckman [91DU1], referring to the convective heat transfer due to the wind over the surface of a solar collector, stated that "from the preceding discussion it is apparent that the calculation of wind induced heat transfer coefficient is not well established".

Sharples and Charlesworth [98SH1] confirmed this statement by stating that, " ...as experiments come closer to resembling "real" collector situations so more discrepancies and inconsistencies are found both between measured results from different experiments and with standard flat plate forced convection relationships for h_w".

More recently in an article, concerning the evaluation of the top loss coefficient (U_t) of solar collectors, Akhtar and Mullick [99AK1] stated: "The wind heat transfer coefficient, h_w, has been taken as an independent variable and the choice of using an appropriate value or correlation for h_w is left to the user." Thus, although Akhtar and Mullick [99AK1] give values for all other heat transfer coefficients they do not commit themselves to the evaluation of h_w.

These uncertainties and discrepancies may be attributed to a number of factors:

Firstly, it is apparent from the literature that the geometry of the apparatus, used by various researchers, and its environment is often not adequately described, with the result that there is often a certain degree of vagueness concerning the validity of the equation.

Secondly, Test et al. [81TE1] found that unless wind tunnel studies are conducted under turbulence levels similar to those found under windy ambient conditions, the resultant heat transfer correlation can not be expected to be in agreement with wind-induced convective heat transfer conditions.

Thirdly, the definition of the convective heat transfer coefficient is not always consistent. Most researchers (McAdams [54MA1], Watmuff [91DU1], Test et al. [81TE1], Kumar et al. [97KU1], Sharples and Charlesworth [98SH1]) used a simple linear correlation of the form

$$h_w = a + b\, v_w^c \tag{2.8}$$

while a second group (Sparrow and Tien [87SH1], Sparrow et al. [87SH1], Sparrow and Lau [87SH1] and Shankerin [87SH1]) chose to used the Colburn j-factor (equation (2.9)) to correlate their findings

$$j = \left(\frac{h_w}{\rho c_p v_w}\right)\left(\frac{\mu c_p}{k}\right)^{2/3} = dRe^{-0.5} \tag{2.9}$$

where a, b, c and d are appropriate constants that are defined differently by each group of researchers.

Since equation (2.8) is not written in a dimensionless form, it does not make provision for changes in the thermophysical properties of the air which exist with varying ambient conditions. Consequently, one can not expect the simple linear equation to model the very complex mixed convective heat transfer process accurately.

Furthermore, equation (2.9) is only valid under windy conditions; thus making no provision for a no-wind condition where natural convection is dominant.

In addition, the majority of researchers who correlate their data by means of equation (2.8), obtain a constant value for "a" by extrapolating the function to $v_w = 0$. However, natural convection strongly depends on the temperature difference between the surface and the ambient. As a result, the value of "a" can not be expected to be a constant with varying surface and ambient temperature.

Therefore, in this study the problems concerning the performance prediction of an upward facing solar air heater will be addressed by following a systematic approach in accordance with which an in-depth analysis will be conducted into those primary areas which govern the performance of such an air heater. The results of this analysis will then be used to derive a set of energy equations for the cover, absorber plate and working fluid (in this case air) for the upward facing solar air heater. Solved simultaneously, these equations will not only yield the efficiency of the solar air heater, but also the individual plate and cover temperatures. The predicted results will then be compared to experimental findings; hence serving as an indication of the validity of the applied theory and the derived energy equations for the prediction of the performance of an upward facing solar air heater.

2.2 Experimental apparatus

The experimental tests were conducted on a specially constructed solar air heater, consisting of a rectangular duct that was coupled to an apparatus used to measure the air mass flow rate through the duct (see Figure 2.2). In the subsequent sections the solar air heater duct and mass flow apparatus will be described.

2.2.1 Solar air heater duct

The solar air heater under consideration had an 8m long rectangular duct with a width of 1m and depth of 0.15m, as shown schematically in Figure 2.3.

The cover of the solar air heater was constructed by placing eight 1m x 1m x 3.88mm thick glass panes next to each other. The eight absorber plates, having dimensions of 1m x 1m x 0.075m, were constructed by bonding a 25mm thick Megaphen high temperature insulation (k = 0.02 W/mK) to 50mm thick polystyrene insulation (k = 0.03 W/mK). To increase the absorbtivity of the absorber plates, the upper surface of the plates were painted with a matt black paint ($\alpha \approx 0.9$). The rectangular test duct was placed on top of a bed of pebbles (see Figure 2.2) at a location 33.98 °South, 18.85 °East and ±100 m above sea level The duct flow axis is in a east-west direction.

2.2.2 Mass flow apparatus and ambient conditions measurements

The air entering the mass flow apparatus (see Figure 2.4), that was connected to the outlet of the solar air heater duct, may have a non-uniform temperature distribution together with a non-uniform velocity distribution (1). Hence, to accurately measure the mean temperature of the air

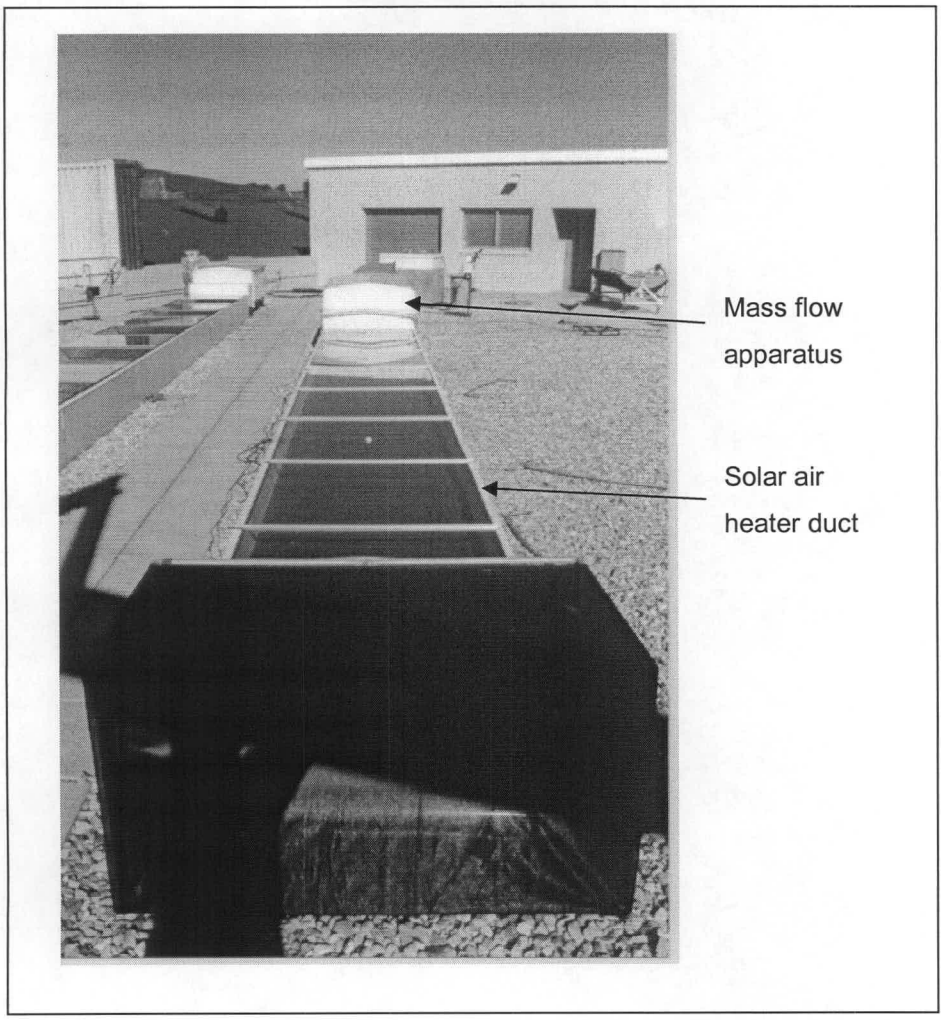

Figure 2.2: Experimental apparatus

stream, the air was first passed through a horizontal (2) mixer and then a vertical mixer (3). Both mixers consisted of a series of vanes, which divided the airflow into small streams that were diverted across each other. From there, the air was passed through a venturi (4). Located in the throat of the venturi (5), were four type-T thermocouples that measured the wet bulb and dry bulb temperatures of the air stream (5).

The mass flow rate through the solar air heater was determined by measuring the pressure drop across any of the three elliptical nozzles (7) mounted in a plate located between two perforated plates (6).

The mass flow rate through a given nozzle, neglecting thermal expansion or contraction of the nozzle, with area A_n, and pressure drop dp_n, is given as [98KR1]

$$m = C_n \phi_g Y A_n \sqrt{2 \rho_n dp_n} \qquad (2.10)$$

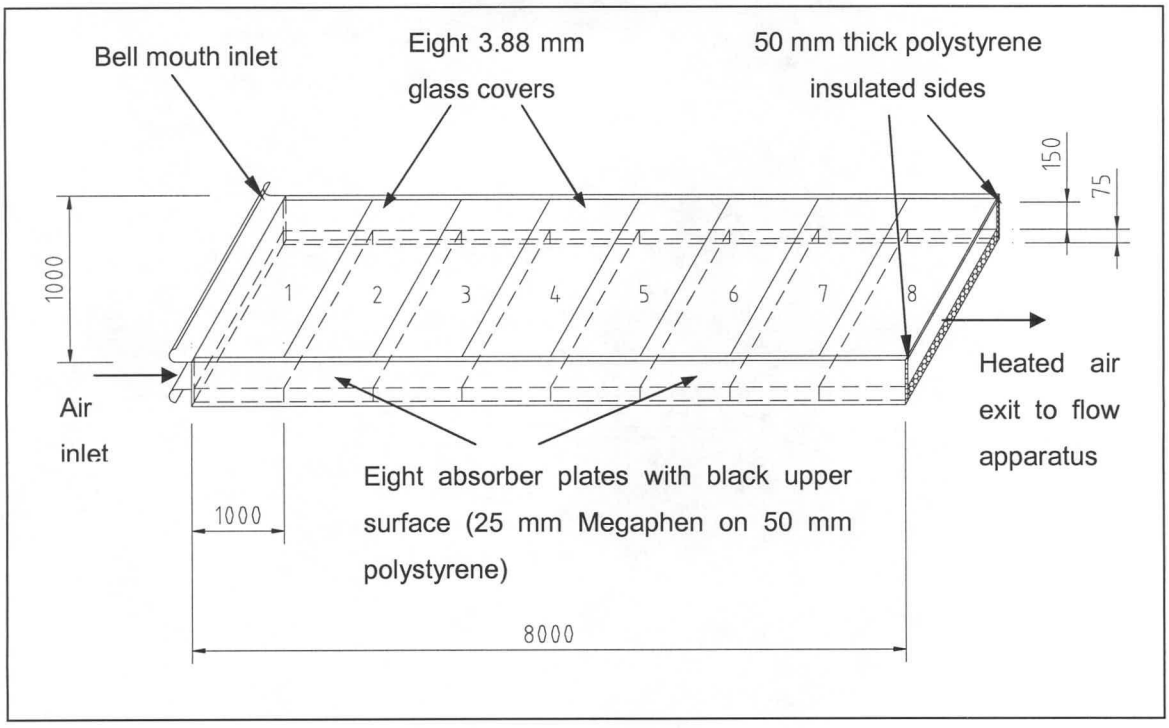

Figure 2.3: Rectangular test duct

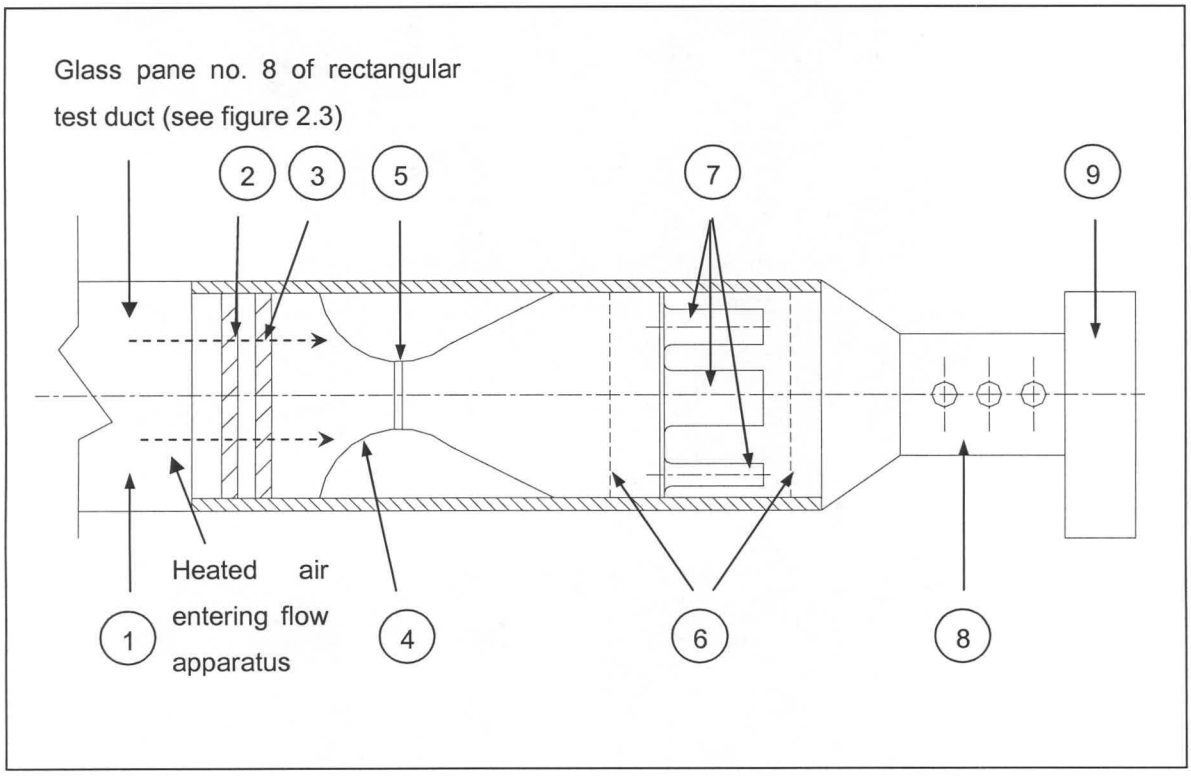

Figure 2.4: Cross-sectional plan view through mass flow apparatus

The nozzle discharge coefficient is a function of the nozzle Reynolds number, Re_n.

$$C_n = 0.954803 + 6.37817\times10^{-7}\,Re_n - 4.65394\times10^{-12}\,Re_n^2 + 1.33514\times10^{-17}\,Re_n^3 \qquad 30000 < Re_n < 100000 \qquad (2.11)$$

$$C_n = 0.9758 + 1.08\times10^{-7}\,Re_n - 1.6\times10^{-13}\,Re_n^2 \qquad 100000 < Re_n < 350000 \qquad (2.12)$$

$$C_n = 0.994 \qquad 350000 < Re_n \qquad (2.13)$$

The gas expansion factor ϕ_g can be approximated by the following correlation

$$\phi_g = 1 - \frac{3\,dp_n}{4\,p_{up}\,(c_p / c_v)} \qquad (2.14)$$

where $(c_p / c_v) = 1.4$ for air and p_{up} defines the nozzle upstream pressure, which can be written as

$$p_{up} = p_a - dp_d \qquad (2.15)$$

with p_a the atmospheric pressure and the dp_d the pressure difference between the upstream nozzle pressure, p_{up}, and the atmospheric pressure. The pressure difference can further be written in terms of a duct lost coefficient, K_d as follows

$$dp_d = K_d\left[\frac{m^2}{2\rho_{av}\,A_d^2}\right] \qquad (2.16)$$

in which m refers to the mass flow rate through the duct in kg/s, A_d the cross-sectional area of the duct and ρ_{av} to the air-vapour density based on the air outlet conditions. Hence, equation (2.15) becomes

$$p_{up} = p_a - K_d\left[\frac{m^2}{2\rho_{av}\,A_d^2}\right] \qquad (2.17)$$

The approach velocity factor for a compressible fluid can be approximated by

$$Y_n = 1 + 0.5\left(\frac{A_n}{A_{tus}}\right)^2 + 2\left(\frac{A_n}{A_{tus}}\right)^2\left(\frac{dp_n}{p_n\,c_p / c_v}\right) \qquad (2.18)$$

with A_{tus} referring to the upstream cross-section area. For the apparatus under consideration $A_{tus} = 0.6\ m^2$.

Therefore, by following an iterative procedure to solve equations (2.10) to (2.18), the massflow rate of the air through the solar air heater can be determined

After the second perforated plate (6) the air passed through the bypass valve (8) and then directly into the radial fan (9) which drives the airflow through the solar air heater. By either opening or closing the bypass valve (8) the mass flow rate through the duct could be adjusted.

Air was sucked into the rectangular duct through a bell mouth, in which four type-T thermocouples were located to measures the inlet air temperature. As air passed through the duct, the individual cover and plate temperatures of sections 1, 3, 6 and 8 of the duct were monitored with the aid of type-T thermocouples that were attached to the respective surfaces.

Ambient conditions (ambient temperature, wind speed, atmospheric pressure) were measured with the aid of a Davis Weather Monitor 2 weather station, while the total incident solar radiation was measured with a Kipp and Zonen solar sensor (Figure 2.5).

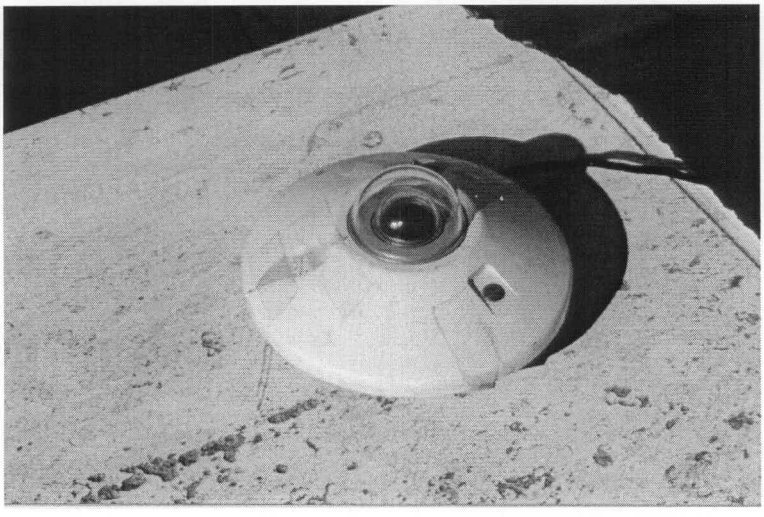

Figure 2.5: Kipp and Zonen solar sensor

2.3 Solar air heater analysis

The main purpose of any solar air heater is to effectively transfer energy from a distant radiant source i.e. the sun, to the air passing through the duct. However, to predict the percentage of energy that is transferred to the air, it is necessary to know how much of the radiant energy is

absorbed by the absorber plates, and secondly, how much of this available energy is then either transferred to the air or lost to the environment.

Set against this background, the subsequent sections of this chapter will initially be directed at establishing an applicable equation for the evaluation of the total heat loss from the heated glass covers to the environment. Then with an equation established for the total heat loss from the glass covers, the focus will shift to the evaluation of the effective absorbtion of the incident solar radiation by the absorber plates. Finally, the heat exchange that occurs between the heated glass covers, absorber plates and air that passes through the solar air heater will also be evaluated.

2.3.1 Total heat loss from cover surface to the environment

According to Duffie and Beckman [91DU1], any heated upward facing surface will tend to lose heat to its surrounding environment through wind-induced convection (q_{ca}) and long-wave sky radiation (q_{rs}).

Consequently, the total heat loss per unit area of heated cover, with emissivity ε and temperature T, to an environment with ambient temperature T_a and equivalent blackbody sky temperature of T_{sky}, is

$$q_t = (q_{ca} + q_{rs}) = \varepsilon\sigma\left(T^4 - T_{sky}^4\right) + h_w\left(T - T_a\right) \tag{2.19}$$

where σ is the Stephan-Boltzman constant.

From the previous discussion it is apparent that no reliable equation exists for the evaluation of h_w. Therefore, to address the ambiguity and discrepancies that surround the wind heat transfer coefficient, a number of experiments are conducted on a specific plate geometry in a particular environment as described in Appendix A.

From Appendix A, it follows that the total heat loss per unit area from a heated horizontal flat surface with temperature T, is

$$q_t = (q_{rs} + q_{ca}) = \varepsilon\sigma\left(T^4 - T_{sky}^{1.5}\right) + \left[(Gr\,Pr)^{1/3}\left(0.227 + 1.406\times10^{-6}\,Re\right)\right]\frac{k}{L_e}\left(T - T_a\right) \tag{2.20}$$

where

$$T_{sky} = 0.0552\, T_a^{1.5} \tag{2.21}$$

It should be noted that equation (2.20) is only applicable to the particular geometry described in Appendix A and valid in the range $6.75 \times 10^8 \leq (GrPr) \leq 26.6 \times 10^8$ and for $0 \leq Re \leq 2.5 \times 10^5$.

Although it may be argued that the sky temperature according to Swinbank [63SW1] (equation (2.21) is not the most accurate of available sky temperature equations, and that this would imply that the effective convective heat transfer coefficient, as defined by equation (2.20), is similarly not very accurate. However, in the evaluation of the heat transfer rate from the plate to the natural environment, this possible inaccuracy will be of little significance if the convection and radiation effects are used in combination, since the derivation of the wind-induced convective heat transfer coefficient, h_w, was done in conjunction with equation (2.21). Consequently, the sky radiation and convection terms should not be used separately to evaluate the individual contributions to the total heat loss.

2.3.2 Solar characteristics of cover and plate

The performance of an upward facing solar air heater is primarily dependent on the percentage of the incident solar radiation that is absorbed by the absorber plates, which in turn is dependent on the effective transmissivity of the cover material.

A literature search revealed that there are two approaches for the evaluation of the solar characteristics of a cover. These are due to Duffie and Beckman [91DU1] and Modest [93MO1] respectively.

Mills [92MI1] states that the sum of the effective reflectivity (ρ'), transmissivity (τ') and absorptivity (α') of transparent medium is equal to unity. Therefore, comparing the equations of Duffie and Beckman [91DU1] (equations (B.1– B.3)) to those proposed by Modest [93MO1] (equations (B.4– B.6)), it is shown in Appendix B that only the latter equations add up to unity. Consequently, the equations of Modest [93MO1] will be used subsequently to determine the solar characteristics of the solar air heater's glass cover.

A closer inspection of the equations of Modest [93MO1], reveals that the solar characteristics of a cover is dependent on the incidence angle of the sun, θ, on the cover as well as the cover's refractive index, n, and coefficient of extinction, C_e.

Although the incidence angle of the sun for the current experimental location was determined from equation (B.24), as given in Appendix B, the refractive index and coefficient of extinction for the glass cover under consideration was unknown.

From the literature [91DU1, 92SE1, 93MO1] it is evident that the refractive indexes for a number of cover materials are readily available (see Table B.1), in contrast to the coefficient of extinction, which depends on the quality of the material that is used to manufacture the cover. For instance, the refractive index of glass was given as 1.526 by a number of authors [91DU1, 93MO1], while the coefficient of extinction for glass was found to vary between $4m^{-1}$, for water white glass, to 32 m^{-1} for greenish glass, according to Duffie and Beckman [91DU1].

Consequently, a number of experiments were conducted on one of the 1m x 1m, 3.88-mm thick glass cover panes of the experimental solar air heater to determine the glass cover's coefficient of extinction. The experimental results, as shown in Appendix C, yielded a value of 13 m^{-1} for the coefficient of extinction of the glass pane. A more detailed description of both the experimental apparatus and analysis is given in Appendix C.

To validate equation (2.17), the proposed equations of Modest [93MO1] as well as the experimentally determined coefficient of extinction for the glass pane, a number of experiments were performed on an well-insulated simple solar collector, as described in Appendix D.

Using the recorded weather data, the cover and plate temperatures were predicted with the aid of the derived equations for the cover and absorber plate of the simple solar collector and compared to the experimentally measured values. The graphical comparison, as shown in figure D.5, reveals that good agreement exists between the theoretically predicted values and the experimentally measured temperatures.

2.3.3 Heat transfer inside rectangular duct

From the work of Duffie and Beckman [91DU1] and Ong [95ON1] it follows that two heat transfer phenomena occur inside the rectangular duct, namely, long-wave radiation heat exchange between the cover and the absorber plate, and forced convection between the two smooth heated surfaces (cover and absorber plate) and the air passing through the duct.

The inner surfaces of the shorter sides of the rectangular duct used in the present analysis were white of colour. Therefore it was assumed that the white inner sides would not participate measurably in the long-wave radiation heat exchange between the cover and absorber plates of the solar air heater. As a result, the long-wave radiation heat exchange between the glass

covers and absorber plates were modelled as two infinite parallel plates. From appendix D it follows that

$$q_{pc} = \sigma\left(\frac{1}{\varepsilon_c} + \frac{1}{\varepsilon_p} - 1\right)^{-1}\left(T_p^4 - T_c^4\right) \tag{2.22}$$

where ε_c and ε_p are the respective emissivities of the cover and absorber plate and T_c and T_p the respective temperatures.

To evaluate the forced convection heat transfer between the heated surfaces and the air, the air mass flow rate through the duct needs to be known. However, to determine the mass flow rate from equations (2.10) – (2.18), the value for the duct loss coefficient, K_d, needs to be known.

Isothermal test were conducted on the experimental solar air heater, as described in Appendix E, which yielded a value of 8.4 for the duct loss coefficient K_d.

During these experiments it was observed that the Reynolds number, based on a hydraulic diameter, Dh, of 4 times the cross sectional flow area, A_d, divided by the wetted perimeter (see equation (2.23)) and outlet conditions, varied between 13779 and 117089. The airflow through the rectangular duct was thus turbulent in nature.

$$Re_{Dh} = \frac{Dh\, m}{\mu A_d} = \frac{m}{\mu A_d} \times \frac{4(W \times H)}{2\mu(W + H)} = \frac{2m}{\mu(W + H)} \tag{2.23}$$

Ong [95ON1,95ON2], referring to the forced convection inside a duct, states that for a duct, with a length to hydraulic diameter ratio (L/Dh) less than 60, the influence of the entrance must be taken into account during the evaluation of the Nusselt number.

For the present rectangular solar air heater duct under consideration, the hydraulic diameter was found to be (Dh = $4A_c$ / P) 0.2608 m, consequently yielding a value of 30.67 for the length to hydraulic diameter ratio (L/Dh) for the rectangular duct.

For a hydraulic diameter to length ratio of less than 60 and Reynolds numbers larger than 10 000, Ong [95ON1, 95ON2] proposes that Nusselt's [31NU1] equation, as given by equation (2.24), be used for the evaluation of the turbulent convective heat transfer inside the upward facing solar air heater.

$$Nu = 0.036\,Re_{Dh}^{0.8}\,Pr^{1/3}\left(\frac{Dh}{x}\right)^{0.055} \qquad 10 < (L/Dh) < 400 \qquad Re_{Dh} > 10000 \qquad (2.24)$$

However, equation (2.24) determines the local Nusselt number at any given point x along length of the duct. Therefore, to obtain a convective heat transfer coefficient that is more representative for any given 1m section of the rectangular duct, starting at a point "a" and ending at point "b", as shown in Figure 2.6, a length weighted average convective heat transfer coefficient was defined as

$$\overline{h_{a-b}} = \sum_{i=1}^{n} Nu_x\left(\frac{k}{Dh}\right)\left(\frac{\Delta x}{b-a}\right) = \sum_{i=1}^{n} 0.036\,Re_{Dh}^{0.8}\,Pr^{1/3}\left(\frac{Dh}{x_i}\right)^{0.055}\left(\frac{k}{Dh}\right)\Delta x \qquad (2.25)$$

The thermophysical properties needed for the evaluation of the above dimensionless Nusselt and Reynolds numbers are to be evaluated at a mean surface-fluid temperature.

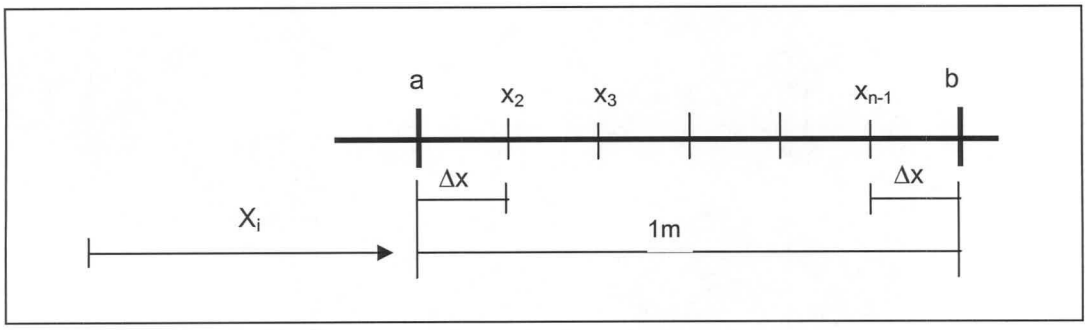

Figure 2.6: Evaluation of the length weighted average convective heat transfer coefficient between a point "a" and "b" for a 1m section of solar air heater

2.4 Solar air heater theoretical model

The objective of the following section is to establish applicable equations with which the respective mean temperatures for the cover, absorber plate, and air for each 1m square section of an 8m long upward facing solar air heater can be predicted with.

Based on the results and findings of the preceding sections of this chapter, Appendix E yields the following energy equation (equation (2.26)) for the cover of a 1m section of the solar air heater.

$$\left[\frac{(1-\rho_{bc})(1-\tau_{bc})}{1+\rho_{bc}\,\tau_{bc}}\right] Ih_b + \left[\frac{(1-\rho_{dc})(1-\tau_{dc})}{1-\rho_{dc}\,\tau_{dc}}\right] Ih_d$$

$$= \bar{h}_c\left(T_c - \bar{T}\right) + \sigma\left[\frac{1}{\varepsilon_c} + \frac{1}{\varepsilon_p} - 1\right]^{-1}\left(T_p^4 - T_c^4\right) \tag{2.26}$$

$$+ \left[\left(Gr_{ca}\,Pr_{ca}\right)^{1/3}\left(0.227 + 1.406\times10^{-6}\,Re_{ca}\right)\right]\frac{k_{ca}}{L_c}\left(T_c - T_a\right) + \varepsilon_c\,\sigma\left[T_c^4 - \left(0.0552\,T_a^{1.5}\right)^4\right]$$

Furthermore, from Appendix E it follows that for an upward facing solar air heater, equation (2.27) is applicable to a 1m long absorber plate

$$\left[\frac{(1-\rho_{bc})^2\,\tau_{\alpha bc}}{1-\rho_{bc}^2\,\tau_{\alpha bc}^2}\right]\left[\frac{\alpha_p}{1-(1-\alpha_p)\rho_d}\right] Ih_b + \left[\frac{(1-\rho_{dc})^2\,\tau_{\alpha dc}}{1-\rho_{dc}^2\,\tau_{\alpha dc}^2}\right]\left[\frac{\alpha_p}{1-(1-\alpha_p)\rho_d}\right] Ih_d$$

$$= \bar{h}_p\left(T_p - \bar{T}\right) + \sigma\left[\frac{1}{\varepsilon_c} + \frac{1}{\varepsilon_p} - 1\right]^{-1}\left(T_p^4 - T_c^4\right) \tag{2.27}$$

and equation (2.28) for the air passing through a 1m section of the experimental solar air heater.

$$\dot{m}c_p\,T_{in} + \bar{h}_p\left(T_p - \bar{T}\right) + \bar{h}_c\left(T_c - \bar{T}\right) = \dot{m}c_p\left(2\bar{T} - T_{in}\right) \tag{2.28}$$

Therefore, by solving the respective energy equations (equations (2.26), (2.27) and (2.28)) for the cover, absorber plate and air simultaneously for each of the eight 1m square sections, the performance of an upward facing solar air heater can be predicted for given ambient conditions.

2.5 Experimental and theoretical results

From the 1st to the 12th of February 2001, experiments were conducted on the experimental upward facing solar air heater described in section 2.2 of this chapter. During the tests the air mass flow rate was varied between 0.09 and 1.02 kg/s.

Using equation (2.26), (2.27) and (2.28), the mean cover and plate temperatures were predicted for each of the eight sections and compared to the experimentally measured values for various mass flow rates (see figures 2.7 – 2.12).

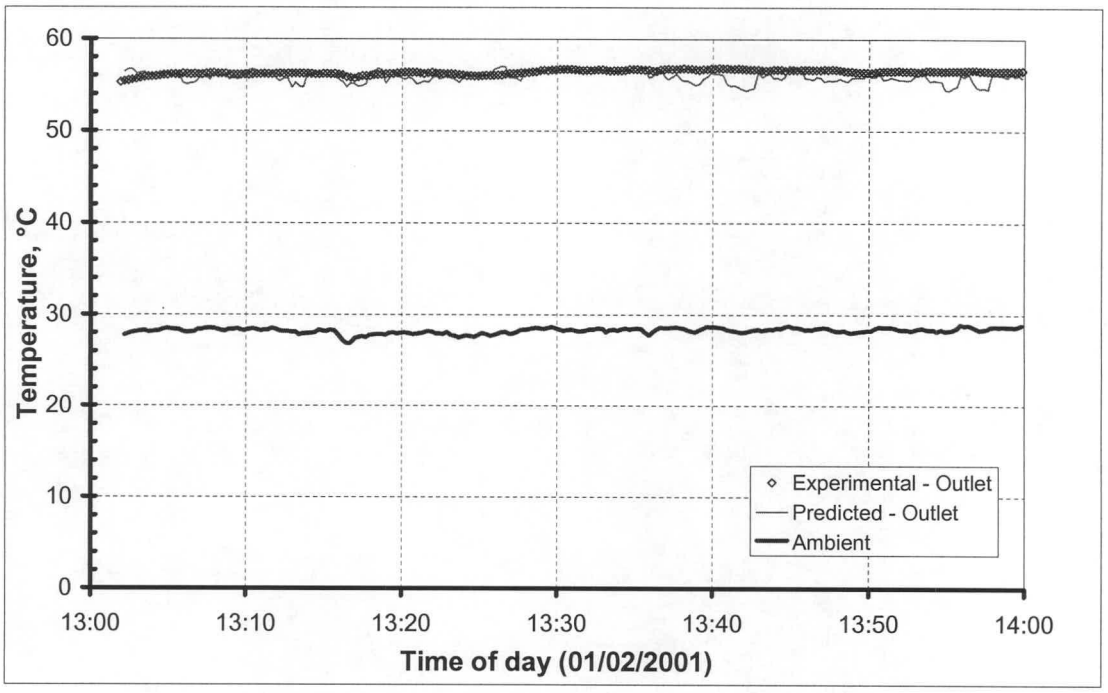

Figure 2.7: Ambient and outlet air temperature for 0.09 kg/s

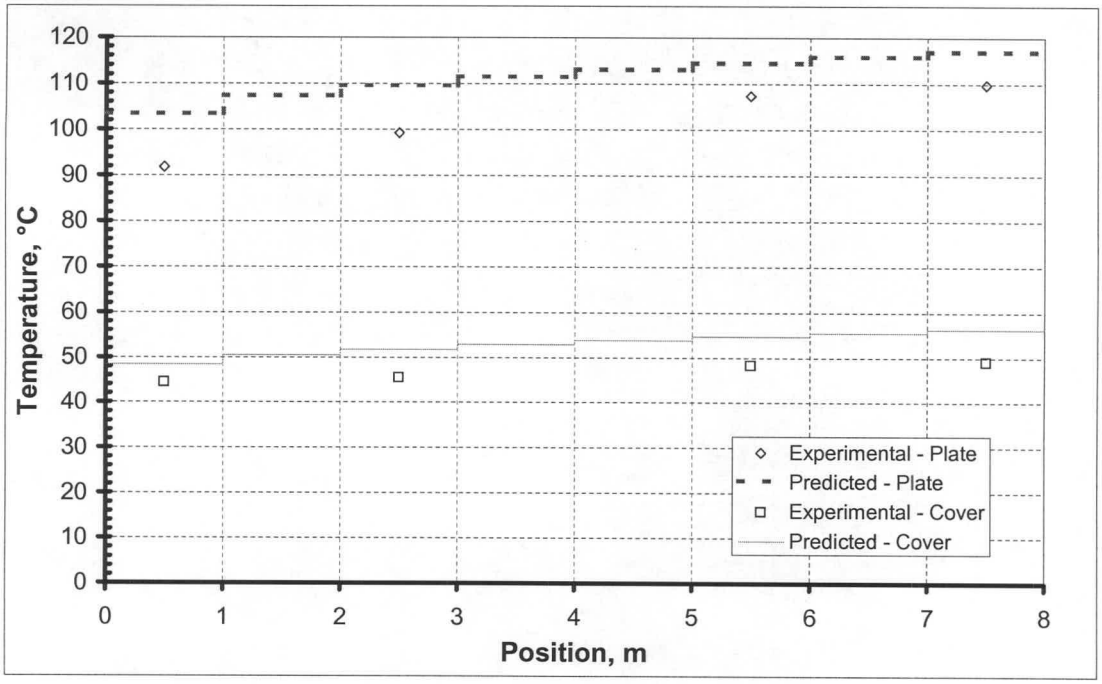

Figure 2.8: Plate and cover temperatures at 13h15 for 0.09 kg/s

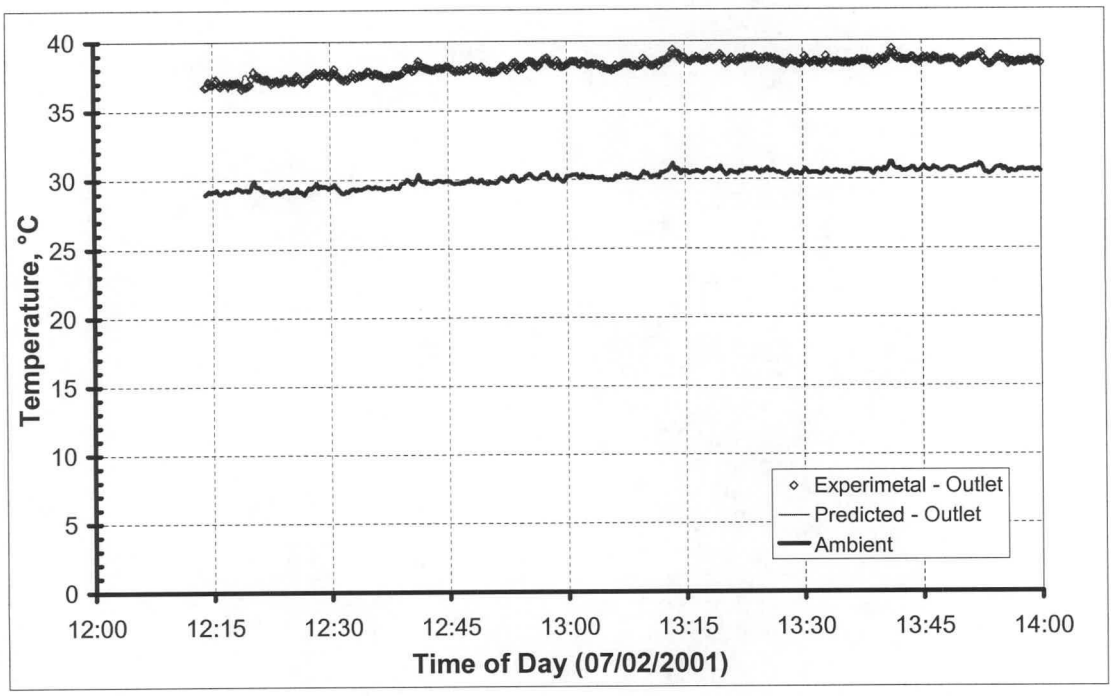

Figure 2.9: Ambient and outlet air temperature for 0.652 kg/s

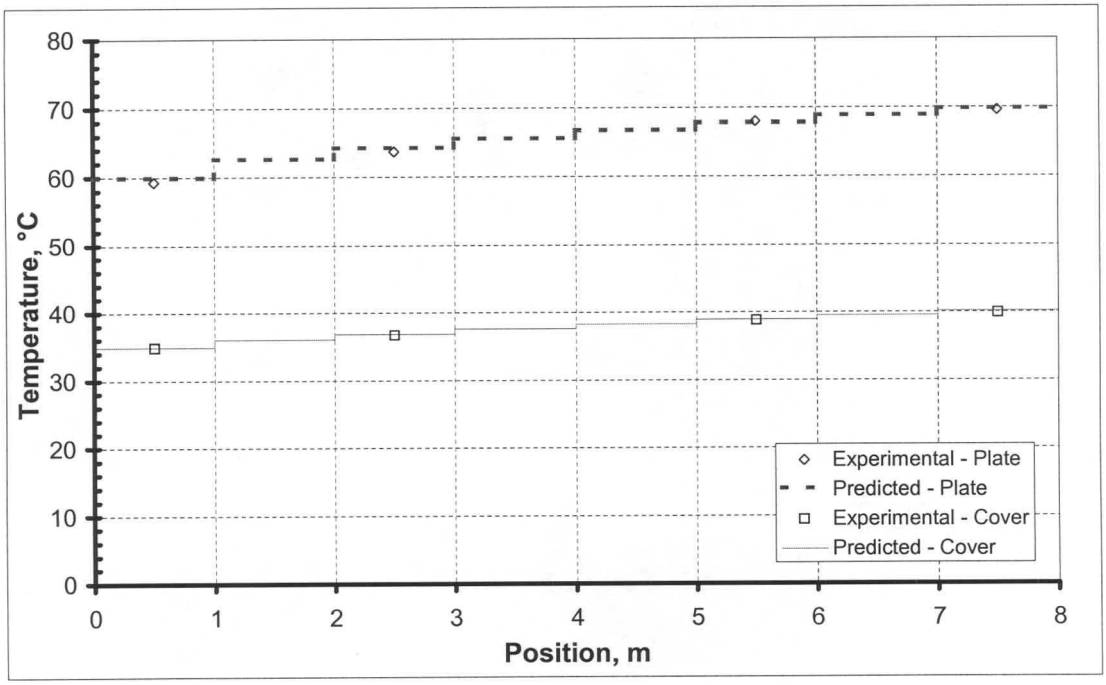

Figure 2.10: Plate and cover temperatures at 13h15 for 0.652 kg/s

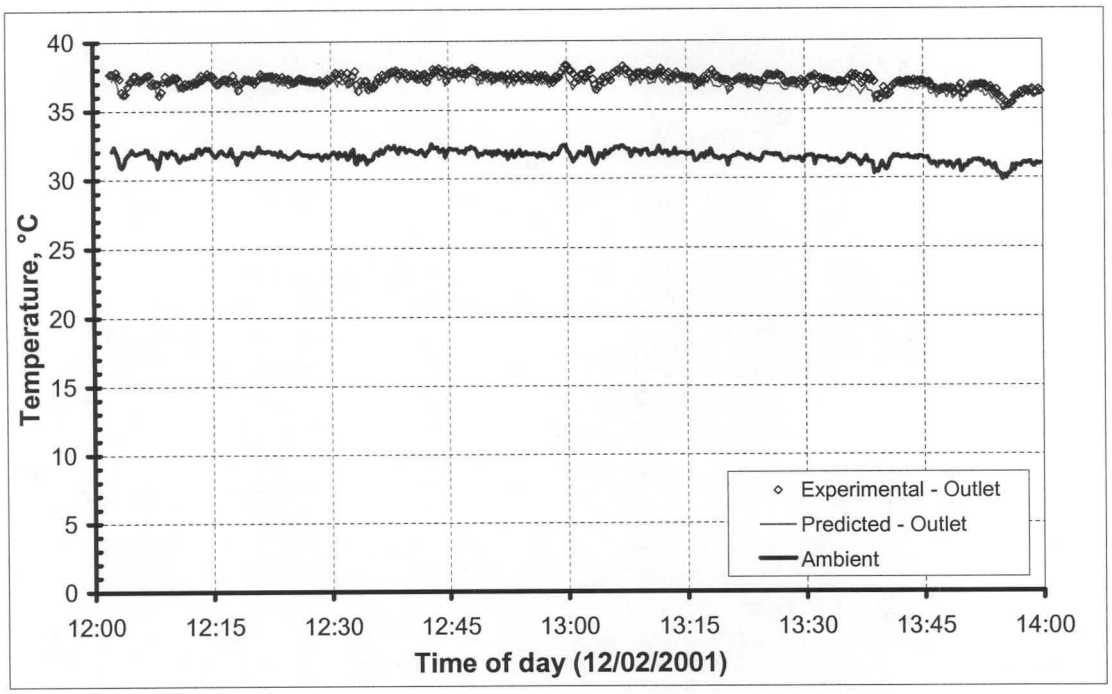

Figure 2.11: Ambient and outlet air temperature for 1.02 kg/s

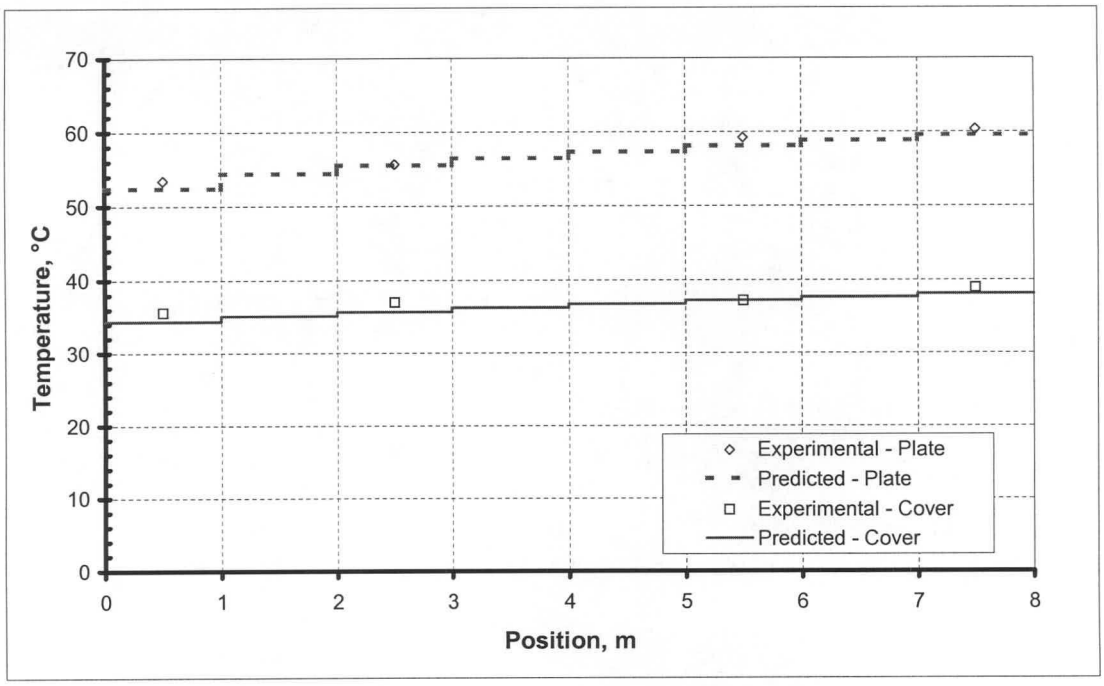

Figure 2.12: Plate and cover temperatures at 12h30 for 1.02 kg/s

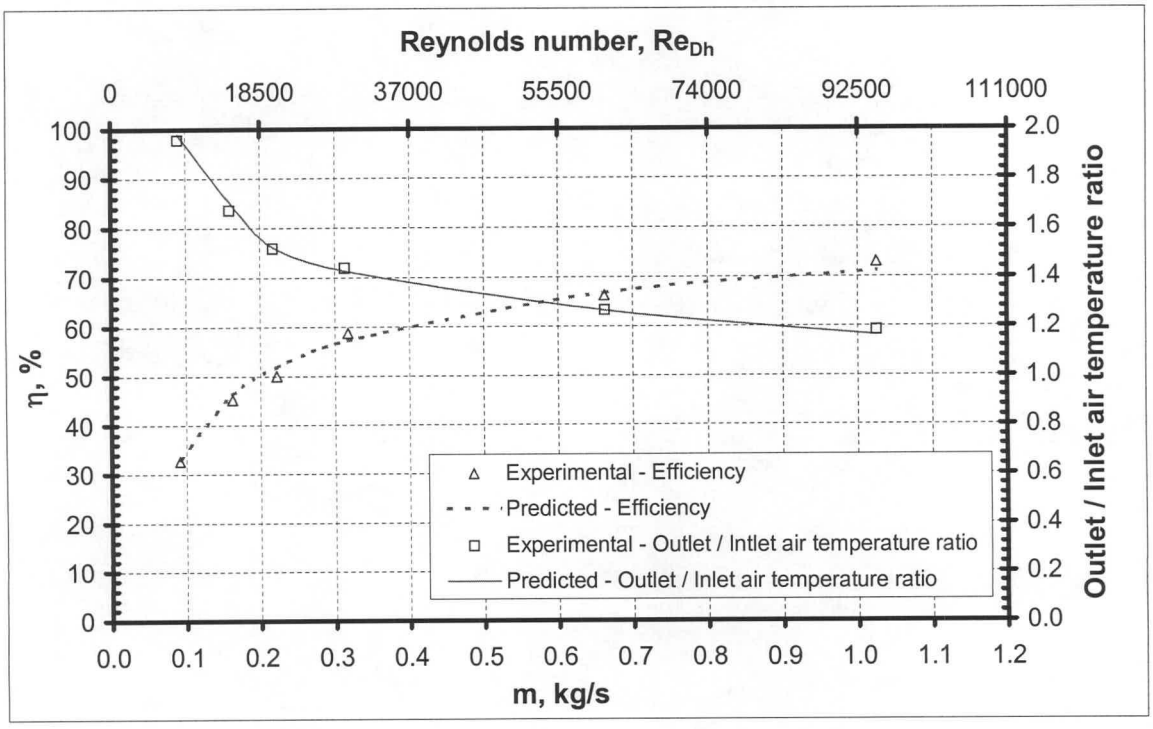

Figure 2.13: Comparison between the theoretically predicted and experimentally measured collector performance of an upward facing solar air heater

From the results, as shown by Figure 2.7 – Figure 2.12, it is evident that except for the case with very low mass flow rate of 0.09 kg/s (Re_{Dh} = 8303), where only moderate agreement exists, good agreement exists between the theoretical model's predicted temperatures and the experimentally measured temperatures for the cover, absorber plate and outlet temperatures.

The reason for the difference between the predicted and experimentally measured values for the low mass flow rate, is in part due to the fact that the equation of Nusselt [31NU1], for the turbulent convective heat transfer inside the passage, is used outside its validity range.

From Figure 2.13 it is evident that, as expected, an increase in the mass flow rate will lead to an increase in the efficiency of the solar air heater. This can be ascribed to the enhanced convective heat transfer between the heated surfaces and the air. However, the increased mass flow rate will also lead to a decrease in the temperature rise across the length of the solar air heater (see Figure 2.13).

In light of the theoretical model's accurate prediction of the outlet fluid temperature, it is also apparent from Figure 2.13, that good agreement exists between the predicted and experimentally determined overall performance of an upward facing solar air heater The

hydraulic diameter based Reynolds number used during calculations in the figure was based on the outlet air conditions.

In Appendix E, sample calculations are presented for both the evaluation of the duct loss coefficient, K_d, from experimental data as well as the prediction of the first section's plate and cover temperature for the 6th of February 2001 at 13h10:04.

2.6 Conclusion

The objective of the chapter was to compare theoretically predicted cover and experimentally measured performance characteristics of an upward facing solar air heater. An in-depth literature study revealed that no reliable equations were available at the time of the study for the evaluation of the convective heat loss from a heated horizontal flat surface to its environment. For this reason, a number of experiments were conducted on a solar heated flat plate exposed to its environment in order to determine an appropriate correlation for the evaluation of the effective wind-convective heat loss from a horizontal heated surface to its surroundings.

Employing the newly derived equation (equation (2.20)) in conjunction with existing equations, it was shown that not only can the cover, absorber plate and air temperature be predicted with a high degree of accuracy but also the overall performance characteristics of an upward facing solar air heater.

Chapter 3: Water energy storage

Household and industrial power consumption, while cyclic, is not necessarily in phase with incident solar radiation. Consequently, if solar energy is to meet substantial portions of energy demands, the storage of solar energy is of utmost importance.

3.1 Storage of solar energy in water

A literature review reveals that although thermal energy can be stored in a various forms (i.e. packed bed [91DU1], phase changing materials [91DU1, 94BE1] and endothermic chemical reaction [91DU1]), water is still the most widely used medium. For instance, Olivetti et al. [98OL1] conducted experiments on a prototype plant for the interseasonal storage of solar energy for the winter heating of buildings in water. Based on the experimental results, Oliveti et al. [98OL1] concluded that the prototype plant was capable of supplying useful energy very close to the required energy needs of the buildings and can therefore can be regarded as an inexpensive and useful medium for thermal energy storage.

Water also has further the ability to absorb solar radiation passing through it; especially the longer wavelengths ($\lambda = 0.7 - 10^3$ μm) of the incident solar radiation spectrum (see Figure 3.1) [90JA1, 91DU1, 93MO1] as is evident from the spectral absorbtion coefficient diagram of water, as shown in Figure 3.2.

Consequently, not only does water have the ability to serve as an excellent storage medium but also to simultaneously serve as a collector of solar energy. As a result, water is able to convert intermittent solar radiation directly into a steady source of thermal energy [89KR1].

The concept of using water as a simultaneous collector and storage device of solar energy is directly exploited in solar ponds, which according to Kreider et al. [89KR1], can be classified into two main categories. Namely those that have reduced heat loss by the prevention of convection within the water storage medium, and those that make use of a covered pond surface to reduce the heat loss from the upper pond surface to its surrounding environment. On a closer inspection of literature, it was apparent that the majority of published articles were concerned primarily with the former.

From literature it follows that two different methods were used to suppress convection within a solar pond. In the first method the density of the water was increased by adding an organic salt to the water; thus creating a salt gradient solar pond (SGSP). This type of solar pond had been studied both experimentally and numerically, and was found to be ideal for long term seasonal storage [84RU1, 89KR1, 91DU1, 94TS1, 96PR1, 00KU1, 00JA1]. However, salt gradient solar

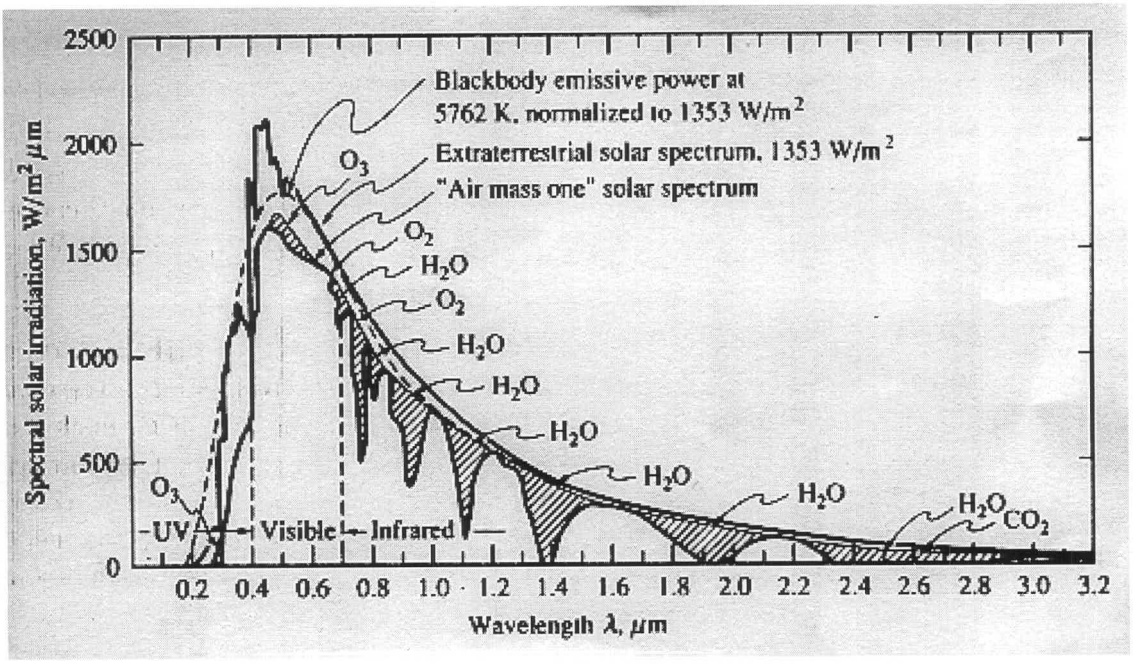

Figure 3.1: Incident solar radiation spectrum [91DU1]

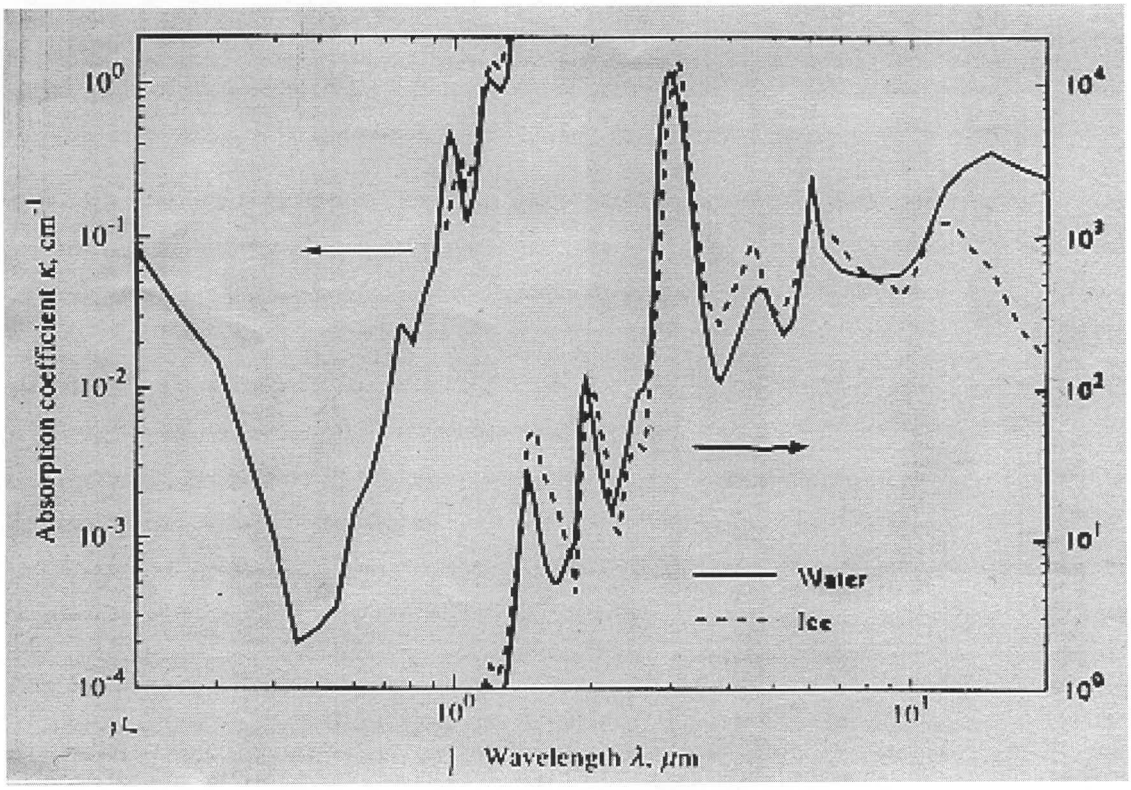

Figure 3.2: Coefficient of extinction for water for various wavelengths [91DU1]

ponds have two shortcomings, namely the potential environmental pollution in case of a salt leakage and the continual maintenance required by the salt gradient layer.

In the second method, thin transparent membranes were used (configured as horizontal sheets, vertical sheets or vertical tubes [80HU1]) to create membrane-stratified solar ponds (MSSP), in order to suppress convection within the water medium. Yeh and Ma [89YE1] conducted a theoretical investigation into the performance of membrane-stratified ponds and found that the MSSP's are more effective than SGSP's. This is due to a more rapid water temperature increase in the membrane-stratified solar ponds than in the salt-gradient solar ponds. However, Hull [80HU1], made it evident that there are certain inherent practical problems to membrane ponds. For instance the optical degradation and membrane stress which results from the formation of air bubbles on the membranes.

The second category of solar ponds is known in literature as either non-salt or freshwater solar ponds [90SO1, 96TA1]. A distinctive characteristic of these solar ponds is that their upper surfaces are covered by a thin transparent cover in order to suppress evaporation. Taga et al. [96TA1] investigated these ponds and found that they are more suitable for short-term energy storage because the temperature rise within the water is more rapid than in salt gradient ponds. In addition, these ponds are easy to construct and have low maintenance cost.

In light of its ability to simultaneously serve as a collector and thermal storage device of solar radiation as well as the more rapid increase in water temperature with which it is associated, a covered freshwater solar pond represents, within the scope of the present study, the best-suited thermal storage device for a solar air heater.

Consequently, in the following sections of this chapter the storage (daytime operation) and discharge (night-time operation) ability of a shallow freshwater covered solar pond, in this case a plastic covered water tank, will be investigated. Thereafter, having established the performance of the plastic covered water tank, the current investigation will be extended to include an evaluation of the influence of a water tank thermal storage device on the performance of a solar collector.

The experimental findings will furthermore be used to validate the ability of available theory to predict the performance of a water tank; either as part of a solar collector system or on its own.

3.2 Experimental apparatus

The apparatus which was used in the experiments, as shown in Figure 3.3, consisted of a 1 m x 1 m x 0.19 m black fibreglass tank which was supported by a square pedestal 1m above the

ground. The pedestal had highly reflective sides in order to ensure that the sides did not contribute to the total heat loss from the covered water surface to the environment.

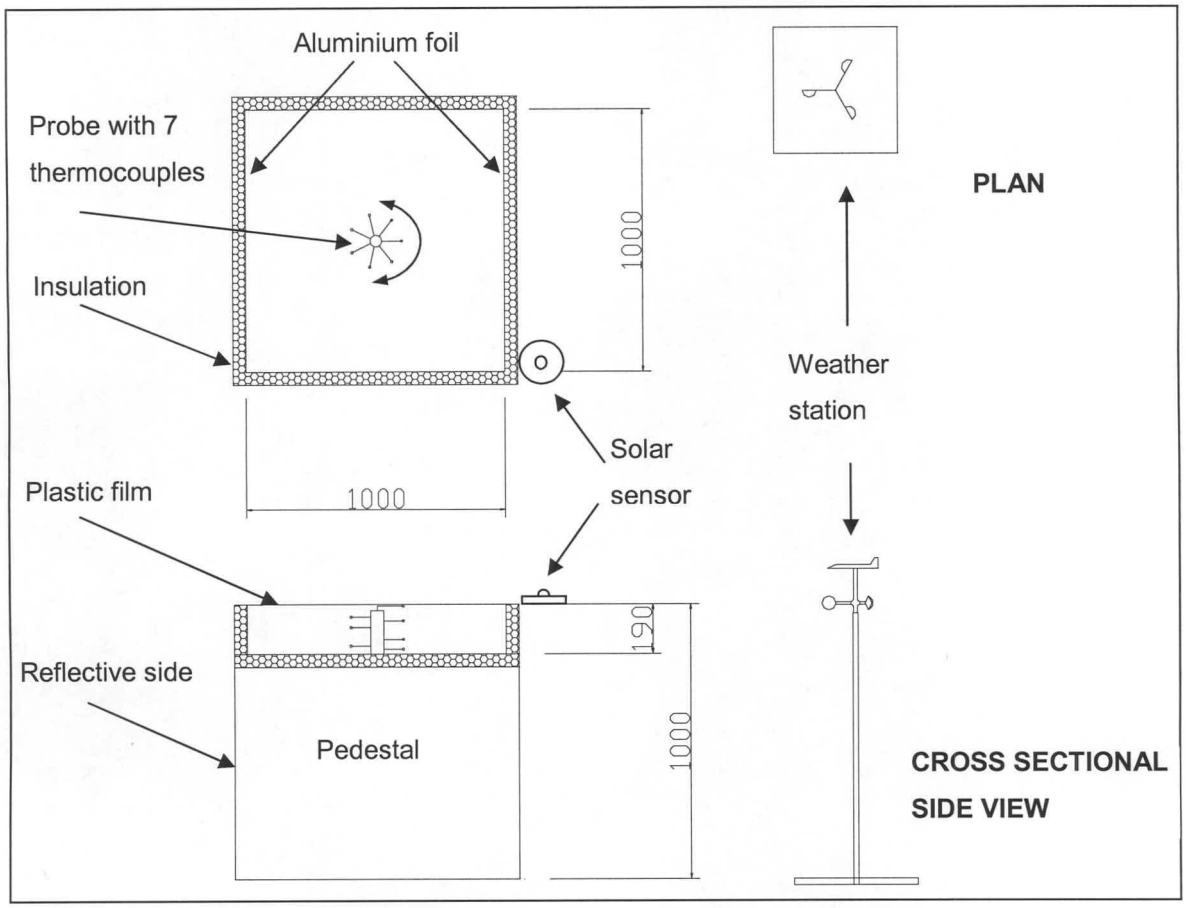

Figure 3.3: Schematic presentation of experimental apparatus

The inner sides of the tank were covered by a highly reflective layer of aluminium foil ($\alpha = \varepsilon \approx 0.1$) to minimise the influence of these surfaces on the convective heat transfer inside in the water and subsequently the water temperature distribution. The sides as well as the bottom were insulated by 50 mm thick polystyrene, while the upper surface of the water was covered by a 0.2 mm thick Luminal Anti-Fog plastic cover, to ensure that no evaporation occurred.

Ambient conditions (temperature, wind speed, atmospheric pressure) are measured with the aid of a weather station (Davis Weather Monitor II) and the total incident solar radiation by means of a solar sensor (Kipp and Zonen) placed next to the surface cover (see Figure 3.3). The facility at which the experiments were conducted was located 100 m above see level at a latitude of 33.98°S and longitude of 18.85°E.

3.2.1 Water temperature measurement

In addition to the water temperature itself, the temperature distribution through the water at any given point in time is also of the utmost importance.

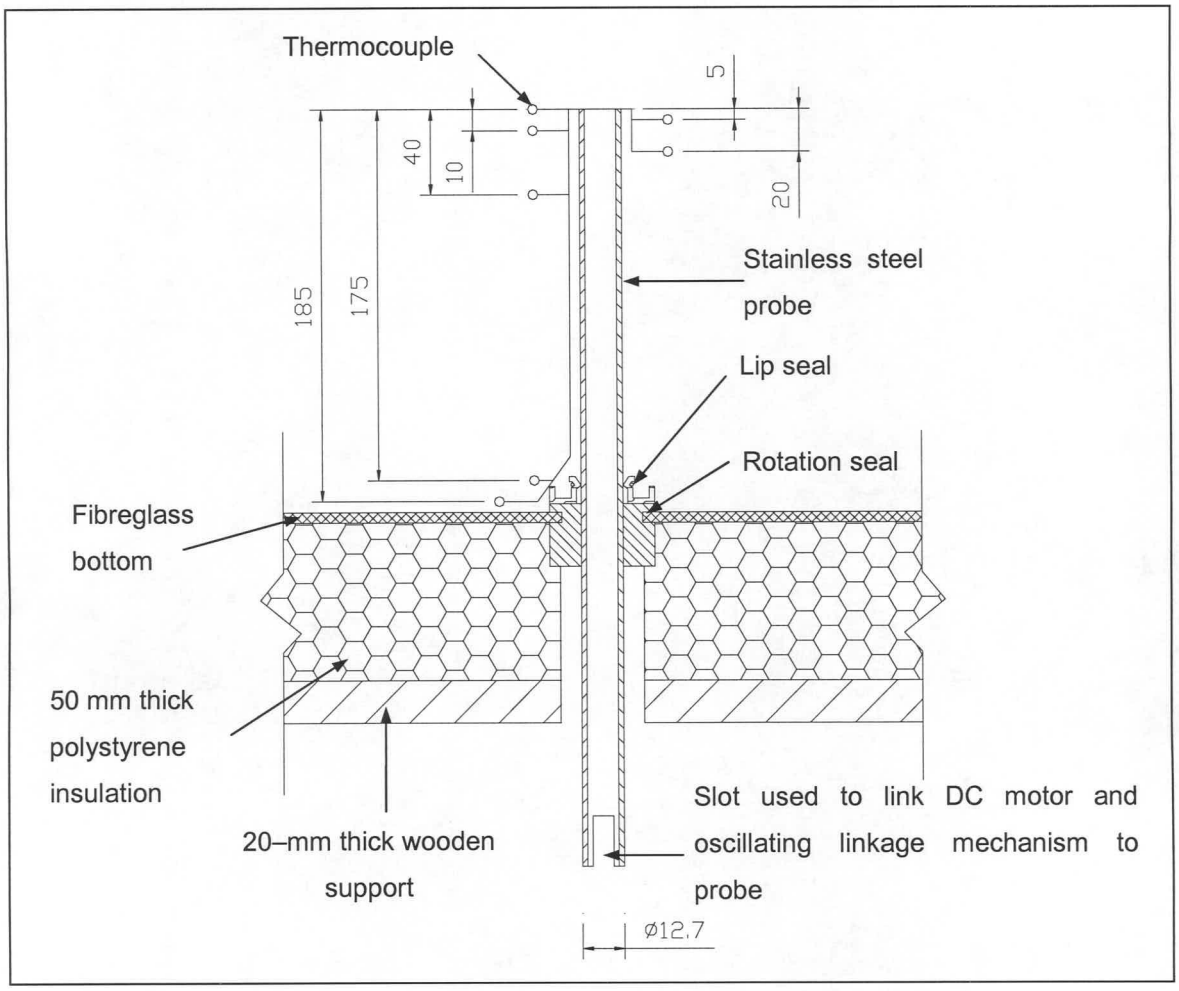

Figure 3.4: Cross-sectional view of oscillating water probe with seven type T thermocouples

With this information available, one would, after all be able to not only understand the absorbtion of solar radiation within water, but also the heat transfer phenomenon which would occur within such a plastic covered water tank, thus enabling one to establish a numerical model that is both representative of a plastic covered water tank and able to accurately predict the performance of these solar ponds. For this reason, an oscillating water temperature probe was installed through the base of the fibreglass tank (see Figure 3.4).

The probe consisted of a 12.7 mm ID stainless steel pipe that was supported at the bottom of the fiberglass tank through a rotating seal. To ensure no leakage occurred, a second lip seal

was attached to the pipe and bonded to the top section of the rotation seal. Seven type-T thermocouples were threaded through the pipe, and positioned to measure the water temperature at various depths as shown in Figure 3.4. Another two thermocouples were bonded to the underside of the tank to record the bottom surface temperature of the tank.

The oscillating movement of the probe was induced by a linkage mechanism and 12V DC motor that were connected to the probe through a slot that was cut into the pipe. The linkage mechanism oscillated through an arc of ± 21.6°, while the frequency of the oscillation was adjusted by changing the input voltage to the electric motor. For the experiments, the frequency of the probe was set at ±8Hz. This low frequency would not only ensure good contact between the thermocouples and the water, but also ensure that the transient water temperature layers in the tank were not disturbed. Furthermore, the movement of the thermocouples also prevented them from heating up due to the absorbtion of solar radiation.

3.3 Analysis and results of plastic covered water tank

To address the uncertainty surrounding the solar properties of the plastic film, experiments were conducted on the 0.2 mm Luminal Anti-Fog plastic film. From these experiments values of 1.6 and 200 m^{-1} were obtained respectively for the refractive index, n_f, and coefficient of extinction, C_{ef}, value for the plastic film (see Appendix F). These experimentally determined properties of the film compare favourable with values quoted in the literature ($1.34 \leq n_f \leq 1.64$ and $9 \leq C_{ef} \leq 205$ [98TS1]).

The second uncertainty surrounding the use of the plastic film pertained to its long-wave emissivity. Heat would be lost from the top of the plastic covered water surface to the surrounding environment through mixed convection and sky radiation. However, to evaluate the long-wave radiation heat exchange between the plastic film and the sky, the long-wave emissivity of the film was required. As a result, experiments were conducted with the aid of a simple solar collector (described in Appendix G) and a value of 0.8 was obtained for the long-wave emissivity of the plastic film, ε_f.

3.3.1 Day operation

With the solar properties and long-wave emissivity of the plastic film known, a number of experiments were conducted during cloudless days. The results for one such day are shown in Figure 3.5.

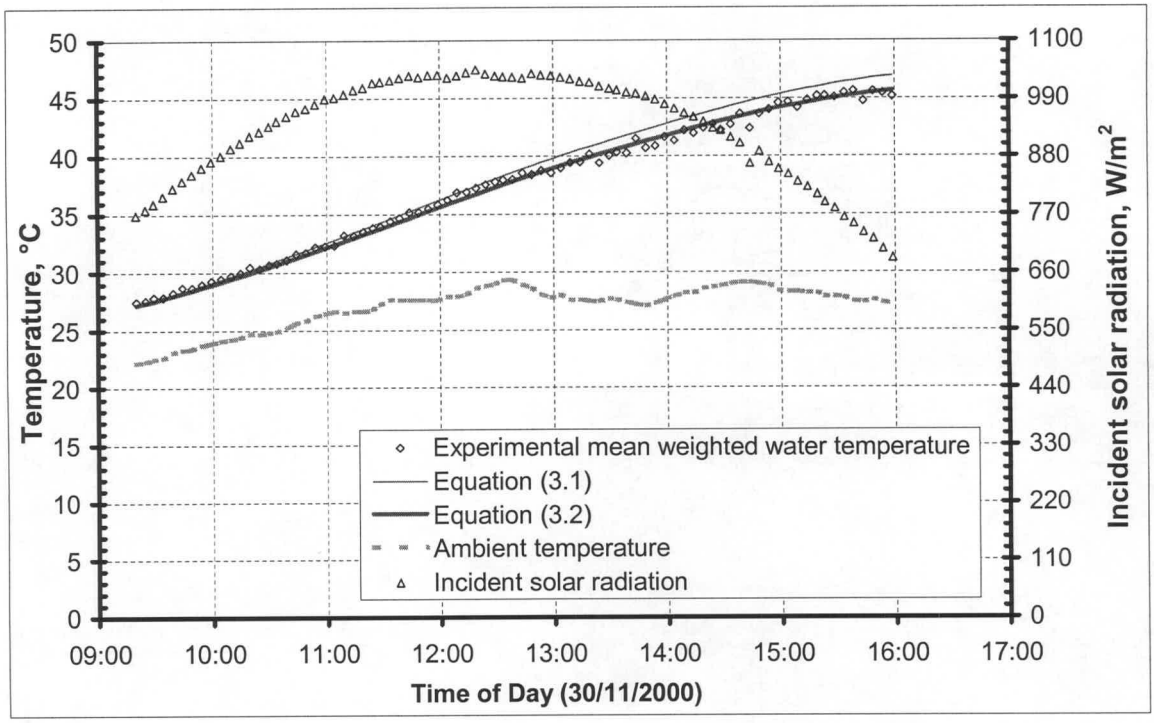

Figure 3.5: Theoretical and experimental mean water temperature for a plastic covered water tank on a cloudless day

Assuming conduction losses through the insulation and the solar absorbtivity of the plastic film to be negligible as well as that there exists perfect contact between the film and water, an analysis of a plastic covered water tank (Figure H.1) is conducted in Appendix H. From the analysis, the following conservation of energy equation is given for the water tank during the day.

$$\left[1-\frac{\rho_{baf}+(1-2\rho_{baf})\rho_{bcw}\tau_{\alpha b}^2}{1-\rho_{baf}\rho_{bcw}\tau_{\alpha b}^2}\right]Ih_b+\left[1-\frac{\rho_{daf}+(1-2\rho_{daf})\rho_{dcw}\tau_{\alpha d}^2}{1-\rho_{daf}\rho_{dcw}\tau_{\alpha d}^2}\right]Ih_d$$

$$-\left[(Gr_{fa}\,Pr_{fa})^{1/3}\left(0.227+1.406\times10^{-6}\,Re_{fa}\right)\right]\frac{k_{fa}}{L_f}(T_w-T_a)-\sigma\,\varepsilon_f\left[T_w^4-\left(0.0552\,T_a^{1.5}\right)^4\right] \qquad (3.1)$$

$$=\rho_w\,c_{pw}\,t_w\frac{dT_w}{dt}$$

In Appendix H, the above equation for the water tank (equation (H.5)) was employed in conjunction with the previously established properties of the plastic film, to predict the water temperature of the water tank, for the given ambient conditions for the 30th of November 2000.

The predicted water temperatures were then compared to experimental measured mean depth-weighted water temperature as shown in Figure 3.5.

From Figure 3.5 it is apparent that as the day progressed, the theoretical and experimental values tend to deviate from each other. Visual observations point to a possible explanation for this phenomenon. During the experiments, it was observed that an air layer formed underneath the plastic cover during the course of the day. An air layer underneath the plastic film would tend to reduce the amount of solar radiation that penetrates the water.

Therefore, assuming an air layer exists from the beginning of the day, the previously derived equation (equation (3.1)) is modified (equation (H.7) in Appendix H), to account for an air layer between the plastic film and the water. The equation is repeated below for clarity.

$$\left[1-\frac{\rho_{bc}(1-\rho_{bc})^2\,\tau_{\alpha b}^2}{1-\rho_{bc}^2\,\tau_{\alpha b}^2}\right](1-\rho_{bw})Ih_b+\left[1-\frac{\rho_{dc}(1-\rho_{dc})^2\,\tau_{\alpha d}^2}{1-\rho_{dc}^2\,\tau_{\alpha d}^2}\right](1-\rho_{dw})\,Ih_d$$
$$-\left[(Gr_{fa}\,Pr_{fa})^{1/3}\left(0.227+1.406\times10^{-6}\,Re_{fa}\right)\right]\frac{k_{fa}}{L_f}(T_w-T_a)-\sigma\varepsilon_f\left[T_w^4-\left(0.0552\,T_a^{1.5}\right)^4\right] \qquad (3.2)$$
$$=\rho_w\,c_{pw}\,t_w\,\frac{dT_w}{dt}$$

Using equation (3.2), the water temperature is again predicted for the 30th of the November 2000 within the water tank and compared to the experimental values (see Figure 3.5).

Figure 3.5, clearly confirms the previous speculation surrounding the influence of the air layer, with the experimental mean weighted water temperature showing good agreement with the predicted water temperature of equation (3.2) during the latter stages of the day.

The instantaneous thermal storage efficiency, η_s, of the plastic covered water tank is defined as

$$\eta_{storage}=\frac{Q_{storage}}{A_c\,Ih}=\frac{\rho_w\,A_c\,t_w\,c_{pw}\,\frac{dT_w}{dt}}{A_c\,Ih}=\frac{\rho_w\,t_w\,c_{pw}\,\frac{dT_w}{dt}}{Ih} \qquad (3.3)$$

Employing equation (3.3), the instantaneous thermal storage efficiency for the plastic covered water tank is calculated and plotted against the time of day as is shown in Figure 3.6.

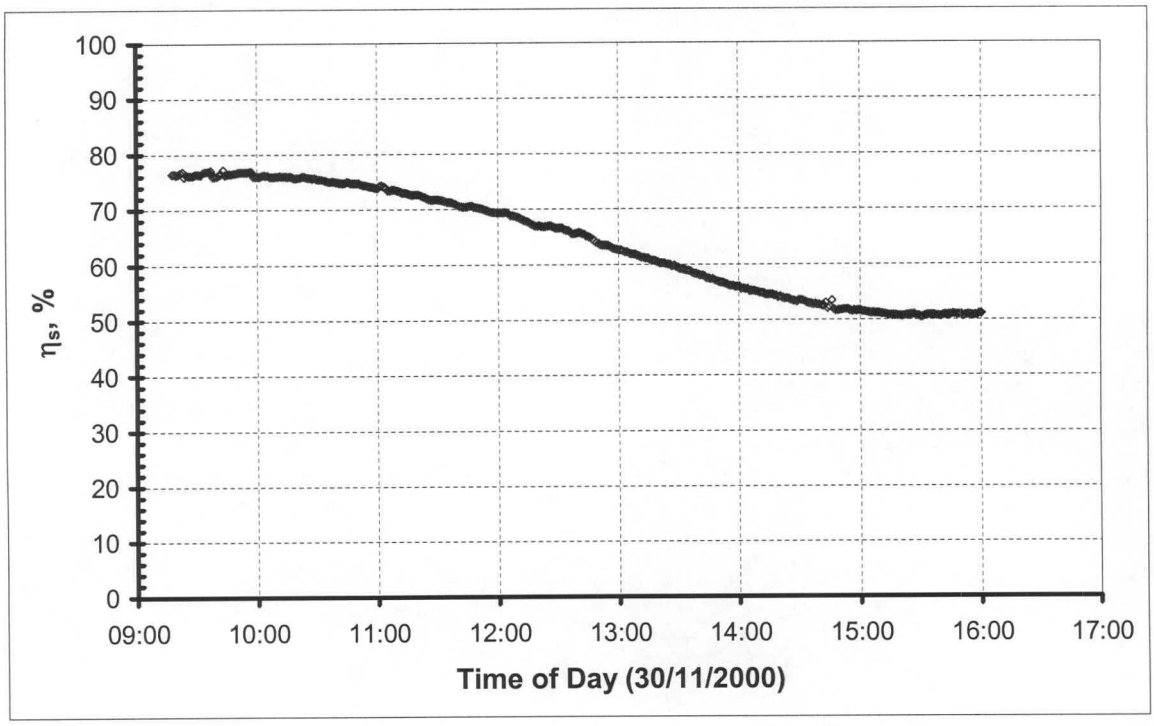

Figure 3.6: Instantaneous storage efficiency for plastic covered water tank on a cloudless day

From the above figure, in conjunction with Figure 3.5, it is evident that an increase in water temperature leads to an increase the amount of energy lost to the environment and therefore leads to a decrease in the storage efficiency of the plastic covered water tank.

3.3.2 Night operation

As in the case of daytime, experiments were conducted during night-time in order to observe the discharge ability of a plastic covered water tank. These experiments were only conducted during cloudless nights, and the results for the night of the 8^{th}-9^{th} of November 2000 are shown in Figure 3.7.

Assuming perfect contact between the plastic film and the water (i.e. no air collected under the plastic film during night-time), and omitting the solar radiation terms in the previously derived conservation of energy equations for the water tank (equation 3.1), Appendix I yields equation (3.4) for the prediction of the water temperature inside the water tank for the night-time.

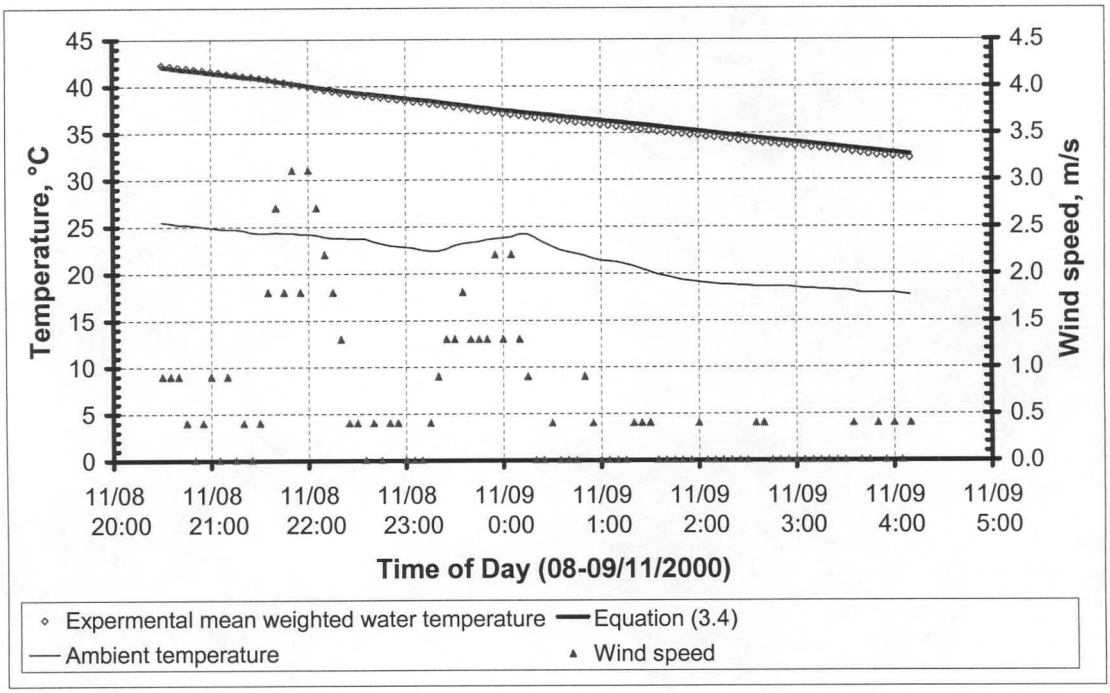

Figure 3.7: Theoretical and experimental mean water temperature for a cloudless night for the plastic covered water tank

$$-\left[\left(Gr_{fa}\,Pr_{fa}\right)^{1/3}\left(0.227+1.406\times10^{-6}\,Re_{fa}\right)\right]\frac{k_{fa}}{L_f}\left(T_w-T_a\right)-\sigma\,\varepsilon_f\left[T_w^4-\left(0.0552\,T_a^{1.5}\right)^4\right] \quad (3.4)$$

$$=\rho_w\,c_{pw}\,t_w\,\frac{dT_w}{dt}$$

Given the ambient conditions for the night of the 8th-9th of November 2000, the water temperature was predicted with the aid of equation (3.4) and compared to the experimental mean depth-weighted water temperature (Figure 3.7).

Figure 3.7 reveals that an excellent agreement exists between the theoretically predicted values and the experimentally measured values, thereby confirming both the validity and the accuracy of the theory used to derive the energy equation for the water tank.

Interestingly, Figure 3.7 also reveals that the output of the thermal energy by the water tank is hardly influenced by either small fluctuations in the wind speed across the plastic film or in ambient temperatures (sky radiation).

3.4 Analysis and results for a solar collector with water storage

In the preceding section the storage and discharge ability of a plastic covered water tank was established. However in the current context of the study, the focus is to evaluate the influence of such an energy storage system on the performance a simple solar collector and an upward facing solar air heater. Consequently a number of experiments were conducted on the simple solar collector (described in Appendix J and shown in Figure 3.3) in which a plastic covered water tank replaced the absorber plate of the solar collector (see Figure 3.3).

3.4.1 Day operation

The 20th of November 2000 was a cloudless day and as a result, experiments were performed on the solar collector with water storage, as described in Appendix J. The experimental results are shown in Figure 3.8.

$$\frac{(1-\rho_{bc})(1-\tau_{\alpha bc})}{1-\rho_{bc}\,\tau_{\alpha bc}} Ih_b + \frac{(1-\rho_{dc})(1-\tau_{\alpha dc})}{1-\rho_{dc}\,\tau_{\alpha dc}} Ih_d$$

$$+\left[1+1.44\left[1-\frac{1708}{Ra_{fc}}\right]+\left[\left(\frac{Ra_{fc}}{5830}\right)^{1/3}-1\right]\right]\frac{k_{cf}}{t_{air}}(T_w-T_c)+\sigma\left(\frac{1}{\varepsilon_c}+\frac{1}{\varepsilon_f}-1\right)^{-1}\left(T_w^4-T_c^4\right) \qquad (3.5)$$

$$=\left[(Gr_{ca}\,Pr_{ca})^{1/3}\left(0.227+1.406\times10^{-6}\,Re_{ca}\right)\right]\frac{k_{ca}}{L_c}(T_c-T_a)+\varepsilon_c\,\sigma\left(T_c^4-\left(0.0552\,T_a^{1.5}\right)^4\right)$$

Using the knowledge gained in Appendix D through the derivation of an energy equation for the cover, Appendix J yields the following equation (see equation (J.2)) for the cover of a solar collector with water storage.

As in the case of the water tank experiments, it was observed that an air layer formed underneath the plastic film, thus reducing the amount of solar radiation that was effectively transmitted to the water.

Therefore, in Appendix J two equations are suggested: the first equation, (equation (J.8)) assuming perfect contact between the plastic film and water, and the second equation (equation (J.10)) assuming that an air layer exist from the beginning of a day. The two equations are repeated below for clarity.

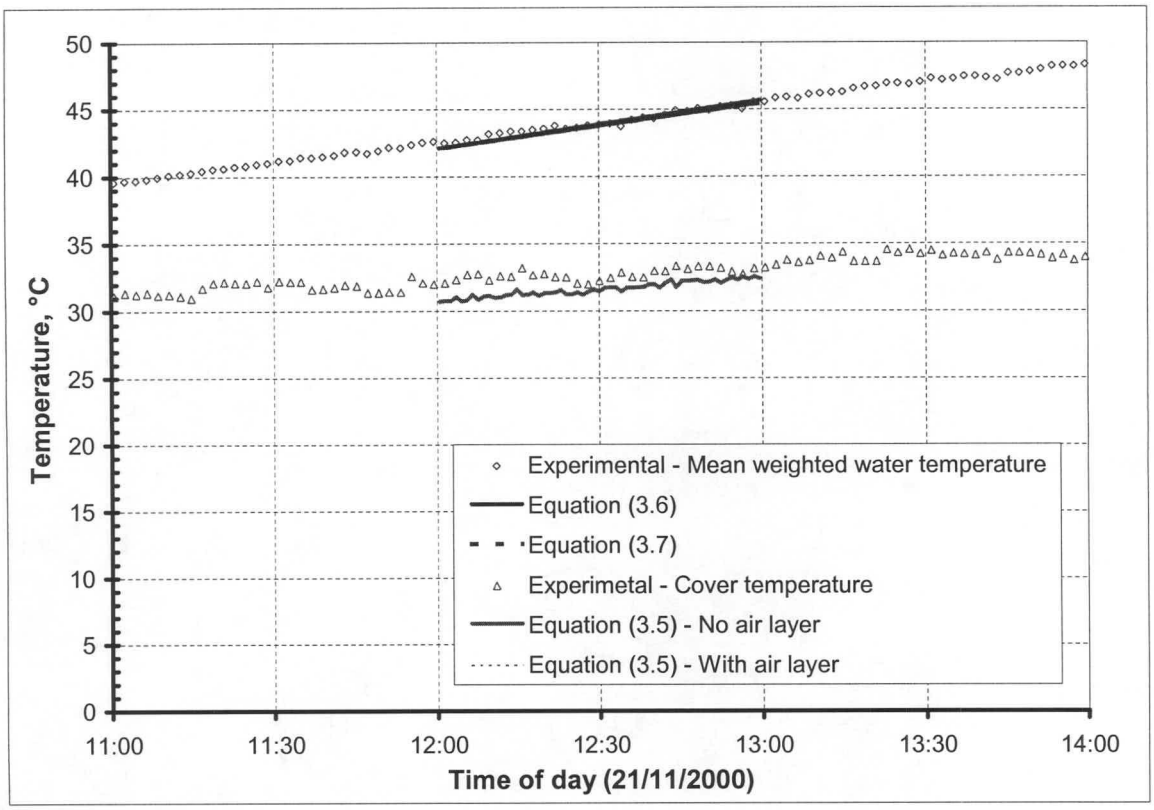

Figure 3.8: Experimentally measured and theoretically predicted cover and mean water temperatures for solar collector with water storage

$$\left[\frac{(1-\rho_{bc})^2\,\tau_{\alpha bc}}{(1-\rho_{bc}^2\,\tau_{\alpha bc}^2)}\right]\left[1-\frac{\rho_{baf}+(1-2\rho_{baf})\rho_{bfw}\,\tau_{\alpha bf}^2}{1-\rho_{baf}\,\rho_{bfw}\,\tau_{\alpha bf}^2}\right]\left[1-\rho_{dc}\,\frac{\rho_{baf}+(1-2\rho_{baf})\rho_{bfw}\,\tau_{\alpha bf}^2}{1-\rho_{baf}\,\rho_{bfw}\,\tau_{\alpha bf}^2}\right]^{-1} Ih_b +$$

$$\left[\frac{(1-\rho_{dc})^2\,\tau_{\alpha dc}}{(1-\rho_{dc}^2\,\tau_{\alpha dc}^2)}\right]\left[1-\frac{\rho_{daf}+(1-2\rho_{daf})\rho_{dfw}\,\tau_{\alpha df}^2}{1-\rho_{daf}\,\rho_{dfw}\,\tau_{\alpha df}^2}\right]\left[1-\rho_{dc}\,\frac{\rho_{daf}+(1-2\rho_{daf})\rho_{dfw}\,\tau_{\alpha df}^2}{1-\rho_{daf}\,\rho_{dfw}\,\tau_{\alpha df}^2}\right]^{-1} Ih_d \qquad (3.6)$$

$$=\left[1+1.44\left[1-\frac{1708}{Ra_{fc}}\right]+\left[\left(\frac{Ra_{fc}}{5830}\right)^{1/3}-1\right]\right]\frac{k_f}{t_{air}}(T_w-T_c)+\sigma\left(\frac{1}{\varepsilon_c}+\frac{1}{\varepsilon_f}-1\right)^{-1}\left(T_w^4-T_c^4\right)$$

$$+\rho_w\,t_w\,c_{pw}\,\frac{dT_w}{dt}$$

$$\left[\frac{(1-\rho_{bc})^2\tau_{\alpha bc}}{(1-\rho_{bc}^2\tau_{\alpha bc}^2)}\right]\left[1-\frac{\rho_{baf}+(1-2\rho_{baf})\rho_{bfw}\tau_{\alpha bf}^2}{1-\rho_{baf}\rho_{bfw}\tau_{\alpha bf}^2}\right]\left[1-\rho_{dc}\frac{\rho_{baf}+(1-2\rho_{baf})\rho_{bfw}\tau_{\alpha bf}^2}{1-\rho_{baf}\rho_{bfw}\tau_{\alpha bf}^2}\right]^{-1}(1-\rho_{bw})Ih_b$$

$$+\left[\frac{(1-\rho_{dc})^2\tau_{\alpha dc}}{(1-\rho_{dc}^2\tau_{\alpha dc}^2)}\right]\left[1-\frac{\rho_{df}+(1-2\rho_{df})\rho_{df}\tau_{\alpha df}^2}{1-\rho_{df}^2\tau_{\alpha df}^2}\right]\left[1-\rho_{dc}\frac{\rho_{df}+(1-2\rho_{df})\rho_{df}\tau_{\alpha df}^2}{1-\rho_{df}^2\tau_{\alpha df}^2}\right]^{-1}(1-\rho_{dw})Ih_d \quad (3.7)$$

$$=\left[1+1.44\left[1-\frac{1708}{Ra_{fc}}\right]+\left[\left(\frac{Ra_{fc}}{5830}\right)^{1/3}-1\right]\right]\frac{k_f}{t_{air}}(T_w-T_c)+\sigma\left(\frac{1}{\varepsilon_c}+\frac{1}{\varepsilon_f}-1\right)^{-1}(T_w^4-T_c^4)$$

$$+\rho_w t_w c_{pw}\frac{dT_w}{dt}$$

Employing these two equations in conjunction with the cover energy equation (equation (3.5)), the respective cover and mean water tank temperatures were predicted for the given ambient conditions of the 21st of November 2000.

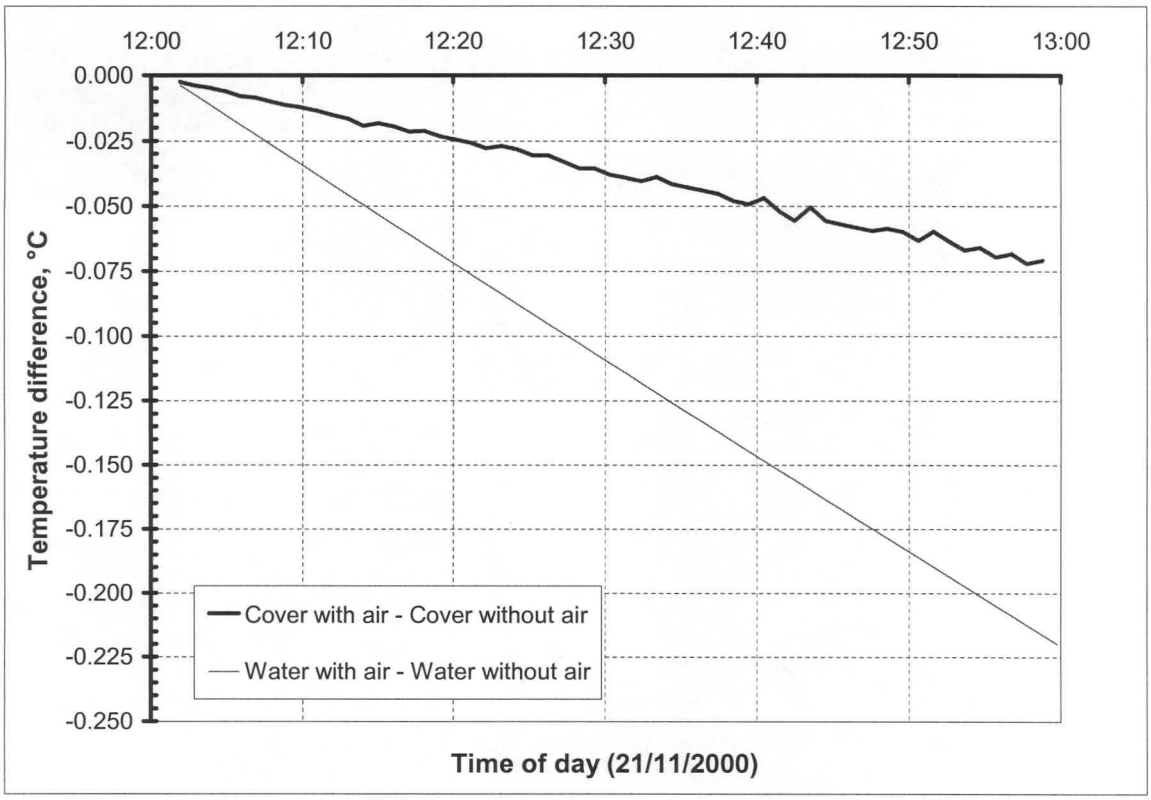

Figure 3.9: Temperature difference between models

In view of Figure J.4, it seems as if both models (equation (3.6) and equation (3.7)) predict similar values, and as a result contradicting the previous findings of the plastic covered water

tank experiments. However, a closer inspection of the predicted cover and mean water temperatures (Figure 3.9) reveals that as in the case of water tank experiments, the air layer (between the cover and water) model tends to predict lower values than the model which assumes good contact between the water and the plastic film. This then again confirms that the formation of an air layer between the film and water leads to a decrease in the effective transmissivity of the film and subsequently the temperature of the water inside the tank.

From Figure 3.8 it also follows that, as in the case of the water tank, good agreement exists between the theoretically predicted and experimentally measured values for both the cover and mean water temperature. The maximum difference between the predicted and the experimental values are 2.0°C and 0.55 °C for the respective cover and water tank temperatures with a respective average errors of 1.075 °C and 0.205 °C for the cover and water tank temperatures.

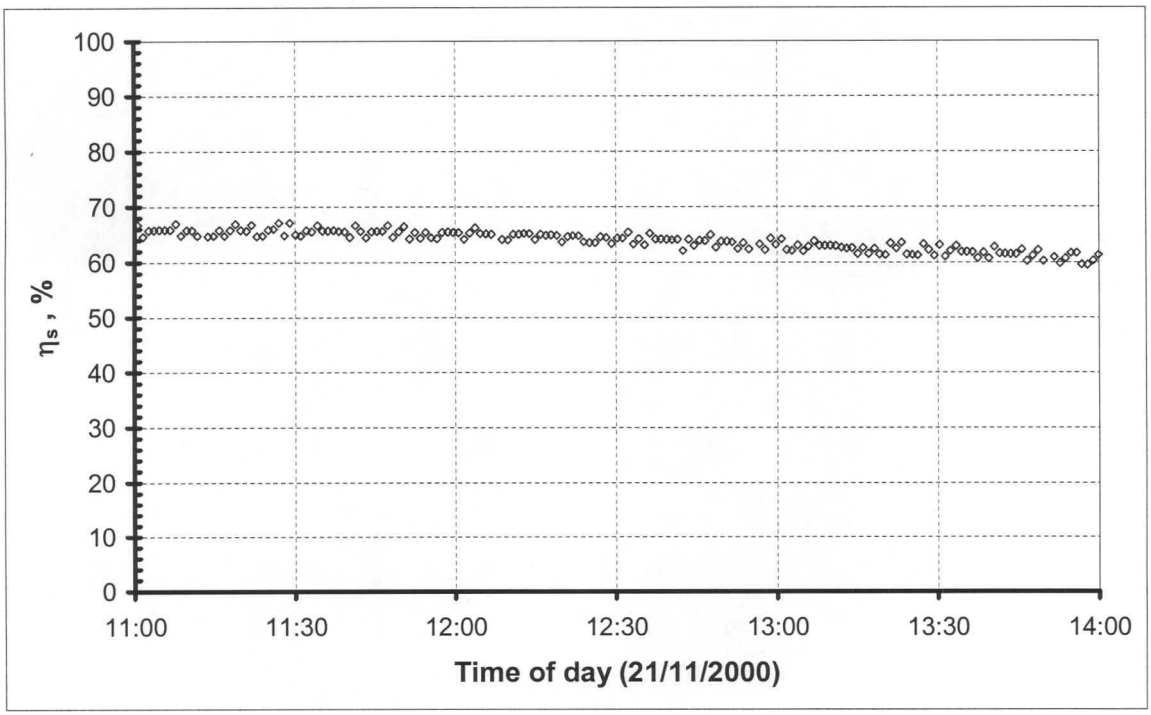

Figure 3.10: Instantaneous storage efficiency for a solar collector with water storage on a cloudless day

Employing equation (3.3) the experimental instantaneous storage efficiency, η_s, of the simple solar collector, incorporating a plastic covered water tank energy storage, is calculated for the period shown in Figure 3.8. From the above figure it is evident that, although the addition of an extra surface (glass cover) would had reduced the amount of solar radiation effectively

transmitted into the water tank, the insulated air layer present in the solar collector reduced the rate against which the storage efficiency decreased with an increase in the water temperature (compare Figure 3.6 to Figure 3.10).

However, the objective of this section is to evaluate the influence of water storage system on the performance of a simple solar collector. Consequently, the previously verified simple solar collector numerical model is used to theoretically predict the cover (equation (D.10)) and absorber plate (equation (D.14)) temperatures of a simple solar collector for the given ambient conditions of the 21st of November 2000. These theoretically predicted values are then compared to the experimental cover and mean water tank temperatures of the simple solar collector in which the absorber plate was replaced by plastic covered water (see Figure 3.8).

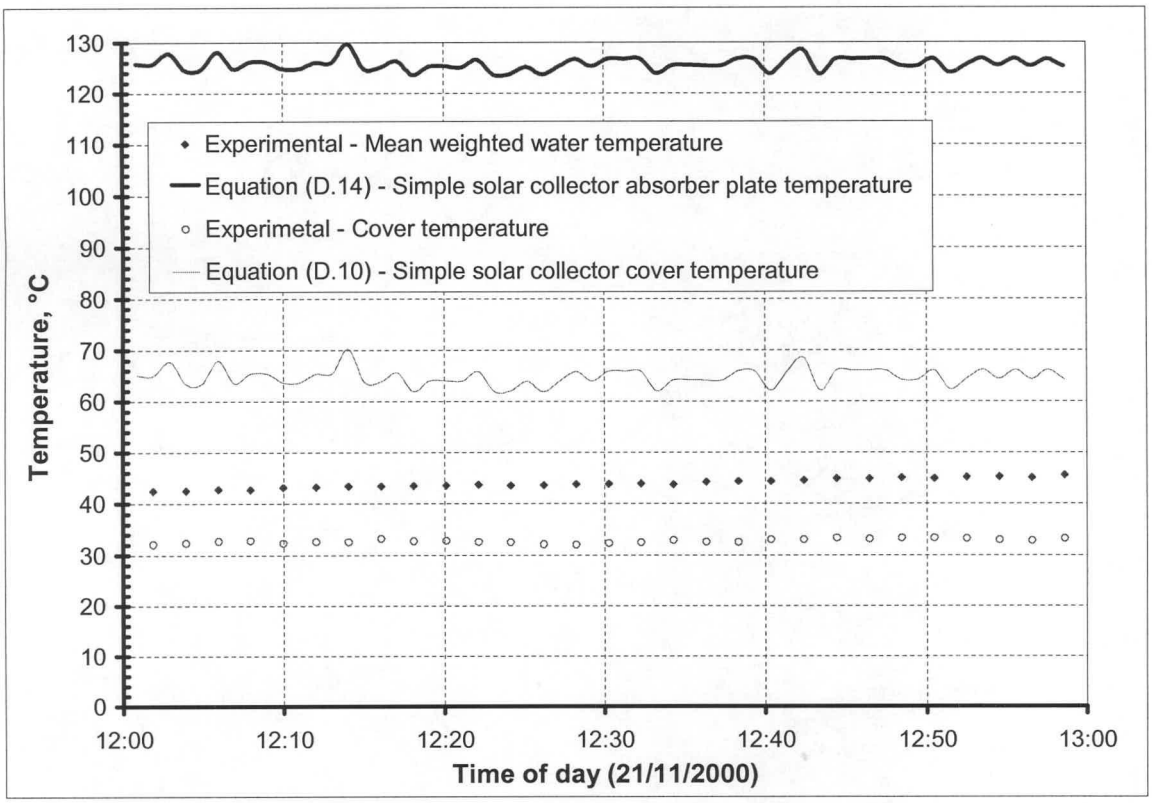

Figure 3.11: Influence of water energy storage on a simple solar collector's cover and "absorber" plate surface temperatures for a solar collector with and without storage

From Figure 3.11 it is apparent that a considerable difference exist between both the cover and "absorber plate" temperature for a solar collector with water energy storage

(experimentally measured values) and for a simple solar collector with a black absorber plate (theoretically predicted values).

From Figure 3.11 the influence of the water storage system on a solar collector tank is quite evident, with the solar collector with the water energy storage's cover and "absorber" plate temperatures being much lower than the respective theoretically predicted surface temperatures for a solar collector with a black absorber plate. Thus, the conclusion can be made that there was much less energy available for the heating of the respective collector surfaces, therefore clearly indicating the storage ability of a plastic covered water tank as well as its influence on the respective surface temperatures of a solar collector.

3.4.2 Night operation

To observe the discharge of thermal energy from the water tank during the night, a number of experiments on the solar collector (described in Appendix J) are conducted on cloudless nights. The experimental results for the night of the 21st – 22nd of November 2000 are shown in Figure 3.12.

Omitting the solar radiation terms in the previously derived equations for the day operation of the solar collector with water storage and assuming perfect contact between the film and the water, the cover energy equation for the solar collector according to Appendix K (equation (K.1)) is

$$\left[1+1.44\left[1-\frac{1708}{Gr_{cf}\,Pr_{cf}}\right]+\left[\left(\frac{Gr_{cf}\,Pr_{cf}}{5830}\right)^{1/3}-1\right]\right]\frac{k_{cf}}{t_{air}}(T_f-T_c)$$
$$+\sigma\left(\frac{1}{\varepsilon_c}+\frac{1}{\varepsilon_f}-1\right)^{-1}\left(T_w^4-T_c^4\right) \qquad (3.8)$$
$$=\left[(Gr_{ca}\,Pr_{ca})^{1/3}\left(0.227+1.406\times10^{-6}\,Re_{ca}\right)\right]\frac{k_{ca}}{L_c}(T_c-T_a)$$
$$+\varepsilon_c\,\sigma\left(T_c^4-\left(0.0552\,T_a^{1.5}\right)^4\right)$$

while the conservation of energy equation for the water (equation (K.2)) can be written as

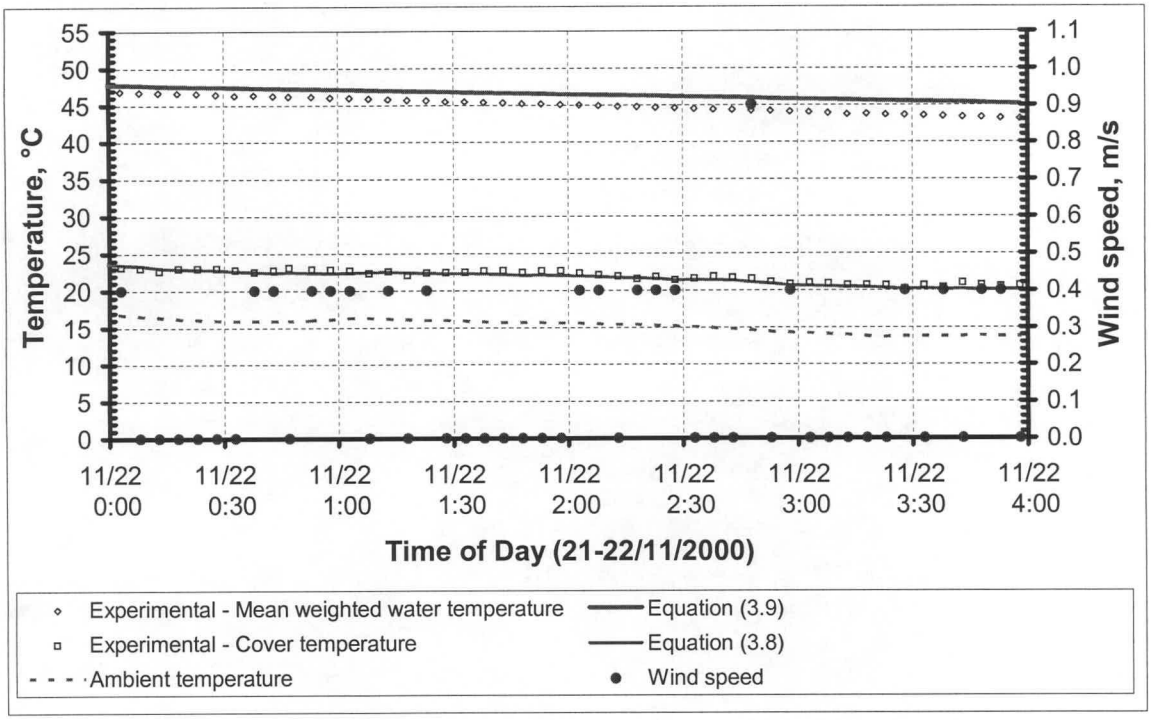

Figure 3.12: Night comparison between predicted and experimentally measured temperatures for a solar collector with water storage

$$-\left[1+1.44\left[1-\frac{1708}{Gr_{cf}\,Pr_{cf}}\right]+\left[\left(\frac{Gr_{cf}\,Pr_{cf}}{5830}\right)^{1/3}-1\right]\right]\frac{k_{cf}}{t_{air}}(T_w-T_c)$$
$$-\sigma\left(\frac{1}{\varepsilon_c}+\frac{1}{\varepsilon_f}-1\right)^{-1}\left(T_w^4-T_c^4\right)=\rho_w\,t_w\,c_{pw}\,\frac{dT_w}{dt} \qquad (3.9)$$

Employing equation (3.8) and equation (3.9), the cover and mean water temperature are predicted for the night of the 21st – 22nd of November 2000 and compared to the experimental values in Figure 3.12 respectively.

From Figure 3.12, it is evident that as in the previous instances, the theoretical predictions for both the cover and water temperatures are in good agreement with the experimentally measured values. It is also evident that the discharge of thermal energy from the water tank is only slightly influenced by a fluctuation in either ambient temperature or in wind speed.

In addition, the ability of the water tank to release its stored energy is clearly evident from Figure 3.12, with the glass cover temperature being kept at a temperature approximately 7°C above the ambient temperature throughout the night.

3.5 Conclusion

In this chapter, the ability of a water solar storage tank to either store or discharge thermal energy was both theoretically and experimentally investigated.

Experimental results revealed that an air layer forms underneath the plastic film. The air layer not only reduces the amount of solar radiation that can penetrate the water, but also in turn, impedes the storage capability of a plastic covered water tank.

On the theoretical side, it was established that available theory is adequate for the predictions of the performance of a plastic covered water tank, whether within a solar collector or on its own.

Chapter 4: Performance of an upward facing solar air heater with water energy storage

The primary focus of the present study is to determine whether or not it is feasible to incorporate a plastic covered water tank storage system into an upward facing solar air heater in order to prolong the output of heated air by the solar air heater. In other words, to what extent can energy stored during the day be recovered during the night.

To answer the above question, a number of experiments are conducted on an upward facing solar air heater with plastic covered water tanks.

In addition, the previously derived energy equations for the upward facing solar air heater and plastic covered water tank (Chapter 2 and Chapter 3), will be used to establish a theoretical model for the prediction of the performance of a water storage solar air heater during both day and night operation. By comparing the predicted temperatures to experimentally measured temperatures, an indication of the validity of the theoretical model will be obtained.

4.1 Experimental apparatus

In the current study, experiments are to be conducted on the upward facing solar air heater described in detail in Chapter 2. The only difference between the experimental set-up in Chapter 2 and the present investigation, is that the eight 75mm thick insulation blocks are replaced by eight plastic covered water tanks with dimensions of 1m x 1m x 0.19m, as shown in Figure 4.1.

The sides of the duct as well as the bottom of the water tanks were insulated by 50 mm thick polystyrene insulation, while the upper surface of each of the water tanks was covered by a Luminal Anti-Fog plastic film with a thickness of 0.2 mm.

Furthermore, four type-T thermocouples were used to measure the respective glass cover temperatures of sections 1,3,6 and 8, while two oscillating temperature probes, as described in Chapter 3, were installed in water tanks 1 and 8 in order to determine the water temperature profile within each of the respective water tanks.

Ambient conditions (ambient temperature, wind speed, atmospheric pressure) were measured with the weather station (Davis Weather Monitor II) and the total incident solar radiation was obtained from a solar sensor (Kipp and Zonen) placed next to the experimental apparatus.

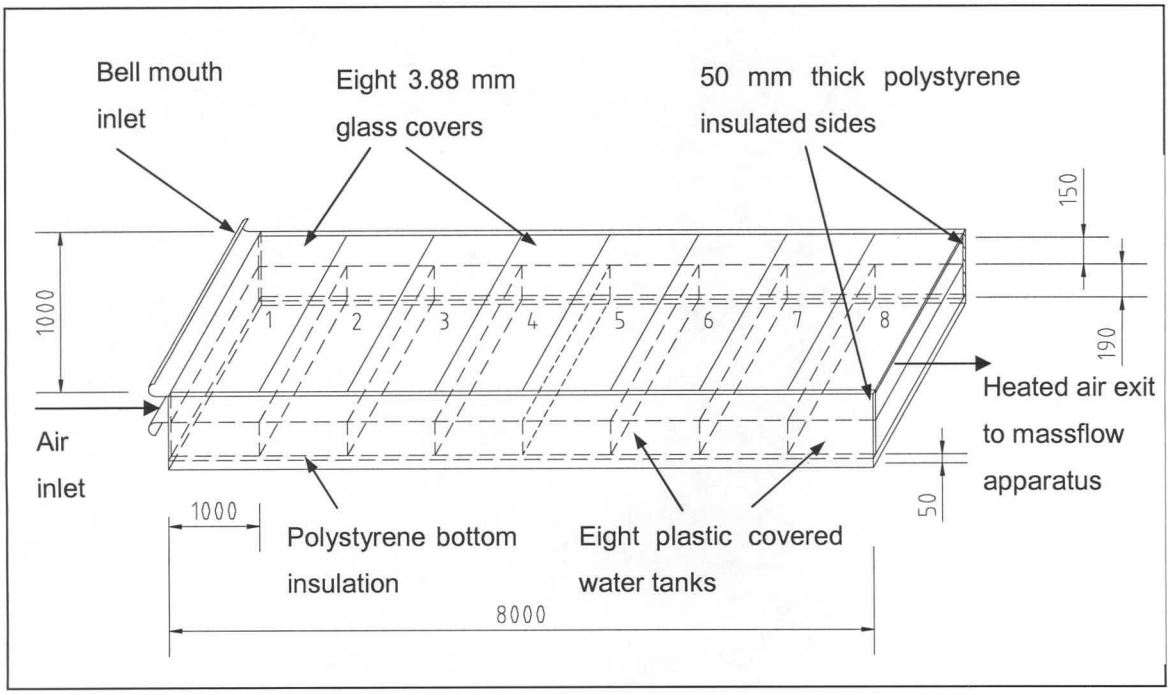

Figure 4.1: Rectangular test duct with water tanks

4.2 Theoretical model for an upward facing solar air heater with water storage

During the preceding analyses and experimental tests on an upward facing solar air heater (Appendix D) and plastic covered water tank (Appendixes H, I, J and K), confidence was established in the available theory.

Combining the knowledge developed through Appendixes D, H and J in Appendix L, a set of equations is obtained for the daytime performance prediction of an upward facing solar air heater with water energy storage.

Assuming perfect contact between the plastic film and the water below it (i.e. no air layer exist between water and plastic film) and assuming conduction losses through the sides of the solar air heater and bottom of the water tank to be negligible, it follows from Appendix L that the conservation of energy equation for the solar air heater cover is

$$\left[\frac{(1-\rho_{bc})(1-\tau_{bc})}{1+\rho_{bc}\,\tau_{bc}}\right] Ih_b + \left[\frac{(1-\rho_{dc})(1-\tau_{dc})}{1-\rho_{dc}\,\tau_{dc}}\right] Ih_d = \bar{h}_c\left(T_c-\bar{T}\right)+\sigma\left[\frac{1}{\varepsilon_c}+\frac{1}{\varepsilon_f}-1\right]^{-1}\left(T_w^4-T_c^4\right)$$
$$+\left[\left(Gr_{ca}\,Pr_{ca}\right)^{1/3}\left(0.227+1.406\times10^{-6}\,Re_{ca}\right)\right]\frac{k_{ca}}{L_c}\left(T_c-T_a\right)+\varepsilon_c\,\sigma\left[T_c^4-\left(0.0552\,T_a^{1.5}\right)^4\right] \tag{4.1}$$

while the corresponding energy equation for the water tanks is

$$\left[\frac{(1-\rho_{bc})^2\,\tau_{\alpha bc}}{\left(1-\rho_{bc}^2\,\tau_{\alpha bc}^2\right)}\right]\left[1-\frac{\rho_{baf}+(1-2\rho_{baf})\rho_{bfw}\,\tau_{\alpha bf}^2}{1-\rho_{baf}\,\rho_{bfw}\,\tau_{\alpha bf}^2}\right]\left[1-\rho_{dc}\,\frac{\rho_{baf}+(1-2\rho_{baf})\rho_{bfw}\,\tau_{\alpha bf}^2}{1-\rho_{baf}\,\rho_{bfw}\,\tau_{\alpha bf}^2}\right]^{-1} Ih_b +$$
$$\left[\frac{(1-\rho_{dc})^2\,\tau_{\alpha dc}}{\left(1-\rho_{dc}^2\,\tau_{\alpha dc}^2\right)}\right]\left[1-\frac{\rho_{daf}+(1-2\rho_{daf})\rho_{dfw}\,\tau_{\alpha df}^2}{1-\rho_{daf}\,\rho_{dfw}\,\tau_{\alpha df}^2}\right]\left[1-\rho_{dc}\,\frac{\rho_{daf}+(1-2\rho_{daf})\rho_{dfw}\,\tau_{\alpha df}^2}{1-\rho_{daf}\,\rho_{dfw}\,\tau_{\alpha df}^2}\right]^{-1} Ih_d \tag{4.2}$$
$$=\bar{h}_f\left(T_w-\bar{T}\right)+\sigma\left[\frac{1}{\varepsilon_c}+\frac{1}{\varepsilon_f}-1\right]^{-1}\left(T_w^4-T_c^4\right)+\rho_w\,t_w\,c_{pw}\,\frac{dT_w}{dt}$$

and for the air the energy equation is found to be

$$\dot{m}c_p\,T_{in}+A\,\bar{h}_f\left(T_w-\bar{T}\right)+A\,\bar{h}_c\left(T_c-\bar{T}\right)=\dot{m}c_p\left(2\bar{T}-T_{in}\right) \tag{4.3}$$

By solving equations (4.1), (4.2) and (4.3) simultaneously, the mean cover, water and air temperature can be respectively predicted with the given ambient conditions for a 1m section of the solar air heater.

In Appendixes I and K, the discharge of thermal energy from a plastic covered water tank during the night, either on its own or within a solar collector system, was both experimentally and theoretically investigated. This investigation, in particular, revealed good agreement between experimental results and theoretically predicted values.

By combining the equations of Appendixes I an K, with the solar air heater analysis of Appendix D, a set of equations is derived in Appendix M for the night-time performance prediction of an upward facing solar air heater with water storage.

For the night operation of a solar air heater with water energy storage, Appendix M yields equation (4.4) for the cover

$$\sigma\left[\frac{1}{\varepsilon_c}+\frac{1}{\varepsilon_f}-1\right]^{-1}\left(T_w^4-T_c^4\right)=\bar{h}_c\left(T_c-\bar{T}\right)$$
$$+\left[\left(Gr_{ca}\,Pr_{ca}\right)^{1/3}\left(0.227+1.406\times10^{-6}\,Re_{ca}\right)\right]\frac{k_{ca}}{L_c}\left(T_c-T_a\right)+\varepsilon_c\,\sigma\left[T_c^4-\left(0.0552\,T_a^{1.5}\right)^4\right] \quad (4.4)$$

and equation (4.5) for a 1m long plastic covered water tank.

$$-\bar{h}_f\left(T_w-\bar{T}\right)-\sigma\left[\frac{1}{\varepsilon_c}+\frac{1}{\varepsilon_f}-1\right]^{-1}\left(T_w^4-T_c^4\right)=\rho_w\,t_w\,c_{pw}\,\frac{dT_w}{dt} \quad (4.5)$$

Furthermore, from Appendix M it follows that the night-time conservation of energy equation for the air is identical to one derived for the daytime operation, i.e. is equation (4.3).

Hence, the respective mean cover, water and air temperatures for a 1m section of an upward facing solar air heater with water storage during night-time, can be predicted for given ambient conditions, by solving equation (4.3), (4.4) and (4.5) simultaneously.

4.3 Experimental and theoretical results

From the 19th to the 29th of March 2001, experiments were conducted during both the day and the night on the upward facing solar air heater with water storage (described in section 4.1). Mass flow rates through the solar air heater were varied between 0.09 – 0.77 kg/s by open or closing the flow nozzles and/or adjusting the bypass valve opening (see Figure 2.4).

4.3.1 Day-time operation

In Figure 4.2 - Figure 4.14 the daytime experimental results for three air mass flow rates are compared to the theoretically predicted mean cover, water tank and air temperatures (equations (4.1), (4.2) and (4.3)).

From the results the following comment can be made concerning the validity of the theoretical model. From Figure 4.14 it is evident that as long as the mass flow rate of the air does not exceed 0.335 kg/s, good agreement is obtained between the theoretical model's collector efficiency and the experimental collector efficiency. However, if this mass flow rate is exceeded, as is evident from Figure 4.14, the theoretical model tends to under predict the collector efficiency of the solar air heater under consideration.

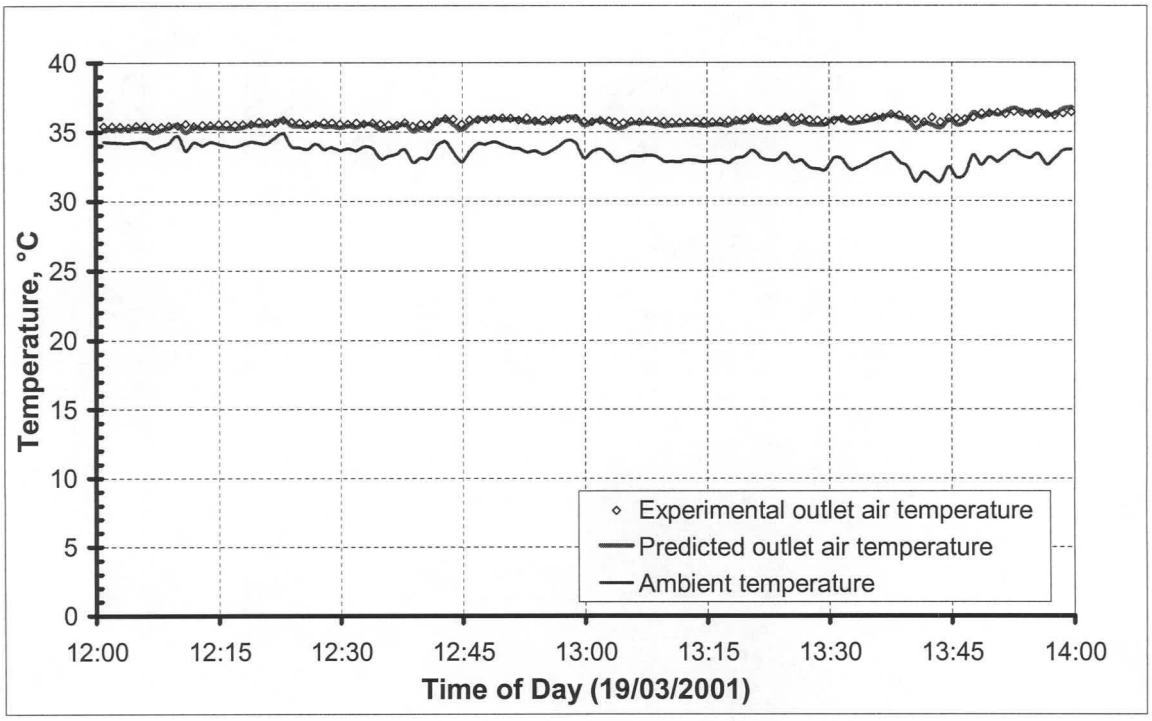

Figure 4.2: Ambient and outlet air temperatures for 0.094 kg/s

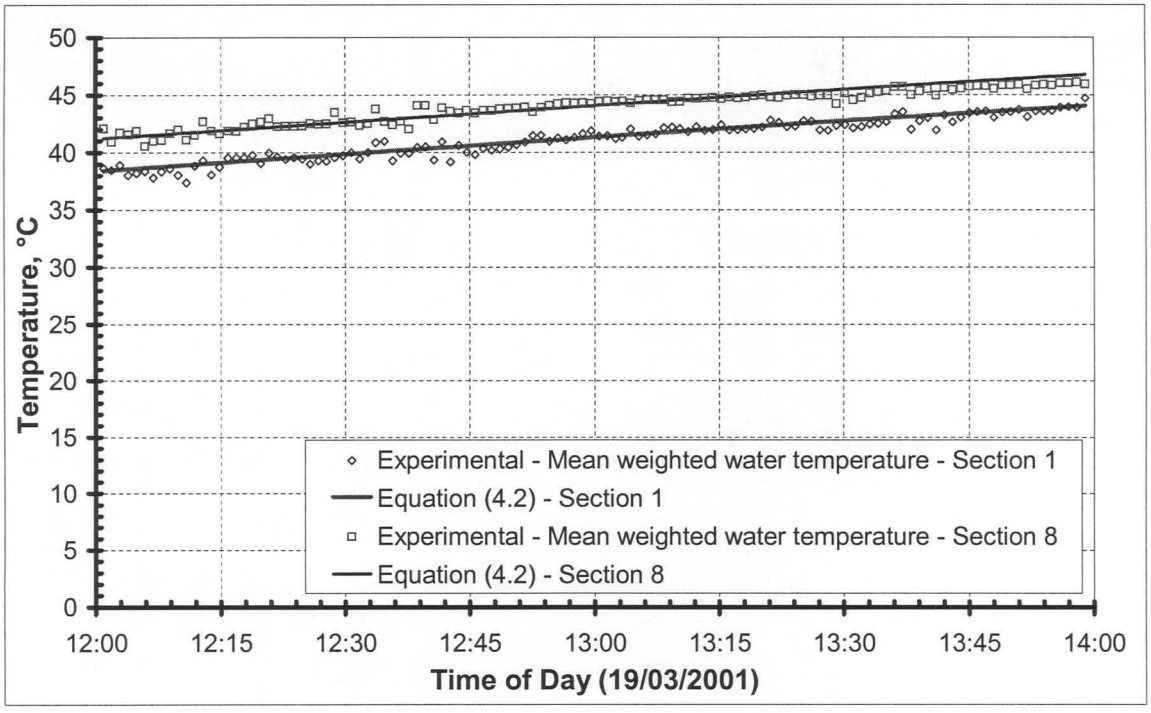

Figure 4.3: Mean water temperatures for sections 1 and 8 (0.094 kg/s)

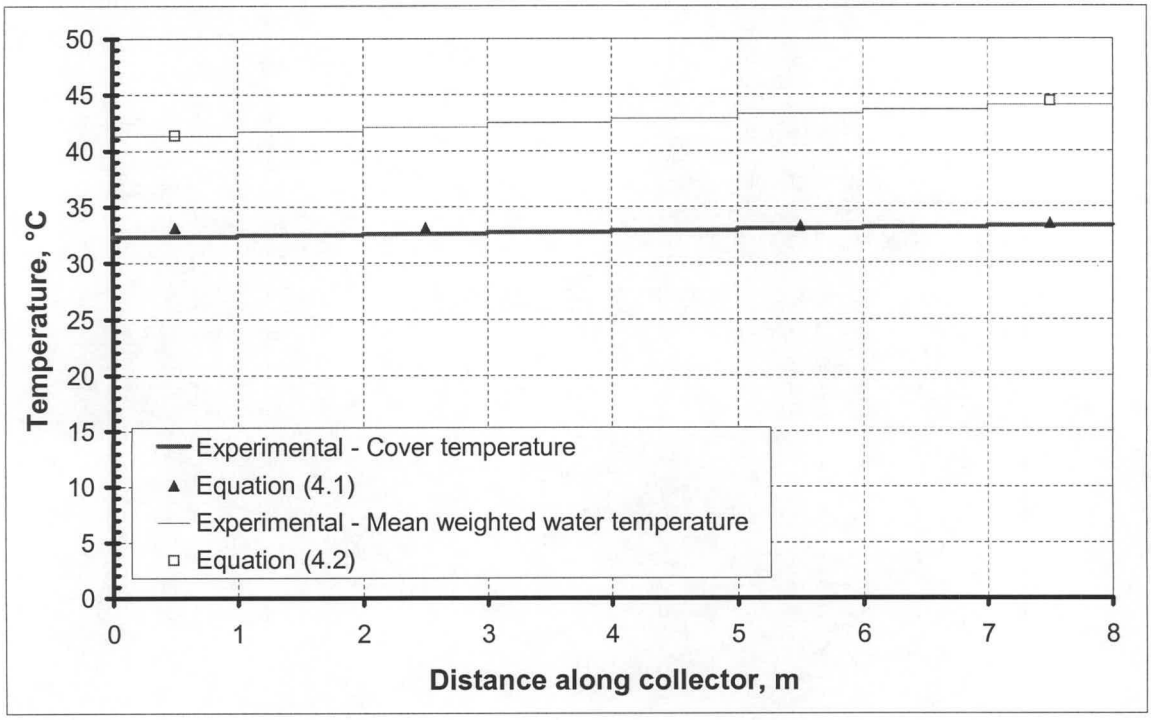

Figure 4.4: Cover and mean water temperatures at 13h00 for 0.094 kg/s

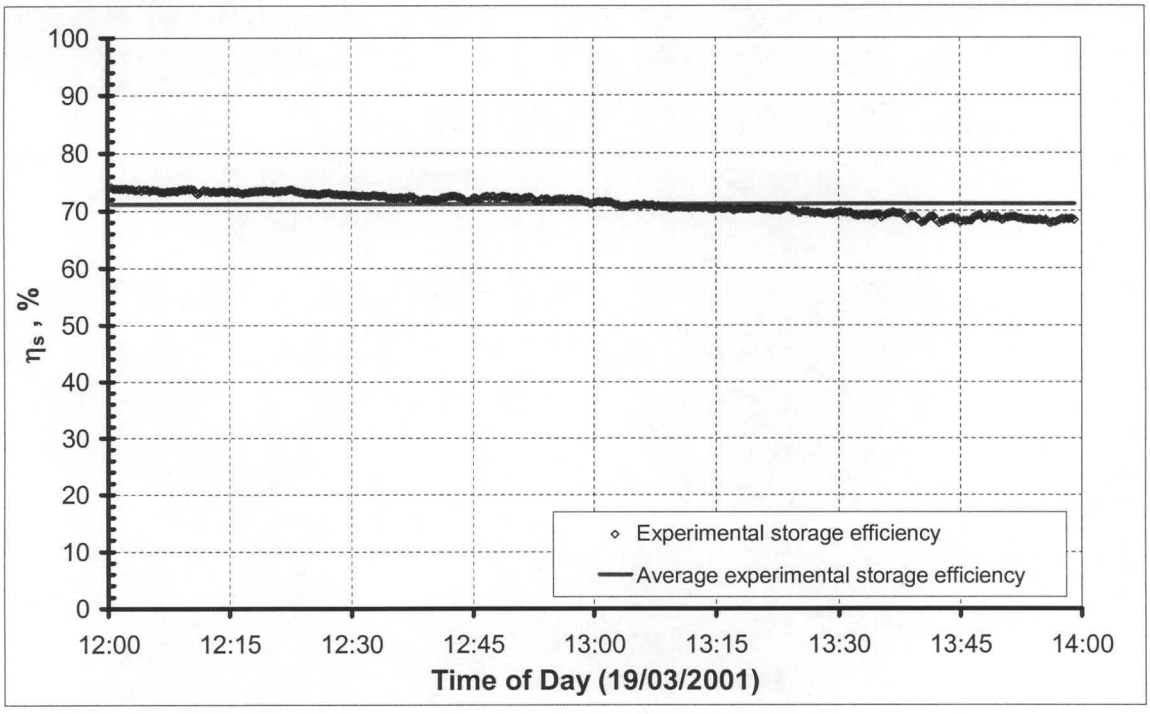

Figure 4.5: Instantaneous storage efficiency of plastic covered water tanks for 0.094 kg/s

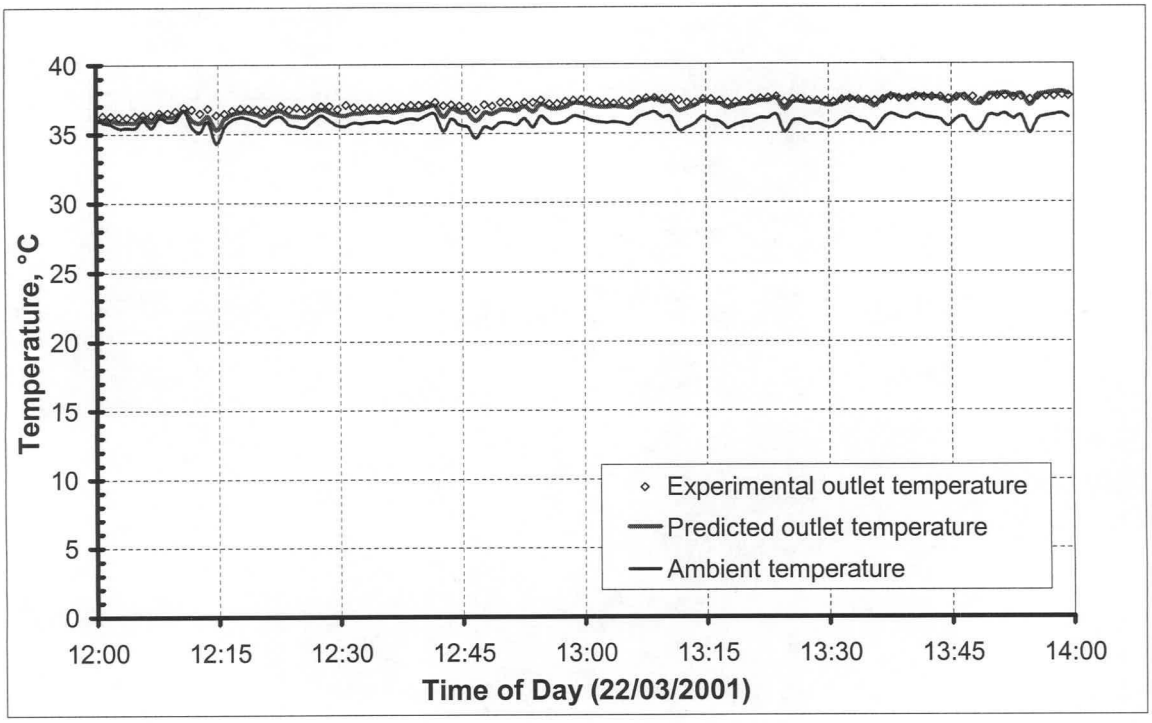

Figure 4.6: Ambient and outlet air temperatures for 0.2538 kg/s

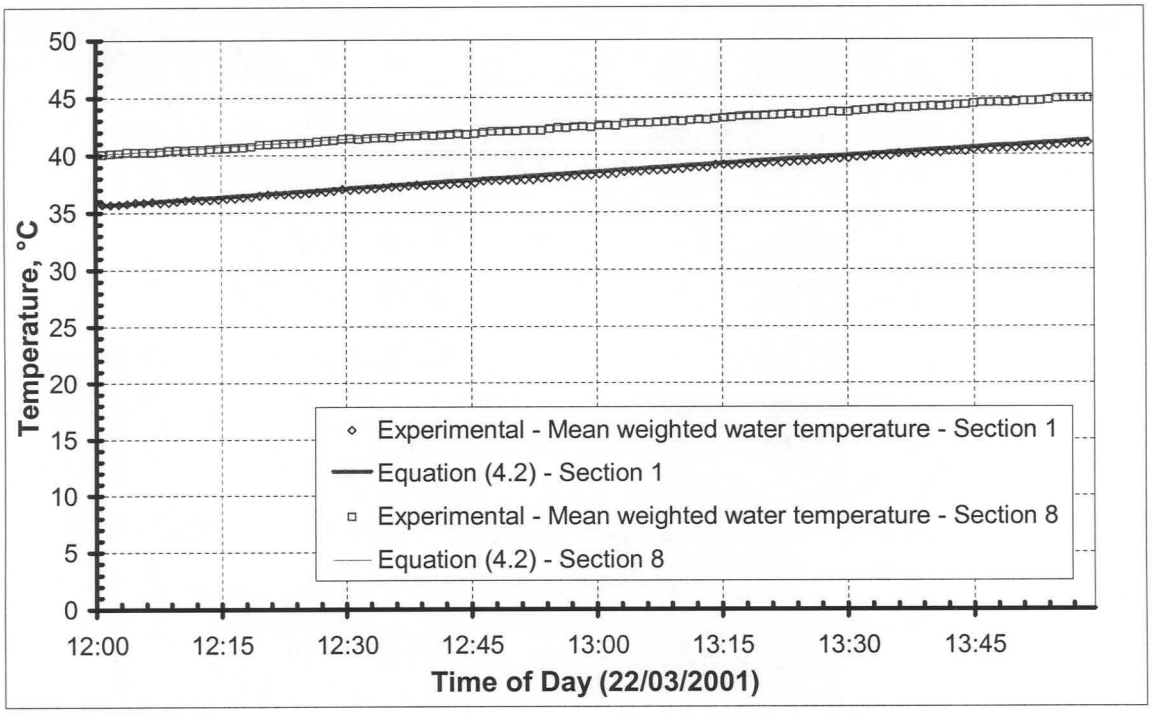

Figure 4.7: Mean water temperatures for sections 1 and 8 (0.2538 kg/s)

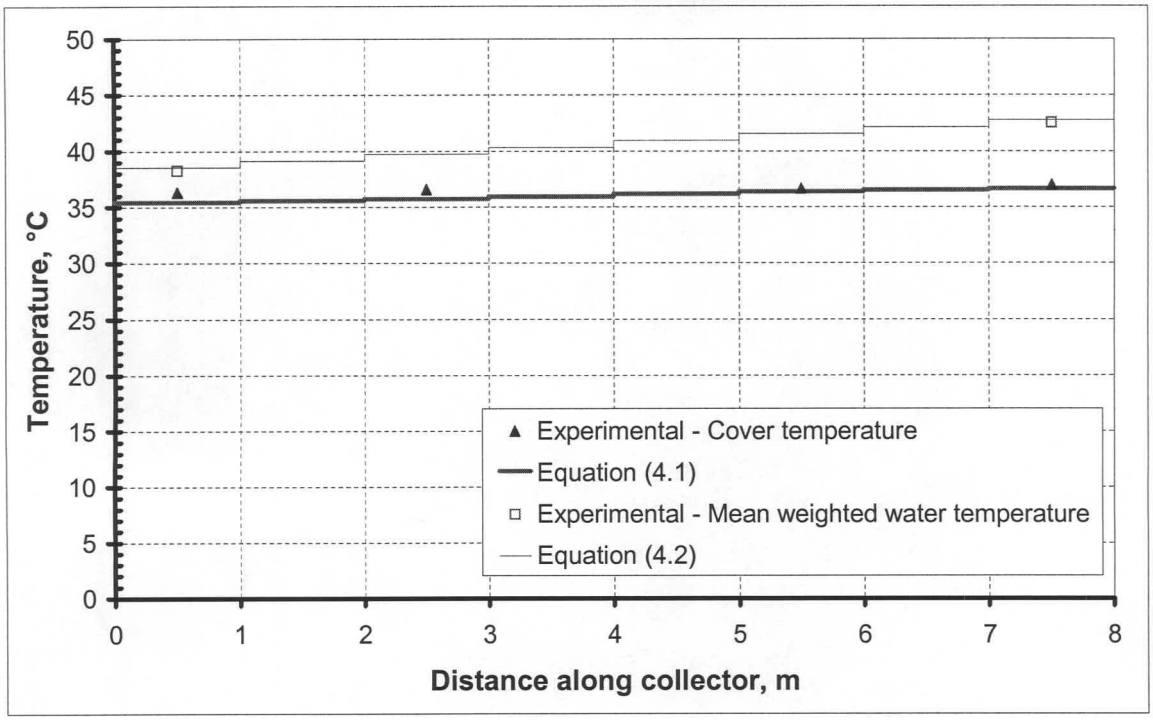

Figure 4.8: Cover and mean water temperatures at 13h00 for 0.2538 kg/s

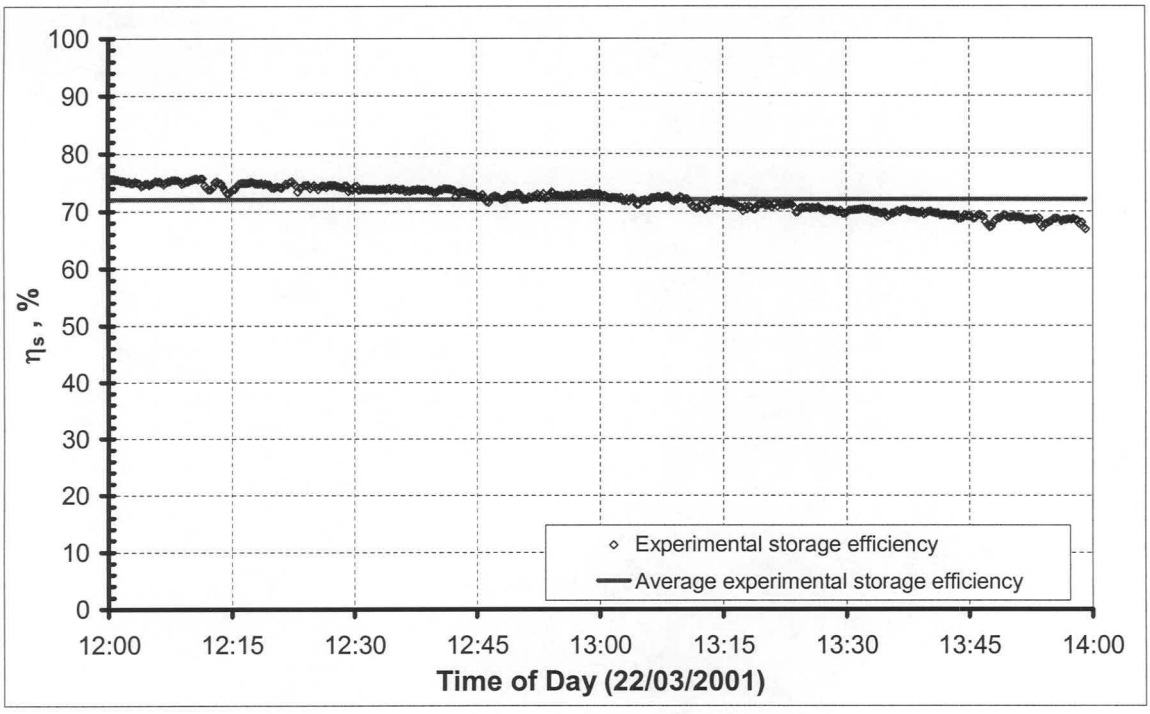

Figure 4.9: Instantaneous storage efficiency of plastic covered water tanks for 0.2538 kg/s

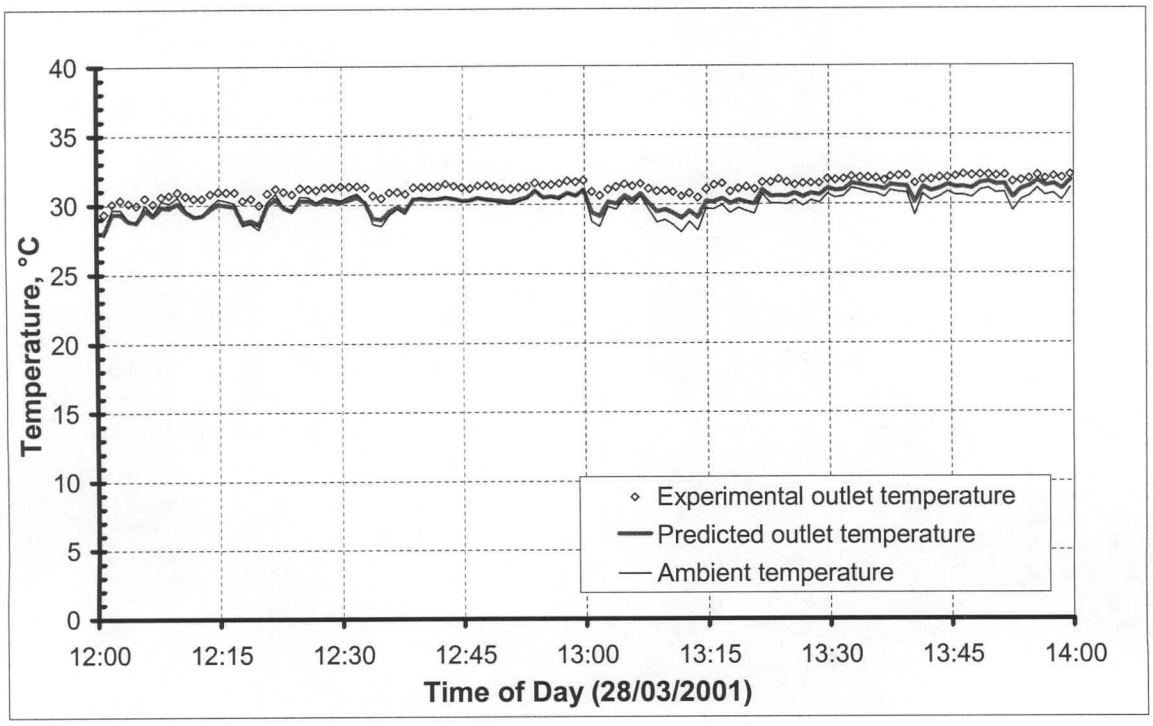

Figure 4.10: Ambient and outlet air temperatures for 0.5172 kg/s

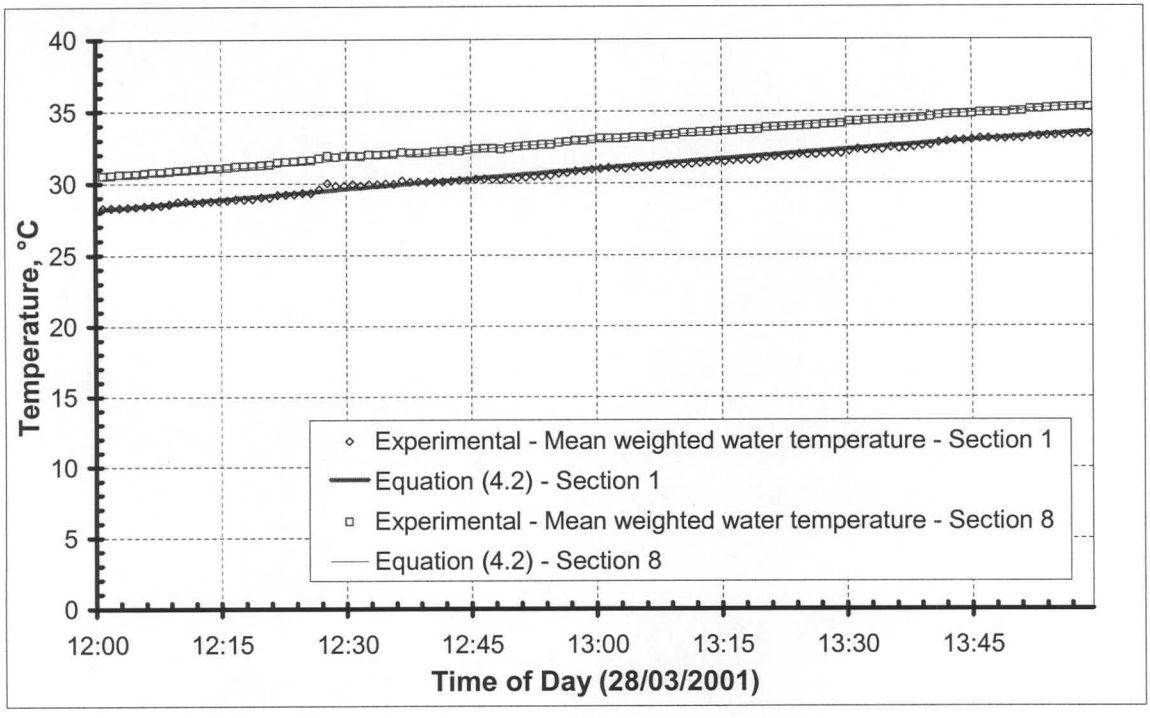

Figure 4.11: Mean water temperatures for sections 1 and 8 (0.5172 kg/s)

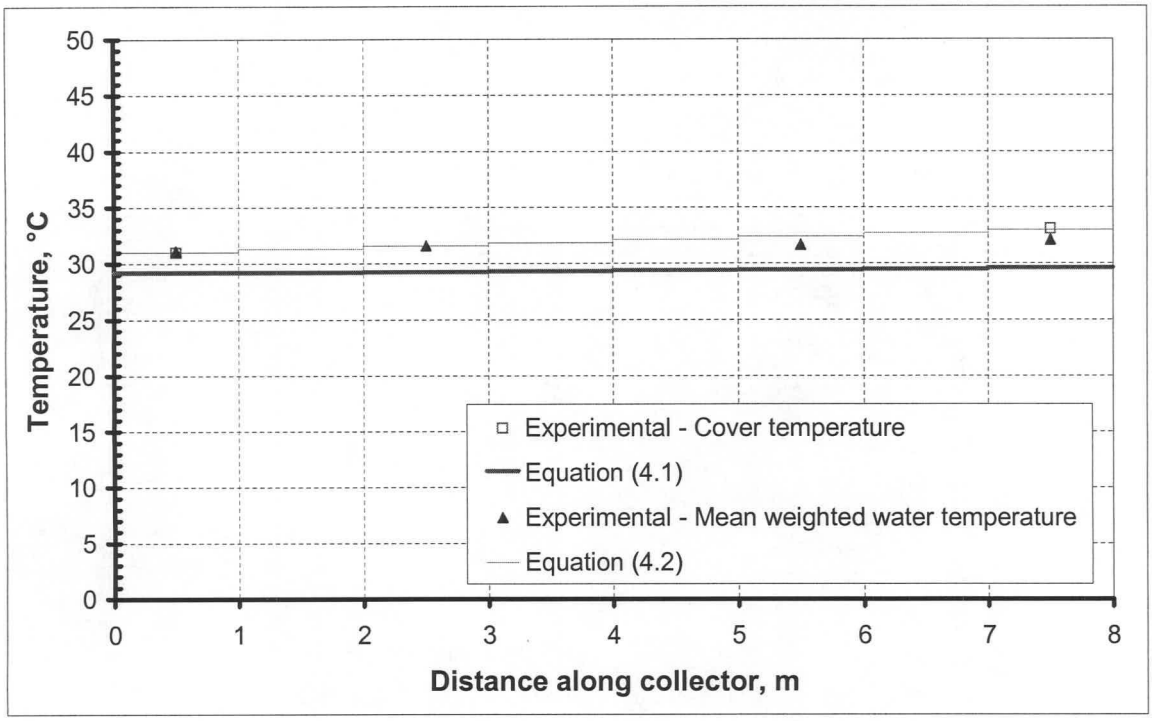

Figure 4.12: Cover and mean water temperatures at 13h00 for 0.5172 kg/s

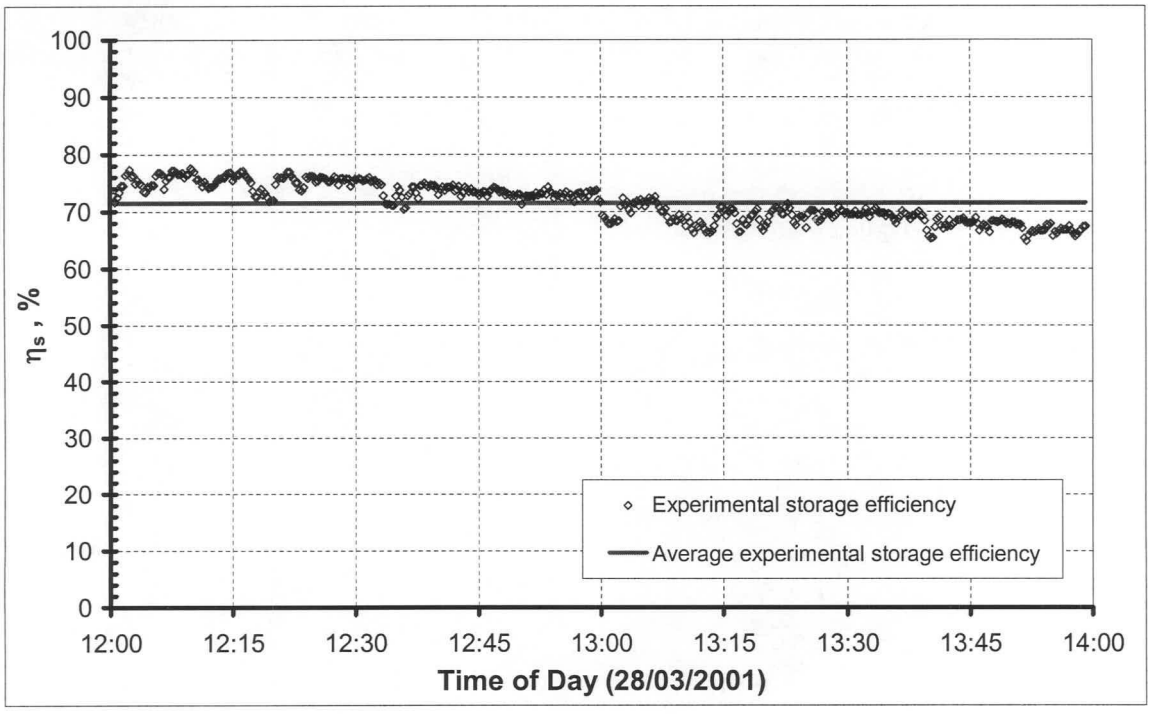

Figure 4.13: Instantaneous storage efficiency of plastic covered water tanks for 0.5172 kg/s

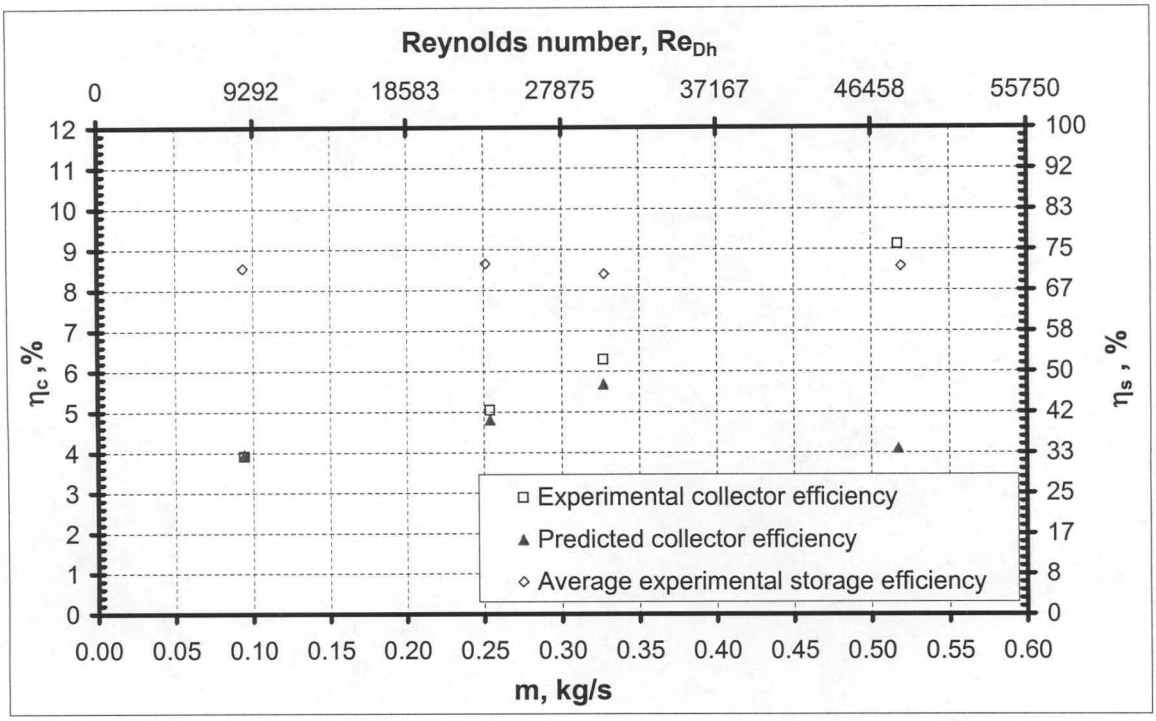

Figure 4.14: Instantaneous storage and collector efficiency for an upward facing solar air heater with 190-mm water energy storage tanks

A possible reason for the "under prediction" behaviour of the theoretically model, for air mass flow rates exceeding 0.335 kg/s, could possible be ascribed to equation (A.8) that is used to evaluate the total heat loss from the cover to the environment due to sky radiation and wind-induced convection.

From Appendix A it follows that equation (A.8) is valid in the range $6.75 \times 10^8 \leq (GrPr) \leq 26.6 \times 10^8$ and for $0 \leq Re \leq 2.5 \times 10^5$. However, on closer inspection of the experimental results for the air mass flow rate of 0.5172 kg/s, it is found that the small temperature difference between the solar air heater cover and ambient temperature led to Grashof-Prandtl numbers in the order of 4.5×10^7. Consequently equation (A.8) is not valid anymore.

Furthermore, during the experimental test the cover-air Reynolds number was in the order of 50×10^3. For these prevailing 0.5172 kg/s experiment conditions ($(GrPr) = 4.5 \times 10^7$, $Re = 50 \times 10^3$), Figure A.4 indicates that the heat transfer from the cover to the environment would be primarily due to forced convection and that the contribution of natural convection to the convective heat loss is negligible. This stands in contrast to equation (A.8) that was based on a state of mixed convection as is evident in Figure A.4.

As a result the possibility exists that equation (A.8) could be predicting a much higher theoretical heat loss than the actual heat loss from the cover of the solar air heater to the natural environment. This would lead to lower cover temperatures and consequently lower air outlet temperatures and collector efficiency, as is apparent from Figure 4.10 and Figure 4.14.

Furthermore, from the storage efficiency graphs for the various mass flow rates it is evident that, as in the case of the simple water tank and solar collector with water energy storage experiments, that an increase in the water temperature led to a decrease in the storage ability of the plastic covered water tanks. However, plotting the average experimental storage efficiencies against their respective mass flow rates (as is shown in Figure 4.14) it seems as though a change in the air mass flow rate did not have any measurable influence on the storage ability of the water tanks.

Comparing the collector efficiency, η_c, of the solar air heater with water storage (Figure 4.14) to the collector efficiency of a solar air heater without storage (Figure 2.13), it is apparent that both systems collector efficiency tends to increase with an increase in the mass flow rate of the air. It is however also evident that, due to the storage of solar energy in the water tanks, the collector efficiency of the solar air heater with water storage is much lower than the solar air heater incorporating no energy storage system.

4.3.2 Night-time operation

Employing equations (4.3), (4.4) and (4.5) the night-time theoretical performance of the solar air heater under consideration is only predicted and compared to experimental values, if and only if the cover temperature exceeds the ambient temperature and $6.75 \times 10^8 \leq (GrPr) \leq 26.6 \times 10^8$ and $0 \leq Re \leq 2.5 \times 10^5$ (see validity criteria of equation (A.8) in Appendix A). Such conditions prevailed during the nights of the 19th-20th of March 2001 and the 22th-23th of March 2001 (Figure 4.15 to Figure 4.21)

In Figure 4.23 to Figure 4.24 the experimentally measured values for the water tank's temperatures, solar air heater cover temperature and outlet air temperature are shown for an air mass flow rate of 0.7734 kg/s. Predicted values are absent due to the ambient temperature exceeding the solar air heater cover's temperature.

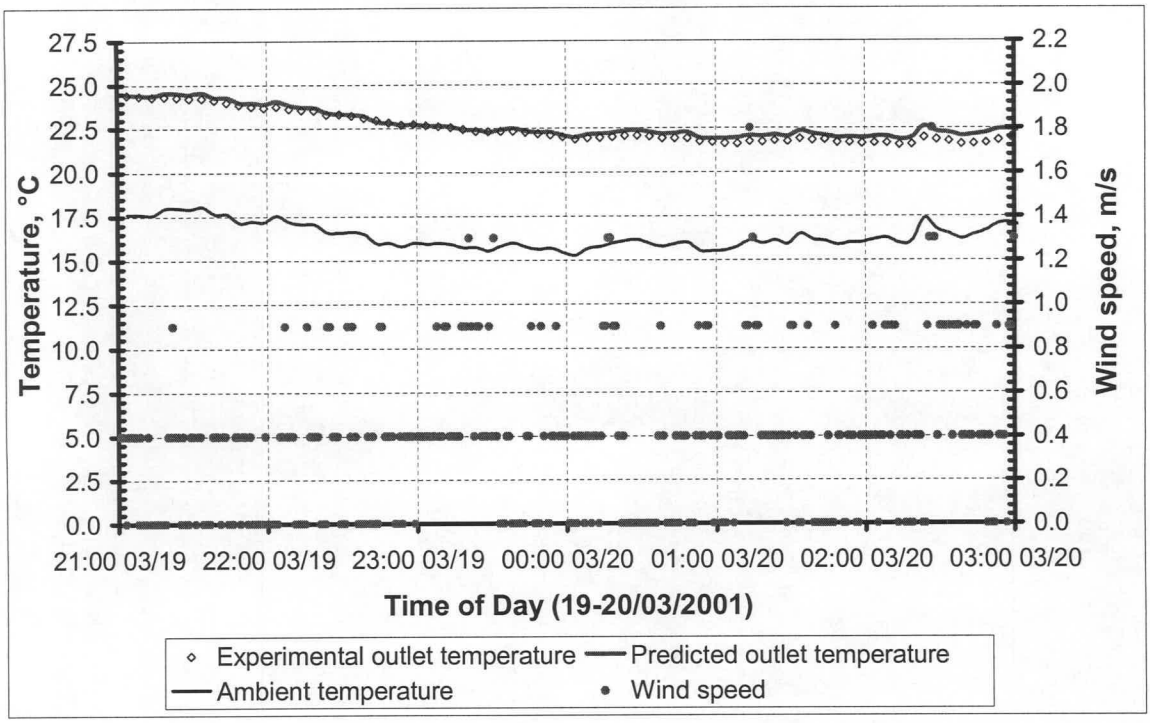

Figure 4.15: Ambient and outlet temperatures for 0.0976 kg/s

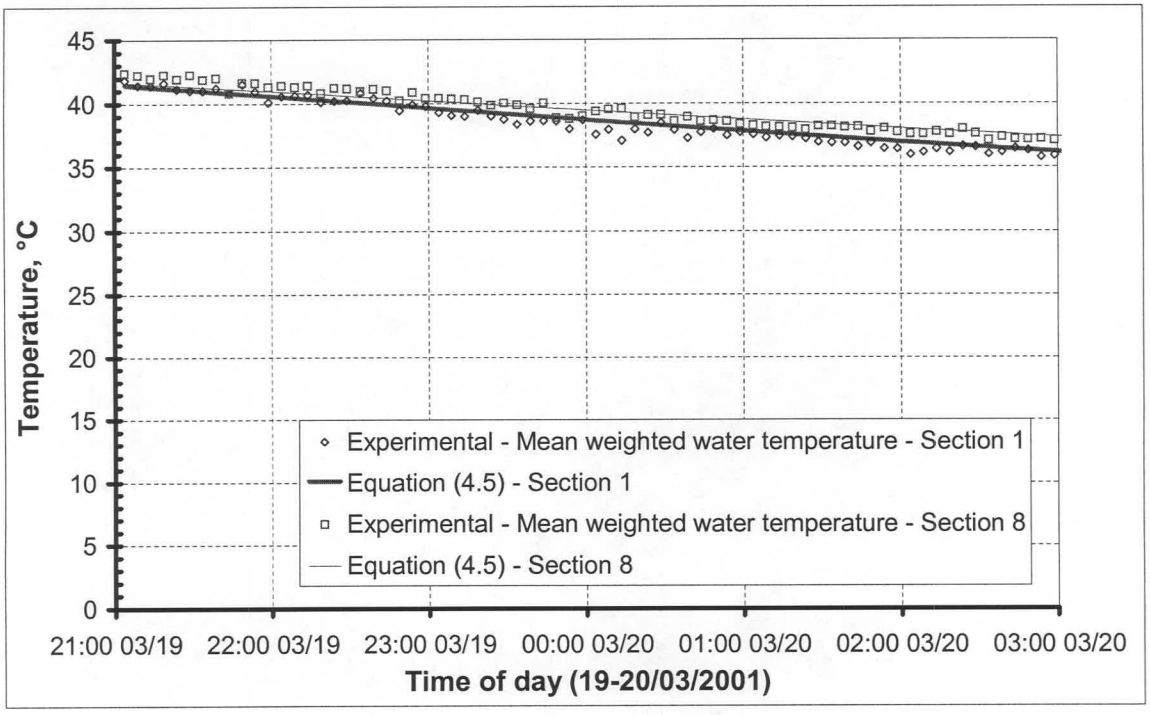

Figure 4.16: Mean water temperatures for section 1 and 8 (0.0976 kg/s)

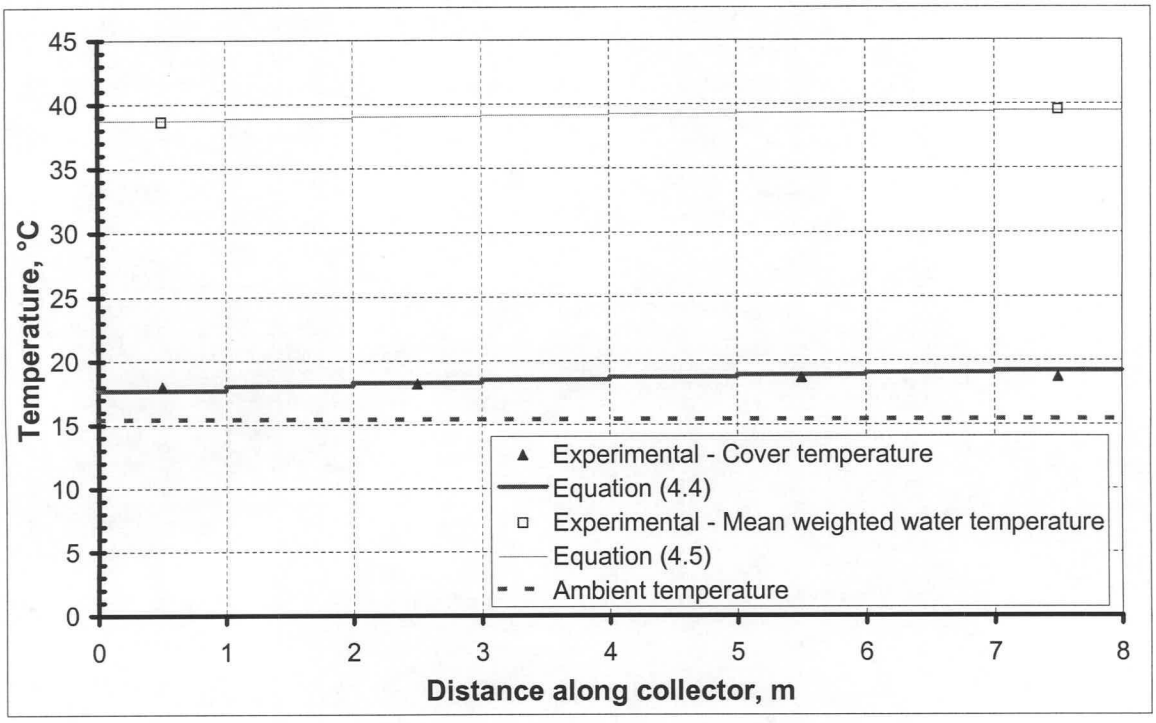

Figure 4.17: Cover and mean water temperatures at 00h00 for 0.0976 kg/s

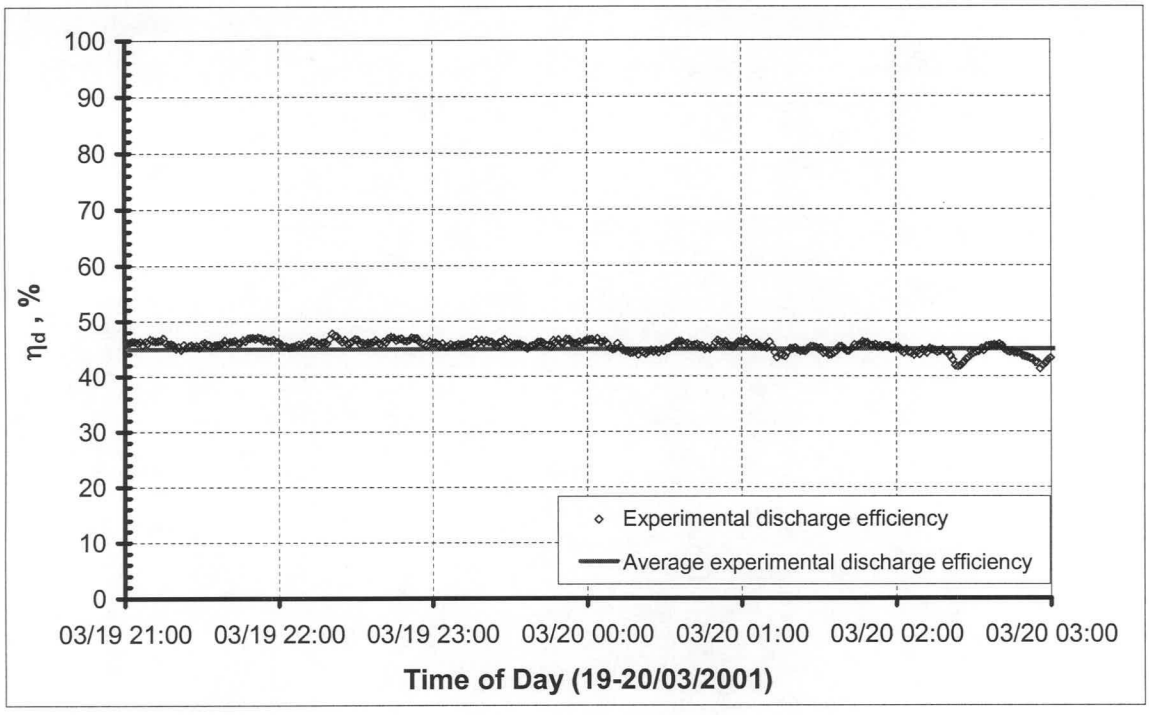

Figure 4.18: Instantaneous discharge efficiency of plastic covered water tanks for 0.0976 kg/s

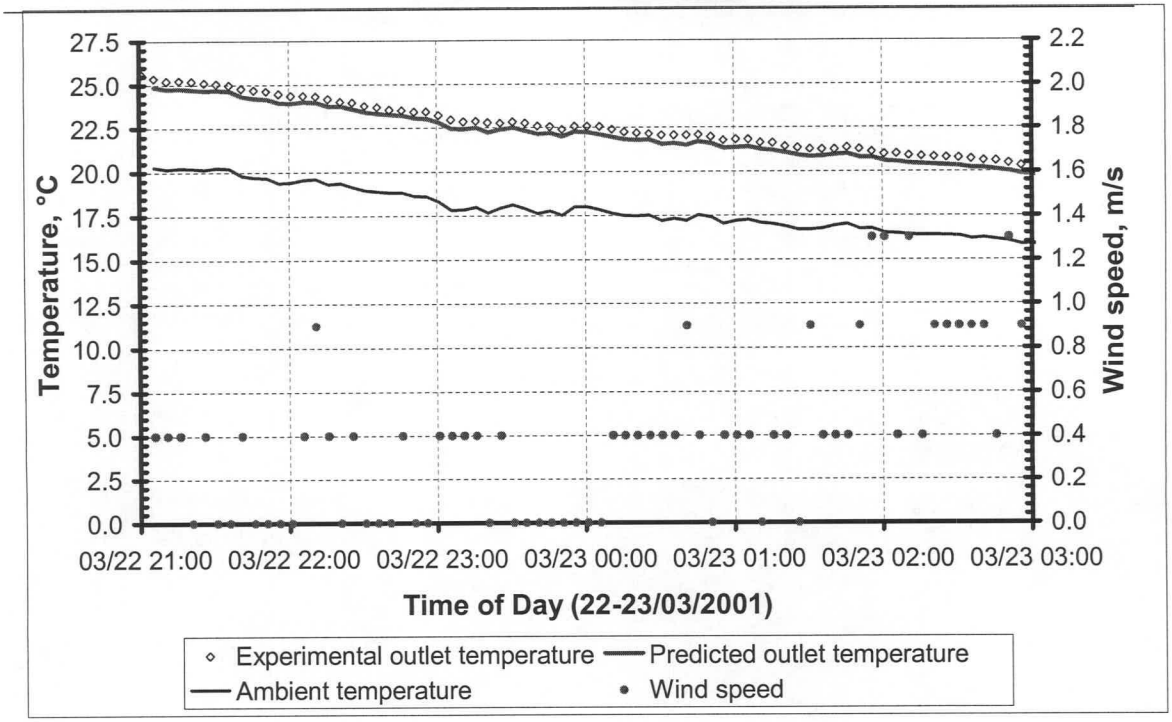

Figure 4.19: Ambient and outlet temperatures for 0.2643 kg/s

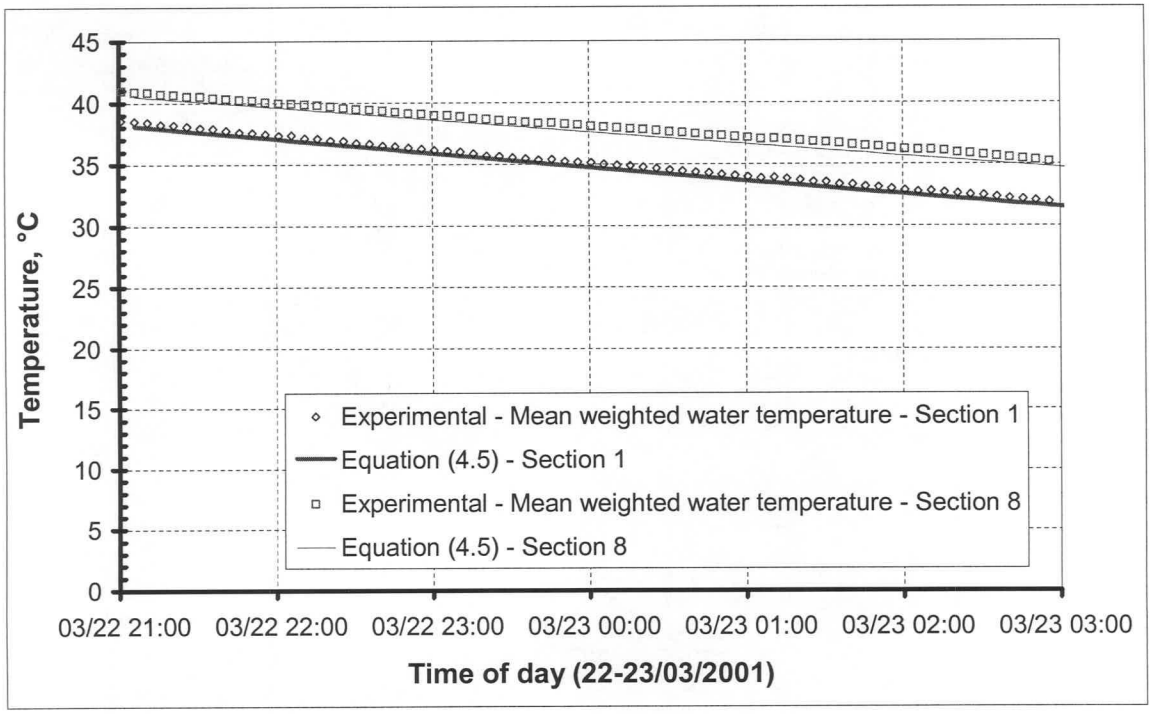

Figure 4.20: Mean water temperatures for section 1 and 8 (0.2643 kg/s)

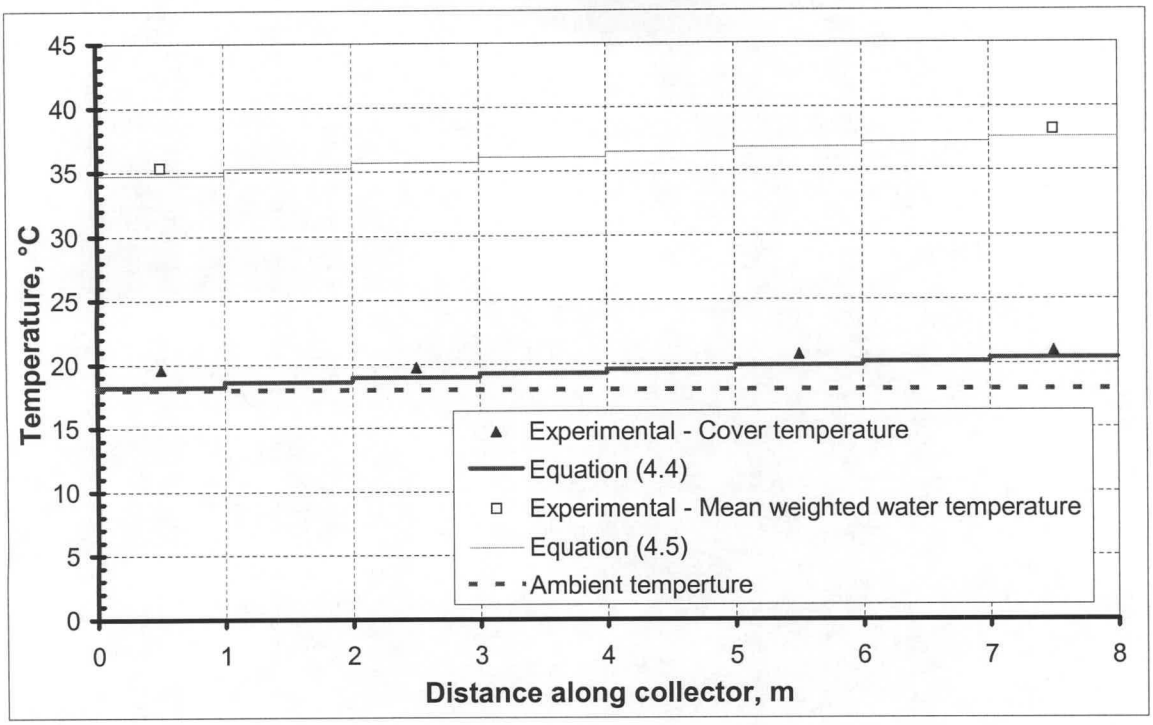

Figure 4.21: Cover and mean water temperatures at 00h00 for 0.2643 kg/s

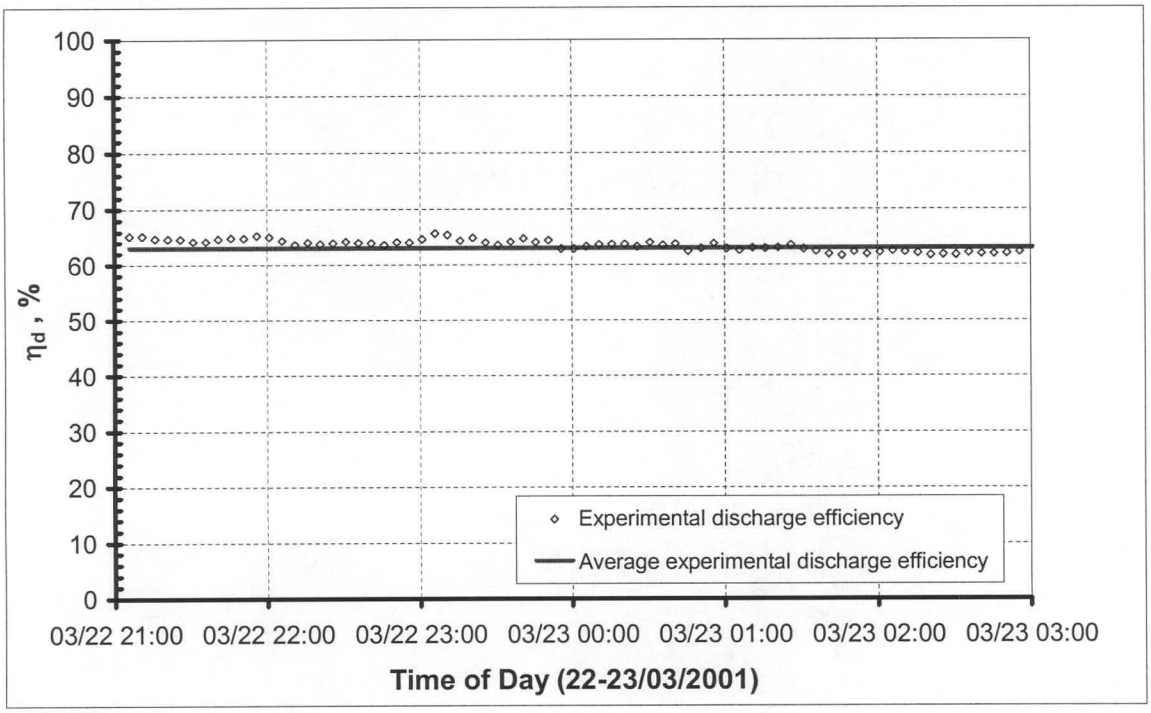

Figure 4.22: Instantaneous discharge efficiency of plastic covered water tanks for 0.2643 kg/s

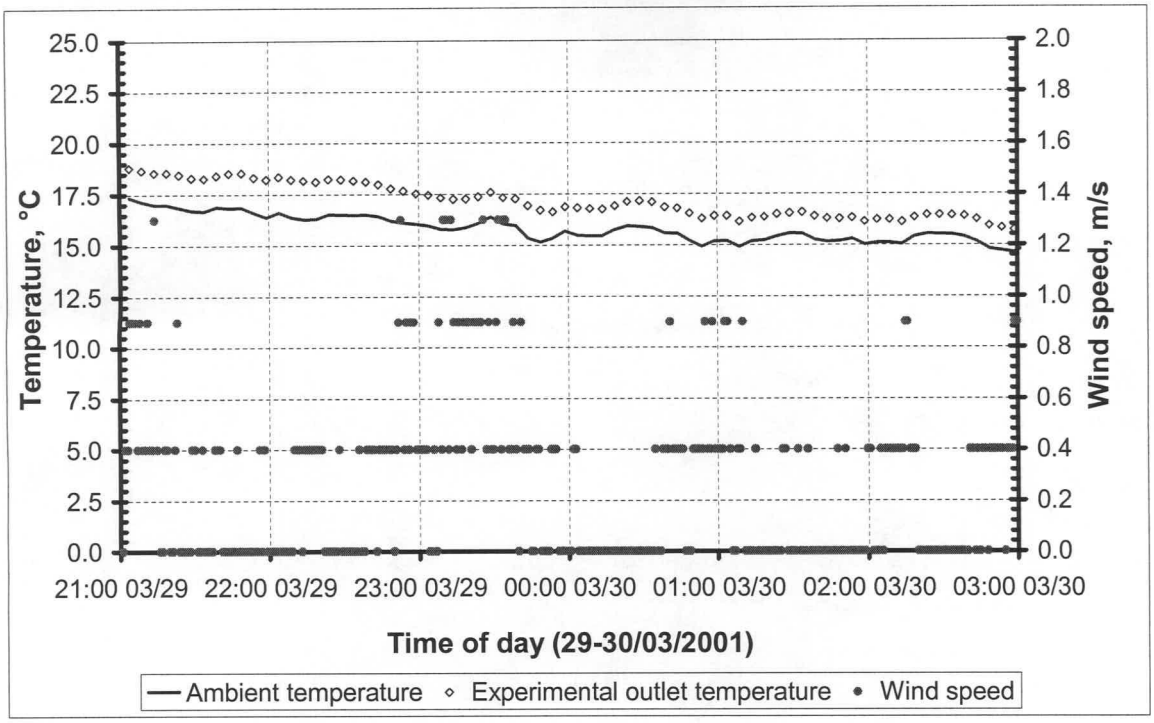

Figure 4.23: Ambient and outlet temperatures for 0.7734 kg/s

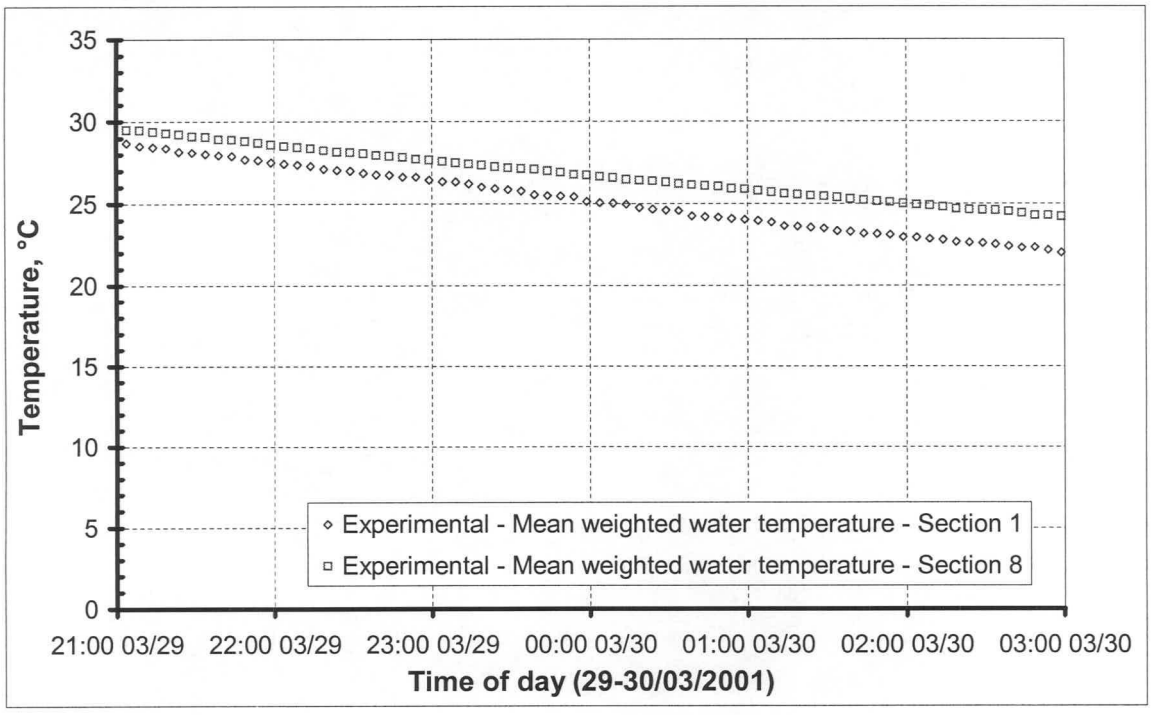

Figure 4.24: Mean water temperatures for section 1 and 8 (0.7734 kg/s)

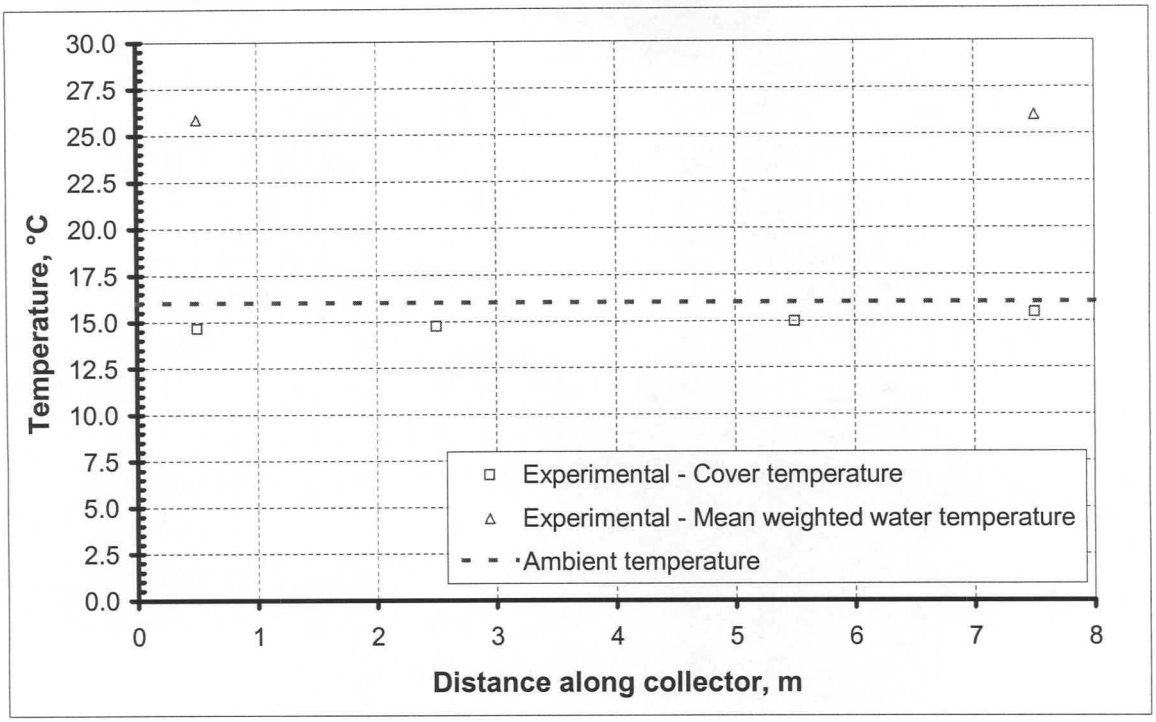

Figure 4.25: Cover and mean water temperatures at 00h00 for 0.7734 kg/s

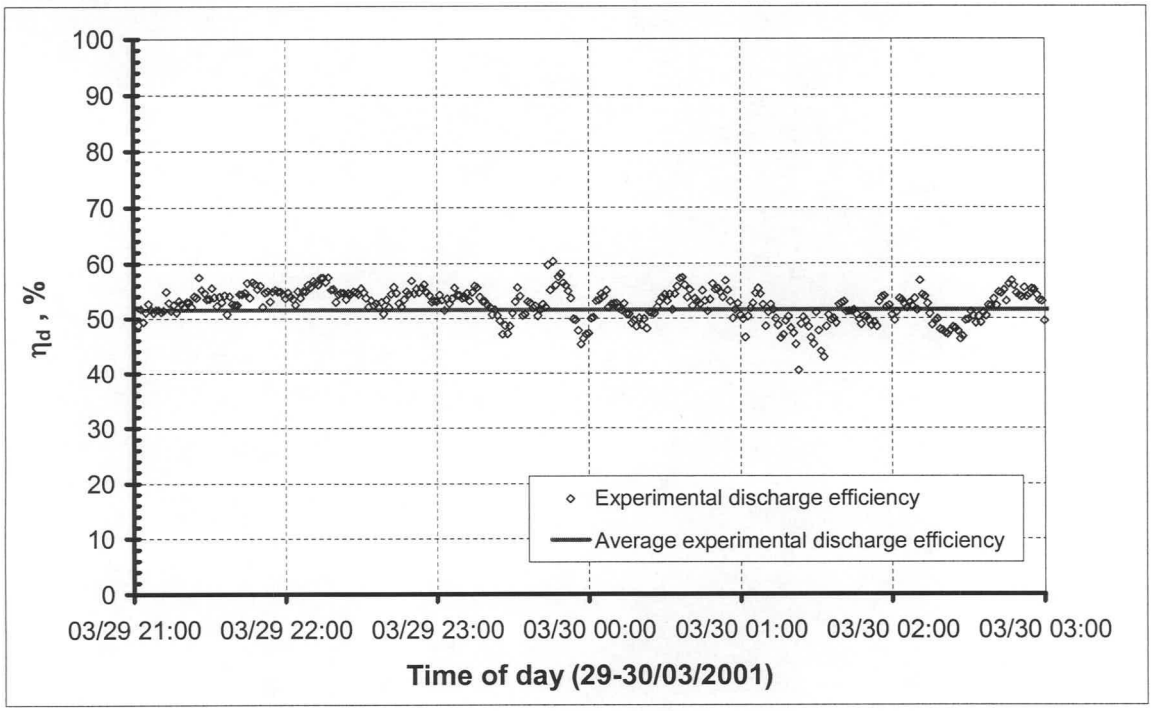

Figure 4.26: Instantaneous discharge efficiency of plastic covered water tanks for 0.7734 kg/s

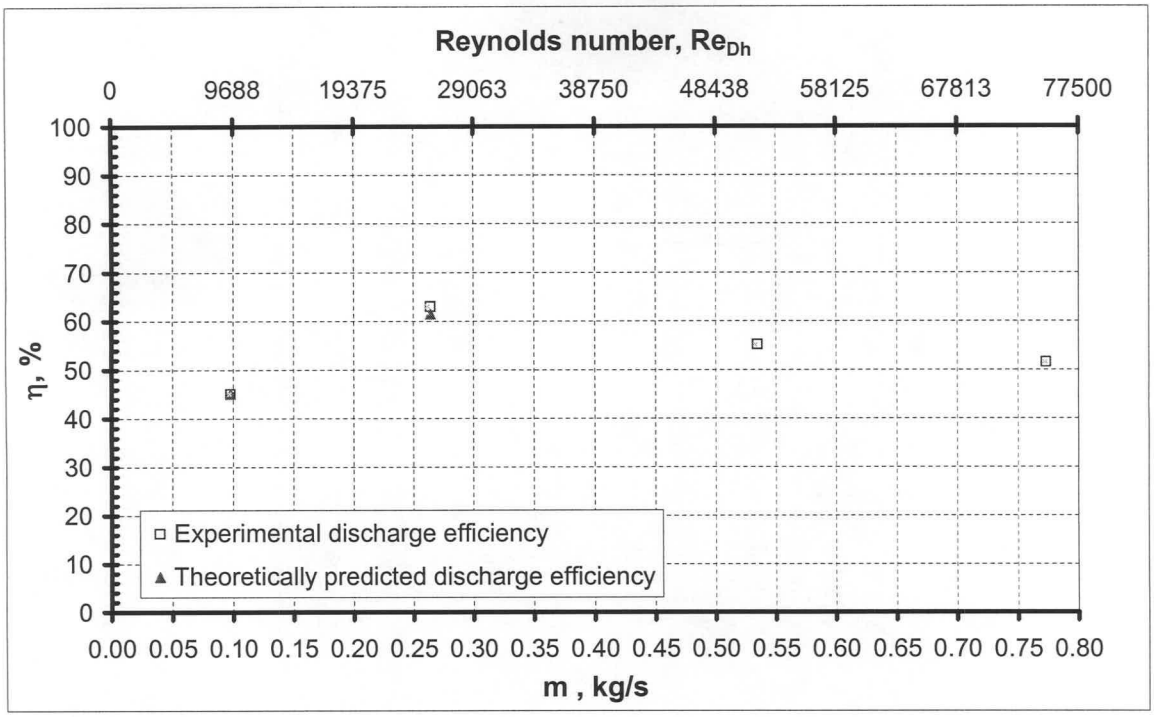

Figure 4.27: Instantaneous discharge efficiency of solar air heater with 190-mm water storage for various mass flow rates

Furthermore, to evaluate the ability of the water storage system to transfer its stored energy to the air sucked through the duct, an instantaneous discharge efficiency, η_d, is defined as

$$\eta_d = \frac{Q_{air}}{Q_{storage}} = \frac{\dot{m} c_{cp} (T_{out} - T_{in})}{\rho_w A_c t_w c_{pw} \frac{dT_w}{dt}} \tag{4.6}$$

Employing equation (4.6), the discharge coefficient is evaluated for experimentally measured values, where after the average experimental discharge efficiencies are plotted against their respective mass flow rates and Reynolds numbers based on outlet conditions (see Figure 4.27).

From the Figure 4.15 to Figure 4.21 it is apparent that as long as the cover and ambient temperature satisfy the validity criteria of equation (A.8), the theoretical model predicts respective mean cover, water and outlet temperatures that show good agreement with experimentally measured results.

Furthermore, on closer inspection of Figure 4.27 it is seems as though there exists an air mass flow rate at which the maximum amount of the available energy from the water tanks are transferred from the water tanks to the air passing though the solar air heater duct.

On closer inspection of the available experimental results it seem as though this phenomenon could be dependent on the ambient and collector conditions. For instances, if the wind-induced and radiative heat loss from the cover to the ambient exceeds the radiative heat transfer between the cover and the absorber plate, a condition could prevail within the collector whereby the radiative heat transfer between the cover and plate exceeds the convective heat transfer between the respective surfaces and the air. Accordingly the cover would then function as a heat sink to the plastic covered water tanks and a result reduce the discharge efficiency of the system.

However, the above-described phenomenon is also dependent on the comparative rate at which the water tanks' temperature and ambient temperature decline. For instance, if the rate at which the water temperature decline is less than the ambient air temperature decline rate, a condition would prevail whereby the cover is warmer than the ambient temperature, and as such most of the available energy would be lost to the cover- water radiative heat exchange. On the other hand, if the opposite condition prevails (i.e. the rate at which the water temperature decline is higher than the ambient temperature rate), both the radiation potential between the cover and water as well as between the ambient air and water tanks' will decline much faster.

Therefore, from the above discussion and Figure 4.27 it follows that for any given ambient condition there exists an optimal air mass flow rate that would optimise the amount of stored energy that is transferred to the air passing through the duct. However, further experimental work is required in order to clarify this phenomenon fully.

4.4 Conclusion

In the present investigation, the influence of water storage (in the form of plastic covered water tanks) on the performance of an upward facing solar air heater was both experimentally and theoretically investigated.

Daytime results revealed that although the efficiency of the solar air heater increases with an increase in the mass flow rate, the storage of solar energy in the water tanks leads to a decrease in the collector efficiency of the solar air heater (compare Figure 2.13 to Figure 4.14), due to the lower "absorber plate" (i.e. plastic covered water tanks) temperatures. Thus, although the solar air heater with water storage tanks makes more effectively use of available solar radiation (i.e. through energy storage and air heating) in comparison to an upward facing solar air heater (compare Figure 2.13 to Figure 4.14), one however has to conclude that the

storage effect of a 190 mm deep water tank system on the daytime collector efficiency of a solar air heater system is to dramatic.

It was also shown in the day-time investigation, that as long as the derived cover, water tank and air energy equations for the solar air heater's are used within the validity boundaries of the equations, good agreement is obtained between the theoretically predicted and experimentally measured values.

From the night-time experimental results it was further evident that water storage has not only the ability to extend the operational period of a solar air heater beyond the limitations of daytime hours but also that the current experimental set-up has the ability to regain 50% of the available energy that was stored during day-time.

Furthermore, the comparison between the predicted theoretical values and experimentally measured values made it evident that, as in the case of the day-time results, good agreement exists as long as the derived energy equations are employed within their validity range.

In addition, from Figure 4.27 it is evident that their exist for every environmental condition during night-time an optimal air mass flow rate at which an upward facing solar air heater, incorporating water energy storage, should be operated. This would ensure that the maximum amount of the stored energy is transferred from the water tanks to the air passing through the duct.

Finally, although the water storage prolonged the operational period of the solar air heater, the influence of the water storage on the daytime operation of the solar air heater was quite significant. Therefore, with regards to the day-night and seasonal fluctuation problem of the solar chimney plant, it is actually very difficult to make any conclusions as to whether the water storage system (i.e. 190 mm deep water plastic covered tank) would be a feasible solution.

Chapter 5: Conclusion and recommendations

The primary objective of the current study was to evaluate the influence of a simple water storage system, in this instance plastic covered water tanks, on the performance of an upward facing solar air heater.

5.1 Research findings

The first step was to conduct a number of experiments on an upward facing solar air heater, as described in Chapter 2, in order to determine the performance characteristics of a solar air heater without energy storage. As expected, an increase in the mass flow rate led to an increase in the collector efficiency (η_c), while it simultaneously led to a decrease in the temperature gain across the solar air heater. In addition, a comparison between the experimental and theoretical results revealed that the equations employed in Chapter 2 for the theoretical model were both reliable and accurate.

In the initial stages of the study, it seemed as though water energy storage would be the ideal solution to the problem of minimising the fluctuation in the output of a solar chimney plant. After all, water has one of the highest specific heat capacities of all natural liquids and is furthermore environmentally friendly. Accordingly, a number of day- and night-time experiments were conducted on a plastic covered water tank to determine the energy storage and discharge capability of such a water energy storage system (Chapter 3).

During experiments conducted in day-time on a plastic covered water tank heated, it was observed that as the day progressed and the water inside the plastic covered water tank heated, an air layer would begin to form underneath the plastic cover. Initially the air layer was assumed to be meaningless, that is, until it became evident from theoretical predictions that the air layer led to a reduction in the effective transmissivity of the air-film-water interface and, consequently, in the storage ability of the water tank.

Furthermore from both the simple plastic covered water tank and solar collector with water storage experiments, it was evident that the plastic covered water tank system is both an excellent storage medium and collector of solar energy. However, a comparison between the predicted performance of a solar collector without storage against the experimental values of the solar collector with water storage (as shown in Figure 3.11), indicated that the energy storage led to a dramatic decrease in the absorber plate temperature, and subsequently, in the ability of the plastic covered water tank system to transfer available solar radiation to the air

passing through the duct during daytime operation as indicated by Figure 2.13 and Figure 4.14.

The plastic covered water tank's primary function is to store the maximum amount of the incident solar radiation, whereafter the stored energy is released during night-time operation. Hence, to evaluate the discharge capability of the plastic covered water tank, a number of night-time experiments were conducted. In this instance, good agreement was obtained between the experimental and theoretical results. In addition, the results also confirmed that the plastic covered water tank is an ideal source of thermal energy during the night. For instance, in the solar collector experiment the solar collector's cover temperature was maintained throughout the night at approximately 7°C above the ambient temperature. Additionally, due to the water's high specific heat capacity, the output of such a storage system is not influenced by sudden fluctuations in the ambient conditions (wind speed and ambient temperature), as is evident from Figure 3.7 and Figure 3.12.

In the present study, an upward facing solar air heater was used to simulate a section of the solar chimney power plant's collector. Therefore, to obtain an indication of the influence of a water storage system on the temperature gain in the collector, during both day- and night-time operation, a number of experiments were conducted on a solar air heater in which the plastic covered water tank energy storage system of Chapter 3 was implemented (see Chapter 4).

Daytime experiments indicated (see Figure 4.14) that although the solar air heater with water storage shows the same collector efficiency tendency as the initial solar air heater of Chapter 2, the energy storage system led to a dramatic decrease in temperature gain in the solar air heater. In contrast to the day-time results, night-time experiments clearly indicated that the stored energy not only prolonged the output of heated air by the solar air heater, but is also able to increase the ambient air temperature by between 7.5 and 1.5 °C; depending on the chosen air mass flow rate. Thus, indicating that an upward facing solar air heater with water energy storage is more effectively making use of the available solar energy in a 24hour period than a normal upward facing solar air heater energy

Furthermore, for both day- and night-time operation, it was evident that, as long as the employed equations in the theoretical model were used within their validity region, good agreement is obtained between the experimentally measured and theoretically predicted values.

It is also interesting to note that, by plotting the discharge coefficient (η_d) against its respective mass flow rates, as shown in Figure 4.27, there appears to exist an optimum mass flow rate that is not determined by the convective heat transfer within the duct, but probably by the rate

at which the ambient temperature decline in comparison to the rate at which water temperature decline within the water tanks. However, a more in-depth study needs to be conducted in order to verify the phenomenon observed in Figure 4.27.

5.2 Remaining questions and recommendations

While the findings of Chapter 4 would appear to indicate that the 190 mm deep plastic covered water tanks might not represent a feasible solution to the day-night and seasonal fluctuation output problem of the solar chimney plant, two further issues still need to be considered, before a final conclusion can be made in this regard.

Firstly, Wang and Seyed-Yagoobi [94WA1] found that the turbidity level of the water plays a critical role on the magnitude of the solar radiation penetration. For instance, by increasing the water turbidity from 1.6 ntu to 4.5 ntu, the solar radiation penetrating to a depth of 1.34 m decreased by a factor of 2.9. However, during the plastic covered water tank experiments of Chapter 3, clean clear water was used and, accordingly, a certain percentage of the incident solar radiation was transmitted through the water and absorbed by the black bottom of the water tank (see Figure H.6 and Figure J.3) Therefore, if one would artificially increase the turbidity of the water, more solar radiation would be directly absorbed in the water; subsequently increasing the storage efficiency of the plastic covered water tank. Furthermore, the increase in the turbidity would decrease the penetration depth of the solar radiation, and as a result, possibly lead to a warmer water layer forming at the film-water interface. Thus, in the context of the solar air heater, this effect would improve the storage efficiency of the plastic covered water tank and collector efficiency of the solar air heater during day-time operation due to a more rapid increase in the water temperature. However, at this point it must be emphasised that the previous discussion is only speculation based on the work of Wang and Seyed-Yagoobi [94WA1], and needs to be confirmed through experimental work.

Secondly, in the present study, experiments were only conducted during a few months. This stands in contrast to the solar chimney power plant where the operation period is expected to be approximately 60 years. Consequently, the scenario exists that the plastic film's effective transmissivity may reduce dramatically due to the constant exposure to solar radiation and, as a result, reduce the storage capability of the water tank. Furthermore, due to the high temperature of the water within the plastic covered water tank as well as organisms existing within such warm water, the possibility exist that the organisms may attach themselves to the lower surface of the plastic film. This would reduce the effective transmissivity of the of the air-film-water interface with time. Yet as for the water turbidity scenario, the effect of the film's effective transmissivity degradation with time as well as the effect of the growth of organisms

on the lower surface of the plastic film on the water tank's storage ability still needs to be investigated through a number of long-term experiments.

Thirdly, the experimental investigation was only conducted on 190 mm deep plastic covered water tanks. As such one still needs to investigate the influence of water depth on the collector, storage and discharge efficiency of an upward facing solar air heater before one would be able to make a final decision on the feasibility of water energy storage on the solar chimney power plant.

5.3 Looking to the future ...

Looking into the future, the biggest question still left answered concerns the long-term prospect of solar energy and its development. Tsur and Zemal [00TS1] addressed the same question, using a dynamic optimisation method to analyse and quantify the development of solar technologies in the light of the increasing scarcity and environmental pollution associated with fossil fuel combustion. From the results, Tsur and Zemal [00TS1] came to two conclusions.

Firstly, their results [00TS1] indicate a smooth transition from conventional to solar technology, during which a period will exist in which both technologies will be employed. This period of transition will continue until the production cost associated with solar energy becomes less than the marginal cost of fossil energy due to the accumulation of knowledge.

Secondly, the model clearly indicates that in order to attain a smooth transition [00TS1] from conventional to solar technology, solar research and development should precede, rather than follow, future increases in the price of fossil fuels.

Both of these conclusions clearly emphasise the need for on-going research in the field of solar energy technologies. It is hoped that the present study represents at least a small, but meaningful contribution to such research. It is indeed envisioned that this study and its findings will not only lead to and inspire further development in the solar energy field, but will also more importantly, lead to the construction of the very first full-scale solar chimney power plant.

References

[31NU1] Nusselt, W., Der Wärmeaustausch zwischen Wand und Wasser im Rohr, Forschung auf dem Gebiete des Ingenieurwesens, Vol. 2, pp. 309, 1931.

[54MA1] McAdams, W,H., Heat Transmission, 3rd edition, McGraw-Hill, New York, 1954.

[63SW1] Swinbank, W.C., Long-Wave Radiation from Clear Skies, Quarterly J. Royal Meteorological Soc., Vol.89, pp. 339 - 384, 1963.

[69DA1] Dake, J.M.K., and Harleman, R.F., Thermal Stratification in Lakes: Analytical and Laboratory Studies, Water Resources Research, Vol. 5, pp. 484 – 495, 1969.

[70TA1] Tan, H.M., and Charters, W.W.S., An Experimental Investigation of Forced-Convective Heat Transfer for Fully-Developed Turbulent Flow in a Rectangular Duct with Asymmetric Heating, Solar Energy, Vol. 13, pp. 121 – 125, 1970.

[76HO1] Hollands K.G.T., Unny T.E., Raithby G.G and Konicek L., Free Convective Heat Transfer across Inclined Air Layers, J. Heat Transfer, Vol. 98, pp. 189 – 193, 1976.

[74LL1] Lloyd, J.R. and Moran W.P., Natural Convection Adjacent to Horizonal Surface of Various Platforms, J. Heat Transfer, Vol. 96, pp. 443, 1977.

[80HU1] Hull, J.R., Membrane Stratified Solar Ponds, Solar Energy, Vol. 26, pp. 317 – 325, 1980.

[81TE1] Test, F.L., Lessmann, R.C. and Johary, A., Heat Transfer During Wind Flow over Rectangular Bodies in the Natural Environment, J. Heat Transfer, Vol. 103, pp. 262 – 267, 1981.

[84CE1] Çengel, Y.A. and Öziçik, M.N., Solar Radiation Absorption in Solar Ponds, Solar Energy, Vol. 33, pp. 581 – 591, 1984.

[84GA1] Garg, H.P. and Datta, G., The Top Loss Calculation for Flat Plate Solar Collectors, Solar Energy, Vol. 32, pp. 141 – 143, 1984.

[84RU1] Rubin, H., and Benedict, B.A., Modelling the Performance of a Solar Pond as a Source of Thermal Energy, Solar Energy, Vol. 32, pp. 771 – 778, 1984.

[85FR1] Francey, J.L.A. and Papaioannou, J., Wind-Related Heat Losses of a Flat-Plate Collector, Solar Energy, Vol. 35, pp. 15 –19, 1985.

[87SH1] Shakerin, S., Wind-Related Heat Transfer Coefficients for Flat-Plate Solar Collectors, ASME J. Solar Energy Engineering, Vol. 109, pp.108 – 110, 1987.

[89KR1] Kreider, J.F., Hoogendoorn, C.J. and Kreith, F., Solar Design: Components, Systems, Economics, Hemisphere Publishing, New York, 1989.

[89YE1] Yeh, H. and Ma, N., Performance of Modified Membrane-Stratified Solar Ponds, Energy, Vol. 14, pp. 207-214, 1989.

[90JA1] Jammal, M.A. and Muaddi, J.A., Solar Energy at Various Depths Below a Water Surface, Int. Journal Energy Research, Vol. 14, pp 859 – 867, 1990.S

[90SO1] Sokolov, M. and Arbel, A,. Freshwater Floating-Collector-Type Solar Pond, Solar Energy, Vol. 44, pp. 13 – 21, 1990.

[91DU1] Duffie, J.A. and Beckman, W.A., Solar Engineering of Thermal Processes, 2nd edition, John Wiley and Sons, 1991.

[92MI1] Mills, A.F., Heat Transfer, Irwin Incorporated, Illinois, 1992.

[92PR1] Prakash, J., Garg, H.P., Jha, R. and Hrishikesan, D.S., Solar Thermal Systems with Transparent Insulation, Energy Convers. Mgmt., Vol. 33, pp. 987 – 996, 1992.

[92SE1] Serway, Raymond A., Physics for Scientists and Engineers, 3rf edition, Saunder College Publishing, Chicago, 1992.

[93MO1] Modest, M.F., Radiative Heat Transfer, McGraw-Hill Inc., New York, 1993.

[94BE1] Bellecci, C., and Conti, M., Phase Change Energy Storage: Entropy Production, Irreversibility and Second Law Efficiency, Solar Energy, Vol. 53, pp. 163 – 170, 1994.

[94HA1] Hahne, E., and Kübler R., Monitoring and Simulation of the Thermal Performance of Solar Heated Outdoor Swimming Pools, Solar Energy, Vol. 53, pp. 9 –19, 1994.

[94KA1] Knagas, M.T., and Lund, P.D., Modelling and Simulation of Aquifer Storage Energy Systems, Solar Energy, Vol. 53, pp. 237 – 247, 1994.

[94SA1] Samdarshi, S.K. and Mullick, S.C., Generalized Analytical Equation for the Top Heat Loss Factor of a Flat-Plate Solar Collector with N Glass Covers, J. Solar Energy Engineering, Vol. 116, pp. 43 – 46, 1994.

[94TS1] Tsilingiris, P.T., Steady-State Modelling Limitations in Solar Pond Design, Solar Energy, Vol. 53, pp. 73 – 79, 1994.

[94WA1] Wang, J. and Seyed-Yagoobi, J., Effects of Water Turbidity and Salt Concentration Levels on Penetration of Solar Radiation under Water, Solar Energy, Vol. 52, pp. 429 – 438, 1994.

[95ON1] Ong, K.S., Thermal Performance of Solar Air Heaters: Mathematical Model and Solution Procedure, Solar Energy, Vol. 55, pp. 93 – 109, 1995.

[95ON2] Ong, K.S., Thermal Performance of Solar Air Heaters: Experimental Correlation, Solar Energy, Vol. 55, pp. 209 – 220, 1995.

[96HE1] Hegazy, A.A., Optimization of Flow-Channel Depth for Conventional Flat-Plate Solar Air Heaters, Renewable Energy, Vol. 7, pp. 15 – 21, 1996.

[96PR1] Prasad, R. and Rao, D.P., Estimation of the Thickness of the Lower Convective Layer of Solar Ponds, Renewable Energy, Vol. 7, pp. 401 – 407, 1996.

[96TA1] Taga, M., Fujimoto, K. and Ochi, T., Field Testing on Nonsalt Solar Ponds, Solar Energy, Vol. 56, pp. 267 – 277, 1996.

[96YE1] Yeh, H. and Lin, C., The Effect of Collector Aspect Ratio on the Collector Efficiency of Upward-type Flat-plate Solar Air Heaters, Energy, Vol. 21, pp. 843 – 850, 1996.

[97HA1] Hachemi, A., Thermal Heat Performance Enhancement by Interaction between the Radiation and Convection in Solar Air Heaters, Renewable Energy, Vol. 12, pp. 419 – 433, 1997.

[97KU1] Kumar, S., Sharma, V.B., Kandpal, T.C. and Mullick, S.C., Wind Induced Heat Losses from Outer Cover of Solar Collectors, Renewable Energy, Vol. 10, pp. 613 –

616, 1997.

[98AL1] Al-nimr M.A., and Damseh, R.A, Dynamic Behaviour of Baffeld Solar Air Heaters, Renewable Energy, Vol. 13, pp. 153 – 163, 1998.

[98KA1] Kabeel, A.E., and Mecárik, K., Shape Optimazation for Absorber Okates of Solar Air Collectors, Renewable Energy, Vol. 13, pp. 121 –131, 1998.

[98KR1] Kröger, D.G., Air-Cooled Heat Exchangers and Cooling Towers, Begell House, New York, 1998.

[98OL1] Oliveti, G., Arcuri, N. and Ruffolo, S., First Experimental Results from a Prototype Plant for the Interseasonal Storage of Solar Energy for the Winter Heating of Buildings, Solar Energy, Vol. 62, pp. 281 – 290, 1998.

[98RO1] Rohsenow, Waren M., Hartnett, James P. and Chou Youbg I., Handbook of Heat Transfer, 3rd edition, Mcgraw-Hill, New York, 1998.

[98SH1] Sharples, S., and Charlesworth, P.S., Full-Scale Measurements of Wind-induced Convective Heat Transfer from a Roof-Mounted Flat Plate Solar Collector, Solar Energy, Vol. 62, pp. 69 – 77, 1998.

[98TS1] Tsilingiris, P.T., On Optical Performance and Directional Characteristics of Plastic Film Liquid Layer Solar Water Heaters, Solar Energy, Vol. 63, pp. 293 – 302, 1998.

[98YE1] Yeh, H., Ho, D. and Lin, C., The Influence of Collector Aspect Ratio on the Collector Efficiency of Baffled Solar Air Heaters, Energy, Vol. 23, pp. 11 – 16, 1998.

[99AK1] Akhtar, N. and Mullick, S.C., Approximate Method for Computation of Glass Cover Temperature and Top Heat-Loss Coefficient of Solar Collectors with Single Glazing, Solar Energy, Vol. 66, pp. 349 – 354, 1999.

[99BA1] Bansal, N.K., Solar Air Heater Application in India, Renewable Energy, Vol. 16, pp. 618 – 623, 1999.

[99HA1] Hachemi, A., Comparative Study on the Thermal Performances of Solar Air Heaters Collectors with Selective and Nonselective Absorber-Plate, Renewable Energy, Vol. 17, pp. 103 – 112, 1999.

[99HA2] Hachemi, A., Experimental Study of Heat Transfer and Flow Friction in Solar Air Heaters with and without Selective Absorbers, Renewable Energy, Vol. 17, pp. 155 – 168, 1999.

[00GA1] Garg, H.P. and Kumar R., Studies on Semi-cylindrical Solar Tunnel Dryers: Thermal Performance of Collector, Applied Thermal Engineering, Vol. 20, pp. 115 – 131, 2000

[00JA1] Jaefarzadeh, M.R., On the Performance of a Salt Gradient Solar Pond, App. Thermal Eng., Vol. 20, pp. 243 – 252, 2000.

[00KU1] Kurt, H., Halici, F. and Binark, A.K., Solar Pond Conception and Theoretical Studies, Energy Convers. Mgmt., Vol. 41, pp. 939 – 951, 2000

[00MV1] Mcveigh, J., Burtraw, D., Darmstadter, J. and Palmer, K., Winner, Loser, or Innocent Victim? Has Renewable Energy Performed as Expected?, Solar energy, Vol. 68, pp. 237 – 255, 2000.

[00NJ1] Njomo, D., Unglazed Selective Absorber Solar Air Collector: Heat Exchange Analysis, Heat and Mass Transfer, Vol. 36, pp. 313 – 317, 2000.

[00SA1] Personal communication with the South African Weather Bureau (SAWB)

[00TS1] Tsur, Y. and Zemel, A., Long-term Perspective on the Development of Solar Energy, Solar Energy, Vol. 68, pp. 379 – 392, 2000.

[01HE1] Hedderwick, R.A., Performance Evaluation of a Solar Chimney Power Plant (Master of Science in Mechanical Engineering Thesis), University of Stellenbosch, 2001.

[01MA1] Martinot, E., Renewable Energy Investment by the World Bank, Energy Policy, Vol. 29, pp. 689 – 699, 2001.

[01PA1] Painuly, J.P., Barriers to Renewable Energy Penetration; a Framework for Analysis, Renewable Energy, Vol. 24, pp. 73 – 89, 2001.

Appendix A: Effective convective heat transfer coefficient

Experiments are conducted on a specific horizontal plate geometry exposed to the incident solar radiation and natural environment, in order to obtain an effective wind-induced convective heat transfer correlation that can be used for the evaluation of the effective convective heat transfer between a flat horizontal plate and the natural environment.

A.1 Analysis

Consider the upper surface of a horizontal flat polystyrene plate that is exposed to the environment as shown in Figure A.1.

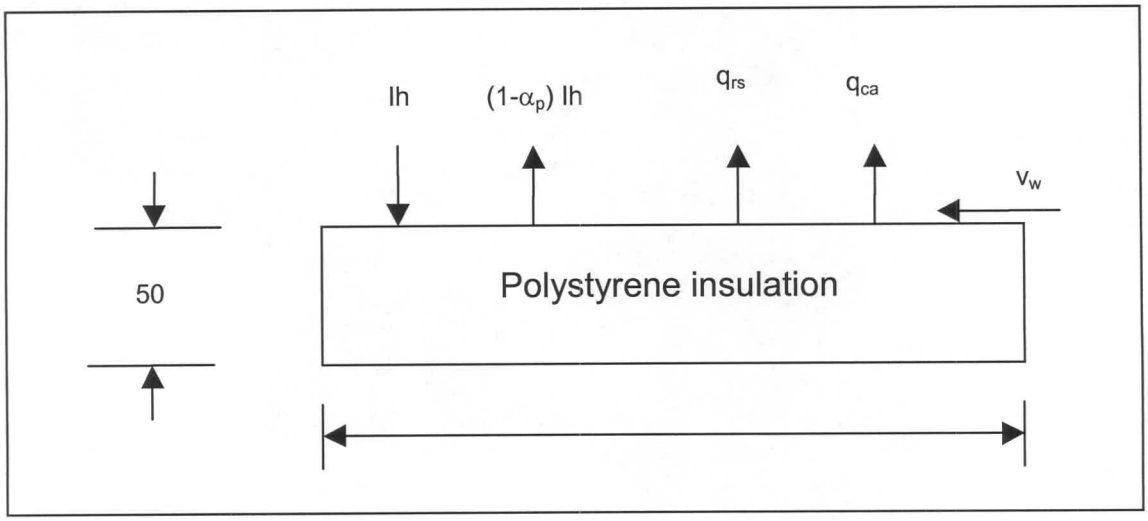

Figure A.1: Polystyrene flat plate exposed to the natural environment

Applying an energy balance to a unit area of the upward facing surface, find

$$Ih = (1-\alpha_p)Ih + q_{rs} + q_{ca} \qquad (A.1)$$

where Ih is the total solar radiation (clear sky in the present investigation) on a unit horizontal surface area, α_p is the plate absorption coefficient and q_{ra} and q_{ca} are the long-wave radiation and convection heat transfer rates in W/m^2. Conduction losses through the polystyrene plate are assumed to be negligible.

The heat flux due to radiation from the plate to the sky can be expressed as

$$q_{rs} = \sigma\varepsilon_p\left(T_p^4 - T_{sky}^4\right) \tag{A.2}$$

where ε_p is the emissivity of the plate, T_p is the mean plate surface temperature, and according to Swinbank [63SW1] the sky temperature in Kelvin is

$$T_{sky} = 0.0552T_a^{1.5} \tag{A.3}$$

where T_a is the ambient air Kelvin temperature.

Although other expressions for sky temperature are available (Brundt [40BR1], Swinbank [63SW1], Whilier [76WH1], Berdahl and Fromberg [82BE1], Berdahl and Martin [84BE1]), this particular expression is chosen in order to define a corresponding convective heat transfer coefficient.

The convective heat flux from the heated polystyrene can be expressed as

$$q_{ca} = h_e\left(T_p - T_a\right) \tag{A.4}$$

with h_e defining the effective convective heat transfer coefficient which will be determined experimentally in this study.

Thus, from equation (A.1), together with equation (A.2), (A.3) and (A.4) it follows that

$$h_e = \frac{\alpha_p Ih - \sigma\varepsilon_p\left[T_p^4 - \left(0.0552T_a^{1.5}\right)^4\right]}{\left(T_p - T_a\right)} \tag{A.5}$$

This relation defines the convective heat transfer coefficient. The latter can be determined experimentally if Ih, α_p, ε_p, T_p and T_a are measured.

A.2 Experiment

Experiments are conducted in order to determine the convective heat transfer coefficient between a 1 m × 1 m horizontal polystyrene plate (50-mm thick polystyrene) on a solid 1 m × 1 m square pedestal having a height of 1.05 m and highly reflective sides. Five fine type-T

thermocouples, having short response times are located on the polystyrene upper surface in positions as shown in Figure A.2.

The test facility is located 100m above sea level at 33.98 °S latitude and 18.85 °E longitude.

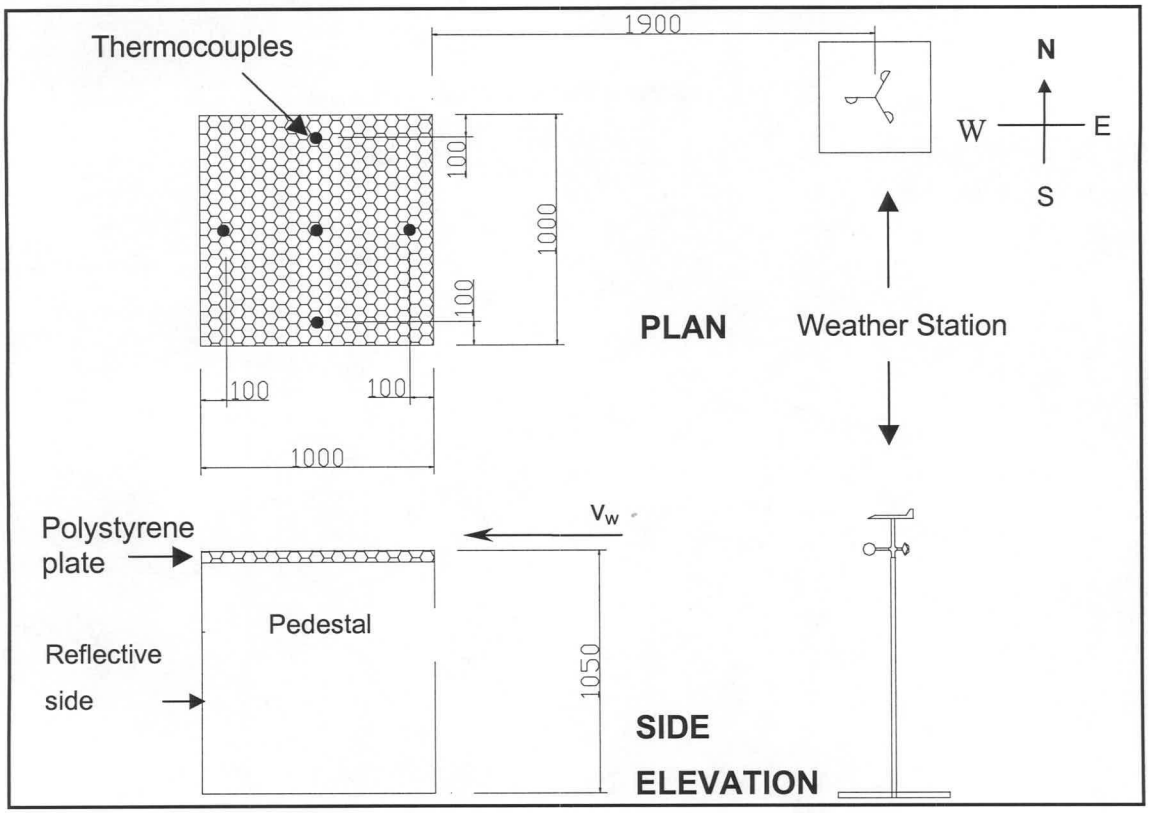

Figure A.2: Experimental apparatus

During the tests solar radiation Ih (on a horizontal surface) ranged between 250 and 1030 W/m^2 while wind velocities v_w (speed and direction) measured at the elevation of the plate (1.05 m above ground level) with the aid of a cup anemometer ranged from 0 m/s to 3.6 m/s. Only data obtained during fairly steady winds in a particular direction perpendicular to one edge of the test plate was retained for evaluation purposes. The ambient air temperature was measured at the anemometer. Only test data obtained during clear sky conditions was used in the evaluation of h_e.

Two sets of experiments were conducted. In one case the upper surface of the polystyrene plate was painted with a matt black paint having an absorbtion coefficient of $\alpha_p \approx 0.9$ and an emissivity of $\varepsilon_p \approx 0.9$. A second set of tests was conducted in which the upper surface of the plate was covered by an aluminium foil with $\alpha_p \approx 0.1$ and $\varepsilon_p \approx 0.03$.

A.3 Results

At wind speeds of $v_w = 0$, heat transfer from the plate to the ambient air is due to natural convection. The heat transfer coefficient determined according to equation (A.6) for the measured data sets can be correlated by the following dimensionless equation

$$\frac{h_e L_e}{k} = Nu_n = 0.227\left[\left(\frac{2(T_p - T_a)gL_e^3\rho^2}{(T_p + T_a)\mu^2}\right)\left(\frac{\mu c_p}{k}\right)\right]^{1/3} = 0.227\,(Gr\,Pr)^{1/3} \qquad (A.6)$$

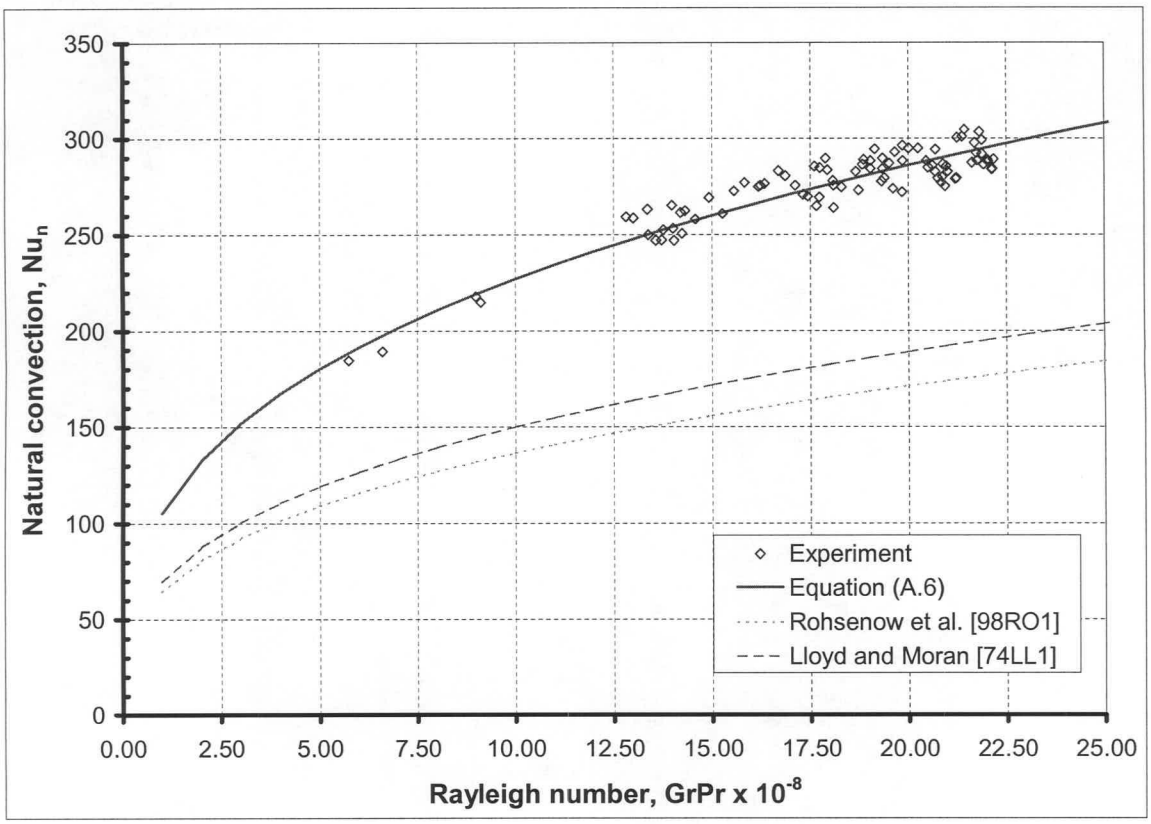

Figure A.3: Heat transfer due to natural convection

Measured experimental data is compared to equation (A.6) as well as to correlations proposed by Lloyd and Moran [74LI1] and Rohsenow et al. [98R01] for a heated horizontal surface facing upwards as shown in Figure A.3. Note that the effective length dimension for the correlations in Figure A.3 is the plate side length L_e

According to Rohsenow et al. [98RO1], natural convection will usually dominate when $Gr \geq 1100\ Re^{3/2}$ while forced convection (windy conditions) will be the primary mechanism when $Gr \leq 11\ Re^{3/2}$ (see Figure A.4).

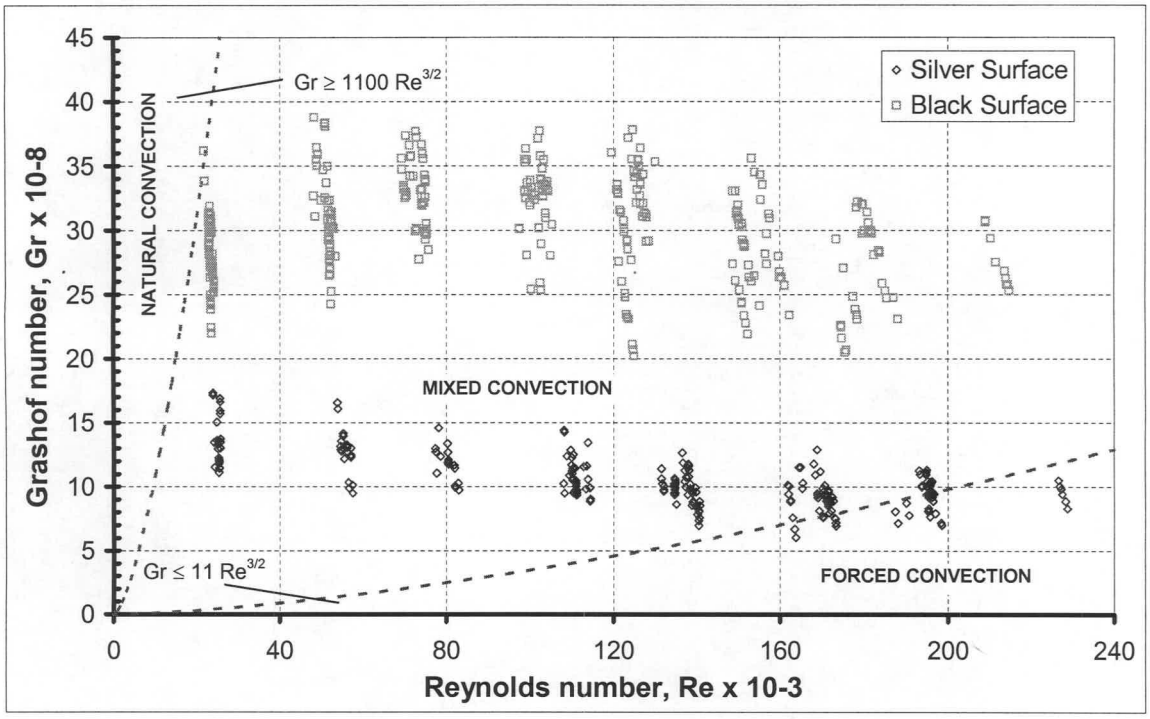

Figure A.4: Dominant convective heat transfer

During windy conditions the airflow pattern across the test surface becomes very complex and the heat transfer coefficient becomes a function of both the Grashof (Gr) and Reynolds (Re) numbers.

As shown in Figure A.5, the present data is well correlated (RMS = 16.2%) by the following equation

$$\frac{h_e L_e}{k} = Nu = (Gr\ Pr)^{1/3}(0.227 + 1.406 \times 10^{-6}\ Re) \qquad (A.7)$$

This equation is valid in the range $6.75 \times 10^8 \leq (GrPr) \leq 26.6 \times 10^8$ and for $0 \leq Re \leq 2.5 \times 10^5$.

A.4 Conclusion

An equation that predicts the effective convective heat transfer on a horizontal heated plate exposed to the environment is presented. It should be noted that equation (A.7) is only applicable to a particular geometry. The range of operating conditions is clearly specified.

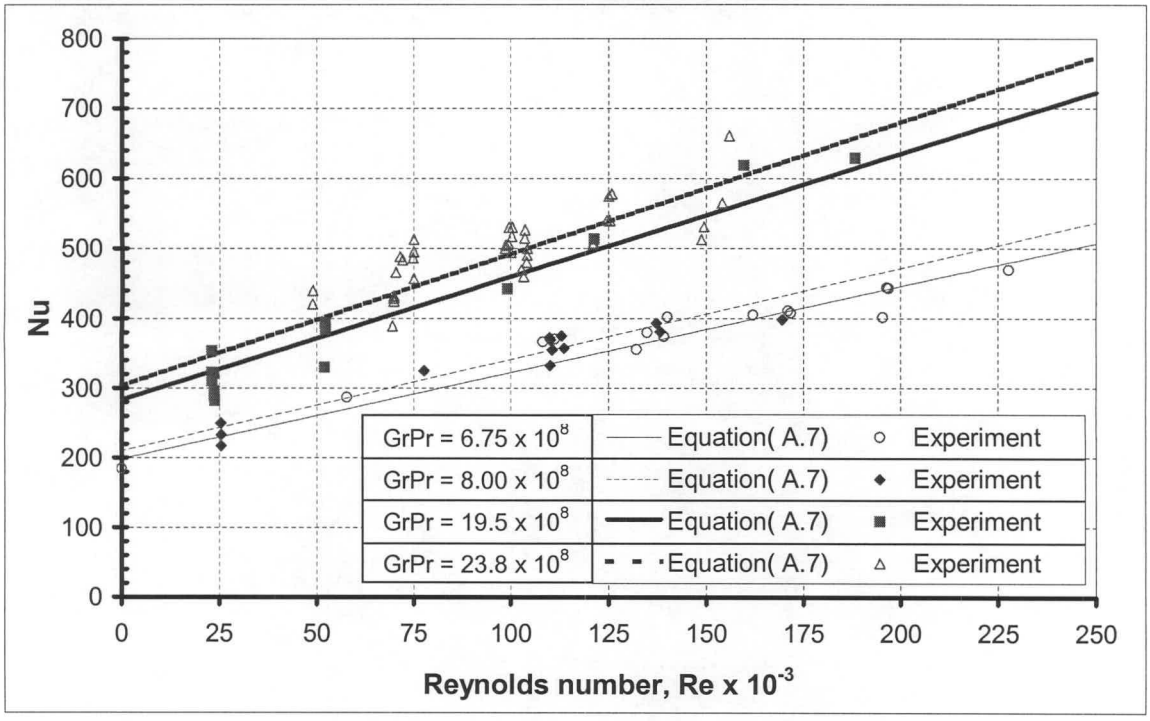

Figure A.5: Convective heat transfer

The fact that the presented correlation (equation (A.6)) for the heat transfer due to natural convection is higher than the predictions of Lloyd and Moran [74LI1] and Rohsenow et al. [98RO1] may in part be due to the nature of the turbulence in the unstable ambient air and the geometry of the particular apparatus.

During windy conditions, the nature of the flow of the air across the test surface will determine the heat transfer coefficient. For laminar flow over a surface $Nu_l \propto Re^{0.5}$ while for turbulent flow $Nu_t \propto Re^{0.8}$. In the present investigation, equation (A.7) shows $Nu \propto Re$. Due to relatively high free stream turbulence a Reynolds number exponent of 0.8 is not unrealistic since it is likely that turbulent flow will predominate although the test surface is not very long in the flow direction. Furthermore, flow distortions due to separation along the edge of the test surface and due to natural convection can be the reason for the Reynolds number exponent of unity over the range tested.

Therefore, from equations (A.2) and (A.7) it follows that the total heat loss per unit area from a heated flat horizontal 1m x 1m plate located 1.05m above the ground is

$$q_t = (q_{rs} + q_{ca}) = \varepsilon_p \sigma \left(T_p^4 - T_{sky}^{1.5}\right) + \left[(Gr\,Pr)^{1/3}\left(0.227 + 1.406\times10^{-6}\,Re\right)\right]\frac{k}{L_e}\left(T_p - T_a\right) \qquad (A.8)$$

where T_{sky} is defined by equation (A.3).

In the following sections, two numerical examples will illustrate the determination of the Nusselt number as well as the appropriate dimensionless numbers for forced and natural convection, applicable to the experimental apparatus.

Numerical example - Natural convection

On the 13th of May 2000, at 10:00, the following temperatures, pressure and incident solar radiation were measured:

T_a = 23.7 °C or 296.85 K
T_p = 44.726 °C or 317.876 K
I_h = 391.152 W/m^2 K
p_a = 100 989 N/m^2

The thermophysical properties of the air as well as the Prandtl and Grashof numbers are evaluated at a mean air-plate temperature of

$$T_{ap} = (23.7 + 44.726)/2 = 34.213\,°C \text{ or } 307.363\,K$$

The thermophysical properties of the air for the above temperatures are [98KR1]

Air density $\rho_{ca} = \dfrac{p_a}{287.08 \times T_{am}} = \dfrac{100989}{287.08 \times 307.363} = 1.1447\ kg/m^3$

Specific heat capacity of air $c_{pca} = 1007.242\ J/kg.K$

Air conductivity $k_{ca} = 0.02679\ W/m.K$

Dynamic viscosity of air $\mu_{ca} = 1.8806 \times 10^{-5}\ N/s.m^2$

and consequently yield a dimensionless Prandtl number of

$$Pr = \frac{\mu\, c_p}{k} = \frac{1.8806 \times 10^{-5} \times 1007.242}{0.02679} = 0.707$$

For the evaluation of the Grashof number, the effective length is set equal to the side length of the square plate. Thus the Grashof number yields a value of

$$Gr = \frac{2(T_p - T_a)gL^3\rho^2}{(T_p + T_a)\mu^2} = \frac{2\times(317.876 - 296.85)\times 9.81\times 1.0^3 \times 1.1447^2}{(317.876 + 296.85)\times\left(1.8806\times 10^{-5}\right)^2} = 2.4864\times 10^9$$

According to equation (A.5), the experimental heat transfer coefficient is

$$h_{nc} = \frac{\alpha_p Ih - \sigma\varepsilon_p\left[T_p^4 - \left(0.0552T_a^{1.5}\right)^4\right]}{\left(T_p - T_a\right)}$$

$$= \frac{0.9\times 391.152 - 5.67\times 10^{-8}\times 0.9\left[317.876^4 - \left(0.0552\times 296.85^{1.5}\right)^4\right]}{(317.876 - 296.85)}$$

$$= 7.382\ W/m^2K.$$

which yields to a corresponding Nusselt number of

$$Nu_{nc} = \frac{h_{nc}L}{k} = \frac{7.382\times 1.0}{0.02679} = 275.55.$$

Numerical example - Forced convection

At 13:40 on the 13th of May 2000 the following pressure, temperatures, wind speed and incident solar radiation were measured:

T_a = 29.9 °C or 303.05 K
T_p = 56.356 °C or 329.506 K
I_h = 574.07 W/m^2 K
p_a = 100 989 N/m^2
v_w = 0.9 m/s

The thermophysical properties of the air are evaluated at a mean air-plate temperature of

$$T_{ap} = (29.9 + 56.356)/2 = 43.128\,°C \text{ or } 316.278\,K$$

For the above mean temperature, the thermophysical properties of the air, according to Kröger [98KR1], are

Air density $$\rho_{ca} = \frac{p_a}{287.08\times T_{am}} = \frac{100989}{287.08\times 316.287} = 1.1125\ kg/m^3$$

Specific heat capacity of air $c_{pca} = 1007.658\ J/kg.K$

Air conductivity $k_{ca} = 0.02747\ W/m.K$

Dynamic viscosity of air $\mu_{ca} = 1.9211 x 10^{-5}\ N/s.m^2$

Using the above determined thermophysical properties, the Prandtl number yields

$$Pr = \frac{\mu\, c_p}{k} = \frac{1.9211 \times 10^{-5} \times 1007.658}{0.02747} = 0.7047$$

Upon substituting the experimental values into the dimensionless Grashof and Reynolds numbers and find

$$Gr = \frac{2(T_p - T_a) g L^3 \rho^2}{(T_p + T_a)\mu^2} = \frac{2 \times (329.506 - 303.05) \times 9.8 \times 1.0^3 \times 1.1125^2}{(329.506 + 303.05) \times \left(1.9211 \times 10^{-5}\right)^2} = 2.7518 \times 10^9$$

$$Re = \frac{\rho v_w L}{\mu} = \frac{1.1125 \times 0.9 \times 1.0}{1.9211 \times 10^{-5}} = 52118.58$$

Hence, the heat transfer coefficient according to equation (A.6) is

$$h = \frac{\alpha_p Ih - \sigma \varepsilon_p \left[T_p^4 - \left(0.0552 T_a^{1.5}\right)^4\right]}{\left(T_p - T_a\right)}$$

$$= \frac{0.9 \times 574.07 - 5.67 \times 10^{-8} \times 0.9 \left[329.506^4 - \left(0.0552 \times 303.05^{1.5}\right)^4\right]}{\left(329.506 - 303.05\right)}$$

$$= 10.663\ W/m^2 K$$

and subsequently the corresponding Nusselt number is

$$Nu = \frac{hL}{k} = \frac{10.663 \times 1.0}{0.02747} = 388.17.$$

Appendix B: Solar characteristics of a cover and absorber plate

From literature, it is evident that in order to evaluate the performance of either a solar collector or solar heater, both the effective transmissivity of the cover as well as the transmittance-absorbtance product for the plate needs to be known. The objective is thus to determine the most applicable equations for the evaluation of these properties.

B.1 Solar characteristics of cover

From a literature search, two sets of equations are obtained for the evaluation of the solar characteristics of a cover [91DU1, 93MO1].

Duffie and Beckman [91DU1] propose the following set of equations for the evaluation of the solar characteristics of a single cover. According to Duffie and Beckman [91DU1] the effective reflectivity of a cover is equal to

$$\rho' \cong \tau_\alpha - \tau_\alpha \left(\frac{1-\rho}{1+\rho} \right) \tag{B.1}$$

with ρ defining the interface reflectivity between the cover and the air, and τ_α the cover's transmittance due to absorbtance. The effective transmissivity of a cover, according to Duffie and Beckman [91DU1], is

$$\tau' \cong \tau_\alpha \left(\frac{1-\rho}{1+\rho} \right) \tag{B.2}$$

with equation (B.3) yielding an equation for the evaluation of the effective absorptivity of a cover

$$\alpha' \cong 1 - \tau_\alpha \tag{B.3}$$

At this point, it must be stressed that the above-proposed equations are only applicable to a cover of which the upper and lower surfaces are surrounded by the same media.

An alternative set of equations is proposed by Modest [93MO1]. These equations are applicable to either a cover that is surrounded by the same media or by different media.

The effective reflectivity of a cover (see Figure B.1), ρ', according to Modest [93MO1], is

$$\rho' = \rho_{12} + \frac{\rho_{23}\,(1-\rho_{12})^2\,\tau_\alpha^2}{1-\rho_{12}\,\rho_{23}\,\tau_\alpha^2} \tag{B.4}$$

while the following equation can be used for the evaluation of the effective transmissivity of the cover.

$$\tau' = \frac{(1-\rho_{12})\,(1-\rho_{23})\,\tau_\alpha}{1-\rho_{12}\,\rho_{23}\,\tau_\alpha^2} \tag{B.5}$$

Modest [93MO1] also suggests, that equation (B.6) be used for the determination of the amount of solar radiation that is effectively absorbed by a cover as solar radiation passes through it.

$$\alpha' = \frac{(1-\rho_{12})(1+\rho_{23}\,\tau_\alpha)(1-\tau_\alpha)}{1-\rho_{12}\,\rho_{23}\,\tau_\alpha^2} \tag{B.6}$$

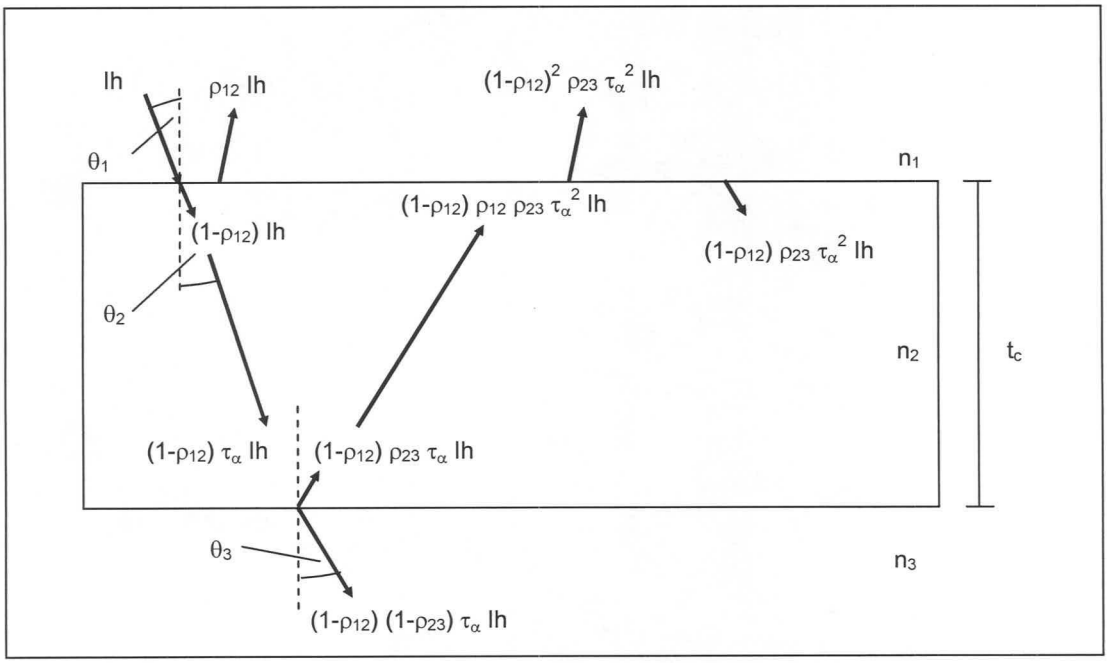

Figure B.1: Solar radiation and transmissivity through a cover with thickness t_c

In the previous equations (equations (B.4), (B.5) and (B.6)), ρ_{12} and ρ_{23} respectively define the reflectivities for the upper and lower surfaces of a cover (see figure B.1).

For the situation where the cover is surrounded by the same media ($\rho_{12} = \rho_{23} = \rho$), the effective reflectivity according to Modest [93MO1] reduces to

$$\rho' = \rho\left[1+\frac{(1-\rho)^2\,\tau_\alpha^2}{1-\rho^2\,\tau_\alpha^2}\right] \tag{B.7}$$

while the effective transmissivity simplifies to

$$\tau' = \frac{(1-\rho)^2\,\tau_\alpha}{1-\rho^2\,\tau_\alpha^2} \tag{B.8}$$

and the effective absorbtivity for a cover yields

$$\alpha' = \frac{(1-\rho)(1+\rho\,\tau_\alpha)(1-\tau_\alpha)}{1-\rho^2\,\tau_\alpha^2} = \frac{(1-\rho)(1-\tau_\alpha)}{1-\rho\,\tau_\alpha} \tag{B.9}$$

Mills [92MI1] states that the sum of the effective reflectivity (ρ'), transmissivity (τ') and absorptivity (α') of transparent medium is equal to one. Therefore comparing the equations of Duffie and Beckman [91DU1] (equations (B.1– B.3)) to those proposed by Modest [93MO1] (equations (B.4– B.6)), it is found that only the latter add up to one. Consequently, the equations of Modest [93MO1] will be used to determine the solar characteristics of the solar air heater's cover.

However, in order to determine these solar characteristics of a cover, the reflectivities of the cover interfaces (ρ_{12}, ρ_{23}) as well as the transmittance due to absorbtance, τ_α, need to be known.

From Figure B.1 it is evident that as solar radiation strikes a surface at an incidence angle θ_1, the incident solar radiation passes from one medium with a refractive index n_1, to a second medium with a refractive n_2. As a result, a certain amount of energy is reflected from the surface.

From the work of Modest [93MO1], it follows that this interface reflectivity can be evaluated with the aid of Fresnel's equation that is given by equation (B.10)

$$\rho_{12} = \frac{1}{2}\left[\frac{\tan^2(\theta_1 - \theta_2)}{\tan^2(\theta_1 + \theta_2)} + \frac{\sin^2(\theta_1 - \theta_2)}{\sin^2(\theta_1 + \theta_2)}\right] \tag{B.10}$$

with θ_2 defining the refractive angle of the interface.

The above defined incident and refractive angles are related to the indexes of refraction by Snell's law (equation (B.11))

$$\theta_2 = \arcsin\left(\frac{n_1 \sin\theta_1}{n_2}\right) \tag{B.11}$$

with n_1 and n_2 referring to the refractive indexes of the respective surfaces. The refractive indexes for a number of cover materials are given in Table B.1.

Table B 1: Refractive indexes for a number of cover materials

Material	Refractive index, n	Ref.
Air	1.0	[91DU1]
Glass	1.526	[91DU1]
Water	1.333	[92SE1]
Polytetrafluoroethylene	1.37	[91DU1]
Polyvinylfluoride	1.45	[91DU1]
Polymethyl methacrylate	1.49	[91DU1]
Polycarbonate	1.60	[91DU1]

Upon substitution of equation (B.11) into equation (B.10), the reflectivity of the upper surface's interface becomes

$$\rho_{12} = \frac{1}{2}\left[\frac{\tan^2(\theta_1 - \arcsin(n_1 \sin\theta_1 / n_2))}{\tan^2(\theta_1 + \arcsin(n_1 \sin\theta_1 / n_2))} + \frac{\sin^2(\theta_1 - \arcsin(n_1 \sin\theta_1 / n_2))}{\sin^2(\theta_1 + \arcsin(n_1 \sin\theta_1 / n_2))}\right] \tag{B.12}$$

Following a similar procedure as before, the refractive angle, θ_3, for the lower surface's interface is related to the incidence angle θ_1

$$\theta_3 = \arcsin\left(\frac{n_2 \sin\theta_2}{n_3}\right) = \arcsin\left(\frac{n_1 \sin\theta_1}{n_3}\right) \tag{B.13}$$

and as a result the reflectivity for the lower surface becomes

$$\begin{aligned}\rho_{23} &= \frac{1}{2}\left[\frac{\tan^2(\theta_2-\theta_3)}{\tan^2(\theta_2+\theta_3)}+\frac{\sin^2(\theta_2-\theta_3)}{\sin^2(\theta_2+\theta_3)}\right] \\ &= \frac{1}{2}\left[\frac{\tan^2(\arcsin(n_1\sin\theta_1/n_2)-\arcsin(n_1\sin\theta_1/n_3))}{\tan^2(\arcsin(n_1\sin\theta_1/n_2)+\arcsin(n_1\sin\theta_1/n_3))}\right] \\ &+ \frac{1}{2}\left[\frac{\sin^2(\arcsin(n_1\sin\theta_1/n_2)-\arcsin(n_1\sin\theta_1/n_3))}{\sin^2(\arcsin(n_1\sin\theta_1/n_2)+\arcsin(n_1\sin\theta_1/n_3))}\right]\end{aligned} \tag{B.14}$$

As solar radiation passes through a cover, a certain amount of the solar energy is absorbed in the cover. From Bouguer's law it follows that the transmissivity due to absorbtance of a partially transparent medium, with a thickness of t_c and coefficient of extinction C_e, is

$$\tau_\alpha = e^{-C_e t_c/\cos(\theta_2)} \tag{B.15}$$

Substituting Snell's law (equation (B.11)) into equation (B.15), Bouguer's law yields

$$\tau_\alpha = e^{-C_e t_c/\cos(\arcsin(n_1\sin\theta_1/n_2))} \tag{B.16}$$

However, to be able to evaluate the reflectivities, ρ_{12} and ρ_{23}, of the upper and lower surfaces of a cover as well as the covers transmissivity due to absorbtance, τ_α, the incidence angle, θ, of the solar radiation on the cover is required.

B.2 Determination of incidence angle

The solar radiation incident on a surface consists of beam and diffuse radiation. Beam radiation is defined as solar radiation that is received from the sun without having been scattered by the atmosphere, while diffuse radiation is solar radiation that has been scattered in the atmosphere.

Since diffuse radiation is incident from all directions, Duffie and Beckman [91DU1] propose that an equivalent incidence angle of 60° should be used for the evaluation of the diffuse solar characteristics of a cover.

In Figure B.2, a flat plate, with any particular orientation, is considered with beam solar radiation incident at an angle θ_b, with respect to the normal to the surface.

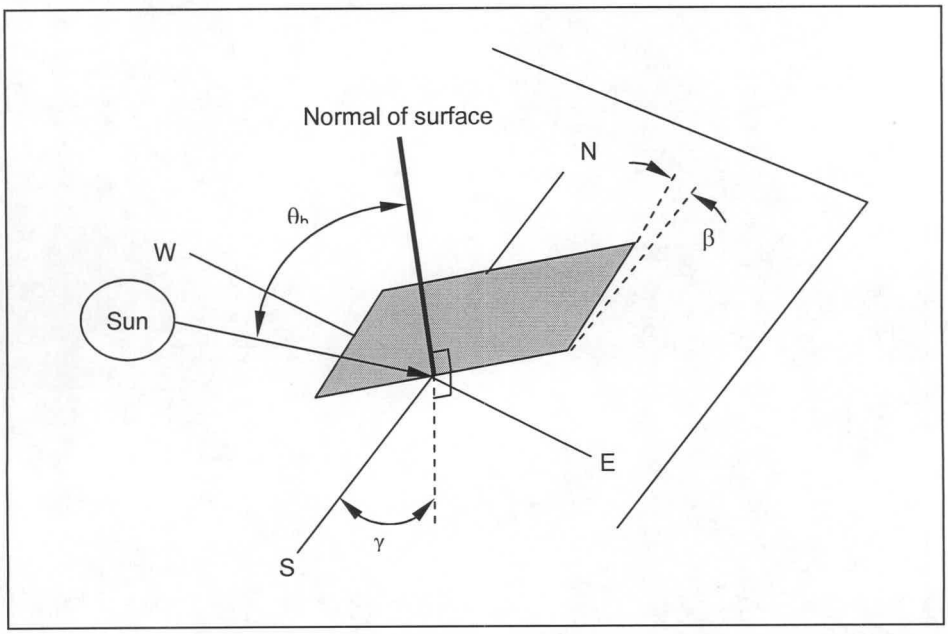

Figure B.2: Angles associated with the evaluation of the beam incidence angle

Duffie and Beckman [91DU1] suggest that the following equation be used for the evaluation of the beam incidence angle for the above shown surface.

$$\cos\theta_b = \sin\delta\sin\phi\cos\beta - \sin\delta\cos\phi\sin\beta\cos\gamma + \cos\delta\cos\phi\cos\beta\cos\omega + \cos\delta\sin\phi\sin\beta\cos\omega\cos\gamma + \cos\delta\sin\beta\sin\omega\sin\gamma \quad \text{(B.17)}$$

In equation (B.17), ϕ is the latitude angle or angular location of the experimental set-up north or south of the equator, with δ defining the declination angle or angular position of the sun at solar noon with respect to the plane of the equator. North is defined as positive for both angles.

The declination angle can be evaluated from equation (B.18), [91DU1]

$$\delta = 23.45\sin\left(360\frac{284+DOY}{365}\right) \quad \text{(B.18)}$$

with DOY defining the respective day of the year, with the 1st of January being the first day of the year.

Through personal communication with the SAWB [00SA1] (South African Weather Bureau) the following alternative equation was obtained for the evaluation of the declination angle

$$\delta = [0.00661 + 0.40602 \sin(P - 1.4075) + 0.00665 \sin(2P - 1.4789) + 0.00298 \sin(3P - 1.0996)] \frac{180}{\pi} \quad \text{(B.19)}$$

with P referring to the annual phase angle on the day of the year, which is to be evaluated according to

$$P = 0.0172028 (DOY + YADJ) \quad \text{(B.20)}$$

In the phase angle equation, YADJ is the leap year adjustment to the day-of–year, as given by the following equation

$$YADJ = 0.25 [2.5 - (Y - 4 (\text{integer}((Y - 1)/4)))] \quad \text{(B.21)}$$

in which Y is the year for which the calculation is conducted. For annual phase angle values at midday SA standard time, the DOY needs to be increased by 0.417 day according to the SAWB [00SA1].

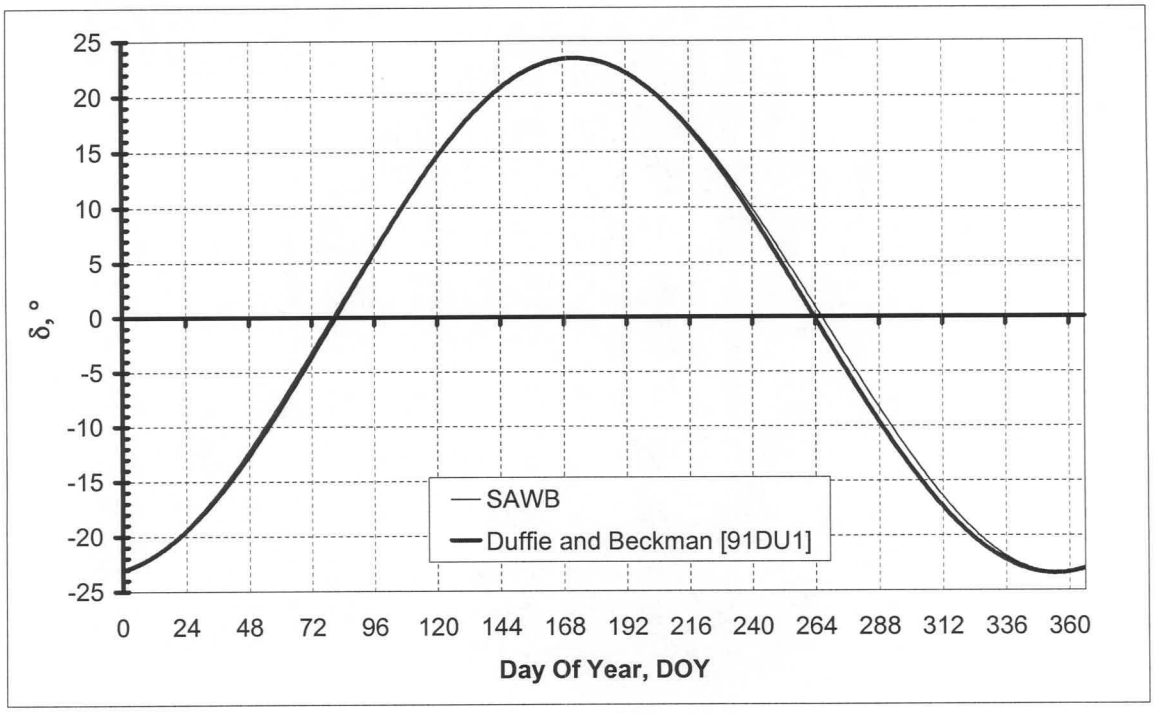

Figure B.3: Declination angle comparison

Comparing the two proposed declination angle equations for the year 2000, it is evident from Figure B.3 that there is a slight deviation at the end of the year, between the SAWB [00SA1] and Duffie and Beckman [91DU1] relations. This deviation can be attributed to the fact that the equation of Duffie and Beckman [91DU1] does not make provision for leap year calculations. Consequently, the SAWB's equations will be used for the determination of the declination angle.

Furthermore, from Figure B.2 it follows that β defines the slope angle between the plane of the surface in question and the horizontal. If $\beta > 90°$ then it means that surface has a downward facing component.

The deviation of the projection on a horizontal plane of the normal to the surface from the local meridian is known as a surface azimuth angle, γ, with an angle of zero defining due south. Any angle east from south is defined as negative.

The hour angle, ω, is defined as the angular displacement of the sun east or west of the local meridian, with morning defined as negative and the afternoon as positive. Taking into consideration the fact that the earth is rotating at 15° per hour, Duffie and Beckman [91DU1] states that the hour angle should be evaluated according to equation (B.22)

$$\omega = 15\left[\psi - 12 - \frac{4(L_{st} - L_{loc}) - EOT}{60}\right] \tag{B.22}$$

In the above equation, ψ refers to the hours after midnight, expressed in decimal format (ex. 16:35 = 16.5833) and ϕ_m and ϕ_l to the respective standard meridian for the specific time zone and longitude angle of the location. For the evaluation of the equation of time, EOT, the SAWB [00SA1] proposed the following equation

$$\begin{aligned} EOT = 1440\,[\,&0.005114\sin(P + 3.0593) + 0.006892\sin(2P + 3.4646) \\ &+ 0.00022\sin(3P + 3.3858) + 0.000153\sin(4P + 3.7766)\,] \end{aligned} \tag{B.23}$$

with the annual phase angle, P, evaluated according to equation (B.20).

For a horizontal surface the slope angle (β) is equal to zero, with the result that the beam incidence angle equation (equation (B.17)) simplifies to

$$\cos\theta_b = \sin\delta\sin\phi + \cos\delta\cos\phi\cos\omega \tag{B.24}$$

B.3 Evaluation of the effective solar absorptivity of an absorber plate

To be able to predict the performance of either a solar collector or heater, the amount of solar radiation that is absorbed by the absorber plate is required.

Therefore, consider the schematic presentation of an absorber plate of either a solar collector or solar collector or solar air heater as shown in Figure B.4. From this figure, it is evident that the solar radiation effectively absorbed by the absorber plate is a function of the effective transmissivity of the cover as well as the solar absorptivity, α_p, of the absorber plate.

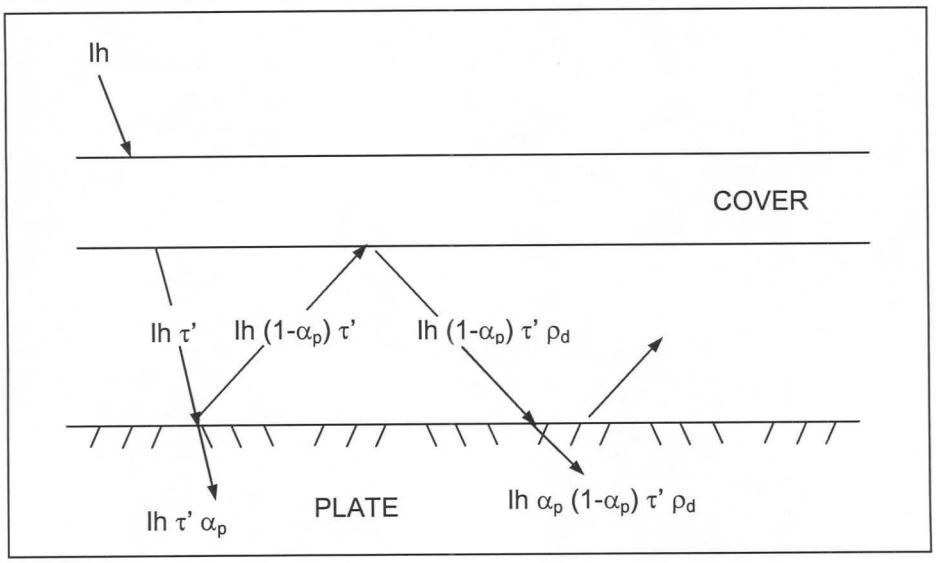

Figure B.4: Effective transmittance-absorbtance product

Accounting for multiple reflections and assuming that the reflected energy is diffuse, the effective transmittance-absorbtance product for the absorber plate considered in Figure B.4, according to Duffie and Beckman [91DU1] is

$$(\tau' \alpha_p) = \alpha_p \left[\frac{\tau'}{1-(1-\alpha_p)\rho_d} \right] \qquad \text{(B.25)}$$

Upon substitution of equation (B.8) into the above equation for the effective transmissivity of the cover, the equation for the evaluation of the plate transmittance-absorbtance product yields

$$\left(\tau'\alpha_p\right)=\left(\frac{\alpha_p}{1-\left(1-\alpha_p\right)\rho_d}\right)\left[\frac{\left(1-\rho\right)^2\tau_\alpha}{1-\rho^2\,\tau_\alpha^2}\right] \tag{B.26}$$

with ρ_d defining the diffuse reflectivity of the bottom surface of the cover.

Appendix C: Glass coefficient of extinction

The refractive index for glass, according to a number of authors [91DU, 92SE1, 93MO1] is equal to 1.526, while the extinction coefficient ranges from 4 m^{-1} to 32 m^{-1}. An experiment was conducted in order to determine the extinction coefficient for the glass cover used in the present investigation.

C.1 Experiment and analysis

The experimental apparatus, as shown by Figure C.1, consisted of a 1m x 1m box, covered by a 3.88 mm glass pane with a 50 mm thick polystyrene base plate. Two different experimental set-ups were used in which the upper side of the plate was covered by either a black painted or a highly reflective aluminium foil. The absorbtivity of the black paint was 0.9 and that of the aluminium foil was 0.1.

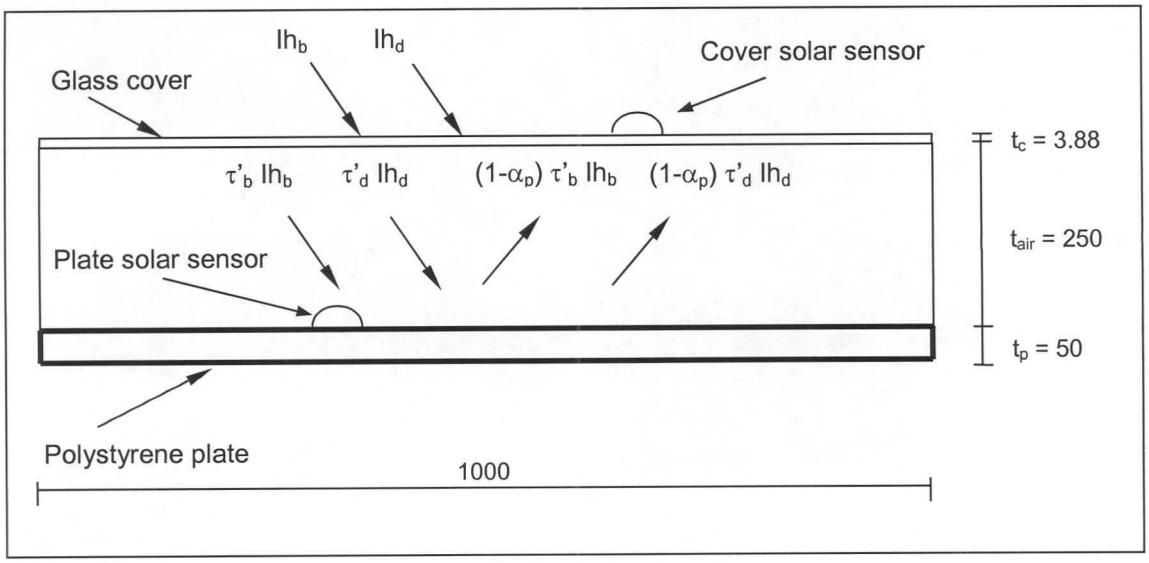

Figure C.1: Apparatus for determining the extinction coefficient of a glass cover.

The total incident solar radiation on the cover and the plate was measured at 10 second intervals by solar sensors placed on the respective surfaces.

Considering the cover's reflectivity and absorptivity of short-wave radiation, the net solar radiation striking the plate was found according to equation (B.25),

$$Ih_p = Ih_b\left(\frac{\tau_b'}{1-(1-\alpha_p)\rho_d}\right) + Ih_d\left(\frac{\tau_d'}{1-(1-\alpha_p)\rho_d}\right) = \left(\frac{1}{1-(1-\alpha_p)\rho_d}\right)\left(\tau_b' Ih_b + \tau_d' Ih_d\right) \quad (C.1)$$

The cover was surrounded by air with a refractive index, n_a, of unity. Thus, upon substituting equation (B.8) into equation (C.1) the equation for the prediction of the incident solar radiation on the plate becomes

$$Ih_p = \left(\frac{1}{1-(1-\alpha_p)\rho_d}\right)\left(\frac{(1-\rho_b)^2\,\tau_{\alpha b}}{1-\rho_b^2\,\tau_{\alpha b}^2} Ih_b + \frac{(1-\rho_d)^2\,\tau_{\alpha d}}{1-\rho_d^2\,\tau_{\alpha d}^2} Ih_d\right) \quad (C.2)$$

C.2 Results

The solar radiation measured on the glass cover and black plate (α_p = 0.9) respectively are shown in Figure C.2. A similar graph is shown in Figure C.3 for the silver plate (α_p = 0.1).

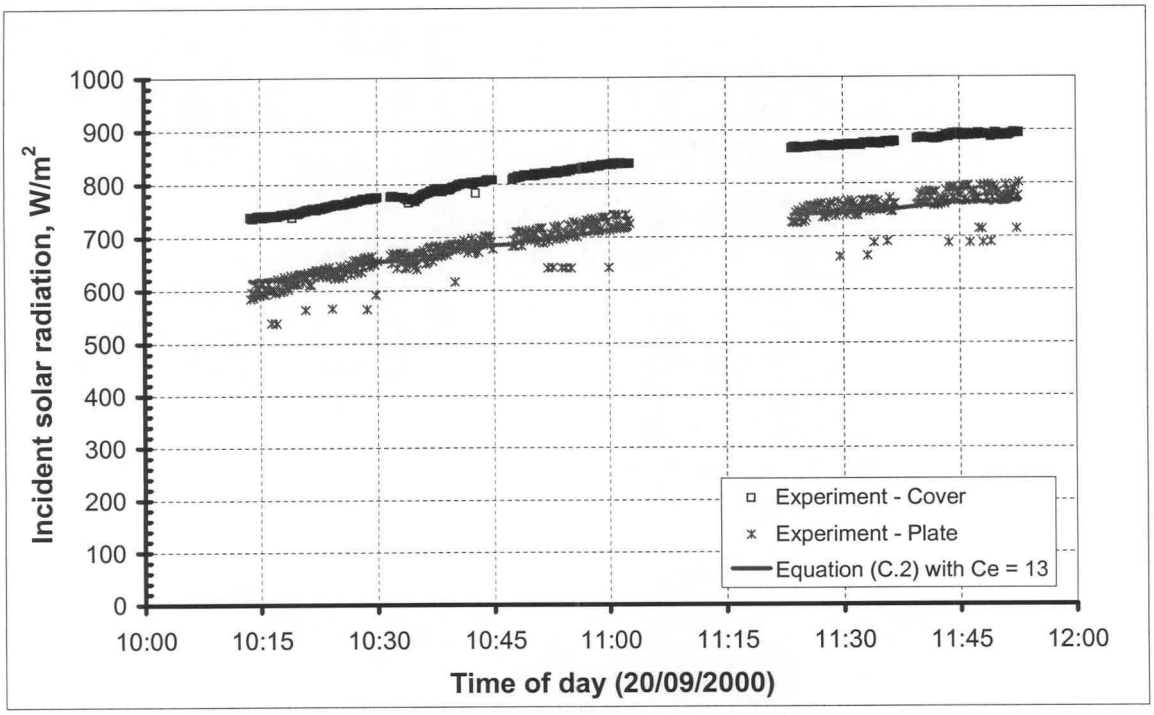

Figure C.2: Solar radiation with black plate

From the available radiation data, it is possible to determine the extinction coefficient, C_e, of the glass cover with the aid of equation (C.2). A numerical example follows.

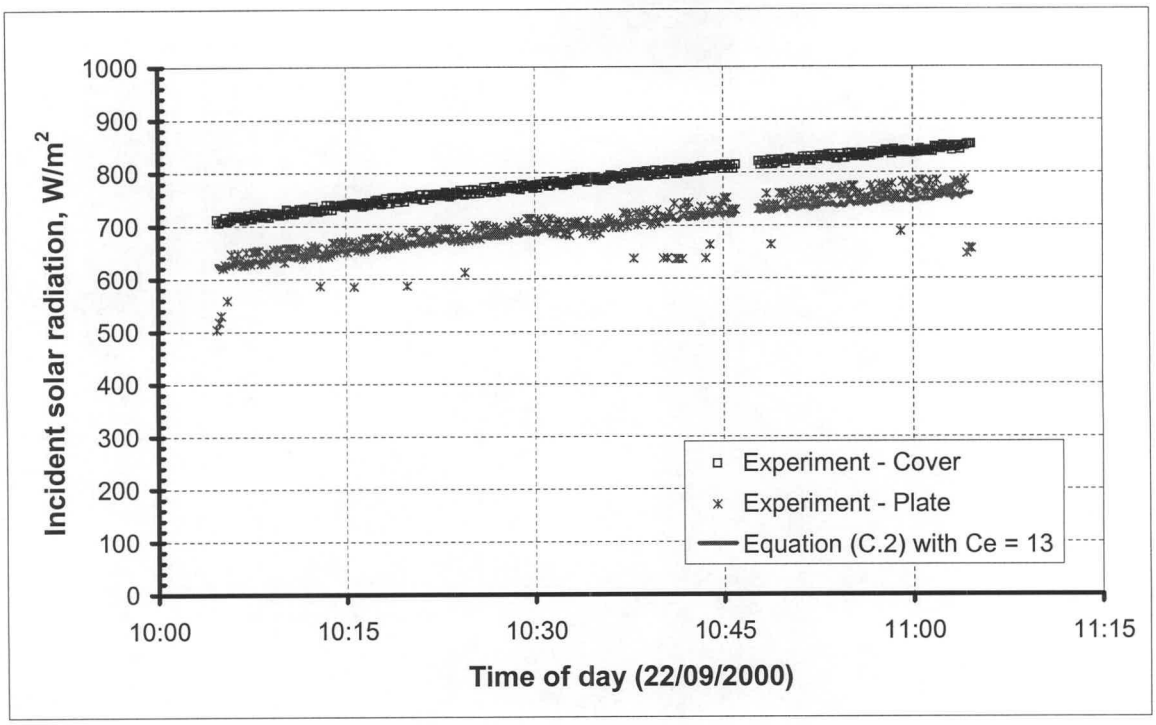

Figure C.3: Solar radiation with silver plate

Numerical example

On the 21st of September 2000 at 11h35:06 the cover solar sensor measured an incident radiation of 877.1 W / m^2, while the sensor on the black plate measured 750.86 W / m^2 for the total incident radiation on the plate. At the same time, the diffuse solar radiation measured by the cover solar sensor was 7.25 % of the total incident solar radiation. Hence the incident beam solar radiation is

$$Ih_b = 0.9275 Ih_T = 0.9275 \times 877.1 = 813.51 \text{ W} / \text{m}^2$$

while the diffuse radiation is

$$Ih_d = 0.0725 Ih_T = 0.725 \times 877.1 = 63.59 \text{ W} / \text{m}^2.$$

According to equation (B.21) the leap year adjustment to the day is

$$YADJ = 0.25\,[2.5 - (Y - 4\,(\text{integer}((Y-1)/4)))] = 0.25 \times [2.5 - (2000 - 4\,(\text{integer}((2000-1)/4)))]$$

$$= -0.375 \text{ days}$$

with the above integer function yielding a value of 499.

The 21st of September is the 265th day of the year 2000. Hence, Duffie and Beckman [91DU1] (equation (B.18)) predict a declination angle of.

$$\delta = 23.45 \sin\left(360\frac{284+\text{DOY}}{365}\right) = 23.45 \sin\left(360\frac{284+265}{365}\right) = -0.6054^{\circ}$$

Using equation (B.20), the annual phase angle is evaluated for the 265th day.

$$P = 0.017208(\text{DOY} + \text{YADJ} + 0.417) = 0.0172028 \times (265 + (-0.375) + 0.417) = 4.561 \text{ rad.}$$

Substituting the annual phase angle into equation (B.19), the declination angle according to the SAWB is found to be

$$\begin{aligned}\delta &= [0.00661 + 0.40602 \sin(P - 1.4075) + 0.00665 \sin(2P - 1.4789) \\ &\quad + 0.00298 \sin(3P - 1.0996)]\frac{180}{\pi} \\ &= [0.00661 + 0.40602 \sin(4.561 - 1.4075) + 0.00665 \sin(2 \times 4.561 - 1.4789) \\ &\quad + 0.00298 \sin(3 \times 4.561 - 1.0996)]\frac{180}{\pi} \\ &= 0.4807^{\circ}\end{aligned}$$

Making use of the previously determined phase angle, the equation of time is calculated from equation (B.23).

$$\begin{aligned}\text{EOT} &= 1440\,[0.005114 \sin(P + 3.0593) + 0.006892 \sin(2P + 3.4646) \\ &\quad + 0.00022 \sin(3P + 3.3858) + 0.000153 \sin(4P + 3.7766)] \\ &= 1440\,[0.005114 \sin(4.561 + 3.0593) + 0.006892 \sin(2 \times 4.561 + 3.4646) \\ &\quad + 0.00022 \sin(3 \times 4.561 + 3.3858) + 0.000153 \sin(4 \times 4.561 + 3.7766) \\ &= 7.045 \text{ min.}\end{aligned}$$

The standard meridian for the time zone, ϕ_m, and longitude angle of the location, ϕ_l, are 30° E and 18.85° E respectively. The measurements taken at 11h35:06 or 11.583 hours after midnight and therefore the hour angle according to equation (B.22), is

$$\omega = 15\left[\psi - 12 - \frac{4(L\phi_m - \phi_l) - EOT}{60}\right] = 15\left[11.583 - 12 - \frac{4(30 - 18.85) - 7.045}{60}\right] = -15.64°.$$

Employing the SAWB declination angle, the beam incidence angle, θ_b, for a horizontal cover, according to equation (B.24) is

$$\theta_b = a\cos(\sin\delta\sin\phi + \cos\delta\cos\phi\cos\omega)$$

$$= a\cos(\sin 0.4809 \times \sin -33.98 + \cos -33.98 \times \cos 0.4809 \times \cos -15.64) = 37.478°.$$

The cover is surrounded by air (n_a =1) and the refractive index of glass, n_c, is given as 1.526 by a number of authors [91DU1, 92SE1, 93MO1]. The beam reflectivity of the cover, according to equation (B.12) is thus

$$\rho_b = \frac{1}{2}\left[\frac{\tan^2(\theta_b - \arcsin(n_a \sin\theta_b / n_c))}{\tan^2(\theta_b + \arcsin(n_a \sin\theta_b / n_c))} + \frac{\sin^2(\theta_b - \arcsin(n_a \sin\theta_b / n_c))}{\sin^2(\theta_b + \arcsin(n_a \sin\theta_b / n_c))}\right]$$

$$= \frac{1}{2}\left[\frac{\tan^2(37.478 - \arcsin(\sin 37.478 / 1.526))}{\tan^2(37.478 + \arcsin(\sin 37.478 / 1.526))} + \frac{\sin^2(37.478 - \arcsin(\sin 37.478 / 1.526))}{\sin^2(37.478 + \arcsin(\sin 37.478 / 1.526))}\right]$$

$$= 0.0477$$

Duffie and Beckman [91DU1] further that an incidence angle of 60° (θ_d) should be used in the evaluation of the diffuse radiation properties. Consequently, the diffuse reflectivity of the cover yields a value of

$$\rho_d = \frac{1}{2}\left[\frac{\tan^2(\theta_d - \arcsin(n_a \sin\theta_d / n_c))}{\tan^2(\theta_d + \arcsin(n_a \sin\theta_d / n_c))} + \frac{\sin^2(\theta_d - \arcsin(n_a \sin\theta_d / n_c))}{\sin^2(\theta_d + \arcsin(n_a \sin\theta_d / n_c))}\right]$$

$$= \frac{1}{2}\left[\frac{\tan^2(60 - \arcsin(\sin 60 / 1.526))}{\tan^2(60 + \arcsin(\sin 60 / 1.526))} + \frac{\sin^2(60 - \arcsin(\sin 60 / 1.526))}{\sin^2(60 + \arcsin(\sin 60 / 1.526))}\right] = 0.09346$$

From an iterative procedure, evolving the solution of equation (C.2) and Bouguer's law repeatedly, a value of 13 is obtained for the coefficient of extinction for the glass. Hence, from equation (B.16) it follows that the transmittance due absorbtance for beam radiation is

$$\tau_{b\alpha} = e^{-C_e t_c / \cos(\arcsin(n_a \sin\theta_b / n_c))} = e^{-13 \times 0.00388 / \cos(\arcsin(\sin 37.935 / 1.526))} = 0.94648$$

and for diffuse radiation

$$\tau_{d\alpha} = e^{-C_e\, t_c / \cos(\arcsin(n_a \sin\theta_d / n_c))} = e^{-13\times 0.00388 / \cos(\arcsin(\sin 60 / 1.526))} = 0.94058$$

Upon substituting of the previously determined beam and diffuse reflectivities and transmittance due to absorbtance values into equation (C.2), the net solar radiation striking the plate is

$$Ih_p = \left(\frac{1}{1-(1-\alpha_p)\rho_d}\right)\left(\frac{(1-\rho_b^2)\tau_{b\alpha}}{1-\rho_b^2\,\tau_{b\alpha}}\, Ih_b + \frac{(1-\rho_d^2)\tau_{d\alpha}}{1-\rho_d^2\,\tau_{d\alpha}} Ih_d\right)$$

$$= \left(\frac{1}{1-(1-0.9)\times 0.09346}\right)\left(\frac{(1-0.0477^2)\times 0.94648}{1-0.0477^2\times 0.94648^2}\times 813.51 + \frac{(1-0.09346^2)\times 0.94058}{1-0.09346^2\times 0.94058^2}\times 63.59\right)$$

$$= 750.21\ W/m^2$$

From the above calculation, it is evident that the theoretical value shows good agreement with the measured radiation for C_e = 13. Similar calculations were conducted for other measured points.

Appendix D: Solar collector test

The objective of this experiment was to measure the glass cover and plate temperatures of a solar collector under given ambient conditions, whereafter experimentally measured temperatures were compared to theoretically predicted values. Good agreement between the predicted and experimental values would imply that the equations employed are reliable.

D.1 Experimental apparatus

The experimental apparatus is shown in Figure D.1.

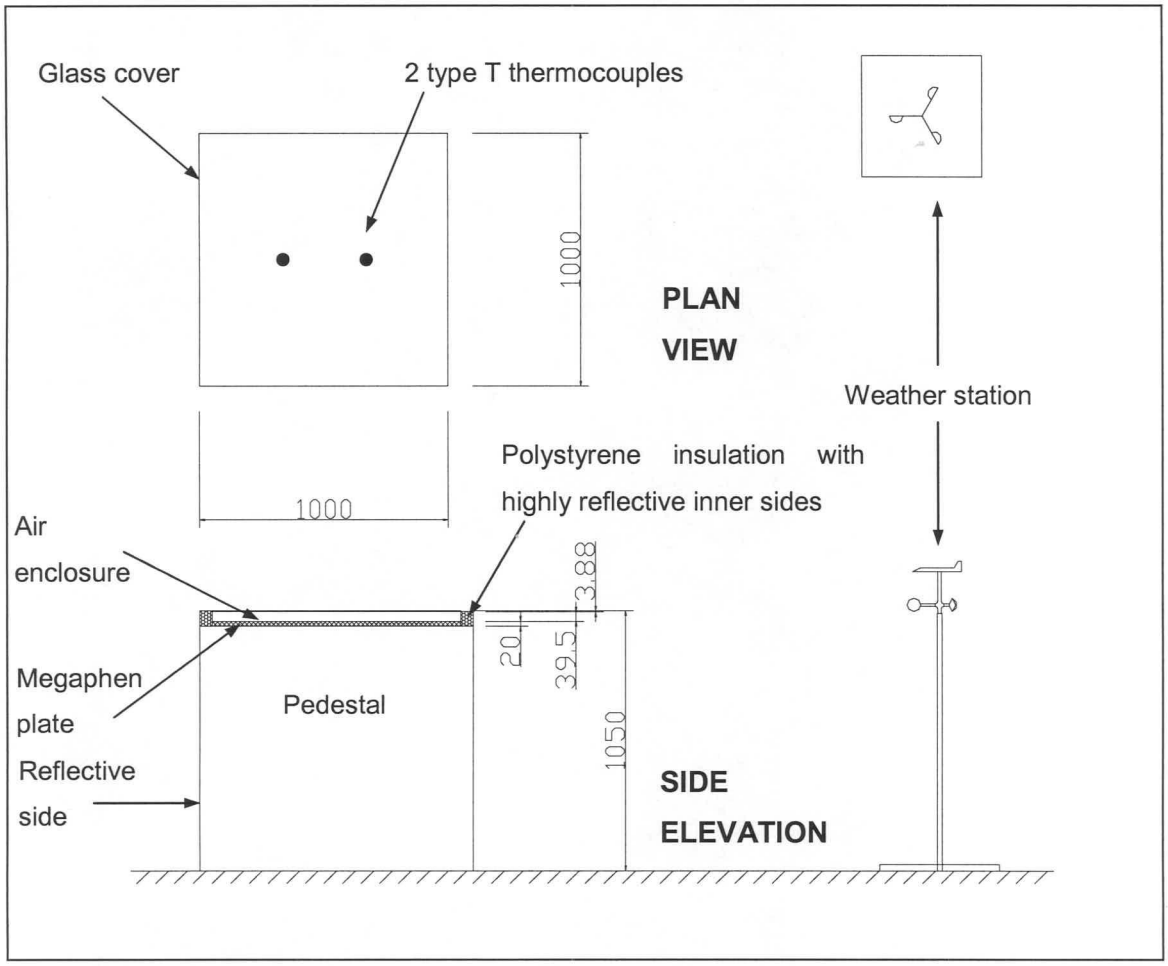

Figure D.1: Schematic representation of solar collector apparatus

The apparatus shown in Figure D.1 consisted of a 3.88 mm thick square glass cover (1m x 1m) and a 20 mm thick black (painted) megaphen solar collector plate (k = 0.02 W/mK). A 39.5 mm air gap separated the cover and plate, while the sides of the collector were insulated by a

50 mm thick polystyrene layer. The sides were covered by a highly reflective aluminium foil ($\alpha = \varepsilon = 0.1$) in order to minimise the side effects on the heat transfer between the plate and cover.

A square pedestal, having highly reflective sides, supported the collector at an elevation of 1.05 m above ground level

The plate and cover temperatures were measured with four type T-thermocouples; two on each surface. Thermocouple readings were taken at 10-second intervals, while the total incident solar radiation was measured by a solar sensor (Kipp and Zonen) placed on the top of the cover. The ambient conditions were monitored by a weather station (Davis Weather Monitor II) positioned next to the experimental set-up as shown in Figure D.2.

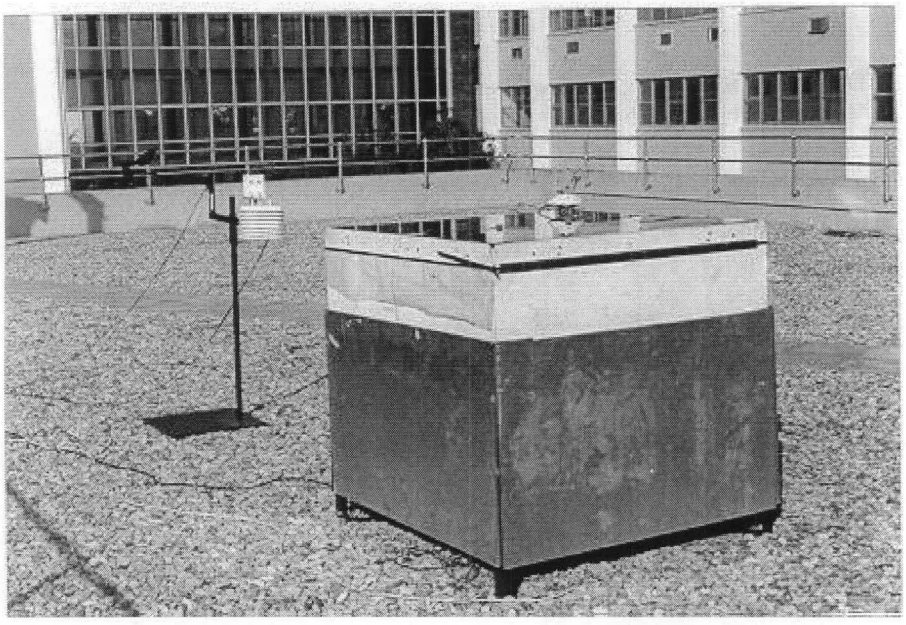

Figure D.2: Experimental apparatus

D.2 Analysis

The respective cover and absorber plate surfaces will be considered separately in the following sections.

D.2.1 Cover

In Figure D.3 the cover of a solar collector is considered.

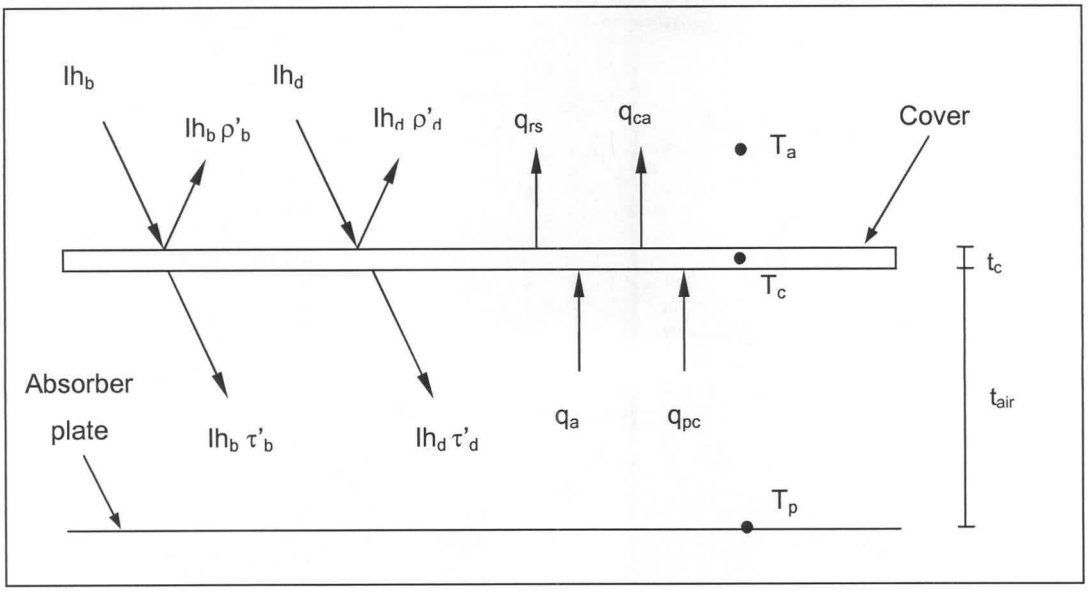

Figure D.3: Energy balance on cover

Applying an energy balance to the cover shown in Figure D.3, the following cover energy equation is obtained

$$Ih_b + Ih_d + q_a + q_{pc} = \rho_b' Ih_b + \rho_d' Ih_d + \tau_b' Ih_b + \tau_d' Ih_d + (q_{ca} + q_{rs}) + \rho_c t_c c_{pc} \frac{dT_c}{dt} \qquad (D.1)$$

Due to the highly reflective sides any radiation heat exchange between the sides and the cover and absorber plate are neglected. Furthermore, the conduction losses through the well-insulated absorber plate and sides of the solar collector are assumed to be negligible. Rearranging terms, equation (D.1) simplifies to

$$(1 - \rho_b' - \tau_b')Ih_b + (1 - \rho_d' - \tau_d')Ih_d + q_a + q_{pc} = (q_{ca} + q_{rs}) + \rho_c t_c c_{pc} \frac{dT_c}{dt} \qquad (D.2)$$

Since $\rho' + \tau' + \alpha' = 1$, equation (D.2) can be simplified to give

$$\alpha_b' Ih_b + \alpha_d' Ih_d + q_a + q_{pc} = (q_{ca} + q_{rs}) + \rho_c t_c c_{pc} \frac{dT_c}{dt} \qquad (D.3)$$

Substitute equation (B.9) for the cover beam and diffuse absorptivity, α', into equation (D.3), find

$$\frac{(1-\rho_b)(1-\tau_{b\alpha})}{1-\rho_b\,\tau_{b\alpha}} Ih_b + \frac{(1-\rho_d)(1-\tau_{d\alpha})}{1-\rho_d\,\tau_{d\alpha}} Ih_d + q_a + q_{pc} = (q_{ca} + q_{rs}) + \rho_c\, t_c\, c_{pc} \frac{dT_c}{dt} \qquad (D.4)$$

For calculations conducted close to solar noon (i.e. steady state conditions prevail), the assumption was made that the rate of change of the glass cover temperature is negligible, with the result that the cover energy equation of the solar collector reduces to

$$\frac{(1-\rho_b)(1-\tau_{b\alpha})}{1-\rho_b\,\tau_{b\alpha}} Ih_b + \frac{(1-\rho_d)(1-\tau_{d\alpha})}{1-\rho_d\,\tau_{d\alpha}} Ih_d + q_a + q_{pc} = (q_{ca} + q_{rs}) \qquad (D.5)$$

with q_{pc} defining the radiative heat transfer between the cover and the plate and q_a the respective convective heat transfer occurring between the cover, enclosed air and absorber plate. The total heat loss from the cover, due to long-wave radiation and convection, is given by (q_{ca} + q_{rs}), while the reflectivity, ρ, as well as the transmittance due to absorbtance of the cover, τ_α, for beam and diffuse radiation are evaluated according to equations (B.12) and (B.16) respectively.

The total heat loss from a square cover with side length, L_c, and emissivity, ε_c, to the environment, according to equation (A.8), is

$$(q_{ca} + q_{rs}) = \left[(Gr_{ca}\, Pr_{ca})^{1/3} \left(0.227 + 1.406\times10^{-6}\, Re_{ca}\right)\right]\frac{k_{ca}}{L_c}(T_c - T_a) + \varepsilon_c\, \sigma \left(T_c^4 - \left(0.0552\, T_a^{1.5}\right)^4\right) \qquad (D.6)$$

with T_c and T_a the respective cover and ambient temperatures expressed in degrees Kelvin, and σ the Stephan-Boltzmann constant.

For steady state conditions (as in the case at solar noon), the convective heat transfer from the entrapped air to the cover is the same as the convective hear transfer from the plate to the entrapped air. Thus, the convective heat exchange between the cover and plate, according to Mills [92MI1], is

$$q_a = h_a (T_p - T_c) \qquad (D.7)$$

For the case where the plate is the warmer of the two surfaces, Holland et al.'s [76HO1] equation is employed for the evaluation of the heat transfer coefficient, h_a.

$$h_a = \left[1+1.44\left[1-\frac{1708}{Gr_{pc}\,Pr_{pc}}\right]+\left[\left(\frac{Gr_{pc}\,Pr_{pc}}{5830}\right)^{1/3}-1\right]\right]\frac{k_{pc}}{t_{air}} \tag{D.8}$$

The above equation is valid for Rayleigh numbers ranging from 0 to 10^8.

Due to the reflective inner sides, the assumption can be made that the cover surface and absorber plate is two infinite parallel plates. Consequently, for two parallel opposing plates (cover and absorber plate), the net long-wave radiation heat exchange, according to Mills [92MI1], is

$$q_{pc} = \sigma\left(\frac{1}{\varepsilon_c}+\frac{1}{\varepsilon_p}-1\right)^{-1}\left(T_p^4 - T_c^4\right) \tag{D.9}$$

in which ε_c and ε_p are the respective cover and absorber plate emissivities.

Substitute equations (D.6), (D.7), (D.8) and (D.9) into equation (D.5), and find

$$\begin{aligned}&\frac{(1-\rho_b)(1-\tau_{\alpha b})}{1-\rho_b\,\tau_{\alpha b}}Ih_b+\frac{(1-\rho_d)(1-\tau_{\alpha d})}{1-\rho_d\,\tau_{\alpha d}}Ih_d+\sigma\left(\frac{1}{\varepsilon_c}+\frac{1}{\varepsilon_p}-1\right)^{-1}\left(T_p^4-T_c^4\right)\\&+\left[1+1.44\left[1-\frac{1708}{Gr_{pc}\,Pr_{pc}}\right]+\left[\left(\frac{Gr_{pc}\,Pr_{pc}}{5830}\right)^{1/3}-1\right]\right]\frac{k_{pc}}{t_{air}}\left(T_p-T_c\right)\\&=\left[\left(Gr_{ca}\,Pr_{ca}\right)^{1/3}\left(0.227+1.406\times10^{-6}\,Re_{ca}\right)\right]\frac{k_{ca}}{L_c}\left(T_c-T_a\right)+\varepsilon_c\,\sigma\left(T_c^4-\left(0.0552\,T_a^{1.5}\right)^4\right)\end{aligned} \tag{D.10}$$

for the steady state conservation of energy equation for the cover of the solar collector.

D.2.2 Absorber plate

From the schematic presentation of the absorber plate (Figure D.4), the following energy equation is written for the top surface of the insulated absorber plate. Neglecting radiation from the sides and conduction losses through the insulated absorber plate, find

$$Ih_b\,\tau_b' + Ih_d\,\tau_d' = (1-\alpha_p)Ih_b\,\tau_b' + (1-\alpha_p)Ih_d\,\tau_d' + q_a + q_{pc} \tag{D.11}$$

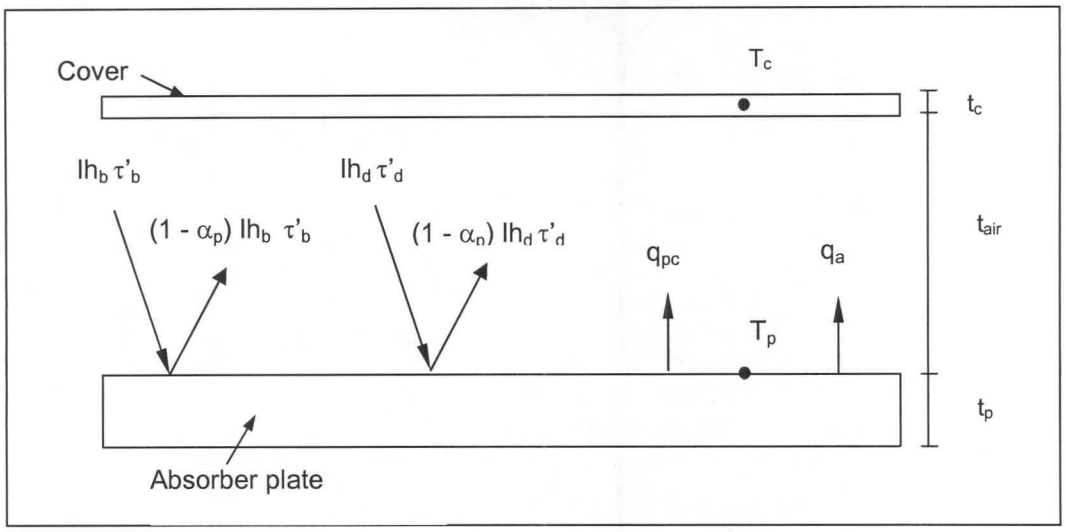

Figure D.4: Energy balance on top surface of insulated absorber plate

From Appendix B (equation (B.26)) the net solar radiation absorbed by the absorber plate is given by

$$\left(\tau' \alpha_p\right) = \left(\frac{\alpha_p}{1-\left(1-\alpha_p\right)\rho_d}\right)\left[\frac{\left(1-\rho\right)^2 \tau_\alpha}{1-\rho^2\ \tau_\alpha^2}\right] \tag{D.12}$$

with α_p defining the solar absorbtance of the absorber plate.

Substituting equation (D.12) for the net absorbed solar radiation into equation (D.11), the, plate surface energy equation yields

$$\left(\frac{\alpha_p}{1-\left(1-\alpha_p\right)\rho_d}\right)\left[\frac{\left(1-\rho_b\right)^2 \tau_{b\alpha}}{1-\rho_b^2\ \tau_{b\alpha}^2}\right] Ih_b + \left(\frac{\alpha_p}{1-\left(1-\alpha_p\right)\rho_d}\right)\left[\frac{\left(1-\rho_d\right)^2 \tau_\alpha}{1-\rho_d^2\ \tau_{d\alpha}^2}\right] Ih_d = q_a + q_{pc} \tag{D.13}$$

Upon substituting equations (D.7), (D.8) and (D.9) into equation (D.13), the following steady state equation is obtained for the conservation of energy equation for the top surface of the insulated absorber plate of the solar collector under consideration.

$$\left(\frac{\alpha_p}{1-(1-\alpha_p)\rho_d}\right)\left[\frac{(1-\rho_b)^2\,\tau_{b\alpha}}{1-\rho_b^2\,\tau_{b\alpha}^2}\right]Ih_b+\left(\frac{\alpha_p}{1-(1-\alpha_p)\rho_d}\right)\left[\frac{(1-\rho_d)^2\,\tau_{\alpha}}{1-\rho_d^2\,\tau_{d\alpha}^2}\right]Ih_d$$

$$=\left[1+1.44\left[1-\frac{1708}{Gr_{pc}\,Pr_{pc}}\right]+\left[\left(\frac{Gr_{pc}\,Pr_{pc}}{5830}\right)^{1/3}-1\right]\right]\frac{k_{pc}}{t_{air}}(T_p-T_c) \qquad \text{(D.14)}$$

$$+\sigma\left(\frac{1}{\varepsilon_c}+\frac{1}{\varepsilon_p}-1\right)^{-1}\left(T_p^4-T_c^4\right)$$

By solving equations (D.10) and (D.14) simultaneously, the cover and plate temperatures of the solar collector can be predicted for given ambient conditions.

D.3 Results and conclusion

The results of measurements conducted during midday on the 27th of October 2000, when essentially steady state conditions prevailed, are shown in Figure D.5. Employing equation (D.10) and equation (D.14), the absorber plate and cover temperatures of the solar collector were predicted for this day.

The agreement between the measured temperatures (T_c and T_p) and the predicted values was very good, as evident from Figure D.5. This suggests that the theoretical approach and equations used make it possible to predict the performance of this type of collector to a high degree of accuracy.

A numerical example, in which the cover and absorber plate temperatures are predicted theoretically at a time during this period, is presented in the following section.

Numerical example

Using the experimental and environmental data given in Table D.1, the cover and absorber plate temperatures for the 1m x 1m solar collector are predicted for the 27th of October 2000 (DOY = 271th day of year) at 12h39:44(ψ = 12.6622 hours after midnight).

In the following sample calculation it will be shown that the energy equations (D.10) and (D.14) are satisfied for T_c = 56.7046 °C (329.8546 K) and T_p = 115.448 °C (388.598 K).

The 21st of September is the 271st day of the year 2000. Consequently, the leap year adjustment (equation (B.21)) is

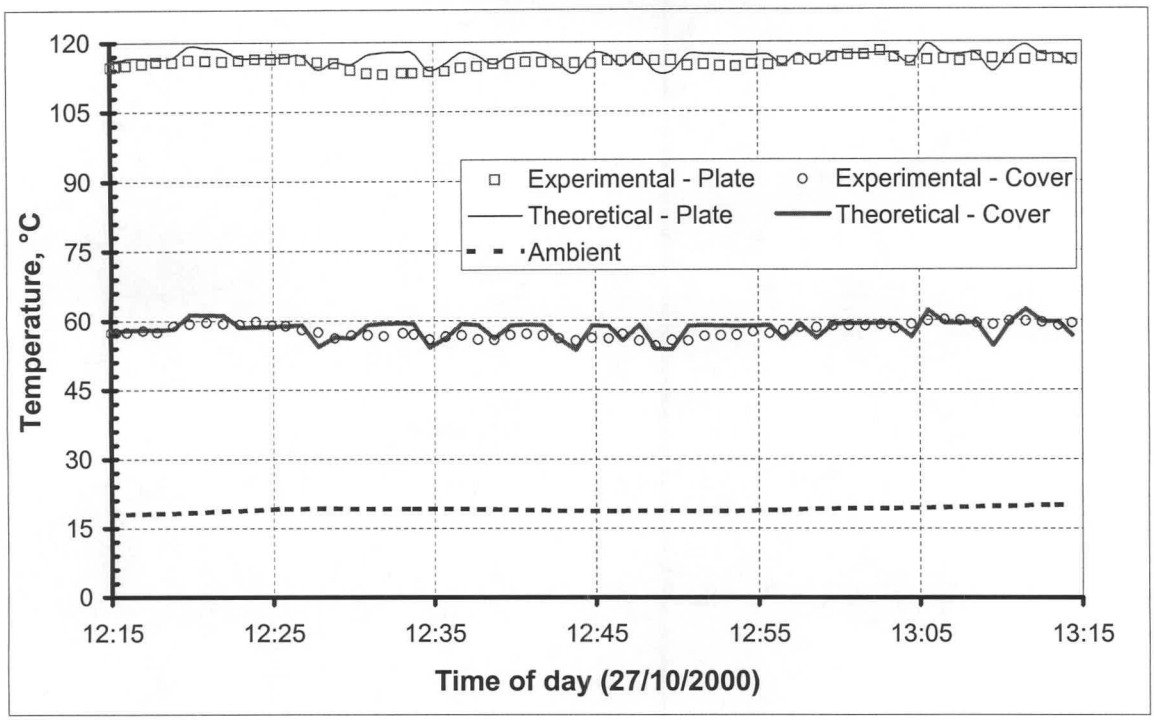

Figure D.5: Experimental and theoretical cover and absorber plate temperatures of a solar collector

$$YADJ = 0.25\,[2.5 - (Y - 4\,(\text{integer}((Y-1)/4)))]$$
$$= 0.25 \times [2.5 - (2000 - 4\,(\text{integer}((2000-1)/4)))] = -0.375 \text{ days}$$

with the integer function in the above equation yielding a value of 499.

For the above YADJ of –0.375 days, equation (B.20) yields an annual phase angle at midday of

$$P = 0.017208\,(DOY + YADJ + 0.417) = 0.0172028 \times (271 + (-0.375) + 0.417) = 4.6627 \text{ rad}$$

Upon substituting the annual phase angle into equation (B.19), the declination angle becomes

Table D.1: Experimental solar collector test data

Experimental mean cover temperature, T_c	56.53 °C (329.68 K)
Cover thickness, t_c	0.00388 m
Side length of cover, L_c	1.0 m
Long-wave emissivity of cover, ε_c [91DU1]	0.88
Cover extinction coefficient, C_e	13 m^{-1}
Cover refractive index, n_c [91DU1]	1.526
Experimental mean plate temperature, T_p	115.44 °C (388.59 K)
Long-wave emissivity of plate, ε_p	0.90
Solar absorptivity of plate, α_p	0.90
Ambient temperature, T_a	19.1 °C (292.25 K)
Total incident solar radiation, Ih_T	895.47 $W/m^2.K$
Wind speed, v_w	0.9 m/s
Atmospheric pressure, p_a	101 049 Pa
Location latitude angle, ϕ	33.98 °S
Location longitude angle, ϕ_l	18.85 °E
Location standard meridian, ϕ_m	30.00 °E
Air enclosure height, t_{air}	0.0395 m
Collector slope angle, β	0 °
%Diffuse radiation of total solar radiation	8.5

$$\delta = [0.00661 + 0.40602 \sin(P - 1.4075) + 0.00665 \sin(2P - 1.4789) + 0.00298 \sin(3P - 1.0996)]\frac{180}{\pi}$$

$$= 0.00661 + 0.40602 \sin(4.6627 - 1.4075) + 0.00665 \sin(2 \times 4.6627 - 1.4789) + 0.00298 \sin(3 \times 4.6627 - 1.0996)] \times \frac{180}{\pi}$$

$$= -1.823°$$

Substitute the determined phase angle into equation (B.23), and find

$$\begin{aligned}EOT &= 1440\,[\,0.005114\sin(P+3.0593)+0.006892\sin(2P+3.4646)\\ &\quad +0.00022\sin(3P+3.3858)+0.000153\sin(4P+3.7766)\,]\\ &= 1440\,[\,0.005114\sin(2.7188+3.0593)+0.006892\sin(2\times 2.7188+3.4646)\\ &\quad +0.00022\sin(3\times 2.7188+3.3858)+0.000153\sin(4\times 2.7188+3.7766)\\ &= 9.0922\ \text{min}.\end{aligned}$$

The experimental measurements were taken at 12h39:44 or 12.6622 hours after midnight. From equation (B.22), it thus follows that the hour angle is

$$\omega = 15\left[\psi - 12 - \frac{4(\phi_m - \phi_l) - EOT}{60}\right] = 15\left[12.6622 - 12 - \frac{4(30 - 18.85) - 9.0922}{60}\right] = 1.053\,^\circ$$

Upon substituting the determined hour angle and declination angle into equation (B.24), find

$$\begin{aligned}\theta_b &= a\cos(\sin\delta\sin\phi + \cos\delta\cos\phi\cos H)\\ &= a\cos(\sin -1.823\times\sin -33.98 + \cos -33.98\times\cos -1.823\times\cos 1.053) = 32.172\,^\circ.\end{aligned}$$

Thus the beam reflectivity from the upper surface of the cover according to equation (B.12) is

$$\begin{aligned}\rho_b &= \frac{1}{2}\left[\frac{\tan^2(\theta_b - \arcsin(n_a\sin\theta_b/n_c))}{\tan^2(\theta_b + \arcsin(n_a\sin\theta_b/n_c))} + \frac{\sin^2(\theta_b - \arcsin(n_a\sin\theta_b/n_c))}{\sin^2(\theta_b + \arcsin(n_a\sin\theta_b/n_c))}\right]\\ &= \frac{1}{2}\left[\frac{\tan^2(32.172 - \arcsin(\sin 32.172/1.526))}{\tan^2(32.172 + \arcsin(\sin 32.172/1.526))} + \frac{\sin^2(32.172 - \arcsin(\sin 32.172/1.526))}{\sin^2(32.172 + \arcsin(\sin 32.172/1.526))}\right]\\ &= 0.045514\end{aligned}$$

Upon substituting the beam incidence angle into equation (B.16) find the beam transmittance due to absorbtance

$$\tau_{b\alpha} = e^{-C_e t_c/\cos(\arcsin(n_a\sin\theta_b/n_c))} = e^{-13\times 0.00388/\cos(\arcsin(1\times\sin 32.172/1.526))} = 0.9476.$$

From Appendix B it follows that an equivalent beam incidence angle of 60° should be used for the evaluation of the diffuse cover characteristics. Thus, repeating the above calculations, the cover reflectivity for diffuse solar radiation is

$$\rho_d = \frac{1}{2}\left[\frac{\tan^2(\theta_d - \arcsin(n_a \sin\theta_d / n_c))}{\tan^2(\theta_d + \arcsin(n_a \sin\theta_d / n_c))} + \frac{\sin^2(\theta_d - \arcsin(n_a \sin\theta_d / n_c))}{\sin^2(\theta_d + \arcsin(n_a \sin\theta_d / n_c))}\right]$$

$$= \frac{1}{2}\left[\frac{\tan^2(60 - \arcsin(1\times \sin 60 / 1.526))}{\tan^2(60 + \arcsin(1\times \sin 60 / 1.526))} + \frac{\sin^2(60 - \arcsin(1\times \sin 60 / 1.526))}{\sin^2(60 + \arcsin(1\times \sin 60 / 1.526))}\right] = 0.09346.$$

while the value for the diffuse transmissivity due to absorbtance of the cover is

$$\tau_{d\alpha} = e^{-C_e t_c / \cos(\arcsin(n_a \sin\theta_d / n_c))} = e^{-13\times 0.00388 / \cos(\arcsin(1\times \sin 60 / 1.526))} = 0.9405$$

Further from Table D.1 it follows that the incident diffuse solar radiation is 8.5 % of the total incident radiation on the cover. Therefore, the incident beam solar radiation on the cover is

$$Ih_b = 0.915 Ih_T = 0.915\times 895.47 = 819.355 \text{ W/m}^2$$

and the incident diffuse solar radiation

$$Ih_d = 0.085 Ih_T = 0.085\times 895.47 = 76.115 \text{ W/m}^2.$$

For the evaluation of the effective convective heat transfer coefficient, the thermophysical properties of the air above the cover is evaluated at a mean cover-ambient temperature of

$$T_{am} = 0.5(T_a + T_c) = 0.5\times(19.1 + 56.7046) = 37.902\,^\circ\text{C or } 311.05\,\text{K}.$$

and the thermophysical properties of he air at this temperature [98KR1] are

Air density	$\rho_{ca} = \frac{p_a}{287.08\times T_{am}} = \frac{101049}{287.08\times 311.05} = 1.13162 \text{ kg/m}^3$
Specific heat capacity of air	$c_{pca} = 1007.4 \text{ J/kg.K}$
Air conductivity	$k_{ca} = 0.027069 \text{ W/m.K}$
Dynamic viscosity of air	$\mu_{ca} = 1.8974 \times 10^{-5} \text{ N/s.m}^2$

with a corresponding Prandtl number of

$$Pr_{ca} = \frac{\mu_{ca}\, c_{pca}}{k_{ca}} = \frac{1.8974\times 10^{-5} \times 1007.4}{0.027069} = 0.7061.$$

The effective length for the square cover was its side length, L_c. The dimensionless Grashof number is thus

$$Gr_{ca} = \frac{2(T_c - T_a)\, g\, L_c^3\, \rho_{ca}^2}{(T_c + T_a)\mu_{ca}^2} = \frac{2\times(329.8546 - 292.25)\text{x}9.8\,\text{x}1.0^3\,\text{x}1.13162^2}{(329.8546 + 292.25)\text{x}\left(1.8974\,\text{x}10^{-5}\right)^2} = 4.21837\ \text{x}10^9$$

while the Reynolds number was

$$Re_{ca} = \frac{\rho_{ca}\, v_w\, L_c}{\mu_{ca}} = \frac{1.13162\,\text{x}0.9\,\text{x}1.0}{1.8974\,\text{x}10^{-5}} = 53675.5$$

To determine the natural convection heat transfer coefficient the thermophysical properties of the entrapped air were required. The entrapped air, according to Mills [82MI1], will be at a mean plate-cover temperature of

$$T_m = 0.5(T_p + T_c) = 0.5\times(115.456 + 56.704) = 86.08\,°\text{C or } 359.23\,\text{K}.$$

For this temperature, the thermophysical properties are found to be

Air density	$\rho_{pc} = \frac{p_a}{287.08\times T_m} = \frac{101049}{287.08\times 359.23} = 0.9798\ \text{kg/m}^3$
Specific heat capacity of air	$c_{ppc} = 1010.6\ \text{J/kg.K}$
Air conductivity	$k_{pc} = 0.030684\ \text{W/m.K}$
Dynamic viscosity of air	$\mu_{pc} = 2.1111\text{x}10^{-5}\ \text{N/s.m}^2$

The dimensionless Rayleigh number is defined as the product of the dimensionless Grashof and Prandtl numbers, with the effective length defined as the air gap distance between the plate and cover. The plate-cover dimensionless Rayleigh number for the enclosure is thus

$$Ra_{pc} = Gr_{pc}\, Pr_{pc} = \frac{2(T_p - T_c)\, g\, t_{air}^3\, \rho_{pc}^2}{(T_p + T_c)\mu_{pc}^2}\left[\frac{\mu_{pc}\, c_{ppc}}{k_{pc}}\right]$$

$$= \frac{2\times(388.6063 - 329.8546)\text{x}9.8\,\text{x}0.0395^3\,\text{x}0.9798^2}{(388.6063 + 329.8546)\text{x}\left(2.1111\text{x}10^{-5}\right)^2}\times\left[\frac{2.1111\text{x}10^{-5}\times 1010.6}{0.030684}\right]$$

$$= 1.481631\times 10^5$$

which falls within the validity region of equation (D.8)

Substituting the previously determined thermophysical properties for the cover and enclosure into equation (D.10), find

$$\frac{(1-0.045514)\times(1-0.9476)}{1-0.045514\times0.9476}\times819.355+\frac{(1-0.09346)\times(1-0.9405)}{1-0.09346\times0.9405}\times76.115$$

$$+\left[1+1.44\left[1-\frac{1708}{1.47829\times10^{5}}\right]+\left[\left(\frac{1.47829\times10^{5}}{5830}\right)^{1/3}-1\right]\right]\times\frac{0.030677}{0.0395}\times(T_p-T_c)$$

$$+5.67\times10^{-8}\times\left(\frac{1}{0.9}+\frac{1}{0.88}-1\right)^{-1}\left(T_p^4-T_c^4\right)$$

$$=\left[\left(4.21531\times10^{9}\times0.7061\right)^{1/3}\times(0.227+1.406\times10^{-6}\times53676.5)\right]\times\frac{0.027069}{1.0}\times(T_c-292.25)$$

$$+0.88\times5.67\times10^{-8}\times\left(T_c^4-\left(0.0552\times292.25^{1.5}\right)^4\right)$$

which simplifies to

$$\begin{aligned}&47.328+3.3878\times(T_p-T_c)+45.4518\times10^{-9}\times\left(T_p^4-T_c^4\right)\\&=11.778\times(T_c-292.25)+49.896\times10^{-9}\times\left(T_c^4-275.785^4\right)\end{aligned}\qquad(D.15)$$

Repeating the above procedure, the absorber plate conservation equation (equation (D.14)) reduces to

$$\frac{0.9}{1-(1-0.9)\times0.09346}\times\left(\frac{(1-0.045514)^2\times0.9476}{1-0.045514^2\times0.9476^2}\times819.355+\frac{(1-0.09346)^2\times0.9405}{1-0.09346^2\times0.9405^2}\times76.115\right)$$

$$=\left[1+1.44\left[1-\frac{1708}{1.47829\times10^{5}}\right]+\left[\left(\frac{1.47829\times10^{5}}{5830}\right)^{1/3}-1\right]\right]\times\frac{0.030677}{0.0395}\times(T_p-T_c)$$

$$+5.67\times10^{-8}\times\left(\frac{1}{0.9}+\frac{1}{0.88}-1\right)^{-1}\left(T_p^4-T_c^4\right)$$

$$3.3878\times(T_p-T_c)+45.4518\times10^{-9}\times\left(T_p^4-T_c^4\right)=697.68\qquad(D.16)$$

Solving equations (D.15) and (D.16) iteratively, find that a cover temperature of 329.84 K and 388.632 K for the absorber plate temperature satisfy equations (D.10) and (D.14).

Upon comparing the predicted cover and absorber plate temperatures to the experimental temperatures in Table D.1, it is evident that good agreement has been obtained between the predicted and experimental values.

Appendix E: Solar air heater

In this appendix, attention is firstly given to the experimental determination of the duct loss coefficient, K_d, for the solar air heater apparatus described in Chapter 2. Thereafter the attention is shifted to the establishment of applicable energy equations for the cover, absorber plate and air for a 1m long section of an upward facing solar air heater. A numerical example is then presented to illustrate the procedure for solving the newly derived energy equations.

E.1 Duct loss coefficient: Experimental apparatus, analysis and results

To be able to determine the mass flow rate of the air through the duct, the upstream nozzle pressure, p_{up}, is required. From Chapter 2 it follows that the upstream nozzle pressure is

$$p_{up} = p_a - dp_d = p_a - K_d \left[\frac{m^2}{2\rho_{av} A_d^2} \right] \tag{E.1}$$

where p_a refers to the atmospheric pressure and m to the mass flow rate of the air. A_d is the duct cross-sectional area, while ρ_{av} is the air-vapour density based on the outlet conditions.

Therefore, to determine an appropriate value for the duct loss coefficient K_d in equation (E.1), a number of isothermal tests were conducted on the 21st of November 2000 on the upward facing solar air heater described in Chapter 2.

The ambient conditions were monitored by the weather station (Davis Weather Monitor II), while two Betz-manometers were used to measure the pressure difference between the atmospheric pressure and the upstream nozzle pressure as well as the pressure drop across the nozzles respectively (see Figure 2.4). The results of the test are shown in Figure E.1.

Using the recorded experimental data in conjunction with equation (E.1), it is possible to determine the duct loss coefficient, K_d, for the specific solar air heater. A numerical example is subsequently presented.

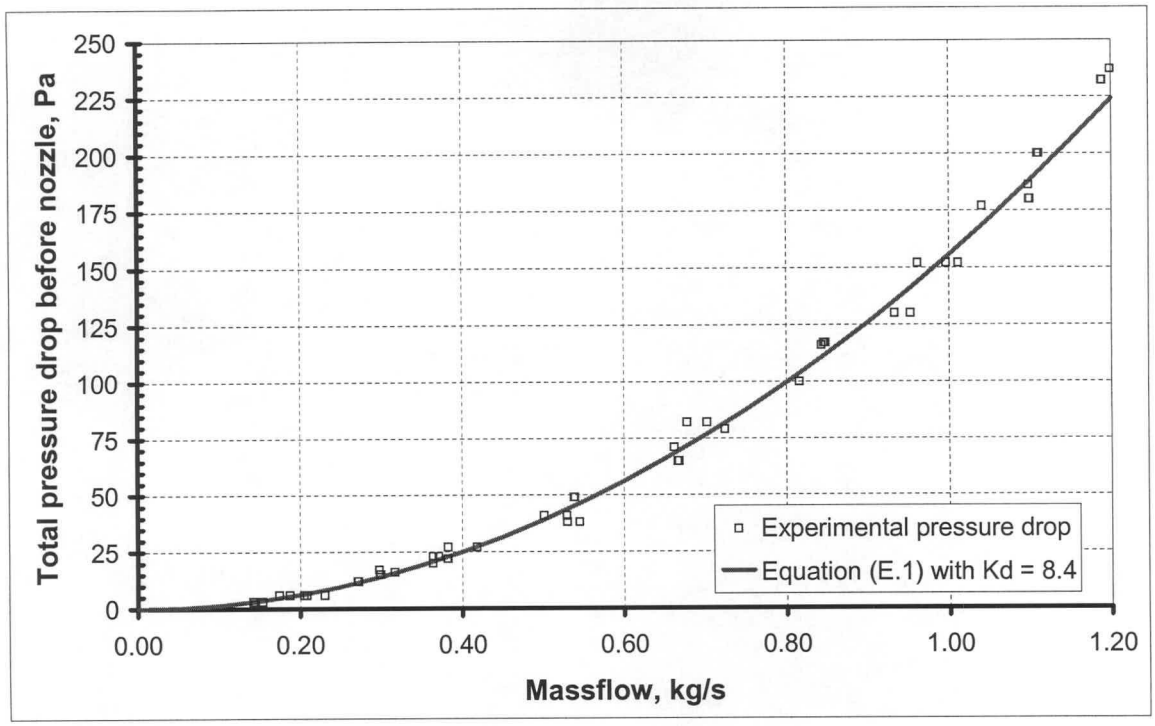

Figure E.1: Pressure difference between atmospheric and upstream nozzle pressure

Numerical example

On the 21st of November 2000 a test was conducted on the solar air heater described in Chapter 2. During the test nozzle 1 was closed while both nozzles 2 and 3 were left open (see Table E.1). In the forthcoming section it will be shown that by following an iterative procedure the air mass flow rates through 2 and 3 are found to be 0.133188 kg/s and 0.52930 kg/s respectively.

During the experiment the pressure difference between the ambient pressure and the pressure just in front of the nozzles was measured as 68 Pa. Thus, from equation (E.1) it follows that the upstream nozzle pressure, $p_{up,}$ is

$$p_{up} = p_a - dp_d = 101295 - 68 = 101227 \text{ Pa}$$

For the above nozzle pressure, and given experimental nozzle pressure drop, dp_n, and outlet temperatures shown in Table E.1, the air-vapour mixture thermophysical properties [98KR1] are

Vapour pressure $p_v = 1569.375$ Pa

Air-vapour density $\rho_{av} = 1.20594\ kg/m^3$

Air-vapour dynamic viscosity $\mu_{av} = 1.79817 \times 10^{-5}\ kg/m.s$

Table E.1: Experimental duct loss coefficient test data

Nozzle 2 diameter, D_2	0.0754875 m
Nozzle 3 diameter, D_3	0.15 m
Nozzle 2 area, A_2	4.47548 x 10^{-3} m^2
Nozzle 3 area, A_3	17.6715 x 10^{-3} m^2
Duct cross-sectional area, A_d	0.15 m^2
Pressure difference between ambient pressure and nozzles upstream pressure, dp_d	68 Pa
Pressure drop across nozzles, dp_n	378.568 Pa
Atmospheric pressure, p_a	101 295 Pa
Dry-bulb temperature, T_{db}	18.114 °C
Wet-bulb temperature, T_{wb}	13.725 °C
Massflow nozzle 2, m_2	0.133188kg/s
Massflow nozzle 3, m_3	0.52930 kg/s.

From equation (2.14) and Table E.1, it follows that the gas expansion for the nozzles is

$$\phi_g = 1 - \frac{3\,dp_n}{4\,p_{up} \times 1.4} = 1 - \frac{3 \times 378.568}{4 \times 101227 \times 1.4} = 0.997996$$

with equation (2.18) yielding respective values of

$$Y_2 = 1 + 0.5\left(\frac{A_2}{A_{tus}}\right)^2 + 2\left(\frac{A_2}{A_{tus}}\right)^2\left(\frac{dp_n}{p_{up}\,c_p/c_v}\right)$$

$$= 1 + 0.5\left(\frac{4.47548 \times 10^{-3}}{0.6}\right)^2 + 2\left(\frac{4.47548 \times 10^{-3}}{0.6}\right)^2\left(\frac{378.568}{101227 \times 1.4}\right) = 1.000028$$

and

$$Y_3 = 1 + 0.5\left(\frac{A_3}{A_{tus}}\right)^2 + 2\left(\frac{A_3}{A_{tus}}\right)^2\left(\frac{dp_n}{p_{up}\, c_p / c_v}\right)$$

$$= 1 + 0.5\left(\frac{17.6715\times10^{-3}}{0.6}\right)^2 + 2\left(\frac{17.6715\times10^{-3}}{0.6}\right)^2\left(\frac{387.568}{101227\times1.4}\right) = 1.000438$$

for the nozzles' approach velocity factors.

From the previously determined thermophysical properties of the air-vapour mixture, and final iteration's results for nozzle 2 and 3's mass flow rates, it follows that the dimensionless Reynolds numbers for the nozzles are respectively

$$Re_2 = \frac{4\,m_2}{\pi D_2\, \mu_{av}} = \frac{4\times0.133188}{\pi\times0.0754875\times1.79817\times10^{-5}} = 124.930\times10^3$$

and

$$Re_3 = \frac{4\,m_3}{\pi D_3\, \mu_{av}} = \frac{4\times0.52930}{\pi\times0.15\times1.79817\times10^{-5}} = 247.3071\times10^3\,.$$

Substitute nozzle two's Reynolds number into the applicable nozzle discharge coefficient equation (equation (2.12)) and find

$$C_2 = 0.9758 + 1.08\times10^{-7}\, Re_2 - 1.6\times10^{-13}\, Re_2^2$$

$$= 0.9758 + 1.08\times10^{-7}\times124.930\times10^3 - 1.6\times10^{-13}\times\left(124.930\times10^3\right)^2 = 0.986795$$

while nozzle 3 equation (2.12) yields

$$C_3 = 0.9758 + 1.08\times10^{-7}\, Re_3 - 1.6\times10^{-13}\, Re_3^2$$

$$= 0.9758 + 1.08\times10^{-7}\times247.3071\times10^3 - 1.6\times10^{-13}\times\left(247.3071\times10^3\right)^2 = 0.992796$$

Upon substituting the respective evaluated nozzle discharge coefficients, approach velocity factors and cross-sectional areas into equation (2.10) find a mass flow rate of

$$m_2 = C_2\,\phi_g\,Y_2\,A_2\sqrt{2\rho_{av}\,dp_n}$$

$$= 0.986795\times0.997996\times1.000028\times4.47548\times10^{-3}\sqrt{2\times1.20594\times378.568}$$

$$= 133.188\times10^{-3}\ kg/s$$

for the second nozzle, and

$$m_3 = C_3\,\phi_g\,Y_3\,A_3\sqrt{2\rho_{av}\,dp_n}$$

$$= 0.992796\times0.997996\times1.000438\times17.6715\times10^{-3}\sqrt{2\times1.20594\times378.568}$$

$$= 529.3\times10^{-3}\ kg/s$$

for the third nozzle. Consequently the total massflow through the rectangular duct is

$$m = m_2 + m_3 = 133.188\times10^{-3} + 529.3\times10^{-3} = 662.488\times10^{-3}\ kg/s$$

Substitute the above determined value into equation (E.1) and find,

$$68 = K_d\left[\frac{\left(662.488\times10^{-3}\right)^2}{2\times1.20594\times0.15^2}\right]$$

From this calculation a value of 8.4 is yielded for the duct loss coefficient, K_d.

Similar calculations were conducted for other measured points, which yielded similar values for the duct loss coefficient K_d. From Figure E.1, it is then also evident that good agreement exists between the experimental results and the theoretically predicted values for a duct loss coefficient value of K_d = 8.4.

E.2 Upward Facing Solar Air Heater Analysis

The objective of the following section is to derive applicable energy equations that can be used to predict the average temperature for the respective cover, absorber plate and working fluid (air) for any 1m long section of an upward facing solar air heater, for a given air inlet temperature and ambient conditions.

E.2.1 Solar air heater cover

The cover of the simple solar collector considered in Appendix D is identical to the cover of the upward facing solar air heater considered in Figure E.2. Thus, from Appendix D it follows that the energy equation for the cover of an upward facing solar air heater under steady state conditions is

$$\alpha_b' Ih_b + \alpha_d' Ih_d = q_c + q_{pc} + (q_{ca} + q_{rs}) \tag{E.2}$$

with q_{pc} and q_c referring to the respective long-wave radiation heat exchange between the plate and cover and the convective heat transfer between the cover and fluid. q_{ca} and q_{rs} define the total heat loss from the heated cover to the natural environment due to convection and sky radiation.

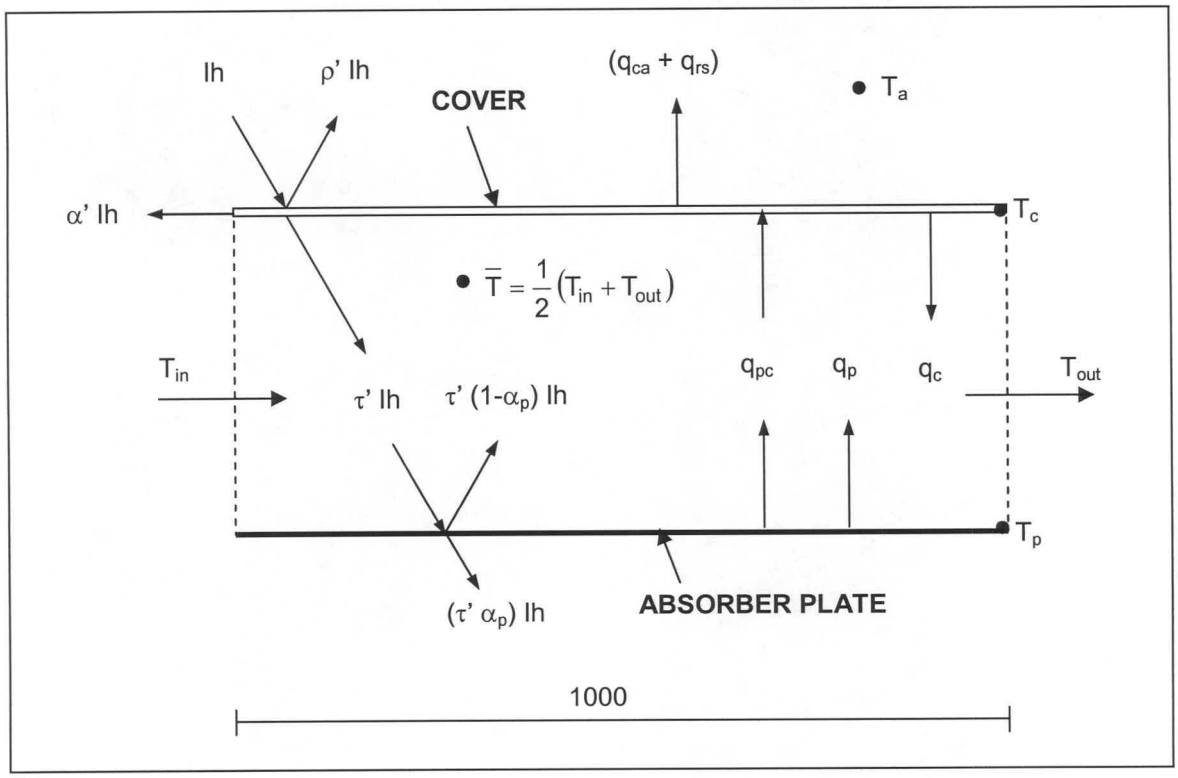

Figure E.2: A 1m long cross-section of an upward facing solar air heater

Upon substitution of equation (A.8) into equation (E.2) for the heat loss from a 1m x 1m cover to the environment, (q_{ca} + q_{rs}), and Modest's [93MO1] equation (equation (B.9)) for the effective absorbtivity of the cover, α', the energy equation for the cover becomes

$$\left[\frac{(1-\rho_{bc})(1-\tau_{bc})}{1+\rho_{bc}\,\tau_{bc}}\right] Ih_b + \left[\frac{(1-\rho_{dc})(1-\tau_{dc})}{1-\rho_{dc}\,\tau_{dc}}\right] Ih_d = q_c + q_{pc}$$
$$+ \left[(Gr_{ca}\,Pr_{ca})^{1/3}\left(0.227 + 1.406\times10^{-6}\,Re_{ca}\right)\right]\frac{k_{ca}}{L_c}(T_c - T_a) + \varepsilon_c\,\sigma\left[T_c^4 - \left(0.0552\,T_a^{1.5}\right)^4\right] \quad \text{(E.3)}$$

The cover and absorber plate of the solar air heater are modelled as two infinite parallel plates due to the highly reflective inner side walls of the duct. Hence, substitute equation (D.9) into the above equation for the radiation heat exchange between the plate and cover, and find

$$\left[\frac{(1-\rho_{bc})(1-\tau_{bc})}{1+\rho_{bc}\,\tau_{bc}}\right] Ih_b + \left[\frac{(1-\rho_{dc})(1-\tau_{dc})}{1-\rho_{dc}\,\tau_{dc}}\right] Ih_d = q_c + \sigma\left[\frac{1}{\varepsilon_c} + \frac{1}{\varepsilon_p} - 1\right]^{-1}\left(T_p^4 - T_c^4\right)$$
$$+ \left[(Gr_{ca}\,Pr_{ca})^{1/3}\left(0.227 + 1.406\times10^{-6}\,Re_{ca}\right)\right]\frac{k_{ca}}{L_c}(T_c - T_a) + \varepsilon_c\,\sigma\left[T_c^4 - \left(0.0552\,T_a^{1.5}\right)^4\right] \quad \text{(E.4)}$$

The convective heat transfer between the cover and air, as well as between the absorber plate and the air, can be expressed as

$$q_c = \bar{h}_c\left(T_c - \bar{T}\right) \quad \text{(E.5)}$$

and

$$q_p = \bar{h}_p\left(T_p - \bar{T}\right) \quad \text{(E.6)}$$

respectively, with T_p and T_c defining the respective mean plate and cover temperatures for the 1m section under consideration, while $\bar{T}$ is the mean temperature of the fluid in the section and $\bar{h}$ the length weighted average heat transfer coefficient defined by equation (2.25). Consequently, the conservation of energy equation for a 1m section of the solar air heater yields

$$\left[\frac{(1-\rho_{bc})(1-\tau_{bc})}{1+\rho_{bc}\,\tau_{bc}}\right] Ih_b + \left[\frac{(1-\rho_{dc})(1-\tau_{dc})}{1-\rho_{dc}\,\tau_{dc}}\right] Ih_d = \bar{h}_c\left(T_c - \bar{T}\right) + \sigma\left[\frac{1}{\varepsilon_c} + \frac{1}{\varepsilon_p} - 1\right]^{-1}\left(T_p^4 - T_c^4\right)$$
$$+ \left[(Gr_{ca}\,Pr_{ca})^{1/3}\left(0.227 + 1.406\times10^{-6}\,Re_{ca}\right)\right]\frac{k_{ca}}{L_c}(T_c - T_a) + \varepsilon_c\,\sigma\left[T_c^4 - \left(0.0552\,T_a^{1.5}\right)^4\right] \quad \text{(E.7)}$$

E.2.2 Solar air heater absorber plate

For an absorber plate with a solar absorptivity of α_p and cover with an effective transmissivity of τ', the following conservation of energy equation can be written for the solar air heater absorber plate(see Figure E.2)

$$\left(\tau' \alpha_p\right)_b Ih_b + \left(\tau' \alpha_p\right)_d Ih_d = q_p + q_{pc} \tag{E.8}$$

with $(\tau' \alpha_p)$ defining the effective transmittance-absorbtance product for the absorber plate.

Substitute equation (E.6) for the convective heat transfer, q_p, and equation (D.9) for the radiative heat transfer between the absorber plate and cover, find

$$\left(\tau' \alpha_p\right)_b Ih_b + \left(\tau' \alpha_p\right)_d Ih_d = \overline{h_p}\left(T_p - \overline{T}\right) + \sigma\left[\frac{1}{\varepsilon_c} + \frac{1}{\varepsilon_p} - 1\right]^{-1}\left(T_p^4 - T_c^4\right) \tag{E.9}$$

Upon substitution of the effective transmittance-absorbtance product of an absorber plate (equation (B.26)) into equation (E.9), the conservation of energy equation for the absorber plate yields

$$\left[\frac{(1-\rho_{bc})^2 \tau_{\alpha bc}}{1-\rho_{bc}^2 \tau_{\alpha bc}^2}\right]\left[\frac{\alpha_p}{1-(1-\alpha_p)\rho_d}\right] Ih_b + \left[\frac{(1-\rho_{dc})^2 \tau_{\alpha dc}}{1-\rho_{dc}^2 \tau_{\alpha dc}^2}\right]\left[\frac{\alpha_p}{1-(1-\alpha_p)\rho_d}\right] Ih_d$$
$$= \overline{h}_p\left(T_p - \overline{T}\right) + \sigma\left[\frac{1}{\varepsilon_c} + \frac{1}{\varepsilon_p} - 1\right]^{-1}\left(T_p^4 - T_c^4\right) \tag{E.10}$$

E.2.3 Air

The 1m long cross-section of an upward facing solar air heater under consideration in Figure E.2, yields the following energy balance for the working fluid (air) with a mass flow rate of m kg/s.

$$\dot{m} c_p T_{in} = A\,\overline{h}_p\left(T_p - \overline{T}\right) + A\,\overline{h}_c\left(T_c - \overline{T}\right) + \dot{m} c_p T_{out} \tag{E.11}$$

The mean fluid temperature of the 1m long section is define as

$$\overline{T} = \frac{1}{2}\left(T_{in} + T_{out}\right) \tag{E.12}$$

where T_{in} and T_{out} are the inlet and outlet air temperatures for the section.

Consequently, for a cover, absorber plate surface area of $1m^2$, equation (E.12) can be written in terms of the mean fluid, $\overline{T}$, and inlet temperature as

$$\dot{m} c_p T_{in} + \bar{h}_p \left(T_p - \overline{T}\right) + \bar{h}_c \left(T_c - \overline{T}\right) = \dot{m} c_p \left(2\overline{T} - T_{in}\right) \tag{E.13}$$

Therefore, with the inlet air temperature and ambient conditions known, the mean temperature for the respective cover, absorber plate and air can be predicted for any 1m long section of an upward facing solar air heater.

To illustrate the solving procedure, the final iteration is shown for the prediction of the solar air heater's performance described in Chapter 2 for the cover, plate and fluid temperature for the first 1m section of the solar air heater on the 6th of February 2001 (DOY = 37th day of year) at 13h10:04 (ψ = 13.16778 hours after midnight).

Numerical example

In the following calculations it will be shown that the solar air heater's first section's cover, plate and fluid energy equations are satisfied by respective cover, plate and air temperatures of 42.508 °C (350.583 K), 77.433 °C (350.583 K) and 33.736 °C (306.886 K), and mass flow rates of m_1 = 0.0949803 kg/s and m_2 = 1.58505 kg/s through nozzles 1 and 2 respectively for the given ambient conditions shown in Table E.2.

The leap year adjustment for the year 2001, according to equation (B.21), is

$$YADJ = 0.25\left[2.5 - \left(Y - 4\left(\text{integer}\left((Y-1)/4\right)\right)\right)\right] = 0.25 \times \left[2.5 - \left(2001 - 4\left(\text{integer}\left((2001-1)/4\right)\right)\right)\right]$$
$$= 0.375 \text{ days}$$

with the above integer function yielding a value of 500.

The 6th of February is the 37th day of the year 2001. The annual phase angle (equation (B.20)), is thus

$$P = 0.0172028\left(DOY + YADJ + 0.417\right) = 0.0172028\left(37 + 0.375 + 0.417\right) = 0.65013 \text{ rad.}$$

Upon substituting the above-evaluated annual phase angle into equation (B.19), the declination angle for the surface is

Table E.2: Values used in the cover and plate temperature prediction of upward facing solar air heater

Cover thickness, t_c	0.00388 m
Side length of cover, L_c	1.0 m
Cover extinction coefficient, C_e	13 m^{-1}
Cover refractive index, n_c	1.562
Air refractive index, n_a [91DU1]	1.0
Long-wave emissivity of cover, ε_c	0.88
Ambient temperature, T_a	32.722 °C (305.872 K)
Total incident solar radiation, Ih_T	988.234 $W/m^2.K$
Wet-bulb temperature, T_{wb}	33.678 °C (306.828 K)
Dry-bulb temperature, T_{db}	49.257 °C (322.407K)
Atmospheric pressure, p_a	99 617.8 Pa
Percentage diffuse radiation	8%
Wind speed, v_w	0.4 m/s
Atmospheric pressure, p_a	99 601 Pa
Location latitude angle, ϕ	33.98 °S
Location longitude angle, ϕ_l	18.85 °E
Location standard meridian, ϕ_m	30.00 °E
Nozzle 1 diameter, D_1	0.0494014 m
Nozzle 2 diameter, D_2	0.0754875 m
Nozzle 1 area, A_1	1.91677 x 10^{-3} m^2
Nozzle 2 area, A_2	4.47548 x 10^{-3} m^2
Mass flow rate for nozzle 1, m_2	0.0949803kg/s
Mass flow rate for nozzle 2, m_3	0.2226375 kg/s.

$$\begin{aligned}\delta &= 180[0.00661 + 0.40602\sin(P - 1.4075) + 0.00665\sin(2P - 1.4789) \\ &\quad + 0.00298\sin(3P - 1.0996)]\pi \\ &= 180[0.00661 + 0.40602\sin(0.65013 - 1.4075) + 0.00665\sin(2\times 0.65013 - 1.4789) \\ &\quad + 0.00298\sin(3\times 0.65013 - 1.0996)]\pi \\ &= -15.543°\end{aligned}$$

The annual phase angle leads to an equation of time value (equation (B.23)) of

$$\begin{aligned}EOT &= 1440\,[\,0.005114\sin(P+3.0593)+0.006892\sin(2P+3.4646)\\ &\quad +0.00022\sin(3P+3.3858)+0.000153\sin(4P+3.7766)\,]\\ &= 1440\,[\,0.005114\sin(0.65013+3.0593)+0.006892\sin(2\times0.65013+3.4646)\\ &\quad +0.00022\sin(3\times0.65013+3.3858)+0.000153\sin(4\times0.65013+3.7766)\,]\\ &= -14.1078\ \text{min}.\end{aligned}$$

The experimental measurements were taken at 13h10:04 or 13.16778 hours after midnight, which, according to equation (B.22) relates to an hour angle of

$$\omega = 15\left[\psi - 12 - \frac{4(\phi_m - \phi_l) - EOT}{60}\right] = 15\left[13.16778 - 12 - \frac{4(30-18.85)-(-14.1078)}{60}\right] = 2.8397°.$$

Form equation (B.24) it follows for a location with a standard meridian, ϕ_m, of 30° E, longitude, ϕ_l, of 18.85° E and latitude of 33.98° S the beam incidence angle is

$$\begin{aligned}\theta_b &= \text{a}\cos(\sin\delta\sin\phi+\cos\delta\cos\phi\cos\omega)\\ &= \text{a}\cos(\sin-15.543\sin-33.98+\cos-15.543\times\cos-33.98\times\cos2.8397) = 18.6139°.\end{aligned}$$

For the above incidence angle, the beam cover reflectivity according to Fresnel's (equation (B.12)) is

$$\begin{aligned}\rho_{bc} &= \frac{1}{2}\left[\frac{\tan^2(\theta_b-\arcsin(n_a\sin\theta_b/n_c))}{\tan^2(\theta_b+\arcsin(n_a\sin\theta_b/n_c))}+\frac{\sin^2(\theta_b-\arcsin(n_a\sin\theta_b/n_c))}{\sin^2(\theta_b+\arcsin(n_a\sin\theta_b/n_c))}\right]\\ &= \frac{1}{2}\left[\frac{\tan^2(18.6139-\arcsin(\sin18.6139/1.526))}{\tan^2(18.6139+\arcsin(\sin18.6139/1.526))}+\frac{\sin^2(18.6139-\arcsin(\sin18.6139/1.526))}{\sin^2(18.6139+\arcsin(\sin18.6139/1.526))}\right]\\ &= 0.04357\end{aligned}$$

and the beam transmittance due to absorbtance (equation (B.16)) is

$$\tau_{\alpha bc} = e^{-C_{ec}\,t_c/\cos(\arcsin(n_a\sin\theta_b/n_c))} = e^{-13\times0.00388/\cos(\arcsin(\sin18.6139/1.526))} = 0.94973$$

From Appendix D's numerical example it follows that the cover's diffuse reflectivity is

$$\rho_{dc} = 0.09346$$

and the transmittance due to absorbtance for diffuse solar radiation is

$\tau_{\alpha dc} = 0.9405$.

From Table E.2, it also follows that the diffuse radiation was 8 % of the total measured incident solar radiation. The incident beam solar radiation on the cover is thus

$$Ih_b = 0.92 Ih_T = 0.92 \times 988.234 = 909.175 \text{ W/m}^2$$

and the diffuse solar radiation

$$Ih_d = 0.09 Ih_T = 0.09 \times 988.234 = 79.059 \text{ W/m}^2$$

To be able to predict the fluid temperature in the section, the mass flow rate of the fluid through the rectangular duct is required.

From Table E.2, it is evident that the final mass flow iteration yielded values of 0.0949803 kg/s and 0.2226375 kg/s for the respective nozzles 1 and 2 for an air-vapour density of 1.58505 kg/m^3. Thus, the upstream nozzle pressure according to equation (E.1) is

$$p_{up} = p_a - K_d \left[\frac{m^2}{2 \rho_{av} A_c^2} \right] = 99617.8 - 8.4 \left[\frac{0.317617^2}{2 \times 1.0585 \times 0.15^2} \right] = 99600 \text{ Pa}$$

Employing the equations of Kröger [98KR1], the thermophysical properties and vapour pressure of the air-vapour mixture are evaluated at the above-determined upstream nozzle pressure and outlet temperatures shown in Table E.2.

Vapour pressure	$p_v = 5227.92$ Pa
Air-vapour density	$\rho_{av} = 1.058505$ kg/m^3
Air-vapour dynamic viscosity	$\mu_{av} = 1.91893 \times 10^{-5}$ kg/m.s

Using the above-determined properties, the gas expansion factor is evaluated according to equation (2.14).

$$\phi_g = 1 - \frac{3 dp_n}{4 p_{up} \times 1.4} = 1 - \frac{3 \times 1206.271}{4 \times 99600.3 \times 1.4} = 0.9935109$$

while equation (2.18) yields values of

$$Y_1 = 1 + 0.5\left(\frac{A_1}{A_{tus}}\right)^2 + 2\left(\frac{A_1}{A_{tus}}\right)^2\left(\frac{dp_n}{p_{up}\, c_p / c_v}\right)$$

$$= 1 + 0.5\left(\frac{1.9677\times10^{-3}}{0.6}\right)^2 + 2\left(\frac{1.9677\times10^{-3}}{0.6}\right)^2\left(\frac{1206.271}{99600.34\times1.4}\right) = 1.000005$$

and

$$Y_2 = 1 + 0.5\left(\frac{A_2}{A_{tus}}\right)^2 + 2\left(\frac{A_2}{A_{tus}}\right)^2\left(\frac{dp_n}{p_{up}\, c_p / c_v}\right)$$

$$= 1 + 0.5\left(\frac{4.47548\times10^{-3}}{0.6}\right)^2 + 2\left(\frac{4.47548\times10^{-3}}{0.6}\right)^2\left(\frac{1206.271}{99600.34\times1.4}\right) = 1.0000287$$

for the approach velocity factors for the two nozzles respectively.

With the thermophysical properties of the air-vapour mixture known, the nozzles' Reynolds number are evaluated.

$$Re_1 = \frac{4\,m_1}{\pi D_1\, \mu_{av}} = \frac{4\times94.9803\times10^{-3}}{\pi\times0.0494014\times1.91893\times10^{-5}} = 127.569\times10^3$$

$$Re_2 = \frac{4\,m_1}{\pi D_1\, \mu_{av}} = \frac{4\times222.6375\times10^{-3}}{\pi\times0.0754875\times1.91893\times10^{-5}} = 195.6925\times10^3\,.$$

From Chapter 2, it is apparent that the discharge coefficient for each nozzle is based on that nozzle's Reynolds number. Subsequently employing equation (2.11), a value of

$$C_1 = 0.9758 + 1.08\times10^{-7}\, Re_1 - 1.6\times10^{-13}\, Re_1^2$$

$$= 0.9758 + 1.08\times10^{-7}\times127.569\times10^3 - 1.6\times10^{-13}\times\left(127.569\times10^3\right)^2 = 0.9869736$$

is obtained for the smaller nozzle, while for the second nozzle it yields

$$C_2 = 0.9758 + 1.08\times10^{-7}\, Re_2 - 1.6\times10^{-13}\, Re_2^2$$

$$= 0.9758 + 1.08\times10^{-7}\times195.6925\times10^3 - 1.6\times10^{-13}\times\left(195.6925\times10^3\right)^2 = 0.9908075$$

From equation (2.10), it follows that the mass flow rate through nozzles 1 and 2 are

$$m_1 = C_1 \phi_g Y_1 A_1 \sqrt{2 \rho_{av} dP_n}$$

$$= 0.9869736 \times 0.9935109 \times 1.000005 \times 1.91677 \times 10^{-3} \sqrt{2 \times 1.058505 \times 1206.271}$$

$$= 94.9803 \times 10^{-3} \text{ kg/s}$$

and

$$m_2 = C_2 \phi_g Y_2 A_2 \sqrt{2 \rho_{av} dP_n}$$

$$= 0.9908075 \times 0.9935109 \times 1.000028 \times 4.47548 \times 10^{-3} \sqrt{2 \times 1.058505 \times 1206.271}$$

$$= 222.637 \times 10^{-3} \text{ kg/s}$$

respectively.

Adding the individual nozzle mass flow rates together, a total mass flow rate of 317.617 x 10^{-3} is obtained.

For the evaluation of the effective convective heat transfer coefficient between the outer cover and the environment, the thermophysical properties of the air above the cover is required.

The final iteration yielded a value of 42.508°C for the cover temperature, while the ambient temperature was measured at 32.722°C. Therefore the air above the cover is at a mean cover-ambient temperature of

$$T_{am} = 0.5(T_a + T_c) = 0.5 \times (32.722 + 42.508) = 37.615 \text{ °C or } 310.765 \text{ K.}$$

For this temperature, the thermophysical properties of air [98KR1] are

Air density	$\rho_{ca} = \frac{p_a}{287.08 \times T_{am}} = \frac{99601}{287.08 \times 310.765} = 1.1164 \text{ kg/m}^3$
Specific heat capacity of air	$c_{pca} = 1007.39 \text{ J/kg.K}$
Air conductivity	$k_{ca} = 0.0270507 \text{ W/m.K}$
Dynamic viscosity of air	$\mu_{ca} = 1.89611 \text{ x} 10^{-5} \text{ N/s.m}^2$

which relates to a corresponding Prandtl number of

$$Pr_{ca} = \frac{\mu_{ca}\, c_{pca}}{k_{ca}} = \frac{1.89611 \times 10^{-5} \times 1007.39}{0.0270507} = 0.7061.$$

The effective length for a square cover is the side length, L_c, of the cover, according to Appendix A. The dimensionless Grashof number is thus

$$Gr_{ca} = \frac{2(T_c - T_a)\, g\, L_c^3\, \rho_{ca}^2}{(T_c + T_a)\mu_{ca}^2} = \frac{2\times(315.658 - 305.872)\times 9.8 \times 1.0^3 \times 1.1164^2}{(315.658 + 305.872)\times\left(1.89611\times 10^{-5}\right)^2} = 1.07091 \times 10^9$$

and the corresponding Reynolds number is

$$Re_{ca} = \frac{\rho_{ca}\, v_w\, L_c}{\mu_{ca}} = \frac{1.1164 \times 0.4 \times 1.0}{1.89611 \times 10^{-5}} = 23551.4$$

To evaluate the length weighted averaged heat transfer coefficient between the cover and air, the thermophysical properties of the air is to be evaluated at a mean air temperature of

$$\overline{T}_m = 0.5\left(\overline{T} + T_c\right) = 0.5\times(33.736 + 42.508) = 38.112\,°C \text{ or } 311.272K.$$

For the above temperature, the thermophysical properties of the air [98KR1] are

Air density	$\rho_c = \frac{p_{up}}{287.08\times\overline{T}_m} = \frac{99601}{287.08\times 311.272} = 1.1146\ kg/m^3$
Specific heat capacity of air	$c_{pc} = 1007.40\ J/kg.K$
Air conductivity	$k_c = 0.027089\ W/m.K$
Dynamic viscosity of air	$\mu_c = 1.8984 \times 10^{-5}\ N/s.m^2$

which relates to a corresponding Prandtl number of

$$Pr_a = \frac{\mu_c\, c_{pc}}{k_c} = \frac{1.8984 \times 10^{-5} \times 1007.4}{0.0271} = 0.706.$$

The rectangular duct's hydraulic diameter is

$$Dh = \frac{4\,(W \times H)}{2\,(W + H)} = \frac{2\,(1.0 \times 0.15)}{(1.0 + 0.15)} = 0.2609\ m$$

which leads to a corresponding Reynolds number (equation (2.23)) of

$$Re_{Dh} = \frac{2\,m}{\mu_c\,(W+H)} = \frac{2\times 0.317617}{1.8984\times 10^{-5}\times(1.0+0.15)} = 29097\ .$$

Setting Δx equal to 0.0204081 m and substitute the previously determined Reynolds number, duct hydraulic diameter and thermophysical properties into equation (2.25), find

$$\bar{h}_c = 0.036\,Re_{Dh}^{0.8}\,Pr^{1/3}\left(\frac{k}{Dh}\right)\sum_{i=1}^{n}\left(\frac{Dh}{x_i}\right)^{0.055}\Delta x$$

$$= 0.036\times 29097^{0.8}\times 0.706^{1/3}\times\left(\frac{0.027089}{0.2609}\right)\sum_{i=1}^{49}\left(\frac{0.2609}{x_i}\right)^{0.055}\times 0.0204081$$

$$= 12.398\times\left[\left(\frac{0.2609}{0.010204}\right)^{0.055}\times 0.0204081 + \Lambda\left(\frac{0.2609}{0.989795}\right)^{0.055}\times 0.0204081\right] = 12.1787\ W/m^2K$$

Repeating the above procedure, a value of

$$h_p = 12.3413\ W/m^2K$$

is yielded for the absorber plate's length averaged heat transfer coefficient.

Upon substitution of the previously determined properties into equation (E.6), the conservation of energy equation for the cover becomes

$$\left[\frac{(1-0.04357)(1-0.94973)}{1-0.04357\times 0.94973}\right]\times 909.175 + \left[\frac{(1-0.09346)(1-0.9405)}{1-0.09346\times 0.9405}\right]\times 79.059$$

$$+ 5.67\times 10^{-8}\left[\frac{1}{0.88}+\frac{1}{0.9}-1\right]^{-1}\left(T_p^4 - T_c^4\right) = 12.1787\times\left(T_c - \bar{T}\right)$$

$$+\left[\left(1.07091\times 10^9\times 0.7061\right)^{1/3}\left(0.227+1.406\times 10^{-6}\times 23551.4\right)\right]\frac{0.0270507}{1.0}\times\left(T_c - 305.872\right)$$

$$+ 0.88\times 5.67\times 10^{-8}\left[T_c^4 - \left(0.0552\times 305.872^{1.5}\right)^4\right]$$

which reduces to

$$50.272 + 45.452\times10^{-9}\times\left(T_p^4 - T_c^4\right) = 12.1787\times\left(T_c - \overline{T}\right) + 6.4103\times\left(T_c - 305.872\right) + 49.896\times10^{-9}\left[T_c^4 - 295.29^4\right] \quad \text{(E.13)}$$

Repeating the above procedure, the plate conservation of energy equation (equation (E.9)) yields

$$\left[\frac{(1-0.04357)^2\times0.94973}{1-0.04357^2\times0.94973^2}\right]\left[\frac{0.9}{1-(1-0.9)\times0.9346}\right]\times909.175 + \left[\frac{(1-0.9346)^2\times0.9405}{1-0.09346^2\times0.9405^2}\right]\left[\frac{0.9}{1-(1-0.9)\times0.9346}\right]\times79.059 = 12.3413\times\left(T_p - \overline{T}\right) + +5.67\times10^{-8}\left[\frac{1}{0.88}+\frac{1}{0.9}-1\right]^{-1}\left(T_p^4 - T_c^4\right)$$

which simplifies to

$$774.792 = 12.3413\times\left(T_p - \overline{T}\right) + 45.45267\times10^{-9}\times\left(T_p^4 - T_c^4\right) \quad \text{(E.14)}$$

The final iteration yielded a value of 33.736 °C (306.886 K) for the average air temperature. The specific heat capacity for the air at this temperature is [98KR1] thus

Specific heat capacity of air $c_p = 1007.22$ J/kg.K

Furthermore, the total mass flow of air through the rectangular duct is 0.317617 kg/s.

Consequently, substituting the specific heat capacity, the mass flow rate and the appropriate cover, h_c, and plate, h_p, convective heat transfer coefficients into equation (E.12)

$$317.617\times10^{-3}\times1007.22\times305.872 + 1\times12.3413\times\left(T_p - \overline{T}\right) + 1\times12.1787\times\left(T_c - \overline{T}\right) = 317.617\times10^{-3}\times1007.22\times\left(2\,\overline{T} - 305.872\right)$$

After simplification the above air conservation of energy equation reduces to

$$97.8516\times10^{3}+12.3413\times\left(T_{p}-\overline{T}\right)+12.1787\times\left(T_{c}-\overline{T}\right)=319.9102\times\left(2\,\overline{T}-305.872\right) \quad \text{(E.15)}$$

Solving equation (E.13), (E.14) and (E.15) simultaneously, temperatures of 42.508 °C (350.583 K), 77.433 °C (350.583 K) and 33.736 °C (306.886 K) are predicted for the first section's respective cover, plate and air temperatures respectively.

Appendix F: Coefficient of extinction

To determine the solar characteristics of a plastic film, the coefficient of extinction as well as the refractive index of the plastic film must to be known. Therefore, a number of experiments were conducted in order to determine these characteristics for a specific plastic film.

F.1 Experiment, analysis and results

Experiments were conducted on the same apparatus as described in appendix C, with the incident solar radiation on the cover and plate measured by two solar sensors placed on the respective surfaces.

From Appendix C, it further follows that the theoretical net solar radiation striking the plate is to be evaluated from equation (C.2). The equation is repeated below for clarity.

$$Ih_p = \left(\frac{1}{1-(1-\alpha_p)\rho_d}\right)\left(\frac{(1-\rho_b)^2\tau_{\alpha b}}{1-\rho_b^2\tau_{\alpha b}^2}Ih_b + \frac{(1-\rho_d)^2\tau_{\alpha d}}{1-\rho_d^2\tau_{\alpha d}^2}Ih_d\right) \quad (F.1)$$

The experimental results for a black insulated plate (α_p = 0.9) are shown in Figure F.1, while Figure F.2 displays the measured results for the silver plate (α_p = 0.1).

With experimental results available for the two surfaces, one is able to determine the unknown characteristics of the plastic cover with the aid of equation (F.1).

From these calculations, respective values of 1.6 and 200 were obtained for the refractive index and coefficient of extinction for the plastic material under consideration. Values quoted from literature for the refractive indexes for cover material range from 1.34 to 1.64 [98TS1], while the coefficient of extinction for various plastics may vary between about 9 m^{-1} (acrylics) to 205 m^{-1} (Mylar), according to Tsilingiris [98TS1].

Consequently, not only are the determined values within the specified ranges quoted in literature, [98TS1] but from Figure F.1 and Figure F.2 it is evident that good agreement exists between the calculated solar radiation incident on the plate and the measured radiation, for a refractive index of 1.6 and coefficient of extinction, C_e, of 200 m^{-1}.

In the following section, a numerical example will be presented to illustrate the solution procedure.

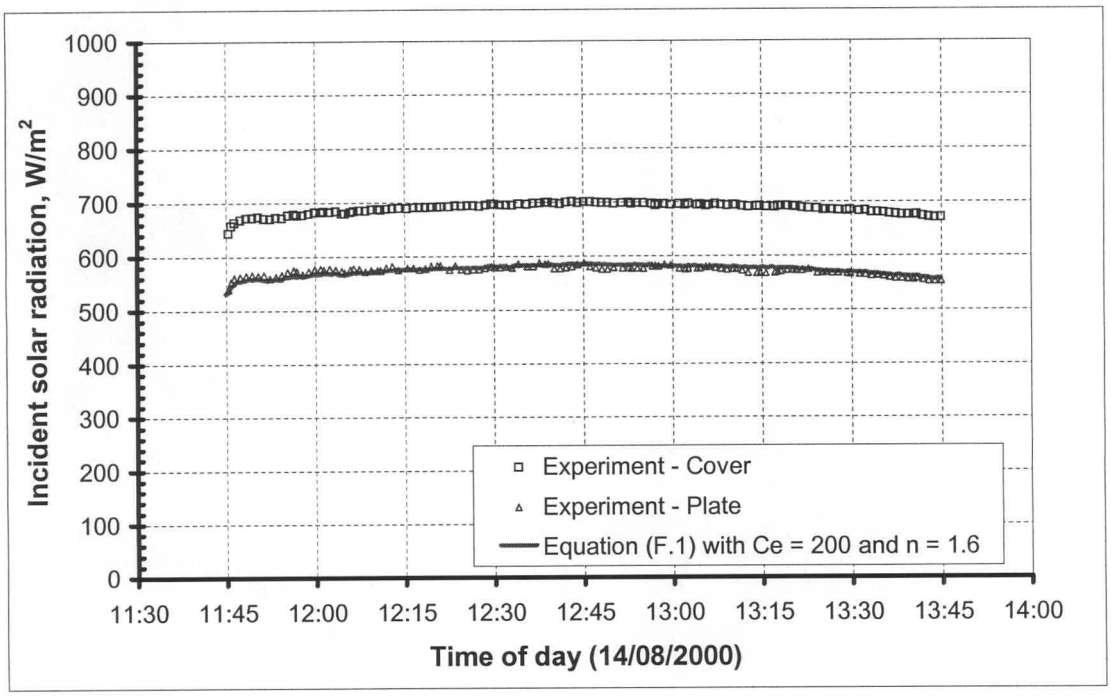

Figure F.1: Incident solar radiation on cover and black plate (14/18/2000)

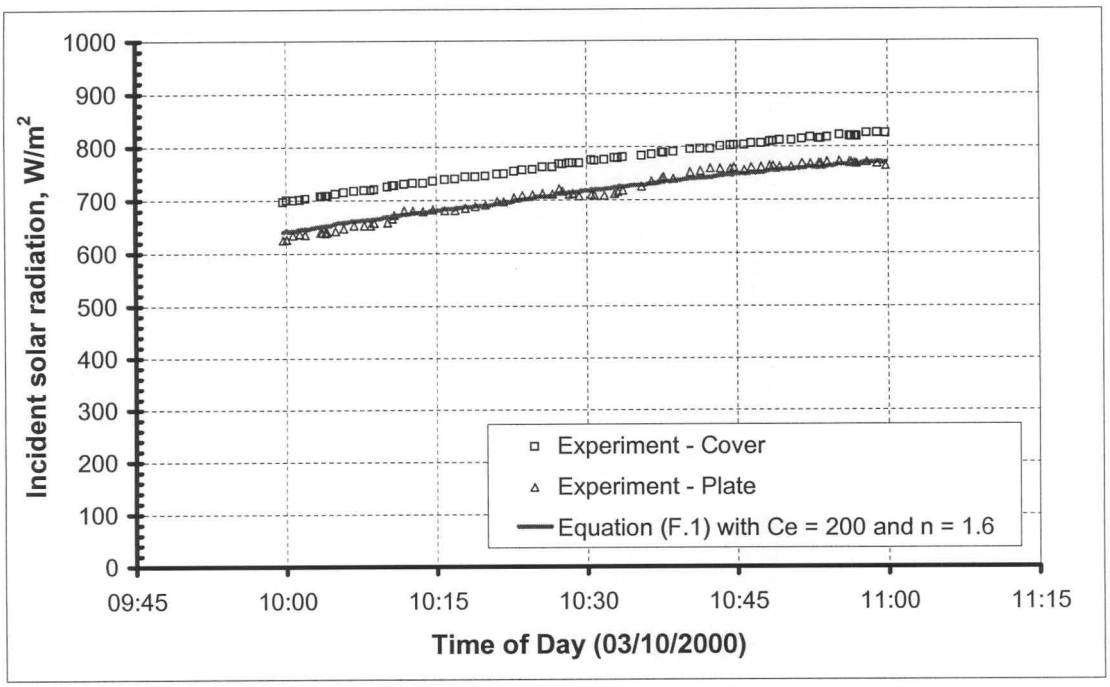

Figure F.2: Incident solar radiation on cover and silver plate (03/10/2000)

Numerical example

To determine the two characteristics of the plastic film, two equations are required. By employing equation (F.1) in conjunction with the experimental black and silver surface's data, two relevant energy equations are obtained which, if solved simultaneously, will yield the unknown solar characteristics for the particular plastic cover material.

On the 14th of August 2000 at 12h44:28, the total solar radiation on the cover was measured as 698.688 W/m^2, while the total solar radiation incident on the black absorber plate was 583.95 W/m^2.

According to equation (B.21) the leap year adjustment to the day for the year, 2000 is

$$YADJ = 0.25\left[2.5 - \left(Y - 4\left(\text{integer}\left((Y-1)/4\right)\right)\right)\right] = 0.25\times\left[2.5 - \left(2000 - 4\left(\text{integer}\left((2000-1)/4\right)\right)\right)\right]$$

$$= -0.375 \text{ days}$$

with the above integer function yielding a value of 499.

The 14th of August is the 227th day of the year. The annual phase angle, according to equation (B.20), is thus

$$P = 0.017208\left(DOY + YADJ + 0.417\right) = 0.0172028\times\left(227 + \left(-0.375\right) + 0.417\right) = 3.9058 \text{ rad.}$$

Substituting the above-evaluated annual phase angle into equation (B.19), the declination angle for the black surface yields

$$\delta = [0.00661 + 0.40602\sin\left(P - 1.4075\right) + 0.00665\sin\left(2P - 1.4789\right)$$
$$+ 0.00298\sin\left(3P - 1.0996\right)]\frac{180}{\pi}$$
$$= [0.00661 + 0.40602\sin\left(3.9058 - 1.4075\right) + 0.00665\sin\left(2\times 3.9058 - 1.4789\right)$$
$$+ 0.00298\sin\left(3\times 3.9058 - 1.0996\right)]\frac{180}{\pi}$$
$$= 14.19°$$

and an equation of time value (equation (B.23)) of

$$\begin{aligned}EOT &= 1440\,[\,0.005114\sin(P+3.0593)+0.006892\sin(2P+3.4646)\\ &\quad +0.00022\sin(3P+3.3858)+0.000153\sin(4P+3.7766)\,]\\ &= 1440\,[\,0.005114\sin(3.9058+3.0593)+0.006892\sin(2\times3.9058+3.4646)\\ &\quad +0.00022\sin(3\times3.9058+3.3858)+0.000153\sin(4\times3.9058+3.7766)\\ &= -4.6\ \text{min}.\end{aligned}$$

Measurements for the black surface were taken at 12h44:28 or 12.7411 hours after midnight, which, according to equation (B.22) relates to an hour angle of

$$\omega = 15\left[\psi - 12 - \frac{4(\phi_m-\phi_l)-EOT}{60}\right] = 15\times\left[12.7411-12-\frac{4(30-18.85)-(-4.6)}{60}\right] = -1.1833°.$$

From equation (B.24) it follows that the beam incidence angle for the location with a standard meridian, ϕ_m, of 30° E, longitude, ϕ_l, of 18.85° E and latitude of 33.98° S is

$$\begin{aligned}\theta_b &= a\cos(\sin\delta\sin\phi+\cos\delta\cos\phi\cos\omega)\\ &= a\cos(\sin 14.19\times\sin-33.98+\cos-33.98\times\cos 14.19\times\cos-1.1833) = 48.187°.\end{aligned}$$

The cover is surrounded by air (n_a = 1); subsequently the beam reflectivity for the cover (equation (B.12)) is

$$\begin{aligned}\rho_b &= \frac{1}{2}\left[\frac{\tan^2(\theta_b-\arcsin(n_a\sin\theta_b/n_c))}{\tan^2(\theta_b+\arcsin(n_a\sin\theta_b/n_c))}+\frac{\sin^2(\theta_b-\arcsin(n_a\sin\theta_b/n_c))}{\sin^2(\theta_b+\arcsin(n_a\sin\theta_b/n_c))}\right]\\ &= \frac{1}{2}\left[\frac{\tan^2(48.43-\arcsin(\sin 48.43/n_c))}{\tan^2(48.43+\arcsin(\sin 48.43/n_c))}+\frac{\sin^2(48.43-\arcsin(\sin 48.43/n_c))}{\sin^2(48.43+\arcsin(\sin 48.43/n_c))}\right]\\ &= \frac{1}{2}\left[\frac{\tan^2(48.43-\arcsin(0.7453/n_c))}{\tan^2(48.43+\arcsin(0.7453/n_c))}+\frac{\sin^2(48.43-\arcsin(0.7453/n_c))}{\sin^2(48.43+\arcsin(0.7453/n_c))}\right]\end{aligned} \qquad (F.2)$$

while the beam transmissivity due to absorbtance for the 0.0002 m thick plastic cover is evaluated from Bouguer's law (equation (B.16)).

$$\begin{aligned}\tau_{b\alpha} &= e^{-C_e t_c/\cos(\arcsin(n_a\sin\theta_b/n_c))} = e^{-C_e\times0.0002/\cos(\arcsin(\sin 48.43/n_c))}\\ &= e^{-C_e\times0.0002/\cos(\arcsin(0.7453/n_c))}\end{aligned} \qquad (F.3)$$

Using an incidence angle of 60°, as suggested by Duffie and Beckman [91DU1], the diffuse reflectivity of the cover yields

$$\begin{aligned}\rho_d &= \frac{1}{2}\left[\frac{\tan^2(\theta_d - \arcsin(n_a \sin\theta_d / n_c))}{\tan^2(\theta_d + \arcsin(n_a \sin\theta_d / n_c))} + \frac{\sin^2(\theta_d - \arcsin(n_a \sin\theta_d / n_c))}{\sin^2(\theta_d + \arcsin(n_a \sin\theta_d / n_c))}\right] \\ &= \frac{1}{2}\left[\frac{\tan^2(60 - \arcsin(\sin 60 / n_c))}{\tan^2(60 + \arcsin(\sin 60 / n_c))} + \frac{\sin^2(60 - \arcsin(\sin 60 / n_c))}{\sin^2(60 + \arcsin(\sin 60 / n_c))}\right] \\ &= \frac{1}{2}\left[\frac{\tan^2(60 - \arcsin(0.866 / n_c))}{\tan^2(60 + \arcsin(0.866 / n_c))} + \frac{\sin^2(60 - \arcsin(0.866 / n_c))}{\sin^2(60 + \arcsin(0.866 / n_c))}\right]\end{aligned} \quad \text{(F.4)}$$

and the diffuse solar radiation transmissivity due to absorbtance

$$\begin{aligned}\tau_{d\alpha} &= e^{-C_e t_c / \cos(\arcsin(n_a \sin\theta_d / n_c))} = e^{-C_e \times 0.0002 / \cos(\arcsin(\sin 60 / n_c))} \\ &= e^{-C_e \times 0.0002 / \cos(\arcsin(0.866 / n_c))}\end{aligned} \quad \text{(F.5)}$$

The diffuse radiation for the black surface was 8 % of the total incident solar radiation on the cover. Consequently, the incident beam solar radiation on the black cover is

$$Ih_b = 0.92 Ih_T = 0.92 \times 698.688 = 642.793 \text{ W/m}^2$$

and the diffuse solar radiation

$$Ih_d = 0.08 Ih_T = 0.08 \times 698.688 = 55.895 \text{ W/m}^2$$

Equation (F.1) can thus be written as follows for the for the black surface

$$\begin{aligned}Ih_p &= \left(\frac{1}{1-(1-\alpha_p)\rho_d}\right)\left(\frac{(1-\rho_b)^2 \tau_{b\alpha}}{1-\rho_b^2 \tau_{b\alpha}} Ih_b + \frac{(1-\rho_d)^2 \tau_{d\alpha}}{1-\rho_d^2 \tau_{d\alpha}} Ih_d\right) \\ 583.95 &= \left(\frac{1}{1-(1-0.9)\times\rho_d}\right)\left(\frac{(1-\rho_b)^2 \tau_{b\alpha}}{1-\rho_b^2 \tau_{b\alpha}} \times 642.793 + \frac{(1-\rho_d)^2 \tau_{d\alpha}}{1-\rho_d^2 \tau_{d\alpha}} \times 55.895\right)\end{aligned} \quad \text{(F.6)}$$

with the cover reflectivities given by equations (F.2) and (F.4) respectively, and the beam transmissivity due to absorbtance by equation (F.3) and the diffuse transmissivity due to absorbtance by equation (F.5).

On the 3rd of October 2000 at 11h10:28, the total solar radiation on the cover was measured as 839.91 W/m^2, while the total solar radiation incident on the silver absorber plate was 785.16 W/m^2.

Following the same procedure as described for the black plate, the characteristics of the cover are determined for the silver plate. The beam reflectivity of the silver plate, according to equation (B.12), is

$$\begin{aligned}\rho_b &= \frac{1}{2}\left[\frac{\tan^2(\theta_b - \arcsin(n_a \sin\theta_b / n_c))}{\tan^2(\theta_b + \arcsin(n_a \sin\theta_b / n_c))} + \frac{\sin^2(\theta_b - \arcsin(n_a \sin\theta_b / n_c))}{\sin^2(\theta_b + \arcsin(n_a \sin\theta_b / n_c))}\right] \\ &= \frac{1}{2}\left[\frac{\tan^2(34.542 - \arcsin(\sin 34.542 / n_c))}{\tan^2(34.542 + \arcsin(\sin 34.542 / n_c))} + \frac{\sin^2(34.542 - \arcsin(\sin 34.542 / n_c))}{\sin^2(34.542 + \arcsin(\sin 34.542 / n_c))}\right] \\ &= \frac{1}{2}\left[\frac{\tan^2(34.542 - \arcsin(0.567 / n_c))}{\tan^2(34.542 + \arcsin(0.567 / n_c))} + \frac{\sin^2(48.43 - \arcsin(0.567 / n_c))}{\sin^2(48.43 + \arcsin(0.567 / n_c))}\right]\end{aligned} \quad (F.7)$$

while the beam transmissivity due to absorbtance for the cover is predicted by Bouguer's law (equation (B.16)) as

$$\begin{aligned}\tau_{b\alpha} &= e^{-C_e t_c / \cos(\arcsin(n_a \sin\theta_b / n_c))} = e^{-C_e \times 0.0002 / \cos(\arcsin(\sin 34.547 / n_c))} \\ &= e^{-C_e \times 0.0002 / \cos(\arcsin(0.567 / n_c))}\end{aligned} \quad (F.8)$$

The diffuse solar radiation is 9 % of the total incident solar radiation. The beam radiation on the cover is thus equal to

$$Ih_b = 0.91 Ih_T = 0.91 \times 839.91 = 764.318 \text{ W/m}^2$$

and the diffuse incident radiation

$$Ih_d = 0.09 Ih_T = 0.09 \times 839.91 = 75.592 \text{ W/m}^2.$$

Upon substituting the above-determined beam and diffuse incident solar radiation into the cover equation (equation (F.1)), the following equation is yielded for the silver plate.

$$Ih_p = \left(\frac{1}{1-(1-\alpha_p)\rho_d}\right)\left(\frac{(1-\rho_b)^2\tau_{b\alpha}}{1-\rho_b^2\tau_{b\alpha}}Ih_b + \frac{(1-\rho_d)^2\tau_{d\alpha}}{1-\rho_d^2\tau_{d\alpha}}Ih_d\right) \quad (F.9)$$

$$785.60 = \left(\frac{1}{1-(1-0.1)\times\rho_d}\right)\left(\frac{(1-\rho_b)^2\tau_{b\alpha}}{1-\rho_b^2\tau_{b\alpha}}\times 764.318 + \frac{(1-\rho_d)^2\tau_{d\alpha}}{1-\rho_d^2\tau_{d\alpha}}\times 75.592\right)$$

The silver plate beam reflectivity is given by equation (F.7) and the transmissivity due to absorbtance for beam radiation by equation (F.8). As in the case of the black plate, the diffuse reflectivity is given by equation (F.4) and the diffuse transmissivity due to absorbtance by equation (F.5).

Following an iterative solving procedure, equations (F.6) and (F.9) are solved simultaneously, in order to obtain the values for the refractive index, n_c, and coefficient of extinction, C_e, for the particular plastic.

Hence, find for n_c = 1.6 and C_e = 200, that the right-hand side of equation (F.6) yields a value of

$$RHS = \left(\frac{1}{1-(1-0.9)\times\rho_d}\right)\left(\frac{(1-\rho_b)^2\tau_{b\alpha}}{1-\rho_b^2\tau_{b\alpha}}\times 642.793 + \frac{(1-\rho_d)^2\tau_{d\alpha}}{1-\rho_d^2\tau_{d\alpha}}\times 55.895\right)$$

$$= \left(\frac{1}{1-0.1\times 0.105238}\right)\left(\frac{(1-0.069)^2\times 0.9558}{1-0.069^2\times 0.9558^2}\times 642.793 + \frac{(1-0.105238)^2\times 0.9535}{1-0.105238^2\times 0.9535^2}\times 55.895\right)$$

$$= 584.09\ W/m^2$$

and the right-hand side of equation (F.9)

$$RHS = \left(\frac{1}{1-(1-0.1)\times\rho_d}\right)\left(\frac{(1-\rho_b)^2\tau_{b\alpha}}{1-\rho_b^2\tau_{b\alpha}}\times 764.318 + \frac{(1-\rho_d)^2\tau_{d\alpha}}{1-\rho_d^2\tau_{d\alpha}}\times 75.592\right)$$

$$= \left(\frac{1}{1-0.9\times 0.105238}\right)\left(\frac{(1-0.05689)^2\times 0.95797}{1-0.05689^2\times 0.95797^2}\times 764.318 + \frac{(1-0.105238)^2\times 0.9535}{1-0.105238^2\times 0.9535^2}\times 75.592\right)$$

$$= 785.92\ W/m^2.$$

Comparing the above-calculated theoretical values against the experimentally measured value (Ih_p = 583.95 W/m^2 for the black surface and Ih_p = 785.16 for silver surface), it is evident that there is good agreement between the values.

Similar calculations were also conducted for a number of other measured points and the results of these calculations are shown in Figure F.1 and Figure F.2.

Appendix G: Long-wave emissivity of plastic film

To determine the long-wave radiation heat exchange between the cover and absorber plate, as well as between the cover and environment, the long-wave emissivity of the cover, ε_c, needs to be known. For that reason, a simple solar collector test is conducted in order to determine the emissivity of the plastic film under consideration.

G.1 Experimental apparatus

The experimental apparatus used in the present investigation is identical to the one described in appendix D, with the only difference being the use of a plastic film for the solar collector's cover.

The temperature of the black absorber plate is measured with the aid of two type-T thermocouples, while the incident solar radiation is measured by means of a solar sensor placed next to the cover surface. Ambient conditions are monitored and recorded by a Davis weather station located near the apparatus.

Due to the negligible thickness of the plastic film (0.0002 m), it is questionable whether one would be able to measure the plastic cover temperature accurately with contact temperature sensors.

To overcome this problem, it was decided that the previously derived cover and plate energy equations for the solar collector (Appendix D) would be used to predict the respective cover and absorber plate temperature for given ambient conditions and assumed plastic film long-wave emissivity.

If an agreement is obtained between the experimental and theoretical absorber plate temperature for a given long-wave emissivity value, it would suggest that the equations employed as well as the cover emissivity is accurate.

G.2 Analysis

The objective of the analysis is to obtain the relevant energy equations for the cover and plate of a simple solar collector with a plastic cover.

G.2.1 Cover

From Appendix D, it follows that the steady state energy equation for the cover (which is essentially the case at solar noon) is

$$\frac{(1-\rho_b)(1-\tau_{\alpha b})}{1-\rho_b\,\tau_{\alpha b}}\,Ih_b+\frac{(1-\rho_d)(1-\tau_{\alpha d})}{1-\rho_d\,\tau_{\alpha d}}\,Ih_d$$

$$+\left[1+1.44\left[1-\frac{1708}{Ra_{pc}}\right]+\left[\left(\frac{Ra_{pc}}{5830}\right)^{1/3}-1\right]\right]\frac{k_{pc}}{t_{air}}\left(T_p-T_c\right)+q_{pc} \qquad (G.1)$$

$$=\left[\left(Gr_{ca}\,Pr_{ca}\right)^{1/3}\left(0.227+1.406\times10^{-6}\,Re_{ca}\right)\right]\frac{k_{ca}}{L_c}\left(T_c-T_a\right)+\varepsilon_c\,\sigma\left(T_c^4-\left(0.0552\,T_a^{1.5}\right)^4\right)$$

with q_{pc} defining the long-wave radiation heat exchange between the plate and cover.

Glass covers are opaque to long-wave radiation, in contrast to plastic covers that tend to transmit a certain percentage of the long-wave radiation. To account for the transmitted solar radiation, Duffie and Beckman [91DU1] suggest that equation (G.2) be used for the evaluation of the net radiation heat exchange between the absorber plate and the partially transparent cover

$$q_{rpc}=\frac{\sigma\,\varepsilon_c\,\varepsilon_p\left(T_p^4-T_c^4\right)}{1-\rho_c\,\rho_p} \qquad (G.2)$$

where ρ_c and ρ_p are the respective cover and absorber plate long-wave reflectivities. According to Mills [92MI1], the long-wave reflectivity of a transparent medium is

$$\rho_c=1-\tau_c-\alpha_c \qquad (G.3)$$

However, for a grey surface the emissivity is equal to its absorptivity ($\alpha_c=\varepsilon_c$) [92MI1]. Thus the long-wave reflectivity of a cover with long-wave transmittance τ_c, becomes

$$\rho_c=1-\tau_c-\varepsilon_c \qquad (G.4)$$

Furthermore, for an opaque surface [92MI1], it follows that

$$\rho_p=1-\alpha_p \qquad (G.5)$$

Upon substituting equations (G.4) and (G.5) into equation (G.3), the following equation is obtained for the evaluation of the net long-wave radiation heat exchange between the absorber plate and the cover

$$q_{pc} = \frac{\sigma \varepsilon_p \varepsilon_c \left(T_p^4 - T_c^4\right)}{1-(1-\alpha_p)(1-\tau_c-\varepsilon_c)} \tag{G.6}$$

With this equation for the plate-cover heat exchange, the cover energy equation becomes

$$\frac{(1-\rho_b)(1-\tau_{\alpha b})}{1-\rho_b \tau_{\alpha b}} Ih_b + \frac{(1-\rho_d)(1-\tau_{\alpha d})}{1-\rho_d \tau_{\alpha d}} Ih_d$$

$$+\left[1+1.44\left[1-\frac{1708}{Ra_{pc}}\right]+\left[\left(\frac{Ra_{pc}}{5830}\right)^{1/3}-1\right]\right]\frac{k_{pc}}{t_{air}}(T_p-T_c)+\frac{\sigma \varepsilon_p \varepsilon_c \left(T_p^4 - T_c^4\right)}{1-(1-\alpha_p)(1-\tau_c-\varepsilon_c)} \tag{G.7}$$

$$=\left[(Gr_{ca}\,Pr_{ca})^{1/3}\left(0.227+1.406\times10^{-6}\,Re_{ca}\right)\right]\frac{k_{ca}}{L_c}(T_c-T_a)+\varepsilon_c \sigma\left(T_c^4-\left(0.0552\,T_a^{1.5}\right)^4\right)$$

G.2.2 Absorber plate

Consider the insulated absorber plate top surface of a plastic cover solar collector, as shown in Figure G.1.

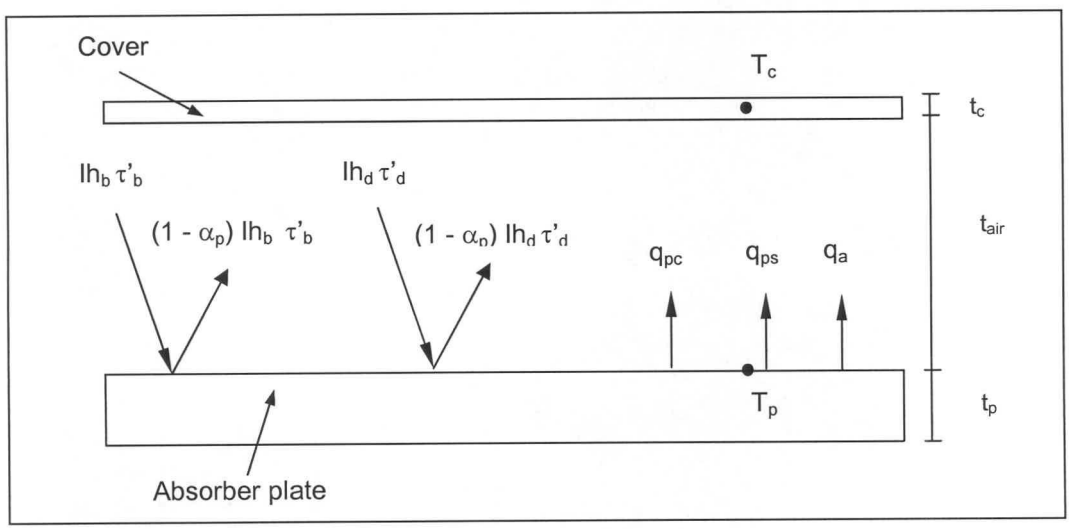

Figure G.1: Energy balance on top surface of insulated absorber plate

For the insulated absorber plate shown in Figure G.1, the following energy balance can be written

$$Ih_b \tau_b' + Ih_d \tau_d' = (1-\alpha_p) Ih_b \tau_b' + (1-\alpha_p) Ih_d \tau_d' + q_{ps} + q_{pc} + q_a \tag{G.8}$$

which, from Appendix D, reduces to

$$\begin{aligned} &\frac{\alpha_p}{1-(1-\alpha_p)\rho_d}\left(\frac{(1-\rho_b)^2 \tau_{\alpha b}}{1-\rho_b^2 \tau_{\alpha b}^2} Ih_b + \frac{(1-\rho_d)^2 \tau_{\alpha d}}{1-\rho_d^2 \tau_{\alpha d}^2} Ih_d\right) \\ &= q_{ps} + q_{pc} + \left[1+1.44\left[1-\frac{1708}{Ra_{pc}}\right]+\left[\left(\frac{Ra_{pc}}{5830}\right)^{1/3}-1\right]\right]\frac{k_{pc}}{t_{air}}(T_p - T_c) \end{aligned} \tag{G.9}$$

In the above equation, q_{ps} defines the net long-wave radiation heat exchange between the plate and the sky, which according to Duffie and Beckman [91DU1], is to be evaluated according to the equation given below

$$q_{ps} = \frac{\sigma \tau_c \varepsilon_p \left(T_p^4 - T_s^4\right)}{1-\rho_p \rho_c} \tag{G.10}$$

Substituting equations (G.4) and (G.5), as well as Swinbank's [63SW1] sky temperature equation (equation (A.3)) into equation (G.10), the plate-sky radiation equation becomes

$$q_{ps} = \frac{\tau_c \varepsilon_p \left(T_p^4 - \left(0.0552\, T_a^{1.5}\right)^4\right)}{1-(1-\alpha_p)(1-\tau_c-\varepsilon_c)} \tag{G.11}$$

Upon substitution of equations (G.6) and (G.11) into equation (G.9), the conservation of energy equation for the insulated plate yields

$$\begin{aligned} &\frac{\alpha_p}{1-(1-\alpha_p)\rho_d}\left(\frac{(1-\rho_b)^2 \tau_{\alpha b}}{1-\rho_b^2 \tau_{\alpha b}^2} Ih_b + \frac{(1-\rho_d)^2 \tau_{\alpha d}}{1-\rho_d^2 \tau_{\alpha d}^2} Ih_d\right) = \frac{\sigma \tau_c \varepsilon_p \left(T_p^4 - \left(0.0552\, T_a^{1.5}\right)^4\right)}{1-(1-\alpha_p)(1-\tau_c-\varepsilon_c)} \\ &+ \frac{\sigma \varepsilon_p \varepsilon_c \left(T_p^4 - T_c^4\right)}{1-(1-\alpha_p)(1-\tau_c-\varepsilon_c)} + \left[1+1.44\left[1-\frac{1708}{Ra_{pc}}\right]+\left[\left(\frac{Ra_{pc}}{5830}\right)^{1/3}-1\right]\right]\frac{k_{pc}}{t_{air}}(T_p - T_c) \end{aligned} \tag{G.12}$$

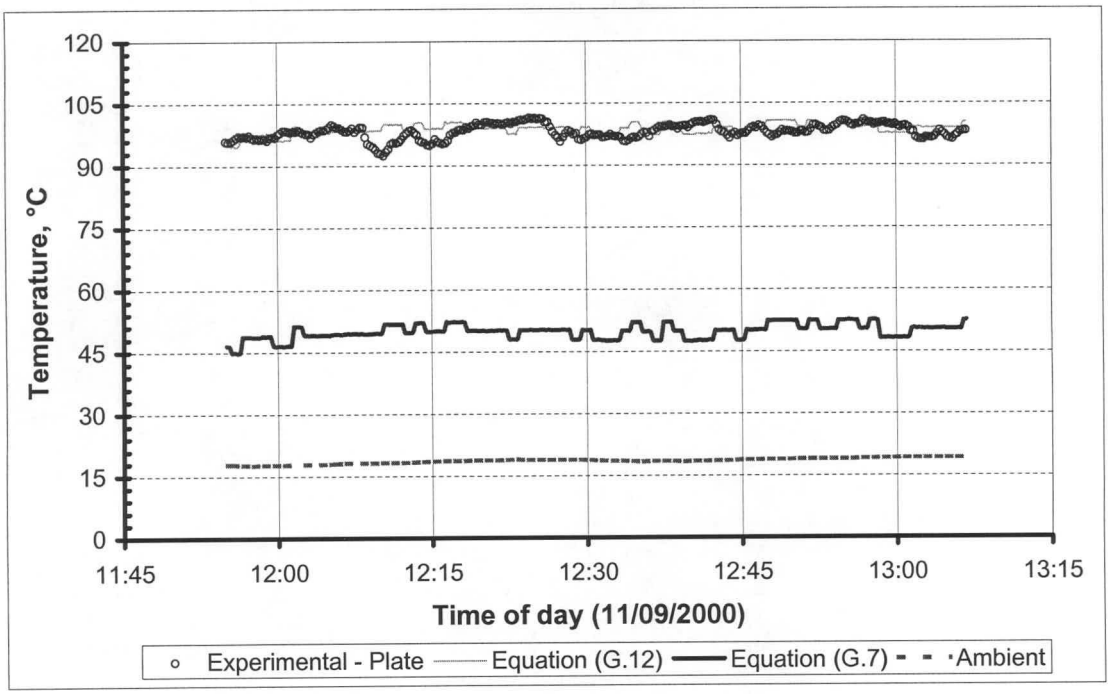

Figure G.2: Experimental absorber plate temperature and theoretically predicted cover and absorber plate temperatures for a cover emissivity of 0.8

G.3 Results

Experiments were conducted on the 11th of September 2000. The experimental results are shown in Figure G.2

By employing equations (G.7) and (G.12), the cover and plate temperatures are predicted for given ambient conditions and a specified cover emissivity. From Figure G.2, it is apparent that for a cover emissivity of 0.8, good agreement is obtained between the predicted and experimentally measured plate temperatures.

In the following section, a numerical example will be used to illustrate the solution procedure.

Numerical example

In Table G.1 the collector specifications as well as the experimental plate temperature and ambient conditions are shown for the 11th September 2000 (DOY = 255th day of year) at 12h12:17 (ψ = 12.20472).

In the subsequent calculations, it will be shown that the cover and plate energy equations (equations (G.7) and (G.12) are satisfied for respective cover and plate temperatures of 49.415 °C (322.565 K) and of 98.666 °C (371.816K) and a given long-wave emissivity, ε_c, of 0.8 for the cover.

Table G.1: Experimental long-wave emissivity test data

Cover thickness, t_c	0.0002 m
Side length of cover, L_c	1.0 m
Cover extinction coefficient, C_e	200 m^{-1}
Cover refractive index, n_c [91DU1]	1.6
Experimental plate temperature, T_p	98.6569 °C (371.806 K)
Long-wave emissivity of plate, ε_p	0.90
Solar absorptivity of plate, α_p	0.90
Ambient temperature, T_a	18.2 °C (291.35 K)
Total incident solar radiation, I_{hT}	788.17 W/m^2K
Wind speed, v_w	0.4 m/s
Atmospheric pressure, p_a	101 290 Pa
Location latitude angle, ϕ	33.98 °S
Location longitude angle, ϕ_l	18.85 °E
Location standard meridian, ϕ_m	30.00 °E
Air enclosure height, t_{air}	0.0395 m
%Diffuse radiation of total solar radiation	9.0

The leap year adjustment to the day for the year 2000, according to equation (B.21), is

$$YADJ = 0.25\left[2.5-\left(Y-4\left(\text{integer}\left((Y-1)/4\right)\right)\right)\right] = 0.25\times\left[2.5-\left(2000-4\left(\text{integer}\left((2000-1)/4\right)\right)\right)\right]$$

$$= -0.375 \text{ days}$$

with the above integer function yielding a value of 499.

For the 255th day of the year, the annual phase angle (equation (B.20)) yields a value of

$$P = 0.0172028\ (DOY + YADJ + 0.417) = 0.0172028\ (255 + (-0.375) + 0.417) = 4.3874 \text{ rad.}$$

Upon substituting the annual phase angle into the declination angle equation (equation (B.19)), the declination angle is found to be

$$\delta = 180\,[0.00661 + 0.40602\sin(P - 1.4075) + 0.00665\sin(2P - 1.4789)$$
$$+ 0.00298\sin(3P - 1.0996)]\,\pi$$
$$= 180\,[0.00661 + 0.40602\sin(4.3874 - 1.4075) + 0.00665\sin(2\times 4.3874 - 1.4789)$$
$$+ 0.00298\sin(3\times 4.3874 - 1.0996)]\,\pi$$
$$= 4.3638°$$

while the previously determined phase angle leads to an equation of time (equation (B.23)) of

$$EOT = 1440\,[0.005114\sin(P + 3.0593) + 0.006892\sin(2P + 3.4646)$$
$$+ 0.00022\sin(3P + 3.3858) + 0.000153\sin(4P + 3.7766)]$$
$$= 1440\,[0.005114\sin(4.3874 + 3.0593) + 0.006892\sin(2\times 4.3874 + 3.4646)$$
$$+ 0.00022\sin(3\times 4.3874 + 3.3858) + 0.000153\sin(4\times 4.3874 + 3.7766)]$$
$$= 3.4751\,\text{min}.$$

The hour angle for the 11th September 2000, according to equation (B.22), at 12h12:17 or 12.20472 hours after midnight, is

$$\omega = 15\left[\psi - 12 - \frac{4(\phi_m - \phi_l) - EOT}{60}\right] = 15\left[12.20472 - 12 - \frac{4(30 - 18.85) - (3.4751)}{60}\right] = -7.2104°.$$

Consequently, for the experimental location, with a standard meridian, ϕ_m, of 30° E, longitude, ϕ_l, of 18.85° E and latitude of 33.98° S, equation (B.24) yields a beam incidence angle of

$$\theta_b = a\cos(\sin\delta\sin\phi + \cos\delta\cos\phi\cos\omega)$$
$$= a\cos(\sin 4.3638\ \sin - 33.98 + \cos 4.3638\ \times\cos - 33.98\ \times\cos - 7.2104) = 38.9437°.$$

For a cover surrounded by air, the beam reflectivity according to equation (B.12), is

$$\rho_b = \frac{1}{2}\left[\frac{\tan^2(\theta_b - \arcsin(n_a\sin\theta_b/n_c))}{\tan^2(\theta_b + \arcsin(n_a\sin\theta_b/n_c))} + \frac{\sin^2(\theta_b - \arcsin(n_a\sin\theta_b/n_c))}{\sin^2(\theta_b + \arcsin(n_a\sin\theta_b/n_c))}\right]$$
$$= \frac{1}{2}\left[\frac{\tan^2(38.9437 - \arcsin(\sin 38.9437/1.6))}{\tan^2(38.9437 + \arcsin(\sin 38.9437/1.6))} + \frac{\sin^2(38.9437 - \arcsin(\sin 38.9437/1.6))}{\sin^2(38.9437 + \arcsin(\sin 38.9437/1.6))}\right]$$
$$= 0.058815$$

while Bouguer's law (equation (B.16)), yields a value of

$$\tau_{b\alpha} = e^{-C_e\, t_c \,/\, \cos(\arcsin(n_a \sin\theta_b \,/\, n_c))} = e^{-200 \times 0.0002 \,/\, \cos(\arcsin(\sin 38.9437 \,/\, 1.6))} = 0.95743$$

for the beam transmissivity due to absorbtance for the 0.0002 m thick plastic cover.

Using an equivalent incidence angle of 60° [91DU1], the respective diffuse reflectivity and transmissivity due to absorbtance for the cover are evaluated with the aid of equations (B.12) and (B.16).

$$\rho_d = \frac{1}{2}\left[\frac{\tan^2(\theta_d - \arcsin(n_a \sin\theta_d / n_c))}{\tan^2(\theta_d + \arcsin(n_a \sin\theta_d / n_c))} + \frac{\sin^2(\theta_d - \arcsin(n_a \sin\theta_d / n_c))}{\sin^2(\theta_d + \arcsin(n_a \sin\theta_d / n_c))}\right]$$

$$= \frac{1}{2}\left[\frac{\tan^2(60 - \arcsin(\sin 60 / 1.6))}{\tan^2(60 + \arcsin(\sin 60 / 1.6))} + \frac{\sin^2(60 - \arcsin(\sin 60 / 1.6))}{\sin^2(60 + \arcsin(\sin 60 / 1.6))}\right]$$

$$= 0.1052$$

$$\tau_{d\alpha} = e^{-C_e\, t_c \,/\, \cos(\arcsin(n_a \sin\theta_d \,/\, n_c))} = e^{-200 \times 0.0002 \,/\, \cos(\arcsin(\sin 60 \,/\, 1.6))} = 0.95354$$

Table G.1 reveals that diffuse radiation was 9 % of the total incident solar radiation on the cover. As a result, the incident beam solar radiation on the cover is

$$Ih_b = 0.91 Ih_T = 0.91 \times 785.61 = 714.91\ W/m^2$$

and the diffuse solar radiation

$$Ih_d = 0.09 Ih_T = 0.09 \times 785.61 = 70.70\ W/m^2$$

For the evaluation of the effective convective heat transfer coefficient, the thermophysical properties of the air above the cover need to be known. The cover temperature is predicted as 51.742 °C. Consequently, the air above the cover is at a mean cover-ambient temperature of

$$T_{am} = 0.5(T_a + T_c) = 0.5 \times (18.3 + 51.742) = 35.021°C \text{ or } 308.17 K.$$

and the thermophysical properties of air at this temperature [98KR1] are

Air density $\rho_{ca} = \frac{p_a}{287.08 \times T_{am}} = \frac{101290}{287.08 \times 308.17} = 1.14409 \text{ kg/m}^3$

Specific heat capacity of air $c_{pca} = 1007.27 \text{ J/kg.K}$

Air conductivity $k_{ca} = 0.026852 \text{ W/m.K}$

Dynamic viscosity of air $\mu_{ca} = 1.8843 \times 10^{-5} \text{ N/s.m}^2$

with a corresponding Prandtl number of

$$Pr_{ca} = \frac{\mu_{ca}\, c_{pca}}{k_{ca}} = \frac{1.8843 \times 10^{-5} \times 1007.27}{0.026852} = 0.7068.$$

The effective length for a square cover is the side length, L_c, of the cover. The dimensionless Grashof number is thus

$$Gr_{ca} = \frac{2(T_c - T_a)\, g\, L_c^3\, \rho_{ca}^2}{(T_c + T_a)\mu_{ca}^2} = \frac{2 \times (324.892 - 291.45) \times 9.8 \times 1.0^3 \times 1.1449^2}{(324.892 + 291.45) \times (1.8843 \times 10^{-5})^2} = 3.93011 \times 10^9$$

To determine the natural convection heat transfer coefficient the thermophysical properties of the entrapped air needs to be evaluated at a mean absorber plate-cover temperature of

$$T_{em} = 0.5(T_p + T_c) = 0.5 \times (100.369 + 51.742) = 76.05\,^{\circ}\text{C or } 349.2\,\text{K}.$$

For the above temperature, the thermophysical properties of the air, according to Kröger [98KR1], are

Air density $\rho_{pc} = \frac{p_a}{287.08 \times T_{em}} = \frac{101290}{287.08 \times 349.2} = 1.0102 \text{ kg/m}^3$

Specific heat capacity of air $c_{ppc} = 1009.8 \text{ J/kg.K}$

Air conductivity $k_{pc} = 0.029947 \text{ W/m.K}$

Dynamic viscosity of air $\mu_{pc} = 2.0675 \times 10^{-5} \text{ N/s.m}^2$

which leads to a corresponding Prandtl number of

$$Pr_{pc} = \frac{\mu_{pc}\, c_{ppc}}{k_{pc}} = \frac{2.0675 \times 10^{-5} \times 1009.8}{0.029947} = 0.6971.$$

The dimensionless Rayleigh number is defined as the product of the dimensionless Grashof and Prandtl numbers, with the effective length defined as the air gap distance between the plate and cover. The absorber plate-cover dimensionless Rayleigh number for the enclosure is thus

$$Ra_{pc} = Gr_{pc}\,Pr_{pc} = \frac{2\left(T_p - T_c\right) g\, t_{air}^3\, \rho_{pc}^2}{\left(T_p + T_c\right)\mu_{pc}^2} Pr_{pc}$$

$$= \frac{2\times(373.519-324.894)\,x\,9.8\,x\,0.0395^3\,x\,1.0102^2}{(373.519+324.894)\,x\,(2.0675\,x\,10^{-5})^2}\times 0.6971 = 140.106\times 10^3$$

Upon substitution of the previously calculated thermophysical properties and solar characteristics into equation (G.7), the left-hand side of the equation yields

$$LHS = \frac{(1-\rho_b)(1-\tau_{\alpha b})}{1-\rho_b\,\tau_{\alpha b}} Ih_b + \frac{(1-\rho_d)(1-\tau_{\alpha d})}{1-\rho_d\,\tau_{\alpha d}} Ih_d$$

$$+\left[1+1.44\left[1-\frac{1708}{Ra_{pc}}\right]+\left[\left(\frac{Ra_{pc}}{5830}\right)^{1/3}-1\right]\right]\frac{k_{pc}}{t_{air}}\left(T_p - T_c\right)+\frac{\sigma\,\varepsilon_p\,\varepsilon_c\left(T_p^4 - T_c^4\right)}{1-(1-\alpha_p)(1-\tau_c-\varepsilon_c)}$$

$$=\frac{(1-0.058815)(1-0.95743)}{1-0.058815\times 0.95743}\times 717.235+\frac{(1-0.1052)(1-0.95354)}{1-0.1052\times 0.95354}\times 70.935$$

$$+\left[1+1.44\left[1-\frac{1708}{140.106\times 10^3}\right]+\left[\left(\frac{140.106\times 10^3}{5830}\right)^{1/3}-1\right]\right]\frac{0.029947}{0.0395}(373.519-324.894)$$

$$+\frac{5.67\times 10^{-8}\times 0.9\times\ 0.8\left(373.519^4 - 324.894^4\right)}{1-(1-0.9)(1-0.15-0.8)} = 534\ W/m^2$$

and the right-hand side of the cover energy equation a value of

$$RHS = \left[\left(Gr_{ca}\,Pr_{ca}\right)^{1/3}\left(0.227+1.406\times 10^{-6}\,Re_{ca}\right)\right]\frac{k_{ca}}{L_c}\left(T_c - T_a\right)+\varepsilon_c\,\sigma\left(T_c^4-\left(0.0552\,T_a^{1.5}\right)^4\right)$$

$$=\left[\left(3.93011\times 10^9\times 0.7068\right)^{1/3}\left(0.227+1.406\times 10^{-6}\times 0\right)\right]\frac{0.026852}{1.0}(324.894-291.45)$$

$$+0.8\times 5.67\times 10^{-8}\left(324.894^4-\left(0.0552\times 291.45^{1.5}\right)^4\right)=534\ W/m^2$$

Consequently, the conservation of energy equation for the cover is satisfied.

Repeating the previous procedure, the relevant thermophysical properties and solar characteristics are substituted into the left-hand side of the plate energy equation (equation G.12), which yields

$$LHS = \frac{\alpha_p}{1-(1-\alpha_p)\rho_d}\left(\frac{(1-\rho_b)^2\,\tau_{\alpha b}}{1-\rho_b^2\,\tau_{\alpha b}^2}Ih_b + \frac{(1-\rho_d)^2\,\tau_{\alpha d}}{1-\rho_d^2\,\tau_{\alpha d}^2}Ih_d\right)$$

$$= \frac{0.9}{1-(1-0.9)0.1052}\left(\frac{(1-0.058815)^2\times 0.95743}{1-0.058815^2\times 0.95743^2}\times 717.235 + \frac{(1-0.1052)^2\times 0.95354}{1-0.1052^2\times 0.95354^2}\times 70.935\right)$$

$$= 604.8\ W/m^2$$

Substitute the dimensionless Rayleigh number and cover characteristics into the right-hand side of equation (G.12), and find

$$RHS = \frac{\tau_c\,\alpha_p\left(T_p^4 - \left(0.0552\,T_a^{1.5}\right)^4\right)}{1-(1-\alpha_p)(1-\tau_c-\varepsilon_c)} + \frac{\sigma\,\varepsilon_p\,\varepsilon_c\left(T_p^4 - T_c^4\right)}{1-(1-\alpha_p)(1-\tau_c-\varepsilon_c)}$$

$$+\left[1+1.44\left[1-\frac{1708}{Ra_{pc}}\right]+\left[\left(\frac{Ra_{pc}}{5830}\right)^{1/3}-1\right]\right]\frac{k_{pc}}{t_{air}}\left(T_p-T_c\right)$$

$$= \frac{5.67\times10^{-8}\times0.15\times0.9\left(373.519^4 - \left(0.0552\times291.45^{1.5}\right)^4\right)}{1-(1-0.9)(1-0.15-0.8)}$$

$$+\left[1+1.44\left[1-\frac{1708}{140.105\times10^5}\right]+\left[\left(\frac{140.105\times10^5}{5830}\right)^{1/3}-1\right]\right]\frac{0.029947}{0.0395}(373.519-324.894)$$

$$+\frac{5.67\times10^{-8}\times0.9\times0.8\left(373.519^4-324.894^4\right)}{1-(1-0.9)(1-0.15-0.8)} = 604.8\ W/m^2$$

As in the case of the solar collector cover, it is shown that the predicted temperatures satisfy the absorber plate energy equation of the simple plastic solar collector, with a cover emissivity of 0.8.

Similar calculations were also conducted for a number of other points, from which it was evident (see Figure G.2) that a cover emissivity of 0.8 yields good agreement between the predicted and experimentally measured absorber plate temperatures.

Appendix H: Plastic covered water tank – Day operation

To evaluate the thermal energy storage ability of water, a number of experiments were conducted on a plastic covered water tank that was exposed to the natural environment. The measured results were then compared to theoretically predicted temperatures.

H.1 Analysis

In Figure H.1 a plastic covered water tank, having plan dimensions of 1m x 1m, was considered. It consisted of a bulk of water, at a mean temperature T_w, and a thin plastic film at temperature, T_f, that suppressed evaporation. The bottom of the tank was black, while a highly reflective material covered the inner sides of the tank.

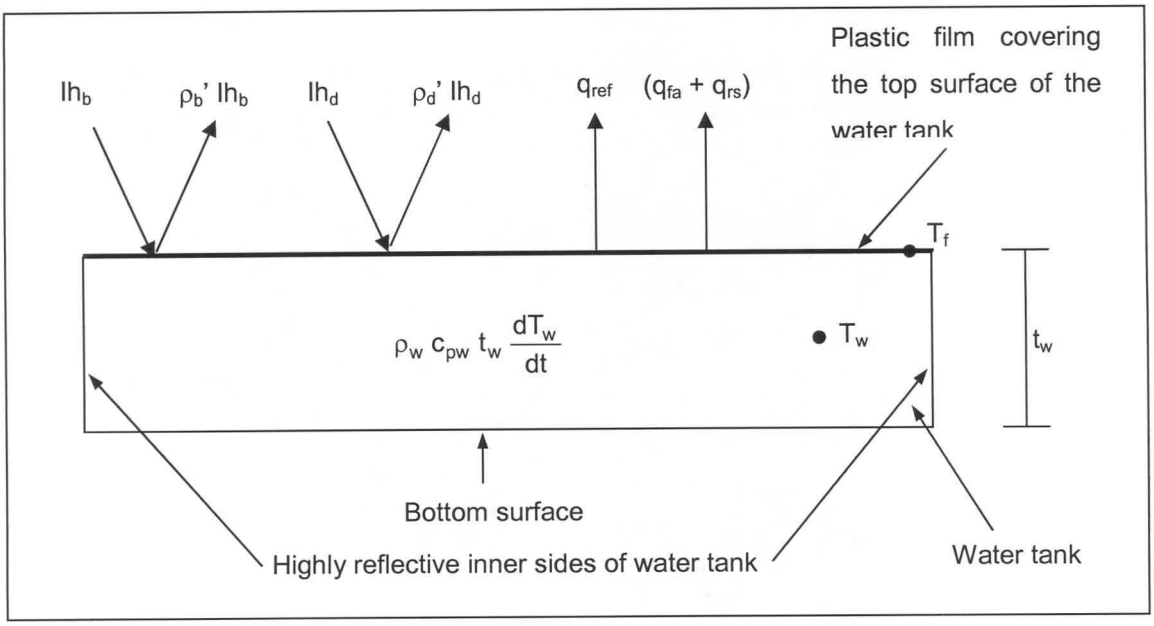

Figure H.1: Schematic presentation of plastic covered water tank

For the above schematic presentation of the plastic covered water tank, the following conservation of energy equation is applicable

$$Ih_b + Ih_d - \rho_b' Ih_b - \rho_b' Ih_b - (q_{fa} + q_{rs}) - q_{ref} = \rho_w c_{pw} t_w \frac{dT_w}{dt} \qquad (H.1)$$

In equation (H.1), (q_{fa} + q_{rs}) represents the total heat loss from the plastic surface to the environment due to convection and sky radiation, and q_{ref} is the transmitted incident solar radiation which is reflected back to the environment, while ρ_b' and ρ_d' define the short-wave reflectivity of the air-cover-water interface for beam and diffuse solar radiation. t_w is the water depth.

The plastic film used in the experiments had a low density and thickness; therefore the assumption was made that the thermal capacitance of the film was negligible. The sides and bottom of the water tank were well insulated. Consequently, the conduction losses through the bottom and the sides of the water tank were assumed to be negligible.

In Figure H.1, provision is made for the possibility that a certain amount of the transmitted incident solar radiation may be reflected by the black bottom back to the environment. This is in contrast to the model proposed by Tsilingiris [94TS1] who assumed that none of the transmitted incident solar radiation is transmitted back to the environment. To clarify this point, a study was undertaken.

Assume a 1000 W/m^2 of solar radiation is incident on the plastic cover. Employing the equation of Modest [93MO1], (equation (B.5)) the effective transmissivity, τ', of the air-film-water interface, and consequently the amount of radiation that is transmitted through the interface, is determined for various incidence angles, θ (see Figure H.2).

The research of Dale and Harleman [69DA1], Rubin and Benedict [84RU1], Modest [93MO1], Tsilingiris [94TS1] and Jamal and Muaddi [90FA1] reveal that solar radiation is absorbed in the water as it passes through it.

From the most recent work of Jamal and Muaddi [90AF1] it follows that for an incidence angle, θ, the available solar radiation, Ih_w, at a water depth of, t_w, of clean water would be

$$Ih_w = (\tau' Ih)\left\{35.22\left[\frac{t_w}{\cos(a\sin(\sin\theta/1.333))}\right]^{0.016}\right\}/100$$

$$\times(\tau' Ih)\left\{\exp\left(-0.05\left[\frac{t_w}{\cos(a\sin(\sin\theta/1.333))}\right]\right)\right\}/100 \qquad \text{(H.2)}$$

$$\times(\tau' Ih)\left\{\exp\left(\exp\left(-2.08\left[\frac{t_w}{\cos(a\sin(\sin\theta/1.333))}\right]^{0.48}\right)\right)\right\}/100$$

with Ih defining the incident solar radiation and τ' the effective transmittance of the film.

Employing equation (H.2), the amount of solar radiation that is absorbed by the water in the water tank is determined (see Figure H.2). Furthermore, by setting t_w in equation (H.2) equal to the water tank depth of 190 mm, and multiplying equation (H.2) by the solar absorbtivity of the bottom of the tank, the amount of solar radiation that is absorbed by the bottom is determined.

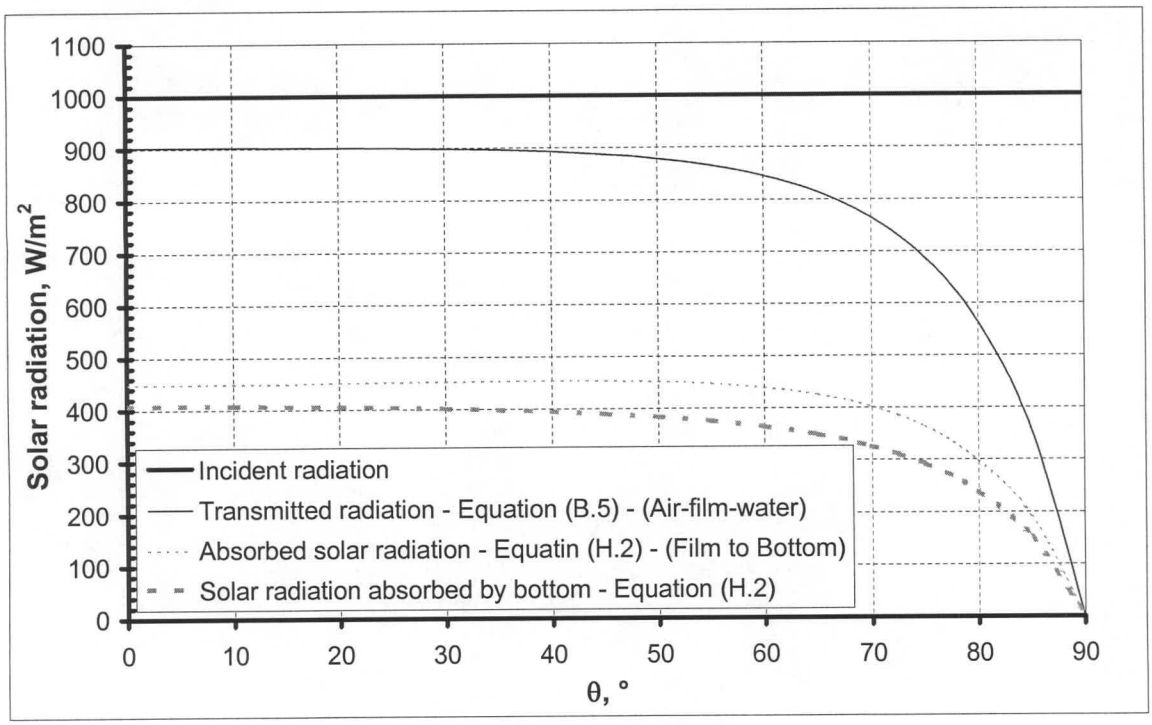

Figure H.2: Solar energy available at various positions

A black surface is a diffuse emitter according to Mills [92MI1]. As a result, the reflected solar radiation is distributed uniformly in all the directions. Duffie and Beckman [91DU1], referring to the diffuse radiation, state that an equivalent angle of 60° should be used for the determination of diffuse properties. Therefore, employing the equivalent diffuse angle in conjunction with equation (H.2), the total amount of solar radiation which reaches the film is determined (see Figure H.3).

From Cengel and Özsik [85CE1] it is apparent that only solar radiation in a small incidence angle band (0° - 48.6° from the normal) is to be transmitted. However, the bottom is a diffuse emitter; with the result, that the incident bottom reflected solar energy is coming from all possible directions. Consequently, the decision was made that an area averaged effective transmissivity would be used to determine the percentage of solar radiation that is transmitted back to the environment.

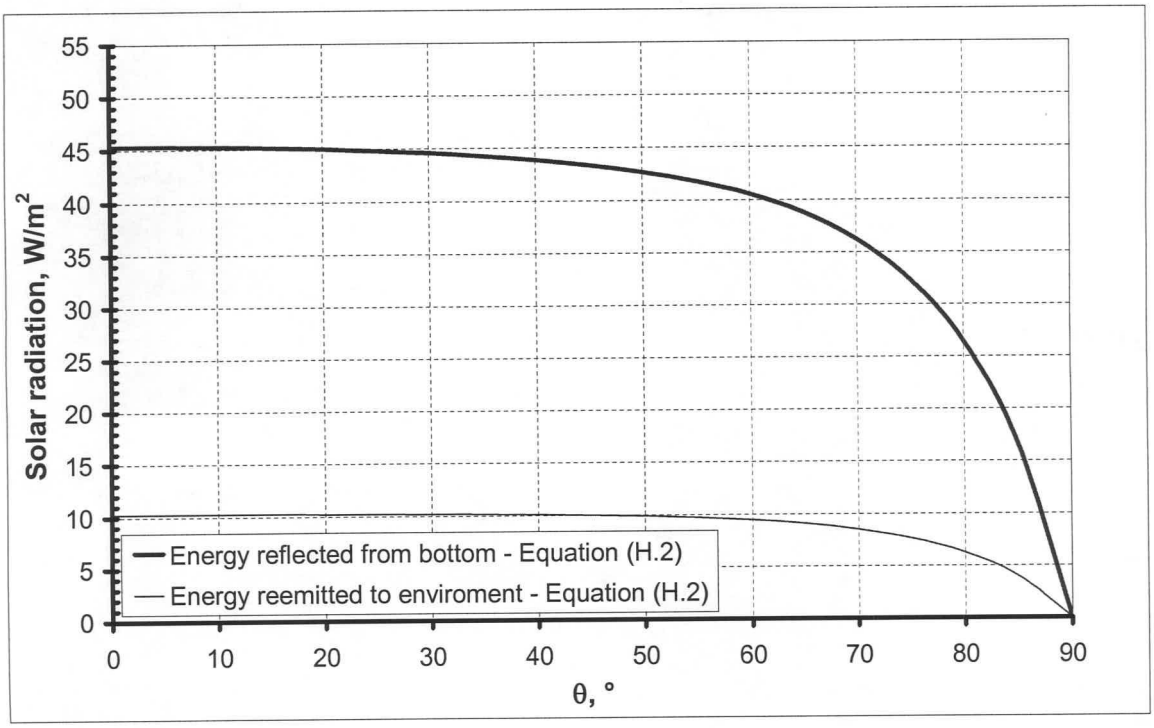

Figure H.3: Reflected and reemitted solar energy

To obtain an area average effective transmissivity for the water-film-air-interface, equation (B.5) is numerically integrated (see Figure H.4) for incidence angles ranging from 0 to π radians, (see equation (H.3)) which yielded a value of 0.273 (27.3%) for the area averaged effective transmissivity of the water-film-air interface.

$$\overline{\tau'} = \frac{1}{2\pi}\int_0^{\pi}\tau' dA = \frac{1}{2\pi}\int_0^{\pi}\tau' 2\pi \sin\theta \, d\theta = \int_0^{\pi}\tau' \sin\theta \, d\theta \qquad \text{(H.3)}$$

Multiplying the above calculated area averaged effective transmissivity for the water-film-air interface with the already determined amount of solar radiation available at the film, an indication is gained of the fraction of the incident solar radiation that escapes back to the environment (see Figure H.4).

From Figure H.4, it is evident that only a small percentage of the total incident solar radiation (± 1%) is emitted back to the environment. Accordingly, it is assumed to be negligible in the current analysis.

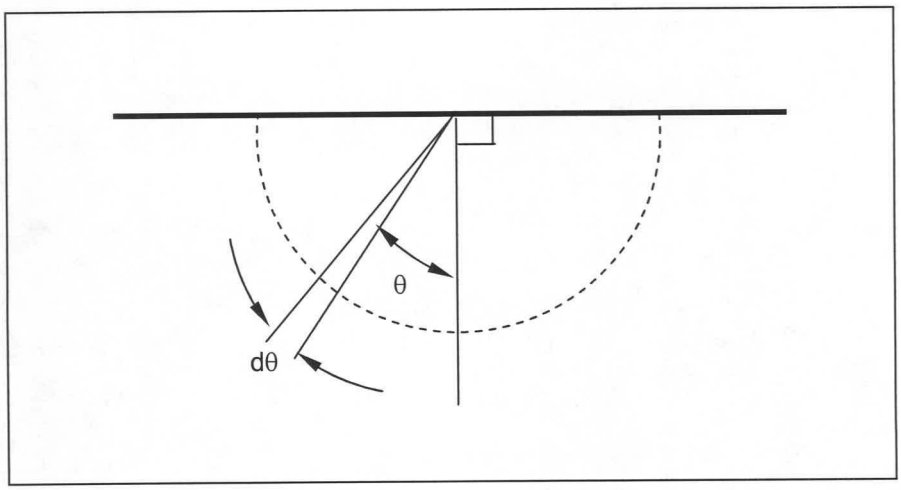

Figure H.4: Numerical integration of effective diffuse transmissivity

Upon substitution of equation (A.8), which accounts for the total heat loss from the film to environment, into equation (H.1), the energy equation for the water tank becomes

$$\left(1-\rho_b^{'}\right)Ih_b+\left(1-\rho_d^{'}\right)Ih_d-\left[\left(Gr_{fa}\,Pr_{fa}\right)^{1/3}\left(0.227+1.406\times10^{-6}\,Re_{fa}\right)\right]\frac{k_{fa}}{L_f}\left(T_c-T_a\right)$$
$$-\sigma\varepsilon_f\left[T_c^4-\left(0.0552\,T_a^{1.5}\right)^4\right]=\rho_w\,c_{pw}\,t_w\,\frac{dT_w}{dt} \qquad \text{(H.4)}$$

As stated previously, the assumption is made that the film's thermal capacitance is negligible, with the result that it is assumed that the film, T_f, and mean water temperature, T_w, will be approximately equal to each other.

Furthermore, upon substituting equation (B.4) into equation (H.4) for the air-film-water interface effective reflectivity, the water tank's conservation of energy equation yields

$$\left[1-\frac{\rho_{baf}+\left(1-2\,\rho_{baf}\right)\rho_{bcw}\,\tau_{\alpha b}^2}{1-\rho_{baf}\,\rho_{bcw}\,\tau_{\alpha b}^2}\right]Ih_b+\left[1-\frac{\rho_{daf}+\left(1-2\,\rho_{daf}\right)\rho_{dcw}\,\tau_{\alpha d}^2}{1-\rho_{daf}\,\rho_{dcw}\,\tau_{\alpha d}^2}\right]Ih_d$$
$$-\left[\left(Gr_{fa}\,Pr_{fa}\right)^{1/3}\left(0.227+1.406\times10^{-6}\,Re_{fa}\right)\right]\frac{k_{fa}}{L_f}\left(T_w-T_a\right)-\sigma\varepsilon_f\left[T_w^4-\left(0.0552\,T_a^{1.5}\right)^4\right] \qquad \text{(H.5)}$$
$$=\rho_w\,c_{pw}\,t_w\,\frac{dT_w}{dt}$$

with ρ_{baf} and ρ_{daf} defining the respective beam and diffuse reflectivity of the air film interface and ρ_{bfw} and ρ_{cfw} the reflectivity of the film water interface for beam and diffuse radiation. The

reflectivity of the upper surface is to be evaluated from equation (B.12), and the lower surface reflectivity with the aid of equation (B.14). Furthermore, equation (H.5) assumes that the water temperature T_w is essentially uniform. Experimental results suggest that this assumption is reasonable.

H.2 Results

As in previous experiments, experimental data are only retained for cases where consecutive cloudless days occur and the daily water temperature profile does not change measurably as to eliminate any secondary heating effects which could influence the water temperature profile. The results for such a test are shown in Figure H.5 and Figure H.6 for the 30th of November 2000.

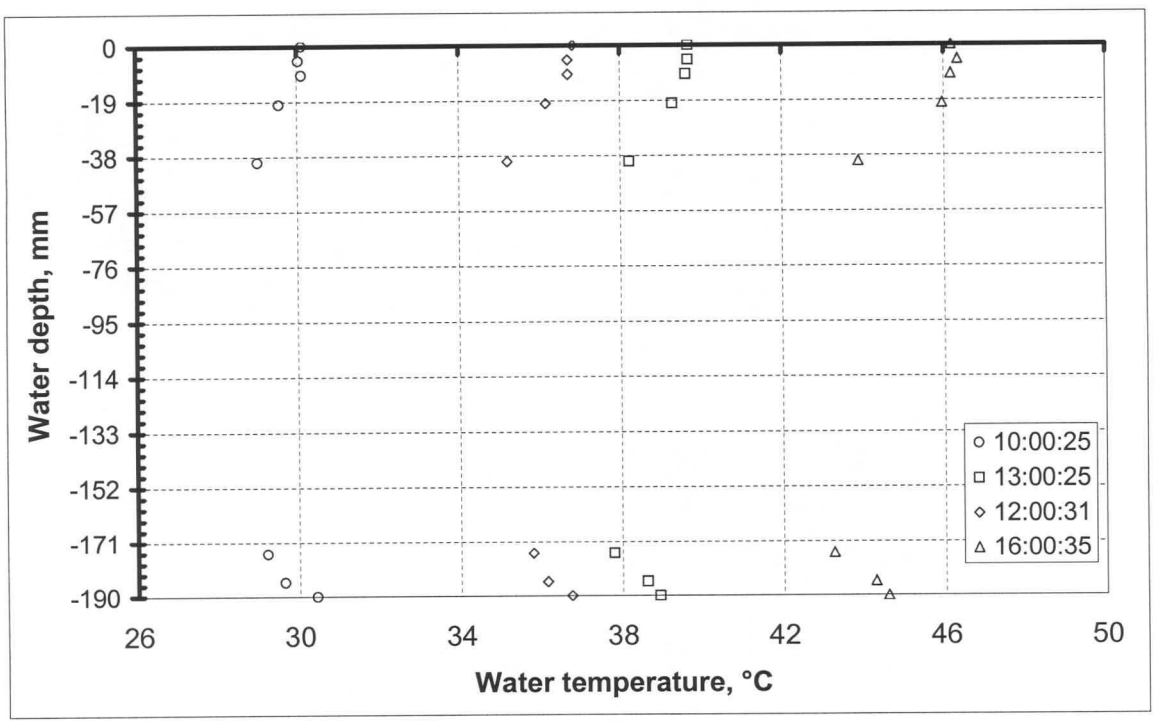

Figure H.5: Water temperature profile

It is clear from Figure H.5, that the warmest water layers occur at the cover and the bottom of the tank. This clearly confirms available theory, which states that the water would be most intensely heated, due to the direct absorbtion of the infrared wavelengths of the solar radiation in the first few millimetres of water underneath the plastic cover, as well as by the bottom which absorbs the transmitted radiation and re-radiates in the long-wave range.

To evaluate equation (H.5) the mean water temperature of the tank temperature is predicted for the 30th of November 2000, and compared to a mean, depth weighted, experimental water temperature.

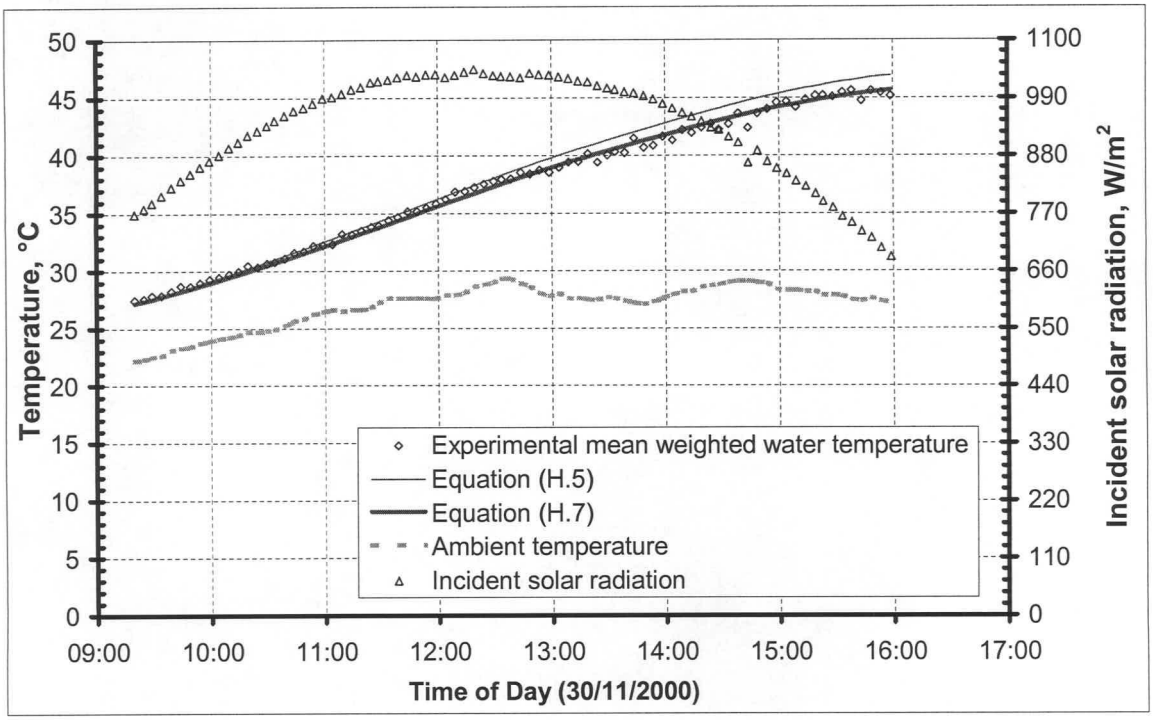

Figure H.6: Theoretically and experimentally mean water temperature for water tank

From Figure H.6, it is evident that as the day progresses the theoretical model tends to predict a higher temperature than that measured experimentally. A possible explanation for this tendency can be deduced from observations made during the execution of the experiments.

As the day progresses (especially from around 13h00 onwards), the water temperature increases and the dissolved air in the water is set free, As a result, air accumulates underneath the plastic cover. So, a second air-water interface is formed under the plastic cover; thus leading to a reduction in the amount of incident solar radiation that is transmitted to the water.

Although attempts were made to remove the bubbles, it quickly became evident that it was a futile process, with bubbles forming as quickly as they were removed.

Assuming the air layer exists from the beginning of the experiment, equation (H.4) is modified in order to account for the influence of the air layer on the mean water temperature inside the water tank.

With air surrounding the plastic cover, equation (B.7) is substituted into equation (H.4) for the effective reflectivity of the cover.

$$\left[1-\frac{\rho_{bc}(1-\rho_{bc})^2\,\tau_{\alpha b}^2}{1-\rho_{bc}^2\,\tau_{\alpha b}^2}\right] Ih_b + \left[1-\frac{\rho_{dc}(1-\rho_{dc})^2\,\tau_{\alpha d}^2}{1-\rho_{dc}^2\,\tau_{\alpha d}^2}\right] Ih_d$$

$$-\left[(Gr_{fa}\,Pr_{fa})^{1/3}\left(0.227+1.406\times10^{-6}\,Re_{fa}\right)\right]\frac{k_{fa}}{L_f}(T_w-T_a)-\sigma\varepsilon_f\left[T_w^4-\left(0.0552\,T_a^{1.5}\right)^4\right] \qquad (H.6)$$

$$=\rho_w\,c_{pw}\,t_w\,\frac{dT_w}{dt}$$

In equation (H.6), ρ_{bc} and ρ_{dc} are the respective beam and diffuse reflectivities evaluated according to Frenel's equation (equation (B.12)).

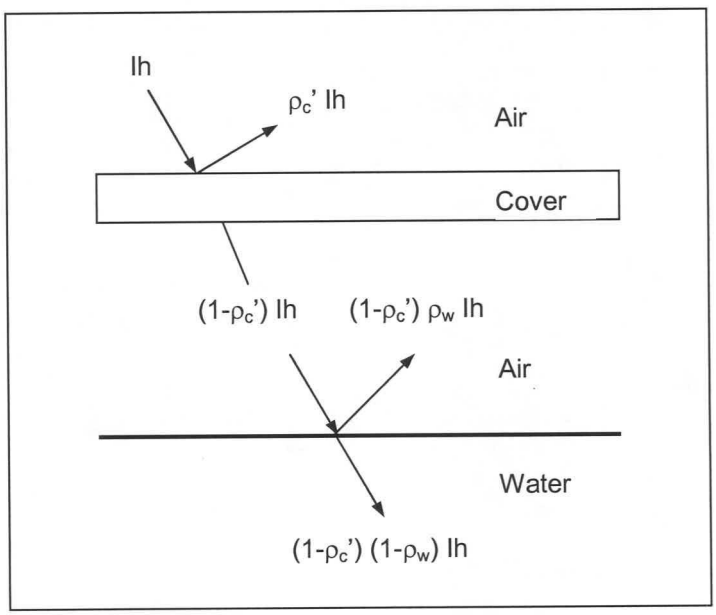

Figure H.7: Air layer influence

The air-water interface under the cover is assumed to be a single interface (see Figure H.7). Therefore, for an air-water reflectivity of ρ_w, the transmittance of the air-water interface is (1 - ρ_w) and the conservation of energy equation for the water tank yields

$$\left[1-\frac{\rho_{bc}(1-\rho_{bc})^2\,\tau_{\alpha b}^2}{1-\rho_{bc}^2\,\tau_{\alpha b}^2}\right](1-\rho_{bw})Ih_b+\left[1-\frac{\rho_{dc}(1-\rho_{dc})^2\,\tau_{\alpha d}^2}{1-\rho_{dc}^2\,\tau_{\alpha d}^2}\right](1-\rho_{dw})\,Ih_d$$

$$-\left[(Gr_{fa}\,Pr_{fa})^{1/3}\left(0.227+1.406\times10^{-6}\,Re_{fa}\right)\right]\frac{k_{fa}}{L_f}(T_w-T_a)-\sigma\varepsilon_f\left[T_w^4-\left(0.0552\,T_a^{1.5}\right)^4\right] \qquad (H.7)$$

$$=\rho_w\,c_{pw}\,t_w\,\frac{dT_w}{dt}$$

Employing the above equation, the mean water temperature of the water tank is once again predicted for the 30th of November 2000 (see Figure H.6).

The results of equation (H.7) confirm the previous speculation concerning the possible influence of the air layer forming underneath the plastic cover on the mean temperature of the water. From Figure H.6, it is evident that in the beginning of the day the experimentally measured water temperature follows equation (H.5), but as the day progresses and the air layer forms, the experimentally measured mean weighted water temperature deviates from equation (H.5) and tends towards the mean water temperature predicted by equation (H.7).

In the following section, the procedure for solving of equation (H.5), and the subsequent prediction of the mean water temperature for the water tank, will be shown for the 30th of November 2000 at 13h00:25.

Numerical example

In Table H.1, the specifications for the plastic covered water tank as well as the ambient conditions, are given for the 30th of November 2000 (DOY = 335th day of year) at 13h00:25 (ψ = 13.007 hours after midnight).

In the following calculations, it will be shown that equation (H.5) is satisfied for a water bulk temperature of 39.794 °C (312.944 K) (see Table H.1) for the given ambient conditions.

According to equation (B.21), the leap year adjustment to the day for the year 2000 is

$$YADJ = 0.25\,[2.5-(Y-4\,(\text{integer}((Y-1)/4)))] = 0.25\times[2.5-(2000-4\,(\text{integer}((2000-1)/4)))]$$

$$= -0.375 \text{ days}$$

with the above integer function yielding a value of 499.

Table H. 1: Experimental data for plastic covered water tank

Water height, t_w	0.190 m
Plastic cover thickness, t_f	0.0002 m
Side length of film, L_f	1.0 m
Film extinction coefficient, C_e	200 m^{-1}
Film refractive index, n_f	1.6
Air refractive index, n_a [91DU1]	1.0
Water refractive index, n_w [92SE1]	1.333
Long-wave emissivity of film, ε_f	0.80
Ambient temperature, T_a	27.8 °C (300.95 K)
Total incident solar radiation, Ih_T	1032.57 W/m^2K
Percentage diffuse radiation	8%
Wind speed, v_w	0.9 m/s
Atmospheric pressure, p_a	100 731 Pa
Location latitude angle, ϕ	-33.98 °N
Location longitude angle, ϕ_l	18.85 °E
Location standard meridian, ϕ_m	30.00 °E
Predicted mean water temperature (13h00:25), T_w^{i-1}	39.794 °C (312.944 K)
Predicted mean water temperature (12h59:24), T_w^{i-1}	39.736 °C (312.886 K)

The 30th of November is the 335th day of the year. Hence, the annual phase angle, according to equation (B.20), is

$$P = 0.0172028\,(DOY + YADJ + 0.417) = 0.0172028\,(3355 + (-0.375) + 0.417) = 5.7636 \text{ rad.}$$

Upon substituting the above-evaluated annual phase angle into equation (B.19), the declination angle for the surface is

$$\begin{aligned}\delta &= 180\,[0.00661 + 0.40602\sin(P - 1.4075) + 0.00665\sin(2P - 1.4789) \\ &\quad + 0.00298\sin(3P - 1.0996)]\,\pi \\ &= 180\,[0.00661 + 0.40602\sin(5.7636 - 1.4075) + 0.00665\sin(2\times 5.7636 - 1.4789) \\ &\quad + 0.00298\sin(3\times 5.7636 - 1.0996)]\,\pi \\ &= -21.725^\circ\end{aligned}$$

which leads to an equation of time (equation (B.23)) of

$$\begin{aligned}EOT &= 1440\,[\,0.005114\sin(P+3.0593)+0.006892\sin(2P+3.4646)\\ &\quad +0.00022\sin(3P+3.3858)+0.000153\sin(4P+3.7766)\,]\\ &= 1440\,[\,0.005114\sin(5.7636+3.0593)+0.006892\sin(2\times5.7636+3.4646)\\ &\quad +0.00022\sin(3\times5.7636+3.3858)+0.000153\sin(4\times5.7636+3.7766)\,]\\ &= 11.208\ \text{min}.\end{aligned}$$

Measurements were taken at 13h00:25 or 13.007 hours after midnight, which, according to equation (B.22) relates to an hour angle of

$$\omega = 15\left[\psi - 12 - \frac{4(\phi_m - \phi_l) - EOT}{60}\right] = 15\left[13.007 - 12 - \frac{4(30-18.85)-(11.208)}{60}\right] = 6.652°.$$

The beam incidence angle (equation (B.24)) for the location with a standard meridian, ϕ_m, of 30° E, longitude, ϕ_l, of 18.85° E and latitude of 33.98° S is thus

$$\begin{aligned}\theta_b &= a\cos(\sin\delta\sin\phi+\cos\delta\cos\phi\cos\omega)\\ &= a\cos(\sin-21.725\sin-33.98+\cos-21.725\times\cos-33.98\times\cos 6.652) = 13.584°.\end{aligned}$$

The top surface of the cover is surrounded by air and the bottom surface by water. From equation (B.12) it follows that the beam reflectivity for the air-film interface is

$$\begin{aligned}\rho_{baf} &= \frac{1}{2}\left[\frac{\tan^2(\theta_b - \arcsin(n_a\sin\theta_b/n_f))}{\tan^2(\theta_b+\arcsin(n_a\sin\theta_b/n_f))}+\frac{\sin^2(\theta_b-\arcsin(n_a\sin\theta_b/n_f))}{\sin^2(\theta_b+\arcsin(n_a\sin\theta_b/n_f))}\right]\\ &= \frac{1}{2}\left[\frac{\tan^2(13.584-\arcsin(\sin 13.584/1.6))}{\tan^2(13.584+\arcsin(\sin 13.584/1.6))}+\frac{\sin^2(13.584-\arcsin(\sin 13.584/1.6))}{\sin^2(13.584+\arcsin(\sin 13.584/1.6))}\right]\\ &= 0.05332\end{aligned}$$

and for the film-water surface equation (B.14) yields

$$\rho_{bfw} = \frac{1}{2}\left[\frac{\tan^2(\arcsin(n_a \sin\theta_b / n_f) - \arcsin(n_a \sin\theta_b / n_w))}{\tan^2(\arcsin(n_a \sin\theta_b / n_f) + \arcsin(n_a \sin\theta_b / n_w))}\right]$$
$$+ \frac{1}{2}\left[\frac{\tan^2(\arcsin(n_a \sin\theta_b / n_f) - \arcsin(n_a \sin\theta_b / n_w))}{\tan^2(\arcsin(n_a \sin\theta_b / n_f) + \arcsin(n_a \sin\theta_b / n_w))}\right]$$
$$= \frac{1}{2}\left[\frac{\tan^2(\arcsin(\sin 13.584/1.6) - \arcsin(\sin 13.584/1.333))}{\tan^2(\arcsin(\sin 13.584/1.6) + \arcsin(\sin 13.584/1.333))}\right]$$
$$+ \frac{1}{2}\left[\frac{\sin^2(\arcsin(\sin 13.584/1.6) - \arcsin(\sin 13.584/1.333))}{\sin^2(\arcsin(\sin 13.584/1.6) + \arcsin(\sin 13.584/1.333))}\right]$$
$$= 0.008498$$

while the beam transmissivity due to absorbtance, according to Bouguer's law (equation (B.16)), for the 0.0002 m thick plastic film is

$$\tau_{b\alpha} = e^{-C_e t_f / \cos(\arcsin(n_a \sin\theta_b / n_f))} = e^{-200 \times 0.0002 / \cos(\arcsin(\sin 13.584/1.6))} = 0.9603$$

Using an equivalent incidence angle of 60° for the diffuse solar radiation, as suggested by Duffie and Beckman [91DU1], the diffuse reflectivity for the air-film interface yields

$$\rho_{daf} = \frac{1}{2}\left[\frac{\tan^2(\theta_b - \arcsin(n_a \sin\theta_d / n_f))}{\tan^2(\theta_d + \arcsin(n_a \sin\theta_d / n_f))} + \frac{\sin^2(\theta_d - \arcsin(n_a \sin\theta_d / n_f))}{\sin^2(\theta_d + \arcsin(n_a \sin\theta_d / n_f))}\right]$$
$$= \frac{1}{2}\left[\frac{\tan^2(60 - \arcsin(\sin 60/1.6))}{\tan^2(60 + \arcsin(\sin 60/1.6))} + \frac{\sin^2(60 - \arcsin(\sin 60/1.6))}{\sin^2(60 + \arcsin(\sin 60/1.6))}\right]$$
$$= 0.1052$$

while the value of

$$\rho_{dfw} = \frac{1}{2}\left[\frac{\tan^2(\arcsin(n_a \sin\theta_d / n_f) - \arcsin(n_a \sin\theta_d / n_w))}{\tan^2(\arcsin(n_a \sin\theta_d / n_f) + \arcsin(n_a \sin\theta_d / n_w))}\right]$$
$$+ \frac{1}{2}\left[\frac{\tan^2(\arcsin(n_a \sin\theta_d / n_f) - \arcsin(n_a \sin\theta_d / n_w))}{\tan^2(\arcsin(n_a \sin\theta_d / n_f) + \arcsin(n_a \sin\theta_d / n_w))}\right]$$
$$= \frac{1}{2}\left[\frac{\tan^2(\arcsin(\sin 60.0/1.6) - \arcsin(\sin 60.0/1.333))}{\tan^2(\arcsin(\sin 60.0/1.6) + \arcsin(\sin 60.0/1.333))}\right]$$
$$+ \frac{1}{2}\left[\frac{\sin^2(\arcsin(\sin 60.0/1.6) - \arcsin(\sin 60.0/1.333))}{\sin^2(\arcsin(\sin 60.0/1.6) + \arcsin(\sin 60.0/1.333))}\right]$$
$$= 0.01102$$

is obtained for the diffuse reflectivity of the cover-water interface. Employing equation (B.16), the diffuse solar radiation transmissivity due to absorbtance is evaluated in accordance with Bouguer's law.

$$\tau_{d\alpha} = e^{-C_e t_f / \cos(\arcsin(n_a \sin\theta_d / n_f))} = e^{-200 \times 0.0002 / \cos(\arcsin(\sin 60 / 1.6))} = 0.95354$$

From Table H.1 it follows that the diffuse radiation for the black surface was 9 % of the total measured incident solar radiation on the cover. Hence, the incident beam solar radiation on the cover is

$$Ih_b = 0.92 Ih_T = 0.92 \times 1032.57 = 949.964 \text{ W/m}^2$$

and the diffuse solar radiation

$$Ih_d = 0.08 Ih_T = 0.08 \times 1032.57 = 82.606 \text{ W/m}^2$$

To evaluate the effective convective heat transfer coefficient between the cover and the environment, the thermophysical properties of the air above the plastic film cover need to be known.

The final iteration yielded a mean bulk water temperature of 39.794°C, while the ambient temperature was measured as 27.80°C. Therefore, the air above the cover is at a mean cover-ambient temperature of

$$T_{am} = 0.5(T_a + T_w) = 0.5 \times (27.80 + 39.794) = 33.80\,°\text{C or } 306.95\text{K}.$$

and the thermophysical properties of air at this temperature [98KR1] are

Air density	$\rho_{fa} = \frac{p_a}{287.08 \times T_{am}} = \frac{100731}{287.08 \times 306.95} = 1.1431 \text{ kg/m}^3$
Specific heat capacity of air	$c_{pfa} = 1007.22 \text{ J/kg.K}$
Air conductivity	$k_{fa} = 0.02675 \text{ W/m.K}$
Dynamic viscosity of air	$\mu_{fa} = 1.87871 \times 10^{-5} \text{ N/s.m}^2$

which gives a corresponding Prandtl number of

$$Pr_{fa} = \frac{\mu_{fa}\, c_{pfa}}{k_{fa}} = \frac{1.87871 \times 10^{-5} \times 1007.22}{0.02675} = 0.7074.$$

The effective length for a square cover is the side length, L_c, of the cover. The dimensionless Grashof number is thus

$$Gr_{fa} = \frac{2(T_w - T_a)\, g\, L_f^3\, \rho_{fa}^2}{(T_w + T_a)\mu_{fa}^2} = \frac{2\times(312.944 - 300.95)\times 9.8 \times 1.0^3 \times 1.1431^2}{(312.944 + 300.95)\times(1.87871 \times 10^{-5})^2} = 1.41912 \times 10^9$$

and the Reynolds number

$$Re_{fa} = \frac{\rho_{fa}\, v_w\, L_f}{\mu_{fa}} = \frac{1.1431 \times 0.9 \times 1.0}{1.87871 \times 10^{-5}} = 54760.45$$

The final iteration yielded a water temperature of 39.70°C or 312.85K as shown in Table H.1. Therefore, at this temperature the water thermophysical properties, according to Kröger [98KR1] are

Water density $\rho_w = 992.412\ kg/m^3$

Specific heat capacity of water $c_{pw} = 4176.80\ J/kg.K$

Upon substituting the previously calculated thermophysical properties for the air and water as well as previously determined solar characteristics of the mixed interface into equation (H.5), the energy equation for the water tank becomes

$$\left[1 - \frac{0.05332 + (1 - 2\times 0.05332)\times 0.008498 \times 0.9603^2}{1 - 0.05332 \times 0.008498 \times 0.9603^2}\right] \times 949.964$$

$$+ \left[1 - \frac{0.1052 + (1 - 2\times 0.1052)\times 0.01102 \times 0.95354^2}{1 - 0.1052 \times 0.01102 \times 0.95354^2}\right] \times 82.606$$

$$- \left[\left(1.41912 \times^{9} \times 0.7074\right)^{1/3} \times \left(0.227 + 1.406 \times 10^{-6} \times 54760.45\right)\right] \times \frac{0.02675}{1.0}(T_w - 300.95)$$

$$- 5.67 \times 10^{-8} \times 0.8 \times \left[T_w^4 - \left(0.0552 \times 300.95^{1.5}\right)^4\right]$$

$$= 992.412 \times 4176.80 \times 0.19 \times \frac{T_w - 312.886}{61}$$

which subsequently reduces to

$$966.487 - 8.1423 \times (T_w - 300.95) - 4.536 \times 10^{-8} \times \left[T_w^4 - 288.909^4\right]$$

$$= 12.911 \times 10^3 \times (T_w - 312.866)$$

and yields a bulk mean water temperature of

$$T_w = 312.944\text{K} = 39.794\ ^{\circ}\text{C}$$

which shows good agreement with the mean depth weighted experimental water temperature of 38.05°C.

Appendix I: Plastic covered water tank – Night operation

In the current study, the ability of a water tank to discharge its stored energy during the night is investigated both experimentally and theoretically.

I.1 Experimental apparatus, results and analysis

The experimental apparatus used in the current study is identical to the one described in Chapter 3 section 2, while the ambient conditions (temperature, wind, and pressure) are monitored by the Davis weather station. Experimental tests are only conducted during cloudless nights.

The results of such an experiment are shown in Figure I.1 and Figure I.2 for the night of the 8/9th of November 2000.

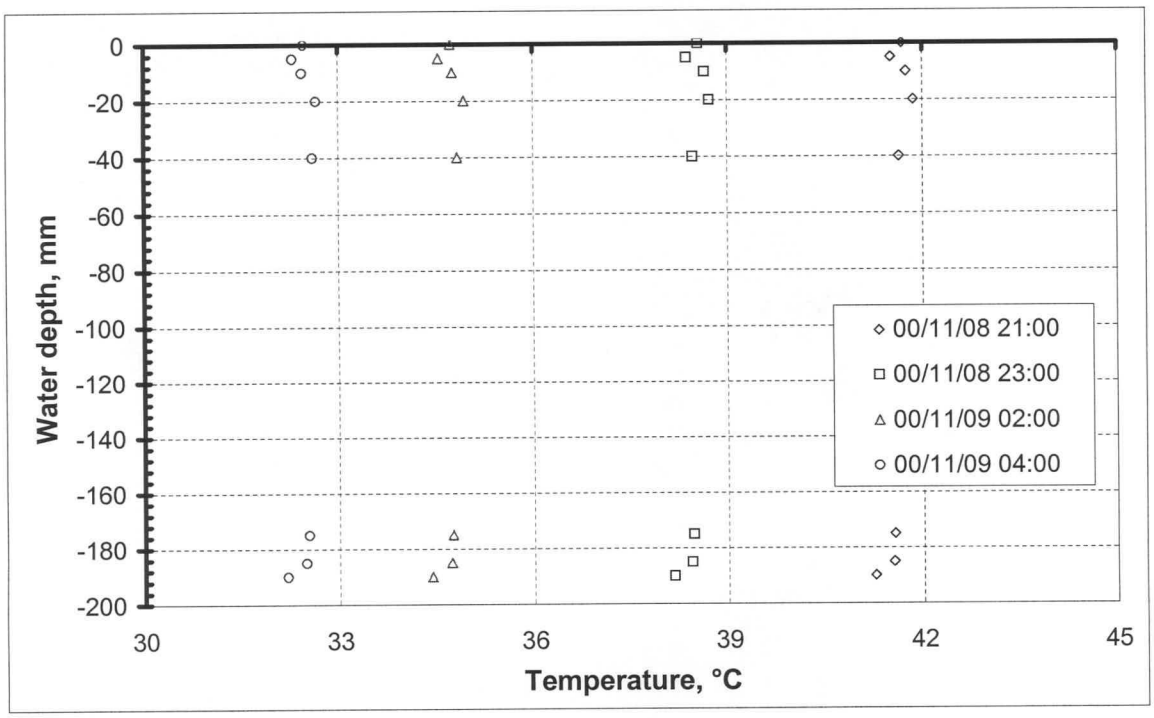

Figure I.1: Water temperature profile

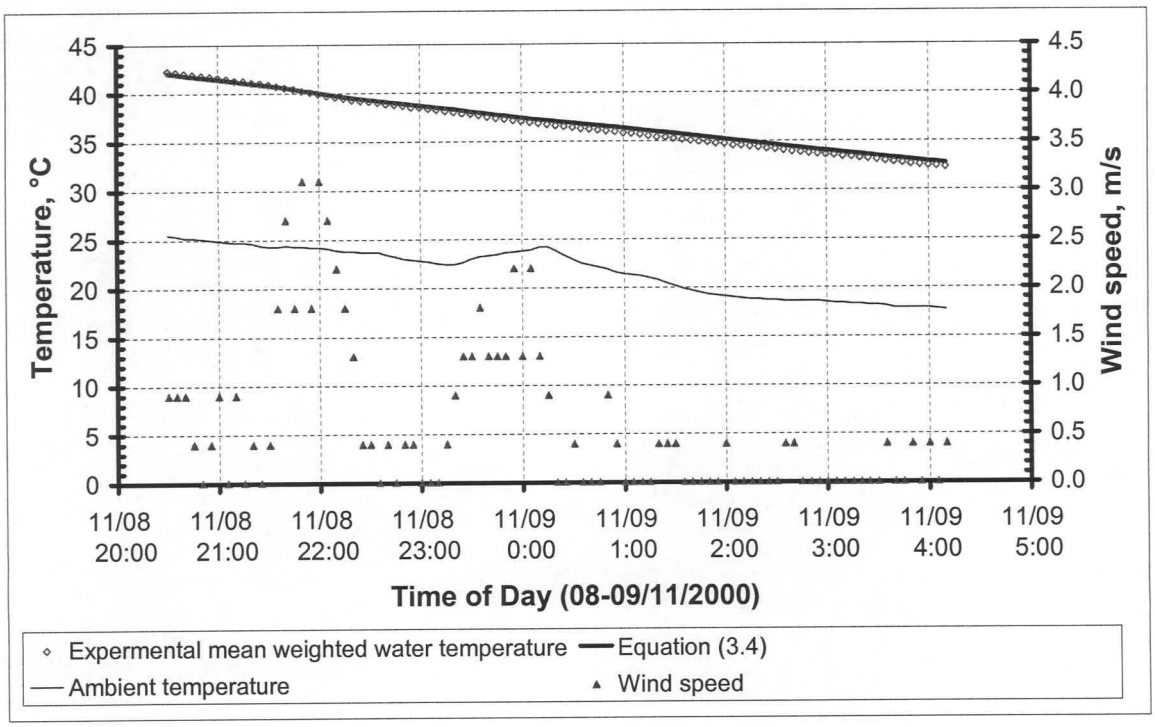

Figure I.2: Experimentally measured and theoretically predicted mean water temperature for the night of the 8th and 9th of November 2000

During the day solar radiation is absorbed by the water tank and the water is heated to a temperature higher than that of the ambient temperature. Consequently, one would expect the water to be at a higher temperature than the ambient temperature throughout the night.

Hence, assuming perfect contact between the plastic film and water and omitting the solar radiation terms in equation (H.5), the mean bulk water temperature can be predicted for the night with the aid of equation (H.5). Equation (H.5), after the omission of the solar radiation terms, is repeated below for clarity.

$$-\left[\left(Gr_{fa}\,Pr_{fa}\right)^{1/3}\left(0.227+1.406\times10^{-6}\,Re_{fa}\right)\right]\frac{k_{fa}}{L_f}\left(T_w-T_a\right)-\sigma\,\varepsilon_f\left[T_w^4-\left(0.0552\,T_a^{1.5}\right)^4\right] = \rho_w\,c_{pw}\,t_w\,\frac{dT_w}{dt} \qquad (I.1)$$

Using the experimentally measured ambient conditions, in conjunction with equation (I.1), the mean water temperature is predicted for the night of the 8/9th of November 2000 and compared to the mean experimental water temperature.

From Figure I.2, in which the experimentally measured mean water temperatures of the water tank are compared to the theoretically predicted values, it is evident that a very good agreement exists, with the maximum difference being less than a degree Celsius.

In the following numerical example, the final iteration is shown for the prediction of the mean bulk water temperature for the 8th of November 2000 at 23h00:39.

Numerical example

In Table I.1 the specifications of the plastic covered water tank as well as the results of the final iteration are shown.

Table I.1: Experimental and numerical data for plastic covered water tank night operation

Water height, t_w	0.190 m
Side length of film, L_f	1.0 m
Long-wave emissivity of film, ε_f	0.80
Ambient temperature, T_a	22.80 °C (295.95 K)
Wind speed, v_w	0.0 m/s
Atmospheric pressure, p_a	100 210 Pa
Experimental mean weighted water temperature	38.48°C (311.63 K)
Predicted mean water temperature (23h00:39), $T_w^{\ i}$	38.73 °C (311.88 K)
Predicted mean water temperature (22h59:40), $T_w^{\ i-1}$	38.749 °C (311.899 K)

To evaluate the effective convective heat transfer coefficient between the cover and the environment, the thermophysical properties of the air above the cover need to be known.

The final iteration for 23h00:39, yielded a mean predicted water temperature of 38.73°C, while the ambient temperature was measured as 22.80°C. Therefore, the air above the cover is at a mean cover-ambient temperature of

$$T_{am} = 0.5\left(T_a + T_w\right) = 0.5 \times \left(22.80 + 38.73\right) = 30.77\,°C \text{ or } 303.92\,K.$$

and the thermophysical properties of air at this temperature [98KR1] are

Air density $\rho_{fa} = \frac{p_a}{287.08 \times T_{am}} = \frac{100210}{287.08 \times 303.92} = 1.1486 \text{ kg/m}^3$

Specific heat capacity of air $c_{pfa} = 1007.10 \text{ J/kg.K}$

Air conductivity $k_{fa} = 0.02653 \text{ W/m.K}$

Dynamic viscosity of air $\mu_{fa} = 1.86484 \times 10^{-5} \text{ N/s.m}^2$

which give a Prandtl number of

$$Pr_{fa} = \frac{\mu_{fa}\, c_{pfa}}{k_{fa}} = \frac{1.86484 \times 10^{-5} \times 1007.10}{0.02653} = 0.7081.$$

The effective length for a square cover is the side length, L_f, of the cover. The dimensionless Grashof number is thus

$$Gr_{fa} = \frac{2(T_w - T_a)\, g\, L_f^3\, \rho_{fa}^2}{(T_w + T_a)\mu_{fa}^2} = \frac{2 \times (311.88 - 295.95) \times 9.8 \times 1.0^3 \times 1.1486^2}{(311.88 + 295.95) \times (1.86484 \times 10^{-5})^2} = 1.95068 \times 10^9$$

The final iteration, as shown in Table I.1, yielded a mean water temperature of 38.73°C or 311.88K. At this temperature the water thermophysical properties, according to Kröger [98KR1], are

Water density $\rho_w = 992.833 \text{ kg/m}^3$

Specific heat capacity of water $c_{pw} = 4176.81 \text{ J/kg.K}$

Upon substitution of the previously determined thermophysical properties for the air and water into equation (I.1), the energy equation for the solar water tank becomes

$$-\left[\left(1.95068 \times {}^{9} \times 0.7081\right)^{1/3} \times \left(0.227 + 1.406 \times 10^{-6} \times 0\right) \right] \times \frac{0.02653}{1.0} (T_w - 295.95)$$

$$-5.67 \times 10^{-8} \times 0.8 \times \left[T_w^4 - \left(0.0552 \times 295.95^{1.5}\right)^4 \right] = 992.833 \times 4176.81 \times 0.19 \times \frac{T_w - 311.899}{59}$$

which reduces to

$$-6.70692 \times (T_w - 295.95) - 4.536 \times 10^{-8} \times \left[T_w^4 - 281.039^4 \right] = 13.35434 \times 10^3 (T_w - 311.889)$$

and yields a bulk water temperature of

$$T_w = 311.88\,K = 38.73\,^{\circ}C$$

Not only does the predicted temperature show good agreement with the experimentally measured temperature of 38.48°C, but also indicates that equation (I.1) is able to predict the water temperature accurately.

Appendix J: Solar collector with water storage – Day operation

Experiments are conducted on a simple solar collector that includes a plastic covered water tank. This is done in order to observe the influence of energy storage on the performance of a simple solar collector. The cover and water temperatures are also theoretically predicted and compared to the experimental results.

J.1 Analysis

The objective of the analysis is to derive a set of equations, which can be used to predict the mean water and cover temperatures, and subsequently the performance of a solar collector (see Figure J.2 and Figure J.2) at approximately solar noon.

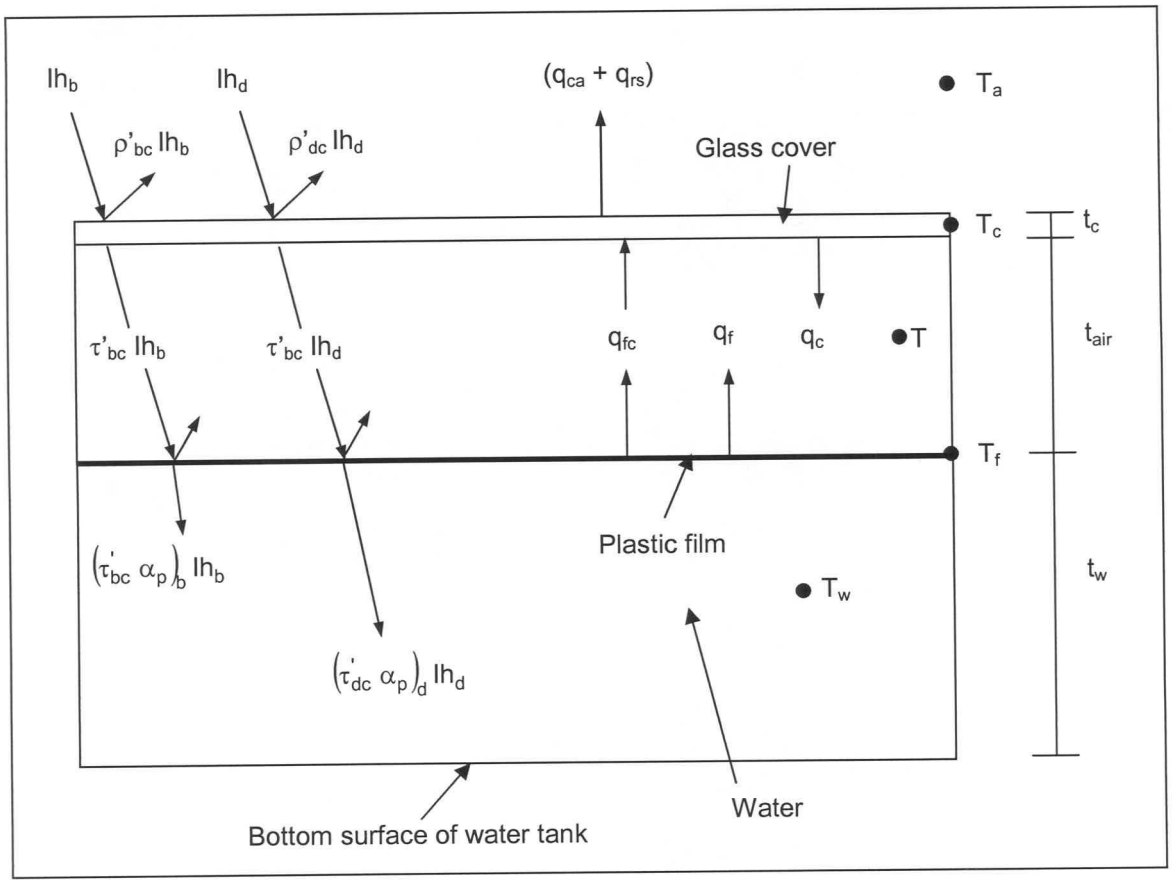

Figure J.1: Schematic presentation of a solar collector with water tank energy storage

The cover of the current experimental set-up is identical to the one studied during the initial solar collector experiments (compare Figure D.3 to Figure D.3). The conservation of energy equation for the cover of the solar collector, according to equation (D.10), is thus

$$\begin{aligned}
&\frac{(1-\rho_{bc})(1-\tau_{\alpha bc})}{1-\rho_{bc}\,\tau_{\alpha bc}} Ih_b + \frac{(1-\rho_{dc})(1-\tau_{\alpha dc})}{1-\rho_{dc}\,\tau_{\alpha dc}} Ih_d \\
&+\left[1+1.44\left[1-\frac{1708}{Ra_{fc}}\right]+\left[\left(\frac{Ra_{fc}}{5830}\right)^{1/3}-1\right]\right]\frac{k_{fc}}{t_{air}}(T_f-T_c)+\sigma\left(\frac{1}{\varepsilon_c}+\frac{1}{\varepsilon_f}-1\right)^{-1}\left(T_f^4-T_c^4\right) \\
&=\left[(Gr_{ca}\,Pr_{ca})^{1/3}\left(0.227+1.406\times10^{-6}\,Re_{ca}\right)\right]\frac{k_{ca}}{L_c}(T_c-T_a) \\
&+\varepsilon_c\,\sigma\left(T_c^4-\left(0.0552\,T_a^{1.5}\right)^4\right)+\rho_c\,t_c\,c_{pc}\frac{dT_c}{dt}
\end{aligned} \tag{J.1}$$

with ρ_{bc} and ρ_{dc} defining the beam and diffuse reflectivity of the cover and $\tau_{\alpha bc}$ and $\tau_{\alpha dc}$ to the respective cover beam and diffuse transmittance due to absorbtance.

From the experimental results of Appendix D, it is apparent that during the period near solar noon a condition prevails in which the cover temperature tends to stay practically constant. Consequently, the transient cover term in equation (J.1) is neglected and the conservation of energy equation for the cover, close to solar noon, reduces to

$$\begin{aligned}
&\frac{(1-\rho_{bc})(1-\tau_{\alpha bc})}{1-\rho_{bc}\,\tau_{\alpha bc}} Ih_b + \frac{(1-\rho_{dc})(1-\tau_{\alpha dc})}{1-\rho_{dc}\,\tau_{\alpha dc}} Ih_d \\
&+\left[1+1.44\left[1-\frac{1708}{Ra_{fc}}\right]+\left[\left(\frac{Ra_{fc}}{5830}\right)^{1/3}-1\right]\right]\frac{k_{fc}}{t_{air}}(T_f-T_c)+\sigma\left(\frac{1}{\varepsilon_c}+\frac{1}{\varepsilon_f}-1\right)^{-1}\left(T_f^4-T_c^4\right) \\
&=\left[(Gr_{ca}\,Pr_{ca})^{1/3}\left(0.227+1.406\times10^{-6}\,Re_{ca}\right)\right]\frac{k_{ca}}{L_c}(T_c-T_a)+\varepsilon_c\,\sigma\left(T_c^4-\left(0.0552\,T_a^{1.5}\right)^4\right)
\end{aligned} \tag{J.2}$$

Assuming that there is good contact between the water and the plastic film, Figure D.3 yields the following energy equation for the plastic covered water tank filled with water at a mean temperature of T_w.

$$\left(\tau'_{bc}\,\alpha_p\right)_b Ih_b + \left(\tau'_{dc}\,\alpha_p\right)_d Ih_d = q_{fc} + q_f + \rho_w\,t_w\,c_{pw}\frac{dT_w}{dt} \tag{J.3}$$

The effective solar transmittance-absorbtance product for a simple solar collector's absorber plate, is given by equation (B.26) as

$$\left(\tau' \alpha_p\right) = \left(\frac{\tau_c' \alpha_p}{1-(1-\alpha_p)\rho_{dc}}\right) \tag{J.4}$$

However, in the current set-up the absorber plate of a simple solar collector is replaced by a plastic covered water tank, and as a result, the absorbtivity of the "absorber plate" is equal to one minus the effective reflectivity of the plastic film, $(1 - \rho'_f)$ that covers the water tank. Assuming the effective solar absorbtivity of the film to be negligible, the effective transmittance-absorbtance product of the water tank for a glass cover with an effective transmissivity of τ'_c is

$$\left(\tau_c' \alpha_p\right) = \left[\tau_c'\left(1-\rho_f'\right)\right] = \left[\frac{\tau_c'\left(1-\rho_f'\right)}{1-\rho_f' \rho_{dc}}\right] \tag{J.5}$$

Substitute equation (J.5) into equation (J.3) and find

$$\frac{\tau_{bc}'\left(1-\rho_{bf}'\right)}{1-\rho_{bf}' \rho_{dc}} Ih_b + \frac{\tau_{dc}'\left(1-\rho_{df}'\right)}{1-\rho_{df}' \rho_{dc}} Ih_d = q_{fc} + q_f + \rho_w t_w c_{pw} \frac{dT_w}{dt} \tag{J.6}$$

Upon substitution of the respective convective and radiative equations (equation (D.8) and (D.9)), into equation (J.6) as well as equations (B.8) and (B.4) for the effective cover transmissivity, τ'_c, and effective reflectivity of the plastic film, ρ'_f, the conservation of energy equation for the water tank becomes

$$\begin{aligned}
&\left[\frac{(1-\rho_{bc})^2 \tau_{\alpha bc}}{\left(1-\rho_{bc}^2 \tau_{\alpha bc}^2\right)}\right]\left[1-\frac{\rho_{baf}+(1-2\rho_{baf})\rho_{bfw}\tau_{\alpha bf}^2}{1-\rho_{baf}\rho_{bfw}\tau_{\alpha bf}^2}\right]\left[1-\rho_{dc}\frac{\rho_{baf}+(1-2\rho_{baf})\rho_{bfw}\tau_{\alpha bf}^2}{1-\rho_{baf}\rho_{bfw}\tau_{\alpha bf}^2}\right]^{-1} Ih_b + \\
&\left[\frac{(1-\rho_{dc})^2 \tau_{\alpha dc}}{\left(1-\rho_{dc}^2 \tau_{\alpha dc}^2\right)}\right]\left[1-\frac{\rho_{daf}+(1-2\rho_{daf})\rho_{dfw}\tau_{\alpha df}^2}{1-\rho_{daf}\rho_{dfw}\tau_{\alpha df}^2}\right]\left[1-\rho_{dc}\frac{\rho_{daf}+(1-2\rho_{daf})\rho_{dfw}\tau_{\alpha df}^2}{1-\rho_{daf}\rho_{dfw}\tau_{\alpha df}^2}\right]^{-1} Ih_d \\
&= \left[1+1.44\left[1-\frac{1708}{Ra_{fc}}\right]+\left[\left(\frac{Ra_{fc}}{5830}\right)^{1/3}-1\right]\right]\frac{k_{fc}}{t_{air}}\left(T_f-T_c\right)+\sigma\left(\frac{1}{\varepsilon_c}+\frac{1}{\varepsilon_f}-1\right)^{-1}\left(T_f^4-T_c^4\right) \\
&+\rho_w t_w c_{pw}\frac{dT_w}{dt}
\end{aligned} \tag{J.7}$$

In equation (J.7) ρ_{baf}, ρ_{daf}, ρ_{bfw}, and ρ_{dfw} define the respective beam and diffuse reflectivities for the air-film and film-water interfaces that are to be evaluated from equations (B.12) and (B.14). $\tau_{\alpha bf}$ and $\tau_{\alpha df}$ refer to the beam and diffuse transmissivity due to absorbtion of the film, which are to be evaluated according to Bouguer's law (equation (B.16)).

During the preceding analysis a number of assumptions were made. Firstly, due to the very small thickness of the plastic film as well as its low density, the thermal capacitance and effective absorbtivity of solar radiation by the plastic film is assumed to be negligible. Secondly, based on the water temperature profile observed in the plastic covered water tank (see Figure D.3) the assumption is made that the water is at a uniform temperature throughout the plastic covered water tank. Thirdly, the conduction heat losses through the sides and bottom of the tank are assumed to be negligible due to the 50 mm thick polystyrene insulation that surrounds these surfaces in the experimental set-up.

The energy equations for both the glass cover and water tank were derived for conditions close to solar noon. Consequently, the assumption was made that the natural convective heat transfer between the cover and entrapped air is equal to the convective heat exchange between the entrapped air and the upper surface of the plastic film i.e. changes in the thermal capacity of the air is neglected.

As in the case of the water tank considered in Appendix H, it is assumed that the film and water temperature ($T_f = T_w$) are equal. The steady state conservation of energy equation for the cover thus becomes

$$\frac{(1-\rho_{bc})(1-\tau_{\alpha bc})}{1-\rho_{bc}\,\tau_{\alpha bc}} Ih_b + \frac{(1-\rho_{dc})(1-\tau_{\alpha dc})}{1-\rho_{dc}\,\tau_{\alpha dc}} Ih_d$$

$$+\left[1+1.44\left[1-\frac{1708}{Ra_{fc}}\right]+\left[\left(\frac{Ra_{fc}}{5830}\right)^{1/3}-1\right]\right]\frac{k_{cf}}{t_{air}}(T_w-T_c)+\sigma\left(\frac{1}{\varepsilon_c}+\frac{1}{\varepsilon_f}-1\right)^{-1}\left(T_w^4-T_c^4\right) \qquad \text{(J.8)}$$

$$=\left[(Gr_{ca}\,Pr_{ca})^{1/3}\left(0.227+1.406\times10^{-6}\,Re_{ca}\right)\right]\frac{k_{ca}}{L_c}(T_c-T_a)+\varepsilon_c\,\sigma\left(T_c^4-\left(0.0552\,T_a^{1.5}\right)^4\right)$$

while the water tank's steady state energy equation reduces to

$$\left[\frac{(1-\rho_{bc})^2\,\tau_{\alpha bc}}{(1-\rho_{bc}^2\,\tau_{\alpha bc}^2)}\right]\left[1-\frac{\rho_{baf}+(1-2\rho_{baf})\rho_{bfw}\,\tau_{\alpha bf}^2}{1-\rho_{baf}\,\rho_{bfw}\,\tau_{\alpha bf}^2}\right]\left[1-\rho_{dc}\,\frac{\rho_{baf}+(1-2\rho_{baf})\rho_{bfw}\,\tau_{\alpha bf}^2}{1-\rho_{baf}\,\rho_{bfw}\,\tau_{\alpha bf}^2}\right]^{-1} Ih_b +$$

$$\left[\frac{(1-\rho_{dc})^2\,\tau_{\alpha dc}}{(1-\rho_{dc}^2\,\tau_{\alpha dc}^2)}\right]\left[1-\frac{\rho_{daf}+(1-2\rho_{daf})\rho_{dfw}\,\tau_{\alpha df}^2}{1-\rho_{daf}\,\rho_{dfw}\,\tau_{\alpha df}^2}\right]\left[1-\rho_{dc}\,\frac{\rho_{daf}+(1-2\rho_{daf})\rho_{dfw}\,\tau_{\alpha df}^2}{1-\rho_{daf}\,\rho_{dfw}\,\tau_{\alpha df}^2}\right]^{-1} Ih_d \qquad \text{(J.9)}$$

$$=\left[1+1.44\left[1-\frac{1708}{Ra_{fc}}\right]+\left[\left(\frac{Ra_{fc}}{5830}\right)^{1/3}-1\right]\right]\frac{k_f}{t_{air}}(T_w-T_c)+\sigma\left(\frac{1}{\varepsilon_c}+\frac{1}{\varepsilon_f}-1\right)^{-1}\left(T_w^4-T_c^4\right)$$

$$+\rho_w\,t_w\,c_{pw}\,\frac{dT_w}{dt}$$

In the case of the water tank experiments (Appendix H), it was observed that a small air layer forms underneath the plastic film during the course of the day, as the dissolved air in the water is set free. In the current experiments, the same phenomenon was observed. Therefore, to observe the influence of the air layer underneath the plastic film on the cover and water temperatures, the effective transmissivity of the film is changed to incorporate the air layer underneath the plastic film (see Appendix H). Consequently, the water tank's energy equation becomes

$$\left[\frac{(1-\rho_{bc})^2\,\tau_{\alpha bc}}{(1-\rho_{bc}^2\,\tau_{\alpha bc}^2)}\right]\left[1-\frac{\rho_{baf}+(1-2\rho_{baf})\rho_{bfw}\,\tau_{\alpha bf}^2}{1-\rho_{baf}\,\rho_{bfw}\,\tau_{\alpha bf}^2}\right]$$

$$\times\left[1-\rho_{dc}\,\frac{\rho_{baf}+(1-2\rho_{baf})\rho_{bfw}\,\tau_{\alpha bf}^2}{1-\rho_{baf}\,\rho_{bfw}\,\tau_{\alpha bf}^2}\right]^{-1}(1-\rho_{bw})\,Ih_b +$$

$$\left[\frac{(1-\rho_{dc})^2\,\tau_{\alpha dc}}{(1-\rho_{dc}^2\,\tau_{\alpha dc}^2)}\right]\left[1-\frac{\rho_{df}+(1-2\rho_{df})\rho_{df}\,\tau_{\alpha df}^2}{1-\rho_{df}^2\,\tau_{\alpha df}^2}\right] \qquad \text{(J.10)}$$

$$\times\left[1-\rho_{dc}\,\frac{\rho_{df}+(1-2\rho_{df})\rho_{df}\,\tau_{\alpha df}^2}{1-\rho_{df}^2\,\tau_{\alpha df}^2}\right]^{-1}(1-\rho_{dw})\,Ih_d$$

$$=\left[1+1.44\left[1-\frac{1708}{Ra_{fc}}\right]+\left[\left(\frac{Ra_{fc}}{5830}\right)^{1/3}-1\right]\right]\frac{k_f}{t_{air}}(T_w-T_c)+\sigma\left(\frac{1}{\varepsilon_c}+\frac{1}{\varepsilon_f}-1\right)^{-1}\left(T_w^4-T_c^4\right)$$

$$+\rho_w\,t_w\,c_{pw}\,\frac{dT_w}{dt}$$

with $(1 - \rho_w)$ accounting for the incident solar radiation that is reflected from the air-water interface that has formed underneath the plastic film.

Employing equations (J.8), (J.9) and (J.10), one would be able to predict the mean water and cover temperatures for both an air layer as well as for a no air layer case for a simple solar collector with a water tank solar storage system.

J.2 Experimental apparatus and results

The solar collector with water tank solar energy storage system under consideration consists of a 3.88 mm thick glass pane and a 1m x 1m x 0.19m black plastic covered fibreglass tank filled with water. An air gap of 60 mm separates the glass cover and water tank (see Figure J.2).

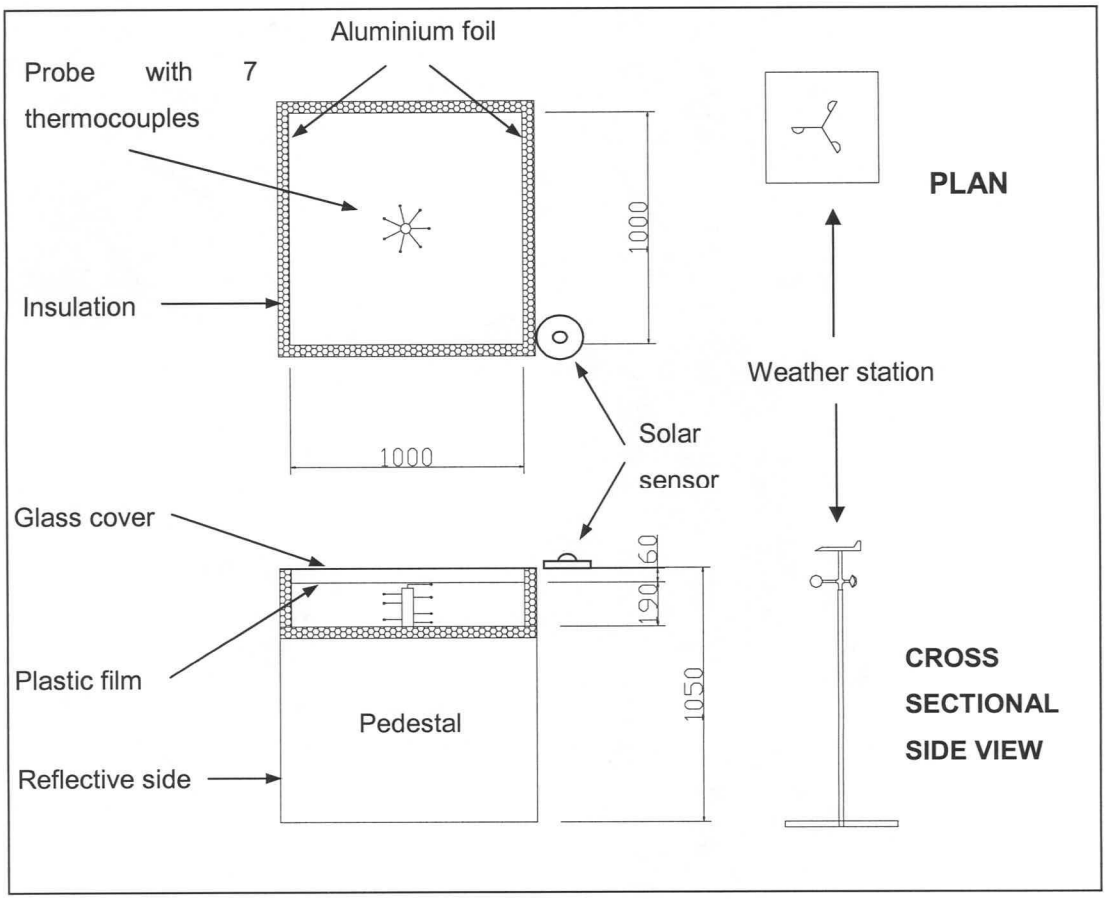

Figure J.2: Experimental apparatus

A square pedestal, having highly reflective sides, supports the solar collector 1.05m above the ground at a location of latitude of 33.98° S and longitude of 18.85 °E.

The sides of the solar collector as well as the bottom of the water tank are insulated by 50 mm thick polystyrene insulation, while the water is covered by a 0.2 mm thick Luminal Anti-Fog plastic cover to suppress evaporation. The inner sides of the tank are covered by a layer of

highly reflective Aluminium foil ($\alpha = \varepsilon \approx 0.1$), to minimise their influence on the heat transfer between themselves and the water and the air gap.

The water temperature probe described in Chapter 3 is used to measure the water temperature at various depths, and two type-T thermocouples monitor the glass cover's temperature. The Kipp and Zonen solar sensor is placed on top of the cover, while the Davis weather station is placed next to the pedestal to monitor the ambient conditions as shown in Figure J.2.

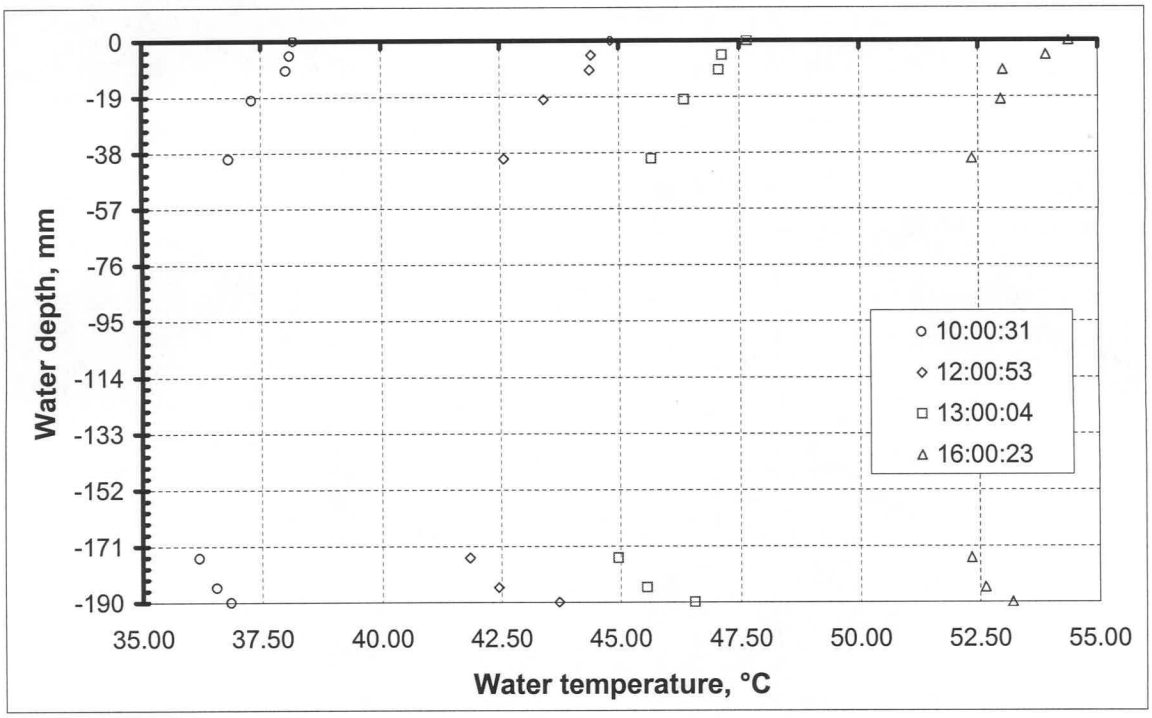

Figure J.3: Water temperature profile

Data was only recorded and retained if consecutive days were cloudless and the water temperature heating and cooling profile did not change measurably. Such a day occurred during the 21st of November 2000. The experimental results for this day are shown in Figure J.3 and Figure J.4.

Employing equations (J.8), (J.9) and (J.10), the mean water and cover temperatures are predicted for both an air layer as well as for a no air layer situation and compared to the experimentally measured values for the 21st of November 2000, as shown in Figure J.4.

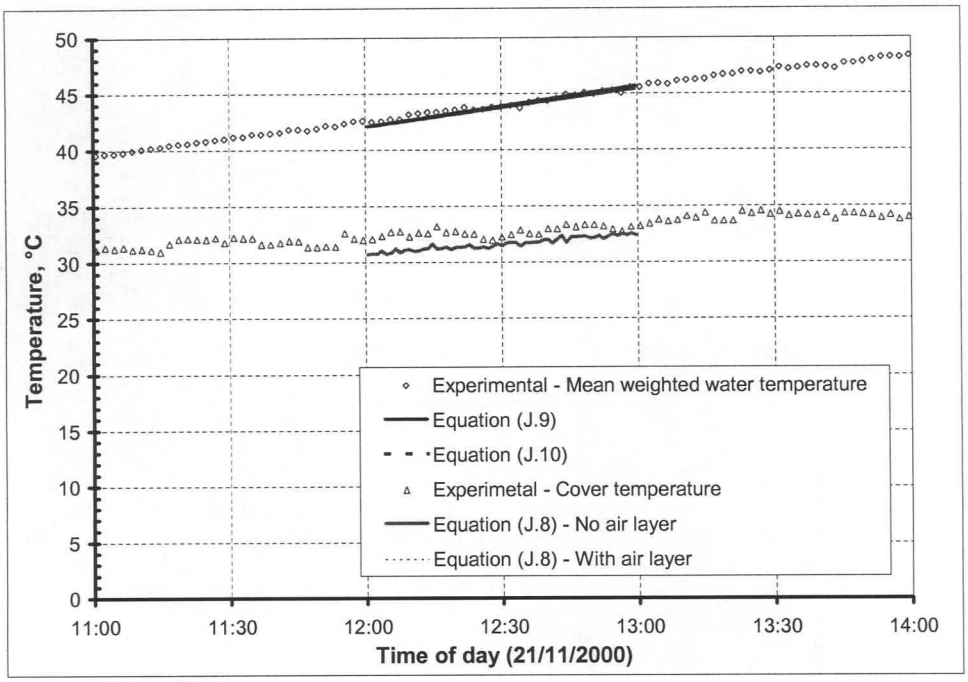

Figure J.4: Experimentally measured and theoretically predicted cover and water temperatures

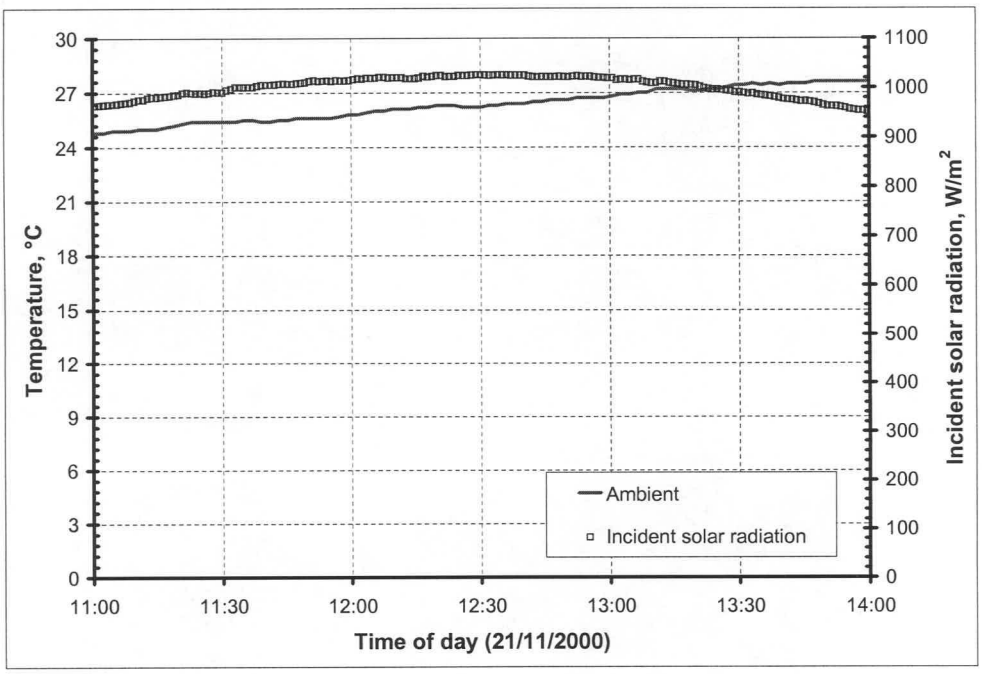

Figure J.5: Ambient conditions

Figure J.4 gives the impression that both models predict similar values (i.e. contradicting the findings of the water tank experiments in Appendix H). However, a closer inspection of the predicted cover and mean water temperatures (Figure J.6) reveals that as in the case of

Appendix H, the air model tends to predict lower values than the model which assumes good contact between the water and the plastic film. This find clearly confirms that the forming air layer decreases the effective transmissivity of the film and subsequently the temperature of the water inside the tank.

Although the air layer is ignored in the initial analysis, it is still apparent that good agreement exists between the predicted cover and mean water temperature of equations (J.8) and (J.9) and the corresponding experimental measurements. The maximum difference between the predicted and the experimental values are 2.0°C and 0.55 °C for the respective cover and water tank temperatures.

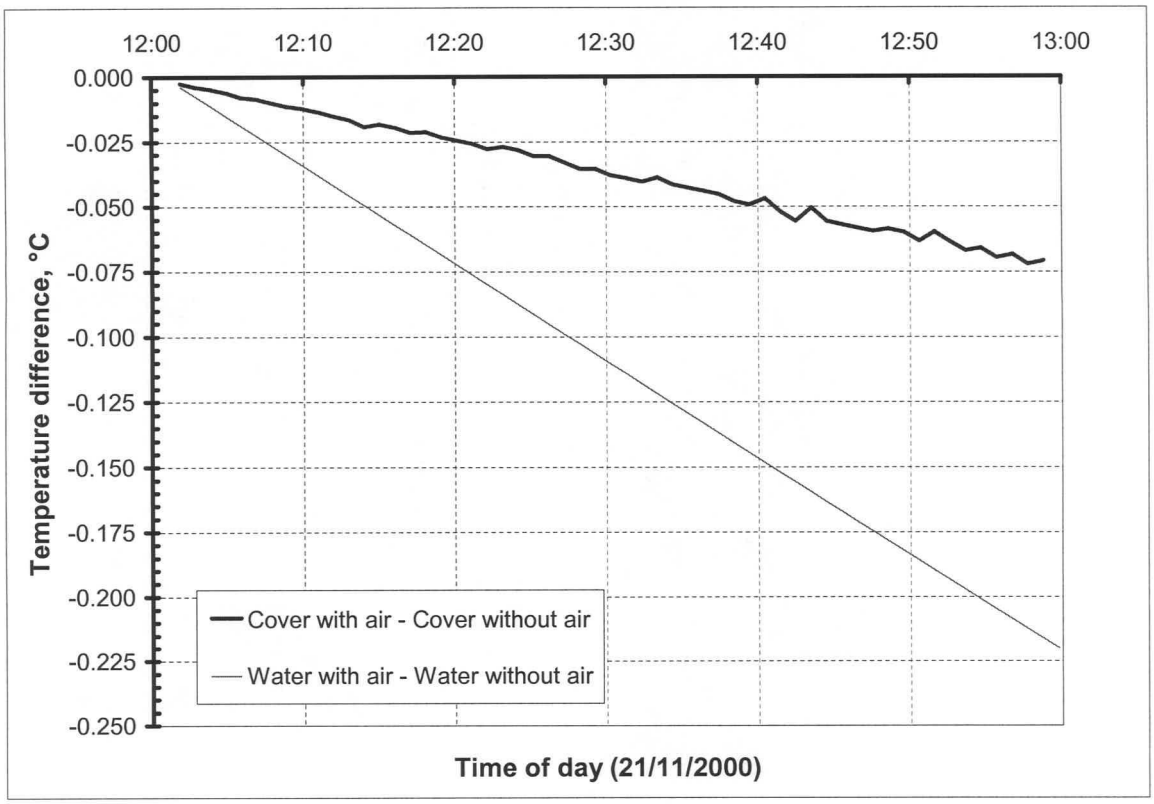

Figure J.6: Temperature difference between models

In the following numerical example, the iterative solving procedure for the cover and mean water temperature is shown for a solar collector with good contact between the plastic film and the water underneath.

Numerical example

In Table J.1 the specifications of the experimental configuration as well as the ambient conditions are given for the 21st of November 2000 (DOY = 326th day of year) at 12h05:58 (ψ = 12.0994 hours after midnight).

In the following calculations, it will be shown that the energy equations for the cover and plastic covered water tank (equation (J.9) and equation (J.10)) are satisfied for a water bulk temperature of 42.407 °C (315.557 K) and cover temperature of 30.834 °C (309.984 K) for the given ambient conditions.

Table J.1: Experimental data for day operation of solar collector with water storage

Water height, t_w	0.190 m
Cover thickness, t_c	0.00388 m
Film thickness, t_f	0.0002 m
Side length of cover, L_c	1.0 m
Cover extinction coefficient, C_{ec}	13 m^{-1}
Cover refractive index, n_c	1.526
Film extinction coefficient, C_{ef}	200 m^{-1}
Film refractive index, n_f	1.6
Air refractive index, n_a [91DU1]	1.0
Water refractive index, n_w [92SE1]	1.333
Long-wave emissivity of cover, ε_c	0.80
Long-wave emissivity of film, ε_f	0.88
Ambient temperature, T_a	26.00 °C (299.15 K)
Total incident solar radiation, Ih_T	1073.20 $W/m^2.K$
Wind speed, v_w	2.2 m/s
Atmospheric pressure, p_a	101 169 Pa
Stellenbosch latitude angle, ϕ	33.98 °S
Stellenbosch longitude angle, ϕ_l	18.85 °E
South African standard meridian, ϕ_m	30.00 °E
Predicted cover temperature, T_c	30.834 °C (309.984 K)
Predicted mean water temperature (12h05:58), T_w^i	42.407 °C (315.557 K)
Predicted mean water temperature (12h04:59), T_w^{i-1}	42.346 °C (315.496 K)

According to equation (B.21), the leap year adjustment to the day for the year 2000 is

$$YADJ = 0.25\,[2.5 - (Y - 4\,(\text{integer}((Y-1)/4)))] = 0.25\times[2.5 - (2000 - 4\,(\text{integer}((2000-1)/4)))]$$

$$= -0.375 \text{ days}$$

with the integer function yielding a value of 499.

The 21st of November is the 326th day of the year. The annual phase angle, according to equation (B.20), is thus

$$P = 0.0172028\,(DOY + YADJ + 0.417) = 0.0172028\,(326 + (-0.375) + 0.417) = 5.6088 \text{ rad.}$$

Upon substituting this annual phase angle into equation (B.19), the declination angle for the surface is

$$\delta = 180\,[0.00661 + 0.40602\sin(P - 1.4075) + 0.00665\sin(2P - 1.4789)$$

$$+ 0.00298\sin(3P - 1.0996)]\,\pi$$

$$= 180\,[0.00661 + 0.40602\sin(5.6088 - 1.4075) + 0.00665\sin(2\times5.6088 - 1.4789)$$

$$+ 0.00298\sin(3\times5.6088 - 1.0996)]\,\pi$$

$$= -20.033°$$

which leads to an equation of time (equation (B.23)) of

$$EOT = 1440\,[0.005114\sin(P + 3.0593) + 0.006892\sin(2P + 3.4646)$$

$$+ 0.00022\sin(3P + 3.3858) + 0.000153\sin(4P + 3.7766)]$$

$$= 1440\,[0.005114\sin(5.6088 + 3.0593) + 0.006892\sin(2\times5.6088 + 3.4646)$$

$$+ 0.00022\sin(3\times5.6088 + 3.3858) + 0.000153\sin(4\times5.6088 + 3.7766)]$$

$$= 14.046 \text{ min.}$$

Measurements were taken at 12h05:58 or 12.0994 hours after midnight, which, according to equation (B.22) relates to an hour angle of

$$\omega = 15\left[\psi - 12 - \frac{4(\phi_m - \phi_l) - EOT}{60}\right] = 15\left[12.0994 - 12 - \frac{4(30 - 18.85) - (14.046)}{60}\right] = -6.1475°.$$

From equation (B.24) it follows that the beam incidence angle for the location with a standard meridian, ϕ_m, of 30° E, longitude, ϕ_l, of 18.85° E and latitude of 33.98° S is

$$\theta_b = a\cos(\sin\delta\sin\phi + \cos\delta\cos\phi\cos\omega)$$
$$= a\cos(\sin-20.033\sin-33.98 + \cos-20.033\times\cos-33.98\times\cos-6.1475) = 14.975°.$$

For the above incidence angle, the beam cover reflectivity is

$$\rho_{bc} = \frac{1}{2}\left[\frac{\tan^2(\theta_b - \arcsin(n_a\sin\theta_b/n_c))}{\tan^2(\theta_b + \arcsin(n_a\sin\theta_b/n_c))} + \frac{\sin^2(\theta_b - \arcsin(n_a\sin\theta_b/n_c))}{\sin^2(\theta_b + \arcsin(n_a\sin\theta_b/n_c))}\right]$$
$$= \frac{1}{2}\left[\frac{\tan^2(14.9749 - \arcsin(\sin 14.9749/1.526))}{\tan^2(14.9749 + \arcsin(\sin 14.9749/1.526))} + \frac{\sin^2(14.9749 - \arcsin(\sin 14.9749/1.526))}{\sin^2(14.9749 + \arcsin(\sin 14.9749/1.526))}\right]$$
$$= 0.04344$$

while the air-film interface yields a beam reflectivity of

$$\rho_{baf} = \frac{1}{2}\left[\frac{\tan^2(\theta_b - \arcsin(n_a\sin\theta_b/n_f))}{\tan^2(\theta_b + \arcsin(n_a\sin\theta_b/n_f))} + \frac{\sin^2(\theta_b - \arcsin(n_a\sin\theta_b/n_f))}{\sin^2(\theta_b + \arcsin(n_a\sin\theta_b/n_f))}\right]$$
$$= \frac{1}{2}\left[\frac{\tan^2(14.9749 - \arcsin(\sin 14.9749/1.6))}{\tan^2(14.9749 + \arcsin(\sin 14.9749/1.6))} + \frac{\sin^2(14.9749 - \arcsin(\sin 14.9749/1.6))}{\sin^2(14.9749 + \arcsin(\sin 14.9749/1.6))}\right]$$
$$= 0.05335$$

and the film-water surface a value of

$$\rho_{bfw} = \frac{1}{2}\left[\frac{\tan^2(\arcsin(n_a\sin\theta_b/n_f) - \arcsin(n_a\sin\theta_b/n_w))}{\tan^2(\arcsin(n_a\sin\theta_b/n_f) + \arcsin(n_a\sin\theta_b/n_w))}\right]$$
$$+ \frac{1}{2}\left[\frac{\tan^2(\arcsin(n_a\sin\theta_b/n_f) - \arcsin(n_a\sin\theta_b/n_w))}{\tan^2(\arcsin(n_a\sin\theta_b/n_f) + \arcsin(n_a\sin\theta_b/n_w))}\right]$$
$$= \frac{1}{2}\left[\frac{\tan^2(\arcsin(\sin 14.9794/1.6) - \arcsin(\sin 14.9794/1.333))}{\tan^2(\arcsin(\sin 14.9794/1.6) + \arcsin(\sin 14.9794/1.333))}\right]$$
$$+ \frac{1}{2}\left[\frac{\sin^2(\arcsin(\sin 14.9794/1.6) - \arcsin(\sin 14.9794/1.333))}{\sin^2(\arcsin(\sin 14.9794/1.6) + \arcsin(\sin 14.9794/1.333))}\right]$$
$$= 0.008296$$

From Bouguer's law (equation (B.16)), it follows that the cover's beam transmittance due to absorbtance is equal to

$$\tau_{\alpha bc} = e^{-C_{ec}\, t_c / \cos(\arcsin(n_a \sin\theta_b / n_c))} = e^{-13 \times 0.00388 / \cos(\arcsin(\sin 14.9749 / 1.526))} = 0.95011$$

while the beam transmittance due to absorbtance for the 0.0002 m thick plastic film is

$$\tau_{\alpha bf} = e^{-C_{ef}\, t_f / \cos(\arcsin(n_a \sin\theta_b / n_f))} = e^{-200 \times 0.0002 / \cos(\arcsin(\sin 14.9749 / 1.6))} = 0.96028$$

From the numerical example presented in Appendix D, it follows that the diffuse cover reflectivity is

$$\rho_{dc} = 0.09346$$

and the transmissivity due to absorbtance for diffuse solar radiation

$$\tau_{\alpha dc} = 0.9405 .$$

The diffuse reflectivity of the air-film and film-water interfaces, according to Appendix H, is respectively

$$\rho_{daf} = 0.1052$$

and

$$\rho_{dfw} = 0.01102$$

while the film's diffuse transmissivity due to absorbtance is

$$\tau_{\alpha df} = 0.95354 .$$

Table J.1 shows that the diffuse radiation was 8 % of the total measured incident solar radiation on the cover. Hence, the incident beam solar radiation on the cover is

$$Ih_b = 0.92 Ih_T = 0.92 \times 1073.20 = 987.34 \text{ W/m}^2$$

and the diffuse solar radiation

$$Ih_d = 0.08 Ih_T = 0.08 \times 1073.20 = 85.86 \text{ W/m}^2$$

To evaluate the effective convective heat transfer coefficient between the outer cover and the environment, the thermophysical properties of the air above the cover are required.

The final iteration yielded a value of 30.834°C for the cover temperature, while the ambient temperature was measured at 26°C. Therefore, the air above the cover is at a mean cover-ambient temperature of

$$T_{am} = 0.5(T_a + T_c) = 0.5\times(26 + 30.834) = 28.417\,°C \text{ or } 301.567\,K.$$

For this temperature, the thermophysical properties of air [98KR1] are

Air density	$\rho_{ca} = \frac{p_a}{287.08 \times T_{am}} = \frac{101169}{287.08 \times 301.19} = 1.1686\ kg/m^3$
Specific heat capacity of air	$c_{pca} = 1007.01\ J/kg.K$
Air conductivity	$k_{ca} = 0.026342\ W/m.K$
Dynamic viscosity of air	$\mu_{ca} = 1.85408\ x10^{-5}\ N/s.m^2$

The above thermophysical properties give a Prandtl number of

$$Pr_{ca} = \frac{\mu_{ca}\, c_{pca}}{k_{ca}} = \frac{1.85408\,x10^{-5}\,x\,1007.01}{0.026342} = 0.7088.$$

The effective length for a square cover is the side length, L_c, of the cover (see Appendix B). The dimensionless Grashof number is thus

$$Gr_{ca} = \frac{2(T_c - T_a)\,g\,L_c^3\,\rho_{ca}^2}{(T_c + T_a)\mu_{ca}^2} = \frac{2\times(303.984 - 299.15)x9.8\,x1.0^3\,x1.1686^2}{(303.984 + 299.15)x\left(1.85408\,x10^{-5}\right)^2} = 634.693\ x10^6$$

and the corresponding Reynolds number is

$$Re_{ca} = \frac{\rho_{ca}\, v_w\, L_c}{\mu_{ca}} = \frac{1.1581x1.8\,x1.0}{1.86515\,x10^{-5}} = 138662.8$$

From Table J.1 it follows that the final iteration yielded a temperature of 42.407°C for the water temperature. Hence, the air within the thin enclosure between the plastic cover and glass cover is at a mean temperature of

$$T_m = 0.5(T_w + T_c) = 0.5 \times (42.407 + 30.834) = 36.621°C \text{ or } 309.771K$$

and the thermophysical properties of air at this temperature [98KR1] are

Air density $\rho_{cf} = \dfrac{p_a}{287.08 \times T_m} = \dfrac{101063}{287.08 \times 309.89} = 1.136 \text{ kg/m}^3$

Specific heat capacity of air $c_{pcf} = 1007.35 \text{ J/kg.K}$

Air conductivity $k_{cf} = 0.026974 \text{ W/m.K}$

Dynamic viscosity of air $\mu_{cf} = 1.89159 \times 10^{-5} \text{ N/s.m}^2$

which relates to a corresponding Prandtl number of

$$Pr_{cf} = \frac{\mu_{cf}\, c_{pcf}}{k_{cf}} = \frac{1.89159 \times 10^{-5} \times 1007.35}{0.026974} = 0.7064.$$

According to Mills [92MI1], the effective length of a thin air enclosure is the distance between the two opposing surfaces. The dimensionless Grashof number for the enclosure is thus

$$Gr_{ce} = \frac{2(T_w - T_c)\, g\, t_{air}^3\, \rho_{cf}^2}{(T_w + T_c)\mu_{cf}^2} = \frac{2 \times (315.557 - 303.984) \times 9.8 \times 0.06^3 \times 1.136^2}{(315.557 + 303.984) \times (1.89159 \times 10^{-5})^2} = 285.5166 \times 10^3$$

Upon substitution of the applicable dimensionless numbers and solar properties into equation (J.8), the cover energy conservation equation becomes

$$\frac{(1-0.04344)(1-0.95011)}{1-0.04344 \times 0.95011} \times 987.34 + \frac{(1-0.09346)(1-0.9405)}{1-0.09346 \times 0.9405} \times 85.86$$

$$+ \left[1 + 1.44 \left[1 - \frac{1708}{285.5166 \times 10^3 \times 0.7064} \right] + \left[\left(\frac{285.5166 \times 10^3 \times 0.7064}{5830} \right)^{1/3} - 1 \right] \right] \frac{0.026974}{0.06} (T_w - T_c)$$

$$+ 5.67 \times 10^{-8} \left(\frac{1}{0.80} + \frac{1}{0.88} - 1 \right)^{-1} \left(T_w^4 - T_c^4 \right)$$

$$= \left[(625.4071 \times 10^6 \times 0.70876)^{1/3} (0.227 + 1.406 \times 10^{-6} \times 138662.8) \right] \frac{0.026342}{1.0} (T_c - 299.15)$$

$$+ 0.88 \times 5.67 \times 10^{-8} \left(T_c^4 - (0.0552 \times (26 + 273.15)^{1.5})^4 \right)$$

which simplifies to

$$49.14704 + 5.07752 + 2.1067\left(T_w - T_c\right) + 40.8984\times10^{-9}\left(T_w^4 - T_c^4\right)$$
$$= 8.47502\left(T_c - 299.15\right) + 49.8960\times10^{-9}\left(T_c^4 - 285.609^4\right) \qquad \text{(J.11)}$$

At a water temperature of 42.407°C (315.557 K), the thermophysical properties of the water, according to Kröger [98KR1], are

Water density $\rho_w = 991.397\ \text{kg/m}^3$

Specific heat capacity of water $c_{pw} = 4176.9\ \text{J/kg.K}$

Upon substituting the water thermophysical properties as well as the dimensionless numbers into equation (J.10), the energy equation of the plastic covered water tank yields

$$\left[\frac{\left(1-0.04344\right)^2\times0.95011}{\left(1-0.04344^2\times0.945011^2\right)}\right]\left[1-\frac{0.05335+\left(1-2\times0.05335\right)\times0.008296\times0.96028^2}{1-0.05335\times0.008296\times0.96028^2}\right]$$
$$\left[1-0.09346\times\frac{0.05335+\left(1-2\times0.05335\right)\times0.008296\times0.96028^2}{1-0.05335\times0.008296\times0.96028^2}\right]^{-1}\times987.34+$$
$$\left[\frac{\left(1-0.09346\right)^2\times0.9405}{\left(1-0.09346^2\times0.9405^2\right)}\right]\left[1-\frac{0.1052+\left(1-2\times0.1052\right)\times0.01102\times0.9603^2}{1-0.1052\times0.01102\times0.9603^2}\right]$$
$$\left[1-0.09346\times\frac{0.1052+\left(1-2\times0.1052\right)\times0.01102\times0.9603^2}{1-0.1052\times0.01102\times0.9603^2}\right]^{-1}\times79.27+$$
$$=\left[1+1.44\left[1-\frac{1708}{285.5166\times10^3\times0.7064}\right]+\left[\left(\frac{285.5166\times10^3\times0.7064}{5830}\right)^{1/3}-1\right]\right]\frac{0.026974}{0.06}\left(T_w-T_c\right)$$
$$+5.67\times10^{-8}\left(\frac{1}{0.80}+\frac{1}{0.88}-1\right)^{-1}\left(T_w^4-T_c^4\right)+991.397\times\ 0.190\times4176.9\times\ \frac{T_w-315.496}{61}$$

and reduces to

$$812.621 + 59.97 =$$
$$2.1067\left(T_w - T_c\right) + 40.8984\times10^{-9}\left(T_w^4 - T_c^4\right) + 12.8981\times\ 10^3\left(T_c - 315.496\right) \qquad \text{(J.12)}$$

Solving equation (J.11) and equation (J.12) simultaneously, temperatures of 30.834°C and 42.407°C are obtained for the respective cover and mean weighted water temperatures respectively, which shows good agreement with the experimentally measured values of 32.48 °C and 42.73 °C.

Appendix K: Solar collector with water storage – Night operation

Experimental tests were conducted to observe the discharge of energy from the plastic covered water tank during the night.

K.1 Experimental apparatus, analysis and results

The experimental apparatus is identical to the one described in Appendix J, with the two thermocouples recording the cover temperature and the oscillating probe monitoring the water temperature at various depths. The ambient conditions were recorded by the Davis weather station.

In Figure K.1 and Figure K.2 the experimental results for the night of the 21 – 22nd of November 2000 are shown.

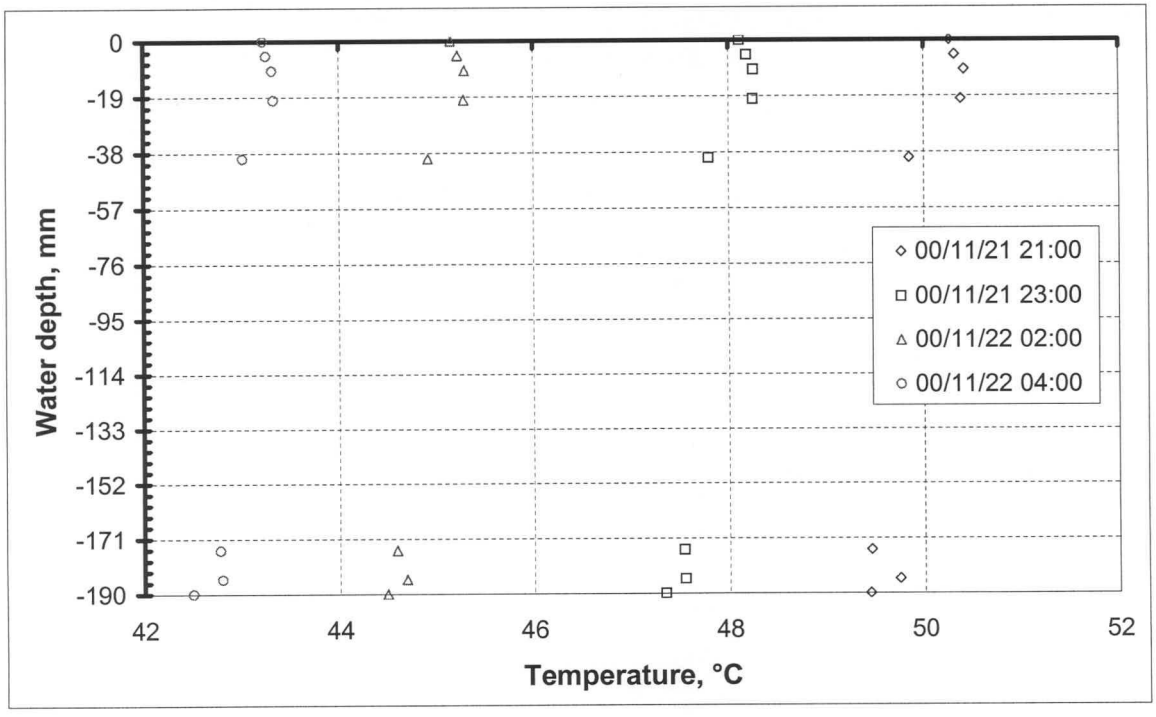

Figure K.1: Water temperature profile for solar collector

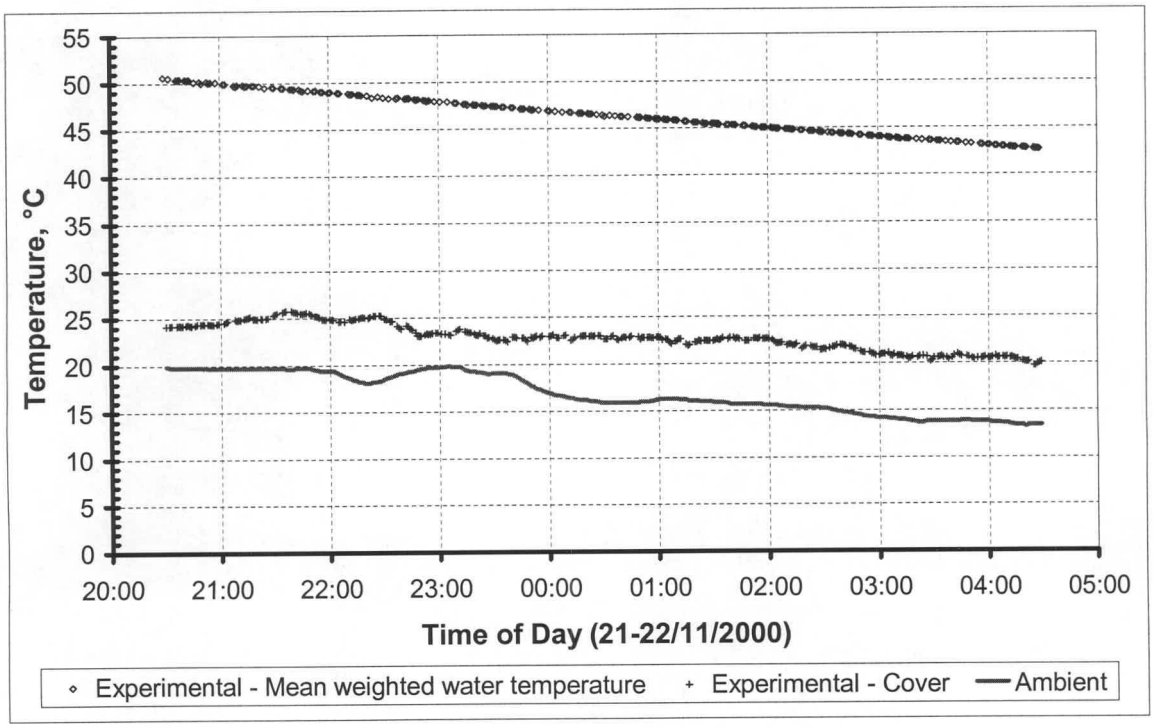

Figure K.2: Experimental cover and water temperatures for solar collector

Omitting the solar radiation terms in the cover and water tank energy equations of Appendix J (equation (J.8) and (J.9)), the following two equations are obtained for the cover and the plastic covered water tank respectively, assuming no air-layer exist between the film and water.

From equation (J.8), it follows that the conservation of energy equations for the cover is

$$\left[1+1.44\left[1-\frac{1708}{Gr_{cf}\ Pr_{cf}}\right]+\left[\left(\frac{Gr_{cf}\ Pr_{cf}}{5830}\right)^{1/3}-1\right]\right]\frac{k_{cf}}{t_{air}}\left(T_f-T_c\right)$$

$$+\sigma\left(\frac{1}{\varepsilon_c}+\frac{1}{\varepsilon_f}-1\right)^{-1}\left(T_w^4-T_c^4\right) \qquad \text{(K.1)}$$

$$=\left[\left(Gr_{ca}\ Pr_{ca}\right)^{1/3}\left(0.227+1.406\times10^{-6}\ Re_{ca}\right)\right]\frac{k_{ca}}{L_c}\left(T_c-T_a\right)$$

$$+\varepsilon_c\ \sigma\left(T_c^4-\left(0.0552\ T_a^{1.5}\right)^4\right)$$

From equation (J.9) the following equation for the plastic covered water tank is obtained

$$-\left[1+1.44\left[1-\frac{1708}{Gr_{cf}\,Pr_{cf}}\right]+\left[\left(\frac{Gr_{cf}\,Pr_{cf}}{5830}\right)^{1/3}-1\right]\right]\frac{k_{cf}}{t_{air}}(T_w-T_c)$$

$$-\sigma\left(\frac{1}{\varepsilon_c}+\frac{1}{\varepsilon_f}-1\right)^{-1}\left(T_w^4-T_c^4\right)=\rho_w\,t_w\,c_{pw}\,\frac{dT_w}{dt} \qquad \text{(K.2)}$$

Under ambient steady state conditions (only a small variation in both the ambient temperature and wind speed over a period of time), equations (K.1) and equation (K.2) can be solved simultaneously to yield the predicted cover and water tank temperature, for given ambient conditions.

Such steady state conditions prevailed during the night of the 21st - 22nd of November 2000, from 00h00 – 04h00. Subsequently, equations (K.1) and (K.2) are used to predict the temperatures for the cover and water tank.

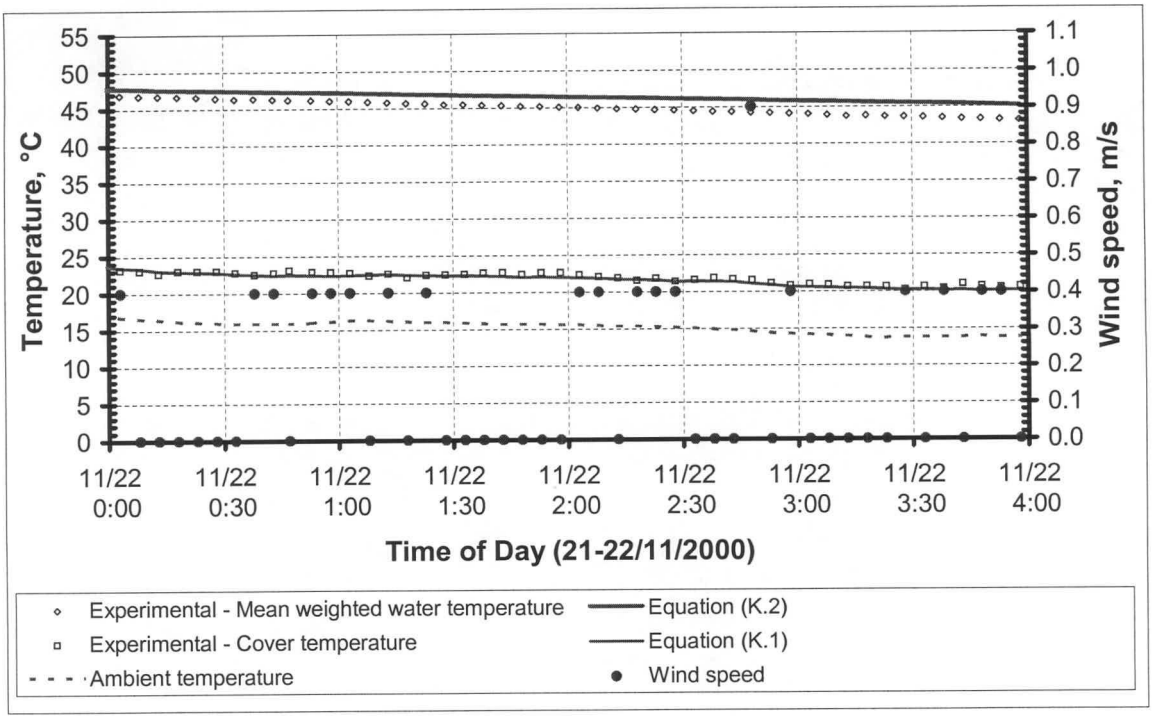

Figure K.3: Comparison between predicted and experimentally measured temperatures for cover and water

From the graphical comparison, as shown in Figure K.3, it is apparent that the previously derived equations for the cover and water tank are in good agreement with the experimentally

measured values. The maximum errors for the cover and water tank temperatures are 1.59 °C and 0.72 °C respectively.

To illustrate the solving procedure, the final iteration is shown for the prediction of the cover and water tank's temperature for the 22nd of November 2000 at 01h00:40.

Numerical example

In this section it will be shown that equation (K.1) and equation (K.2) are satisfied by a cover temperature of 24.1039 °C (297.2529 K) and mean water tank temperature of 46.1899 °C (319.3399 K).

In Table K.1 the specifications of the experimental configuration as well as the ambient conditions are given for the 22nd of November 2000 at 01h00:12.

Table K. 1: Experimental and numerical data for night operation of solar collector with water storage

Water height, t_w	0.190 m
Side length of cover, L_c	1.0 m
Long-wave emissivity of film, ε_f	0.80
Long-wave emissivity of cover, ε_c	0.88
Thin enclosure thickness, t_{air}	0.06 m
Ambient temperature, T_a	16.2 °C (289.35 K)
Wind speed, v_w	0.0 m/s
Atmospheric pressure, p_a	100 904 Pa
Predicted cover temperature, T_c	24.1039 °C (297.2529 K)
Predicted mean water temperature (01h00:12), T_w^i	46.1899 °C (319.3399 K)
Predicted mean water temperature (00h59:11), T_w^{i-1}	46.3824 °C (319.5324 K)

To evaluate the effective convective heat transfer coefficient between the outer cover and the environment, the thermophysical properties of the air above the cover need to be known.

From Table K.1 it follows that the final iteration yielded a cover temperature of 24.1039°C, while the ambient temperature for this given point in time was measured as 16.20°C. Therefore, the air above the cover is at a mean cover-ambient temperature of

$$T_{am} = 0.5(T_a + T_c) = 0.5 \times (16.20 + 24.1039) = 20.152\,°C \text{ or } 293.302\,K.$$

For this temperature, the thermophysical properties of air [98KR1] are

Air density $\rho_{ca} = \dfrac{p_a}{287.08 \times T_{am}} = \dfrac{100904}{287.08 \times 293.302} = 1.1984\ kg/m^3$

Specific heat capacity of air $c_{pca} = 1006.733\ J/kg.K$

Air conductivity $k_{ca} = 0.025701\ W/m.K$

Dynamic viscosity of air $\mu_{ca} = 1.81594 \times 10^{-5}\ N/s.m^2$

The above thermophysical properties result in a Prandtl number of

$$Pr_{ca} = \frac{\mu_{ca}\, c_{pca}}{k_{ca}} = \frac{1.81594 \times 10^{-5} \times 1006.733}{0.025701} = 0.7113.$$

The effective length for a square cover is the side length, L_c, of the cover. Thus, the dimensionless Grashof number is

$$Gr_{ca} = \frac{2(T_c - T_a)\, g\, L_c^3\, \rho_{ca}^2}{(T_c + T_a)\mu_{ca}^2} = \frac{2 \times (297.2539 - 289.35) \times 9.8 \times 1.0^3 \times 1.1984^2}{(297.2539 + 289.35) \times (1.81594 \times 10^{-5})^2} = 1.15132 \times 10^9$$

The water tank temperature is predicted as 46.1899 °C. Thus, the enclosed air, according to Mills [92MI1], is at a mean temperature of

$$T_m = 0.5(T_w + T_c) = 0.5 \times (46.1899 + 24.1039) = 35.147\,°C \text{ or } 308.297\,K.$$

and the thermophysical properties of air at this temperature [98KR1] are

Air density $\rho_{cf} = \dfrac{p_a}{287.08 \times T_m} = \dfrac{100904}{287.08 \times 308.297} = 1.1401\ kg/m^3$

Specific heat capacity of air $c_{pcf} = 1007.28\ J/kg.K$

Air conductivity $k_{cf} = 0.026861\ W/m.K$

Dynamic viscosity of air $\mu_{cf} = 1.88487 \times 10^{-5}\ N/s.m^2$

These values result in a Prandtl number of

$$Pr_{cf} = \frac{\mu_{cf}\, c_{pcf}}{k_{cf}} = \frac{1.88487\,x10^{-5}\,x\,1007.28}{0.026861} = 0.7068.$$

According to Mills [92MI1], the effective length of a thin air enclosure is the distance between the opposing surfaces. Hence, the dimensionless Grashof number for the thin enclosure is

$$Gr_{cf} = \frac{2(T_w - T_c)\,g\,t_{air}^3\,\rho_{cf}^2}{(T_w + T_c)\mu_{cf}^2} = \frac{2\times(319.3399 - 297.2539)x9.8\,x0.06^3\,x1.1401^2}{(319.3399 + 297.2539)x\left(1.88487x10^{-5}\right)^2} = 555.384\ x10^3$$

Upon substitution of the applicable dimensionless numbers and solar properties into equation (K.1), the cover energy conservation equation becomes

$$\left[1+1.44\left[1-\frac{1708}{555.384\times10^3\times0.7068}\right]+\left[\left(\frac{555.384\times10^3\times0.7068}{5830}\right)^{1/3}-1\right]\right]\frac{0.026861}{0.06}(T_w - T_c)$$

$$+5.67\times10^{-8}\left(\frac{1}{0.80}+\frac{1}{0.88}-1\right)^{-1}\left(T_w^4 - T_c^4\right)$$

$$=\left[\left(1.15132\times10^9\times0.7113\right)^{1/3}\left(0.227+1.406\times10^{-6}\times0\right)\right]\frac{0.025701}{1.0}(T_c - 289.35)$$

$$+0.88\times5.67\times10^{-8}\left(T_c^4 - \left(0.0552\times(16.2+273.15)^{1.5}\right)^4\right)$$

which simplifies to

$$\begin{aligned}&2.4631(T_w - T_c) + 40.8984\times10^{-9}\left(T_w^4 - T_c^4\right)\\&= 5.4583\,(T_c - 289.35) + 49.8960\times10^{-9}\left(T_c^4 - 271.69^4\right)\end{aligned} \qquad \text{(K.3)}$$

At a water temperature of 46.1899°C (319.3399 K), the thermophysical properties of the water, according to Kröger [98KR1], are

Water density $\rho_w = 989.581\,kg/m^3$

Specific heat capacity of water $c_{pw} = 4177.84\ J/kg.K$

Substituting the above determined thermophysical properties of the water, as well as the previously determined properties of the enclosed air, into equation (K.2), find

$$-\left[1+1.44\left[1-\frac{1708}{555.384\times10^{3}\times0.7068}\right]+\left[\left(\frac{555.384\times10^{3}\times0.7068}{5830}\right)^{1/3}-1\right]\right]\frac{0.026861}{0.06}(T_w-T_c)$$

$$+5.67\times10^{-8}\left(\frac{1}{0.80}+\frac{1}{0.88}-1\right)^{-1}\left(T_w^4-T_c^4\right)=989.581\times 0.190\times4177.84\times\frac{T_w-319.3524}{61}$$

After simplifying the above equation, the conservation of energy equation for the water tank reduces to

$$-2.4631(T_w-T_c)-40.8984\times10^{-9}\left(T_w^4-T_c^4\right)=12.8774\times10^{3}\left(T_w-319.3524\right) \qquad \text{(K.4)}$$

Solving equation (K.3) and (K.4) simultaneously, the mean temperature for the water tank temperature is predicted to be 46.1899°C (319.3399 K) and the cover temperature as 24.1039°C (297.2539 K). Comparing these values to the experimentally measured values of 22.83°C and T_w = 46.01 °C respectively, it s evident that good agreement exists between the experimental and theoretical values.

Appendix L: Solar air heater with water storage – Day operation

To observe the influence of water energy storage system on the daytime performance of a solar air heater, experiments were conducted on the solar air heater (described in Chapter 4). The experimental results were compared to theoretically predicted values.

L.1 Analysis

Consider the 1m cross-section of an upward facing solar air heater with a plastic covered water tank shown in Figure L.1.

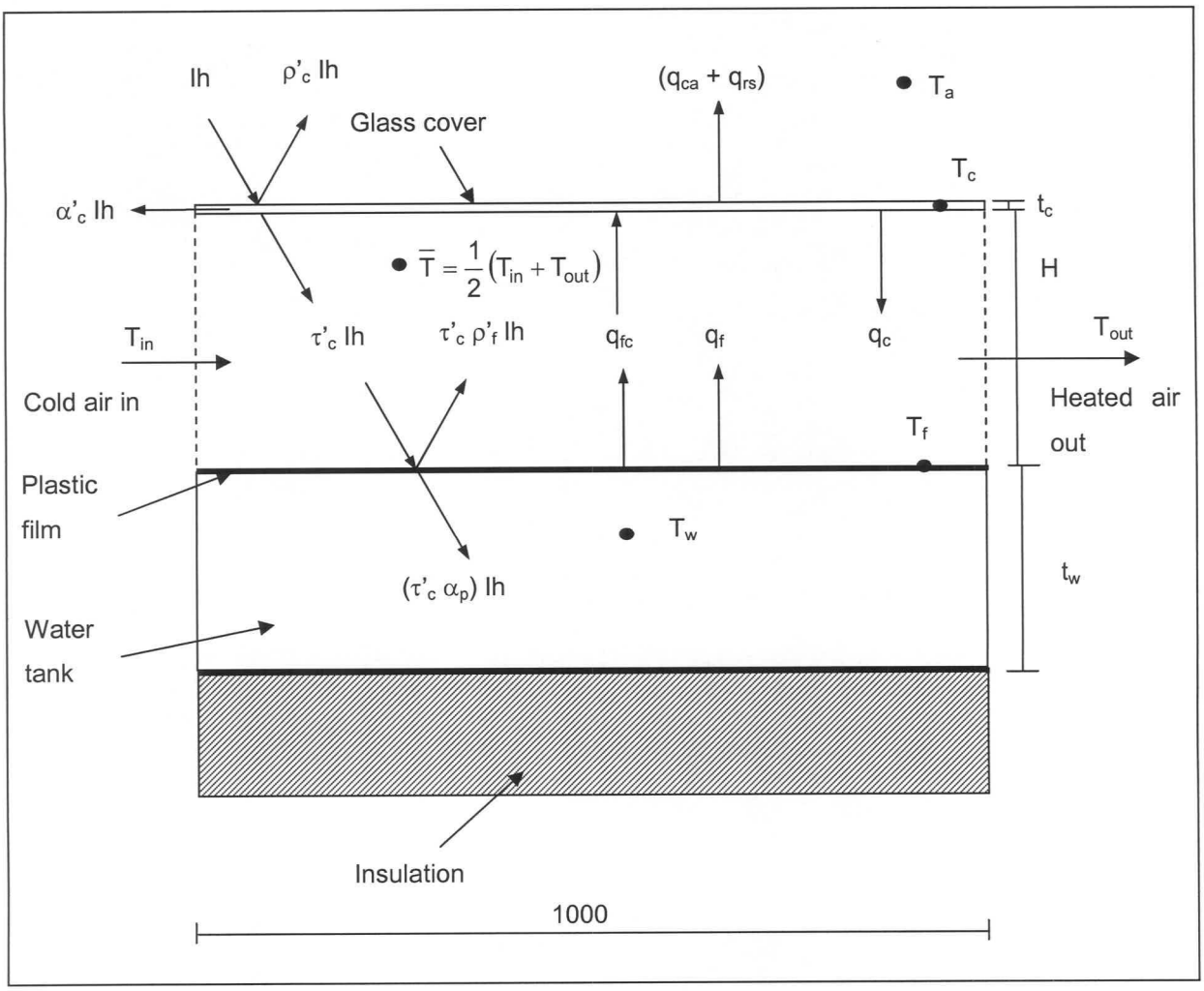

Figure L.1: A 1m-cross section of an upward facing solar air heater with plastic covered water tank

The 1m cover considered in the previous schematic presentation (Figure L.1) is identical to the solar air heater cover considered in Appendix E. Hence, the conservation of energy equation for the cover under consideration in Figure L.1 is

$$\left[\frac{(1-\rho_{bc})(1-\tau_{bc})}{1+\rho_{bc}\,\tau_{bc}}\right] Ih_b + \left[\frac{(1-\rho_{dc})(1-\tau_{dc})}{1-\rho_{dc}\,\tau_{dc}}\right] Ih_d + \sigma\left[\frac{1}{\varepsilon_c}+\frac{1}{\varepsilon_f}-1\right]^{-1}\left(T_f^4 - T_c^4\right) = \bar{h}_c\left(T_c - \bar{T}\right)$$
$$+\left[(Gr_{ca}\,Pr_{ca})^{1/3}\left(0.227 + 1.406\times10^{-6}\,Re_{ca}\right)\right]\frac{k_{ca}}{L_c}\left(T_c - T_a\right) + \varepsilon_c\,\sigma\left[T_c^4 - \left(0.0552\,T_a^{1.5}\right)^4\right] \qquad \text{(L.1)}$$

with ε_f and T_f defining the respective emissivity and temperature respectively of the plastic film which covers the water tank. However, at this point it must be stressed that the above derived cover energy equation for the solar air heater is only valid if the cover temperature exceeds the ambient temperature and $6.75 \times 10^8 \le (GrPr) \le 26.6 \times 10^8$ and for $0 \le Re \le 2.5 \times 10^5$.

In the present experimental set-up, the insulation blocks of the solar air heater in Appendix E are replaced by 8 plastic covered water tanks, having dimensions of 1m x 1m x 0.19m. Assuming perfect contact between the plastic film and the water, and conduction losses through the 50-mm thick polystyrene insulation to be negligible, Figure L.1 yields the following energy equation for the water tank

$$\left(\tau'\,\alpha_p\right)_b Ih_b + \left(\tau'\,\alpha_p\right)_d Ih_d = q_f + q_{fc} + \rho_w\,t_w\,c_{pw}\frac{dT_w}{dt} \qquad \text{(L.2)}$$

Substitute equations (2.25) and (D.9) into equation (L.2) for the convective and radiative terms, and equation (J.5) for the effective transmittance-absorbtance product for the water tank, and find

$$\left[\frac{\tau_c'\left(1-\rho_f'\right)}{1-\rho_f'\,\rho_{dc}}\right]_b Ih_b + \left[\frac{\tau_c'\left(1-\rho_f'\right)}{1-\rho_f'\,\rho_{dc}}\right]_d Ih_d = \bar{h}_f\left(T_f - \bar{T}\right) + \sigma\left[\frac{1}{\varepsilon_c}+\frac{1}{\varepsilon_f}-1\right]^{-1}\left(T_f^4 - T_c^4\right)$$
$$+\rho_w\,t_w\,c_{pw}\frac{dT_w}{dt} \qquad \text{(L.3)}$$

Upon substitution of the respective effective cover transmissivity, τ_c', and effective reflectivity of the plastic film ρ_f', (equations (B.8) and (B.4)), into equation (L.3), the conservation of energy equation for the water tank becomes

$$\left[\frac{(1-\rho_{bc})^2\,\tau_{\alpha bc}}{\left(1-\rho_{bc}^2\,\tau_{\alpha bc}^2\right)}\right]\left[1-\frac{\rho_{baf}+(1-2\rho_{baf})\rho_{bfw}\,\tau_{\alpha bf}^2}{1-\rho_{baf}\,\rho_{bfw}\,\tau_{\alpha bf}^2}\right]\left[1-\rho_{dc}\,\frac{\rho_{baf}+(1-2\rho_{baf})\rho_{bfw}\,\tau_{\alpha bf}^2}{1-\rho_{baf}\,\rho_{bfw}\,\tau_{\alpha bf}^2}\right]^{-1} Ih_b +$$

$$\left[\frac{(1-\rho_{dc})^2\,\tau_{\alpha dc}}{\left(1-\rho_{dc}^2\,\tau_{\alpha dc}^2\right)}\right]\left[1-\frac{\rho_{daf}+(1-2\rho_{daf})\rho_{dfw}\,\tau_{\alpha df}^2}{1-\rho_{daf}\,\rho_{dfw}\,\tau_{\alpha df}^2}\right]\left[1-\rho_{dc}\,\frac{\rho_{daf}+(1-2\rho_{daf})\rho_{dfw}\,\tau_{\alpha df}^2}{1-\rho_{daf}\,\rho_{dfw}\,\tau_{\alpha df}^2}\right]^{-1} Ih_d \qquad (L.4)$$

$$=\bar{h}_f\left(T_f-\bar{T}\right)+\sigma\left[\frac{1}{\varepsilon_c}+\frac{1}{\varepsilon_f}-1\right]^{-1}\left(T_f^4-T_c^4\right)+\rho_w\,t_w\,c_{pw}\,\frac{dT_w}{dt}$$

From a comparison between Figure L.1 and Figure E.2, it is evident that the energy balance for the air stream for each of the experimental set-ups is identical. Consequently, from equation (E.13) it follows

$$\dot{m}c_p\,T_{in}+A\,\bar{h}_f\left(T_f-\bar{T}\right)+A\,\bar{h}_c\left(T_c-\bar{T}\right)=\dot{m}c_p\left(2\bar{T}-T_{in}\right) \qquad (L.5)$$

During the above water tank energy equation derivation, the assumption was made that both the effective absorbtance and thermal capacitance of the plastic film is negligible. Consequently, the film temperature, T_f, and mean water temperature, T_w are assumed to be approximately equal to each other. As a result, equation (L.1) becomes

$$\left[\frac{(1-\rho_{bc})(1-\tau_{bc})}{1+\rho_{bc}\,\tau_{bc}}\right]Ih_b+\left[\frac{(1-\rho_{dc})(1-\tau_{dc})}{1-\rho_{dc}\,\tau_{dc}}\right]Ih_d=\bar{h}_c\left(T_c-\bar{T}\right)+\sigma\left[\frac{1}{\varepsilon_c}+\frac{1}{\varepsilon_f}-1\right]^{-1}\left(T_w^4-T_c^4\right)$$
$$+\left[\left(Gr_{ca}\,Pr_{ca}\right)^{1/3}\left(0.227+1.406\times10^{-6}\,Re_{ca}\right)\right]\frac{k_{ca}}{L_c}\left(T_c-T_a\right)+\varepsilon_c\,\sigma\left[T_c^4-\left(0.0552\,T_a^{1.5}\right)^4\right] \qquad (L.6)$$

while the conservation of energy equation for the plastic covered water tank (equation (L.4)) reduces to

$$\left[\frac{(1-\rho_{bc})^2\,\tau_{\alpha bc}}{\left(1-\rho_{bc}^2\,\tau_{\alpha bc}^2\right)}\right]\left[1-\frac{\rho_{baf}+(1-2\rho_{baf})\rho_{bfw}\,\tau_{\alpha bf}^2}{1-\rho_{baf}\,\rho_{bfw}\,\tau_{\alpha bf}^2}\right]\left[1-\rho_{dc}\,\frac{\rho_{baf}+(1-2\rho_{baf})\rho_{bfw}\,\tau_{\alpha bf}^2}{1-\rho_{baf}\,\rho_{bfw}\,\tau_{\alpha bf}^2}\right]^{-1} Ih_b +$$

$$\left[\frac{(1-\rho_{dc})^2\,\tau_{\alpha dc}}{\left(1-\rho_{dc}^2\,\tau_{\alpha dc}^2\right)}\right]\left[1-\frac{\rho_{daf}+(1-2\rho_{daf})\rho_{dfw}\,\tau_{\alpha df}^2}{1-\rho_{daf}\,\rho_{dfw}\,\tau_{\alpha df}^2}\right]\left[1-\rho_{dc}\,\frac{\rho_{daf}+(1-2\rho_{daf})\rho_{dfw}\,\tau_{\alpha df}^2}{1-\rho_{daf}\,\rho_{dfw}\,\tau_{\alpha df}^2}\right]^{-1} Ih_d \qquad (L.7)$$

$$=\bar{h}_f\left(T_w-\bar{T}\right)+\sigma\left[\frac{1}{\varepsilon_c}+\frac{1}{\varepsilon_f}-1\right]^{-1}\left(T_w^4-T_c^4\right)+\rho_w\,t_w\,c_{pw}\,\frac{dT_w}{dt}$$

Table L.1: Experimental data for day operation of solar air heater with water storage

Water height, t_w	0.190 m
Cover thickness, t_c	0.00388 m
Film thickness, t_f	0.0002 m
Side length of cover, L_c	1.0 m
Duct height, H	0.15 m
Duct width, W	1.0 m
Cover extinction coefficient, C_{ec}	13 m^{-1}
Cover refractive index, n_c	1.526
Film extinction coefficient, C_{ef}	200 m^{-1}
Film refractive index, n_f	1.6
Air refractive index, n_a [91DU1]	1.0
Water refractive index, n_w [92SE1]	1.333
Long-wave emissivity of cover, ε_c	0.80
Long-wave emissivity of film, ε_f	0.88
Ambient temperature, T_a	31.94 °C (305.09 K)
Wet-bulb temperature, T_{wb}	26.255 °C (299.405 K)
Dry-bulb temperature, T_{db}	35.807 °C (308.957 K)
Massflow nozzle 2, m_2	0.09359 kg/s
Total incident solar radiation, Ih_T	886.394 $W/m^2.K$
Wind speed, v_w	0.4 m/s
Percentage diffuse radiation	9 %
Atmospheric pressure, p_a	99 933.4 Pa
Location latitude angle, ϕ	33.98 °S
Location longitude angle, ϕ_l	18.85 °E
Location standard meridian, ϕ_m	30.00 °E
Predicted cover temperature	34.128 °C (307.278 K)
Predicted air temperature	32.239 °C (305.389 K)
Predicted water temperature (13h24:02), T_w^i	42.444 °C (315.594 K)
Predicted water temperature (13h23:47), T_w^{i-1}	42.4321 °C (315.5281 K)

and the air energy equation simplifies to

$$mc_p T_{in} + A\bar{h}_f\left(T_w - \bar{T}\right) + A\bar{h}_c\left(T_c - \bar{T}\right) = mc_p\left(2\bar{T} - T_{in}\right) \tag{L.8}$$

Therefore, to predict the performance of an upward facing solar air heater with water storage for given ambient conditions, equations (L.6), (L.7) and (L.8) need to be solved simultaneously.

To illustrate the solution procedure used during this solution, the final iteration is shown for the prediction of the first 1m section of the solar air heater's mean cover, plate and air temperature of the water tank for the 19th of March 2001 (DOY = 78th day of year) at 13h24:02 (ψ = 13.16778 hours after midnight).

Numerical example

In the following calculations, it will be shown that equations (L.6), (L.7) and (L.8) are satisfied for the 19th of March 2001 by a cover temperature of 34.128 °C (307.278 K), a mean water temperature of 42.444 °C (315.594 K) and a air temperature of 32.239 °C (305.389 K) for the given ambient conditions in Table L.1 and mass flow rate of 0.09359 kg/s through nozzle number 2.

According to equation (B.21), the leap year adjustment to the day for the year 2001 is

$$YADJ = 0.25\left[2.5 - \left(Y - 4\left(\text{integer}\left(\left(Y-1\right)/4\right)\right)\right)\right] = 0.25\times\left[2.5 - \left(2001 - 4\left(\text{integer}\left(\left(2001-1\right)/4\right)\right)\right)\right]$$

$$= 0.375 \text{ days}$$

with the above integer function yielding a value of 500.

The 19th of March is the 78th day of the year. The annual phase angle, according to equation (B.20), is thus

$$P = 0.0172028\left(DOY + YADJ + 0.417\right) = 0.0172028\left(78 + 0.375 + 0.417\right) = 1.35544 \text{ rad.}$$

Substituting the above-evaluated annual phase angle into equation (B.20), the declination angle for the surface becomes

$$\delta = 180\left[0.00661 + 0.40602\sin\left(P - 1.4075\right) + 0.00665\sin\left(2P - 1.4789\right)\right.$$

$$\left. + 0.00298\sin\left(3P - 1.0996\right)\right]\pi$$

$$= 180\left[0.00661 + 0.40602\sin\left(1.35544 - 1.4075\right) + 0.00665\sin\left(2\times 1.35544 - 1.4789\right)\right.$$

$$\left. + 0.00298\sin\left(3\times 1.35544 - 1.0996\right)\right]\pi$$

$$= -0.4427°$$

which leads to an equation of time (equation (B.23)) of

$$\begin{aligned}EOT &= 1440\,[\,0.005114\sin(P+3.0593)+0.006892\sin(2P+3.4646)\\ &\quad +0.00022\sin(3P+3.3858)+0.000153\sin(4P+3.7766)\,]\\ &= 1440\,[\,0.005114\sin(1.35544+3.0593)+0.006892\sin(2\times1.35544+3.4646)\\ &\quad +0.00022\sin(3\times1.35544+3.3858)+0.000153\sin(4\times1.35544+3.7766)\,]\\ &= -7.7661\,\text{min.}\end{aligned}$$

Measurements were taken at 13h24:03 or 13.40056 hours after midnight, which, according to equation (B.22) relates to an hour angle of

$$\omega = 15\left[\psi - 12 - \frac{4(\phi_m - \phi_l) - EOT}{60}\right] = 15\left[13.40056 - 12 - \frac{4(30-18.85)-(-7.7661)}{60}\right] = 7.9169°.$$

For the location with a standard meridian, ϕ_m, of 30° E, longitude, ϕ_l, of 18.85° E and latitude of 33.98° S, the beam incidence angle according to equation (B.22) is

$$\begin{aligned}\theta_b &= \text{a}\cos(\sin\delta\sin\phi+\cos\delta\cos\phi\cos\omega)\\ &= \text{a}\cos(\sin-0.4427\sin-33.98+\cos-0.4427\times\cos-33.98\times\cos-7.7661) = 34.318°.\end{aligned}$$

For the above incidence angle, the beam cover reflectivity is

$$\begin{aligned}\rho_{bc} &= \frac{1}{2}\left[\frac{\tan^2(\theta_b-\arcsin(n_a\sin\theta_b/n_c))}{\tan^2(\theta_b+\arcsin(n_a\sin\theta_b/n_c))}+\frac{\sin^2(\theta_b-\arcsin(n_a\sin\theta_b/n_c))}{\sin^2(\theta_b+\arcsin(n_a\sin\theta_b/n_c))}\right]\\ &= \frac{1}{2}\left[\frac{\tan^2(34.318-\arcsin(\sin 34.318/1.526))}{\tan^2(34.318+\arcsin(\sin 34.318/1.526))}+\frac{\sin^2(34.318-\arcsin(\sin 34.318/1.526))}{\sin^2(34.318+\arcsin(\sin 34.318/1.526))}\right]\\ &= 0.04625\end{aligned}$$

while the air-film interface yields a beam reflectivity of

$$\begin{aligned}\rho_{baf} &= \frac{1}{2}\left[\frac{\tan^2(\theta_b-\arcsin(n_a\sin\theta_b/n_f))}{\tan^2(\theta_b+\arcsin(n_a\sin\theta_b/n_f))}+\frac{\sin^2(\theta_b-\arcsin(n_a\sin\theta_b/n_f))}{\sin^2(\theta_b+\arcsin(n_a\sin\theta_b/n_f))}\right]\\ &= \frac{1}{2}\left[\frac{\tan^2(34.318-\arcsin(\sin 34.318/1.6))}{\tan^2(34.318+\arcsin(\sin 34.318/1.6))}+\frac{\sin^2(34.318-\arcsin(\sin 34.318/1.6))}{\sin^2(34.318+\arcsin(\sin 34.318/1.6))}\right]\\ &= 0.05636\end{aligned}$$

and the film-water surface a value of

$$\rho_{bfw} = \frac{1}{2}\left[\frac{\tan^2(\arcsin(n_a \sin\theta_b / n_f) - \arcsin(n_a \sin\theta_b / n_w))}{\tan^2(\arcsin(n_a \sin\theta_b / n_f) + \arcsin(n_a \sin\theta_b / n_w))}\right]$$

$$+ \frac{1}{2}\left[\frac{\tan^2(\arcsin(n_a \sin\theta_b / n_f) - \arcsin(n_a \sin\theta_b / n_w))}{\tan^2(\arcsin(n_a \sin\theta_b / n_f) + \arcsin(n_a \sin\theta_b / n_w))}\right]$$

$$= \frac{1}{2}\left[\frac{\tan^2(\arcsin(\sin 34.318 / 1.6) - \arcsin(\sin 34.318 / 1.333))}{\tan^2(\arcsin(\sin 34.318 / 1.6) + \arcsin(\sin 34.318 / 1.333))}\right]$$

$$+ \frac{1}{2}\left[\frac{\sin^2(\arcsin(\sin 34.318 / 1.6) - \arcsin(\sin 34.318 / 1.333))}{\sin^2(\arcsin(\sin 34.318 / 1.6) + \arcsin(\sin 34.318 / 1.333))}\right]$$

$$= 0.008536$$

From Bouguer's law (equation (B.16)) it follows that the cover's beam transmissivity due to absorbtance is equal to

$$\tau_{\alpha bc} = e^{-C_{ec} t_c / \cos(\arcsin(n_a \sin\theta_b / n_c))} = e^{-13 \times 0.00388 / \cos(\arcsin(\sin 34.318 / 1.526))} = 0.94717$$

while the beam transmissivity due to absorbtance for the 0.0002 m thick plastic film is

$$\tau_{\alpha bf} = e^{-C_{ef} t_f / \cos(\arcsin(n_a \sin\theta_b / n_f))} = e^{-200 \times 0.0002 / \cos(\arcsin(\sin 34.318 / 1.6))} = 0.95816$$

From Appendix C's numerical example it follows that the diffuse cover reflectivity is

$$\rho_{dc} = 0.09346$$

and the transmissivity due to absorbtance for diffuse solar radiation

$$\tau_{\alpha dc} = 0.9405 .$$

The diffuse reflectivity of the air-film and film-water interfaces, according to Appendix H, is respectively

$$\rho_{daf} = 0.1052$$

and

$\rho_{dfw} = 0.01102$

while Appendix D yields a value of

$\rho_{dc} = 0.09346$

for the cover's diffuse reflectivity. Furthermore, from Appendix D it follows that the diffuse transmittance for the cover is

$\tau_{\alpha dc} = 0.9405$

while the film's diffuse transmissivity due to absorbtance for the film, according to Appendix H, is

$\tau_{\alpha df} = 0.95354$.

Table L.1 indicates that the diffuse radiation was 9 % of the total measured incident solar radiation on the cover during the period of time under consideration. The incident beam solar radiation on the cover is thus

$I_{hb} = 0.92 I_{hT} = 0.91 \times 886.394 = 806.619 \text{ W/m}^2$

and the diffuse solar radiation

$I_{hd} = 0.09 I_{hT} = 0.09 \times 886.394 = 79.775 \text{ W/m}^2$

To predict the mean air temperature, $\overline{T}$, for the section the air mass flow rate through the rectangular duct is required. From Table L.1, it is evident that the final iteration yielded an air mass flow rate of 0.09359 kg/s through the 75.48-mm diameter nozzle 2.

Employing the equations of Kröger [98KR1], the thermophysical properties and vapour pressure of the air-vapour mixture are evaluated at the outlet wet- and dry-bulb temperatures given in Table L.1.

Vapour pressure	$p_v = 3451.2$ Pa
Air-vapour density	$\rho_{av} = 1.1127 \text{ kg/m}^3$

Air-vapour dynamic viscosity $\mu_{av} = 1.8711\times10^{-5}$ kg/m.s

From equation (E.1) it follows that for a mixed density of 1.1127 kg/m^3 the upstream pressure is

$$p_{up} = p_a - K_d\left[\frac{m^2}{2\rho_{av}A_d^2}\right] = 99933.4 - 8.4\left[\frac{0.09359^2}{2\times1.1127\times0.15^2}\right] = 99931.9 \text{ Pa}$$

Using these properties, the gas expansion factor is evaluated according to equation (2.14)

$$\phi_g = 1-\frac{3\,dp_n}{4\,p_{up}\times1.4} = 1-\frac{3\times203.589}{4\times99931.9\times1.4} = 0.998909$$

while equation (2.18) yields an approach velocity factor of

$$Y_2 = 1+0.5\left(\frac{A_2}{A_{tus}}\right)^2+2\left(\frac{A_2}{A_{tus}}\right)^2\left(\frac{dp_n}{p_n\,c_p/c_v}\right)$$

$$= 1+0.5\left(\frac{4.47548\times10^{-3}}{0.6}\right)^2+2\left(\frac{4.47548\times10^{-3}}{0.6}\right)^2\left(\frac{203.589}{99931.9\times1.4}\right) = 1.000028$$

Using the previously determined thermophysical properties for the air-vapour mixture, the nozzle's Reynolds number is evaluated.

$$Re_2 = \frac{4\,m_2}{\pi D_2\,\mu_{av}} = \frac{4\times0.09359}{\pi\times0.0754875\times1.8711\times10^{-5}} = 84.366\times10^3$$

The nozzle discharge coefficient for each nozzle is based on the nozzle's particular Reynolds number. Consequently, from equation (2.12) it follows

$$C_n = 0.954803+6.37817\times10^{-7}\,Re_n-4.65394\times10^{-12}\,Re_n^2+1.33514\times10^{-17}\,Re_n^3$$

$$= 0.954803+6.37817\times10^{-7}\times84.366\times10^3-4.65394\times10^{-12}\times\left(84.366\times10^3\right)^2$$

$$+1.33514\times10^{-17}\times\left(84.366\times10^3\right)^3 = 0.983509$$

From equation (2.10), it follows that the mass flow rate through the nozzle is

$$m_2 = C_2\,\phi_g\,Y_2\,A_2\sqrt{2\,\rho_{av}\,dP_n}$$

$$= 0.983509 \times 0.998909 \times 1.000028 \times 4.47548 \times 10^{-3}\sqrt{2 \times 1.1127 \times 203.589}$$

$$= 0.09359 \text{ kg/s}$$

To evaluate the effective convective heat transfer coefficient between the outer cover and the environment, the thermophysical properties of the air above the cover need to be known.

For a cover temperature of 34.128°C and ambient temperature of 31.94°C the mean cover-ambient temperature is

$$T_{am} = 0.5\left(T_a + T_c\right) = 0.5 \times \left(31.94 + 34.128\right) = 33.03\,°C \text{ or } 306.18\,K.$$

For this temperature, the thermophysical properties of air [98KR1] are

Air density	$\rho_{ca} = \dfrac{p_a}{287.08 \times T_{am}} = \dfrac{99933.4}{287.08 \times 306.18} = 1.1369 \text{ kg/m}^3$
Specific heat capacity of air	$c_{pca} = 1007.19 \text{ J/kg.K}$
Air conductivity	$k_{ca} = 0.026698 \text{ W/m.K}$
Dynamic viscosity of air	$\mu_{ca} = 1.87522 \text{ x} 10^{-5} \text{ N/s.m}^2$

The above thermophysical properties give a Prandtl number of

$$Pr_{ca} = \frac{\mu_{ca}\,c_{pca}}{k_{ca}} = \frac{1.87522 \text{ x} 10^{-5} \text{ x } 1007.19}{0.026698} = 0.7074.$$

The effective length for a square cover is the side length, L_c, of the cover (see Appendix A). The dimensionless Grashof number is thus

$$Gr_{ca} = \frac{2\left(T_c - T_a\right) g\, L_c^3\, \rho_{ca}^2}{\left(T_c + T_a\right)\mu_{ca}^2} = \frac{2 \times \left(307.278 - 305.09\right) \text{x} 9.8 \text{ x} 1.0^3 \text{ x} 1.1369^2}{\left(307.278 + 305.09\right) \text{x} \left(1.87522 \text{ x} 10^{-5}\right)^2} = 257.676 \text{ x} 10^6$$

and the corresponding Reynolds number is

$$Re_{ca} = \frac{\rho_{ca}\,v_w\,L_c}{\mu_{ca}} = \frac{1.1369 \text{ x} 0.4 \text{ x} 1.0}{1.87522 \text{ x} 10^{-5}} = 24251$$

To evaluate the length weighted averaged heat transfer coefficient between the cover and air, the thermophysical properties of the air is to be evaluated at a mean air temperature of

$$\overline{T}_m = 0.5\left(\overline{T} + T_c\right) = 0.5 \times (34.128 + 32.239) = 33.184\,°C \text{ or } 306.334\,K.$$

For the above temperature, the thermophysical properties of the air [98KR1] are

Air density	$\rho_c = \dfrac{p_{up}}{287.08 \times \overline{T}_m} = \dfrac{99933.4}{287.08 \times 306.334} = 1.1364\ kg/m^3$
Specific heat capacity of air	$c_{pc} = 1007.19\ J/kg.K$
Air conductivity	$k_c = 0.02671\ W/m.K$
Dynamic viscosity of air	$\mu_c = 1.87591 \times 10^{-5}\ N/s.m^2$

which relates to a corresponding Prandtl number of

$$Pr_a = \frac{\mu_c\, c_{pc}}{k_c} = \frac{1.87591 \times 10^{-5} \times 1007.19}{0.02671} = 0.707.$$

The rectangular duct's hydraulic diameter is

$$Dh = \frac{4\,(W \times H)}{2\,(W + H)} = \frac{2\,(1.0 \times 0.15)}{(1.0 + 0.15)} = 0.2609\ m$$

which leads to a corresponding Reynolds number (equation (2.23)) of

$$Re_{Dh} = \frac{2\,m}{\mu_c\,(W + H)} = \frac{2 \times 0.09359}{1.87591 \times 10^{-5} \times (1.0 + 0.15)} = 8676.6.$$

Setting Δx equal to 0.0204081 m and substitute the previously determined Reynolds number, duct hydraulic diameter, Dh, and thermophysical properties into equation (2.25), find

$$\bar{h}_c = 0.036\, Re_{Dh}^{0.8}\, Pr^{1/3} \left(\frac{k}{Dh}\right) \sum_{i=1}^{n} \left(\frac{Dh}{x_i}\right)^{0.055} \Delta x$$

$$= 0.036 \times 8676.6^{0.8} \times 0.707^{1/3} \times \left(\frac{0.02671}{0.2609}\right) \sum_{i=1}^{49} \left(\frac{0.2609}{x_i}\right)^{0.055} \times 0.0204081$$

$$= 4.6450 \times \left[\left(\frac{0.2609}{0.010204}\right)^{0.055} \times 0.0204081 + \Lambda \left(\frac{0.2609}{0.989795}\right)^{0.055} \times 0.0204081\right] = 4.5643\ W/m^2K$$

Repeating the previous procedure, a value of

$$\bar{h}_f = 4.5793\ W/m^2\,K$$

is yielded for the absorber plate's length averaged heat transfer coefficient.

Under the above circumstances, (very low Reynolds number and ± 8°C temperature difference between the water and cover temperature) the possibility exist that the actually heat transfer coefficient between the two smooth surfaces might be higher than the theoretically predicted values, due to added contribution of natural convection to the total convective heat transfer within the duct.

To evaluate the effect of natural convection between two surfaces, Hollands et al [76HO1] states that the thermophysical properties of the air is to be evaluated at a mean temperature of the two surfaces. Thus

$$T_m = 0.5(T_c + T_w) = 0.5(34.128 + 42.444) = 38.286°C \text{ or } 311.436K$$

For this temperature the thermophysical properties of he air [98KR1] are

Air density	$\rho = \frac{p_a}{287.08 \times T_m} = \frac{99933.49}{287.08 \times 311.436} = 1.1177\ kg/m^3$
Specific heat capacity of air	$c_p = 1007.42\ J/kg.K$
Air conductivity	$k = 0.027102\ W/m.K$
Dynamic viscosity of air	$\mu = 1.8992 \times 10^{-5}\ N/s.m^2$

with a corresponding Prandtl number of

$$Pr = \frac{\mu\, c_p}{k} = \frac{1.8992 \times 10^{-5} \times 1007.42}{0.027102} = 0.706.$$

The effective length for the rectangular duct, according to Hollands et al. [76HO1], is the height, H, of the duct. The dimensionless Grashof number is thus

$$Gr = \frac{2(T_w - T_c)\, g\, H^3\, \rho^2}{(T_w + T_c)\mu^2} = \frac{2\times(315.594 - 307.278)\times 9.8 \times 0.15^3 \times 1.1177^2}{(315.594 + 307.278)\times(1.8992 \times 10^{-5})^2} = 3.05882 \times 10^6$$

From equation (D.8) it follows that the natural convection between the cover and water tank is

$$h = \left[1 + 1.44\left[1 - \frac{1708}{Gr\,Pr}\right] + \left[\left(\frac{Gr\,Pr}{5830}\right)^{1/3} - 1\right]\right]\frac{k}{H}$$

$$= \left[1 + 1.44\left[1 - \frac{1708}{3.05882 \times 10^6 \times 0.706}\right] + \left[\left(\frac{3.05882 \times 10^6 \times 0.706}{5830}\right)^{1/3} - 1\right]\right] \times \frac{0.027102}{0.15}$$

$$= 1.5575\ W/m^2.K$$

Therefore, from the previous calculation it is apparent that the natural convection has the same order of magnitude as the forced convection. Consequently, the actual convective heat transfer coefficient between the surfaces and the air in between will be marginally higher than the previously theoretically predicted values.

Upon substitution of the applicable dimensionless numbers and solar properties into equation (L.6), the cover energy conservation equation becomes

$$\left[\frac{(1-0.04625)(1-0.94717)}{1-0.04625\times 0.94717}\right]\times 806.619 + \left[\frac{(1-0.09346)(1-0.9405)}{1-0.09346\times 0.9405}\right]\times 79.775 +$$

$$5.67\times 10^{-8}\left[\frac{1}{0.88} + \frac{1}{0.88} - 1\right]^{-1}\left(T_w^4 - T_c^4\right) = 4.5643\left(T_c - \bar{T}\right) +$$

$$+\left[\left(257.676\times 10^6 \times 0.7074\right)^{1/3}\left(0.227 + 1.406\times 10^{-6}\times 24251\right)\right]\frac{0.026698}{1.0}\left(T_c - 305.09\right)$$

$$+ 0.88\times 5.67\times 10^{-8}\left[T_c^4 - \left(0.0552\times 305.09^{1.5}\right)^4\right]$$

which simplifies to

$$42.505 + 4.718 + 40.898\times10^{-9}\left(T_w^4 - T_c^4\right) = 4.5643\left(T_c - \overline{T}\right) + \\ + 3.952\left(T_c - 305.09\right) + 49.896\times10^{-9}\left(T_c^4 - 294.158^4\right) \tag{L.9}$$

At a water temperature of 42.444°C (315.594 K), the thermophysical properties of the water, according to Kröger [98KR1], are

Water density $\rho_w = 991.382\ \text{kg/m}^3$

Specific heat capacity of water $c_{pw} = 4176.9\ \text{J/kg.K}$

Repeating the previous procedure, the energy equation for the water tank (equation (L.7)) yields

$$\left[\frac{(1-0.04625)^2\times0.94717}{\left(1-0.04625^2\times0.94717^2\right)}\right]\left[1-\frac{0.05636+(1-2\times0.05636)\times0.008536\times0.95816^2}{1-0.05636\times0.008536\times0.95816^2}\right]$$
$$\times\left[1-0.09346\times\frac{0.05636+(1-2\times0.05636)\times0.008536\times0.95816^2}{1-0.05636\times0.008536\times0.95816^2}\right]^{-1}\times806.619 +$$
$$\left[\frac{(1-0.09346)^2\times0.9405}{\left(1-0.09346^2\times0.9405^2\right)}\right]\left[1-\frac{0.1052+(1-2\times0.1052)\times0.01102\times0.95354^2}{1-0.1052\times0.01102\times0.95354^2}\right]$$
$$\times\left[1-0.09346\times\frac{0.1052+(1-2\times0.1052)\times0.01102\times0.95354^2}{1-0.1052\times0.01102\times0.95354^2}\right]^{-1}\times79.775$$
$$= 4.5793\left(T_w - \overline{T}\right) + 5.67\times10^{-8}\times\left[\frac{1}{0.88}+\frac{1}{0.8}-1\right]^{-1}\left(T_w^4 - T_c^4\right)$$
$$+ 991.382\times0.19\times4176.9\times\frac{T_w - 315.5821}{15}$$

and reduces to

$$656.687 + 55.693 = 4.5793\left(T_w - \overline{T}\right) + 40.898\times10^{-9}\times\left(T_w^4 - T_c^4\right) \\ + 52.45144\times10^3\times\left(T_w - 315.5821\right) \tag{L.10}$$

The specific heat capacity for the air at a temperature of 32.239 °C (305.389 K), according to Kröger [98KR1], is

Specific heat capacity of air $c_p = 1007.16\ \text{J/kg.K}$

Substitute the above-determined specific heat capacity, length-averaged cover-air and plate-air heat transfer coefficients as well as the mass flow rate into the air conservation of energy equation (equation (L.8)), and find

$$0.09359\times1007.16\times305.09+1.0\times4.5793\times\left(T_w-\overline{T}\right)+1.0\times4.5643\times\left(T_c-\overline{T}\right)$$
$$=0.09359\times1007.16\times\left(2\overline{T}-305.09\right)$$

The above equation simplifies to

$$28.7578\times10^3+4.5793\times\left(T_w-\overline{T}\right)+4.5643\times\left(T_c-\overline{T}\right)=94.2601\times\left(2\overline{T}-305.09\right) \quad \text{(L.11)}$$

Solving equations (L.9), (L.10) and (L.11) simultaneously, the cover, water tank and air temperatures are predicted as 34.128 °C (307.278 K), 42.444 °C (315.594 K) and 32.239 °C (305.389 K) respectively. These values show good agreement with the experimental cover temperature of 35.603 °C and the experimental mean weighted water temperature of 42.340 °C.

Appendix M: Solar air heater with water storage – Night operation

A number of experiments are conducted on a solar air heater with plastic covered water tanks in order to observe the amount of energy that is transferred from the plastic covered water tanks to the air in the duct during night-time. The experimental results are also compared to theoretically predicted values.

M.1 Analysis

The solar air heater with plastic covered water tanks under consideration is identical to the one considered in Appendix L.

Hence, omitting solar radiation terms in Appendix L, the following energy equation is yielded for a 1m section of the cover of the solar air heater with a plastic covered water tank

$$\sigma\left[\frac{1}{\varepsilon_c}+\frac{1}{\varepsilon_f}-1\right]^{-1}\left(T_w^4-T_c^4\right)=\bar{h}_c\left(T_c-\bar{T}\right)$$
$$+\left[\left(Gr_{ca}\,Pr_{ca}\right)^{1/3}\left(0.227+1.406\times10^{-6}\,Re_{ca}\right)\right]\frac{k_{ca}}{L_c}\left(T_c-T_a\right)+\varepsilon_c\,\sigma\left[T_c^4-\left(0.0552\,T_a^{1.5}\right)^4\right] \quad (M.1)$$

while the conservation of energy equation for the plastic covered water tank (equation (L.4)) becomes

$$-\bar{h}_f\left(T_w-\bar{T}\right)-\sigma\left[\frac{1}{\varepsilon_c}+\frac{1}{\varepsilon_f}-1\right]^{-1}\left(T_w^4-T_c^4\right)=\rho_w\,t_w\,c_{pw}\,\frac{dT_w}{dt} \quad (M.2)$$

and the air energy equation simplifies to

$$\dot{m}c_p\,T_{in}+A\,\bar{h}_f\left(T_w-\bar{T}\right)+A\,\bar{h}_c\left(T_c-\bar{T}\right)=\dot{m}c_p\left(2\bar{T}-T_{in}\right) \quad (M.3)$$

However, at this point it must be stresses that, as in the case of Appendix L, the cover energy equation (equation (M.1), would only be valid if the cover temperature exceeds the ambient temperature and $6.75 \times 10^8 \leq (GrPr) \leq 26.6 \times 10^8$ and for $0 \leq Re \leq 2.5 \times 10^5$.

Thus, if the above criteria is satisfied and equations (M.1), (M.1) and (M.3) are solved simultaneously for given ambient conditions, the performance of the solar air heater can be predicted for night-time.

In the following numerical example the simultaneous solution of equations (M.1) (M.2) and (M.3) will be illustrated for the first section of the solar air heater with water storage on the 20th of March 2001 at 00h23.

Numerical example

In the following calculations, it will be shown that a cover temperature of 17.622 °C (290.772 K), a mean water temperature of 38.3911 °C (311.541 K) and a air temperature of 16.8116 °C (289.961 K), satisfy equations (M.1), (M.2) nd (M.3) for the ambient conditions and mass flow rate of 0.09656 kg/s for the 20th of March 2001.

Table M.1: Experimental data for night operation of solar air heater with water storage

Time	00h23:02
Water height, t_w	0.190 m
Ambient temperature, T_a	16.275 °C
Wet-bulb temperature, T_{wb}	18.193 °C
Dry-bulb temperature, T_{db}	22.068 °C
Wind speed, v_w	0.4 m/s
Atmospheric pressure, p_a	100 066 Pa
Nozzle pressure drop, dp_n	205.368 Pa
Predicted water temperature (00h22:02), T_w^{i-1}	38.405 °C (311.555 K0

To predict the mean air temperature, $\overline{T}$, for the section the mass flow rate of the air through the rectangular duct needs to be known.

From the calculation procedure used it follows that a mass flow rate of 0.09656 kg/s through the 75.48-mm diameter nozzle for a mixed density of 1.1127 kg/m^3. From equation (E.1) it follows that the upstream nozzle pressure is

$$p_n = p_a - K_d\left[\frac{m^2}{2\rho_{av}A_d^2}\right] = 100066 - 8.4\left[\frac{0.09656^2}{2\times1.1725\times0.15^2}\right] = 100064.5\ \text{Pa}$$

Employing the equations of Kröger [98KR1], the thermophysical properties and vapour pressure of the air-vapour mixture are evaluated.

Vapour pressure	$p_v = 2089.2\ \text{Pa}$
Air-vapour density	$\rho_{av} = 1.1725\ \text{kg/m}^3$
Air-vapour dynamic viscosity	$\mu_{av} = 1.8125\times10^{-5}\ \text{kg/m.s}$

Using these properties, the gas expansion factor is evaluated according to equation (2.14)

$$\phi_g = 1-\frac{3\,dp_n}{4p_n\times1.4} = 1-\frac{3\times205.368}{4\times100064.5\times1.4} = 0.9989$$

while equation (2.18) yields an approach velocity factor of

$$Y_2 = 1+0.5\left(\frac{A_2}{A_{tus}}\right)^2+2\left(\frac{A_2}{A_{tus}}\right)^2\left(\frac{dp_n}{p_{up}\,c_p/c_v}\right)$$

$$= 1+0.5\left(\frac{4.47548\times10^{-3}}{0.6}\right)^2+2\left(\frac{4.47548\times10^{-3}}{0.6}\right)^2\left(\frac{205.368}{100064.5\times1.4}\right) = 1.0000279$$

Using the previously determined thermophysical properties for the air-vapour mixture, the nozzle's Reynolds number is evaluated.

$$Re_2 = \frac{4m_2}{\pi D_2\,\mu_{av}} = \frac{4\times0.09656}{\pi\times0.0754875\times1.8125\times10^{-5}} = 89.857\times10^3$$

The nozzle discharge coefficient for each nozzle is based on the nozzle's particular Reynolds number. Consequently, from equation (2.12) it follows

$$C_n = 0.954803+6.37817\times10^{-7}\,Re_n-4.65394\times10^{-12}\,Re_n^2+1.33514\times10^{-17}\,Re_n^3$$

$$= 0.954803+6.37817\times10^{-7}\times89.857\times10^3-4.65394\times10^{-12}\times\left(89.857\times10^3\right)^2$$

$$+1.33514\times10^{-17}\times\left(89.857\times10^3\right)^3 = 0.984225$$

From equation (2.10), the mass flow rate through the nozzle is

$$m_2 = C_2\,\phi_g\,Y_2\,A_2\sqrt{2\rho_{av}\,dp_n}$$

$$= 0.984225\times0.9989\times1.0000279\times4.47548\times10^{-3}\sqrt{2\times1.1725\times205.368}$$

$$= 0.09656\times10^{-3}\ \text{kg/s}$$

To evaluate the effective convective heat transfer coefficient between the outer cover and the environment, the thermophysical properties of the air above the cover need to be known.

For a cover temperature of 17.622°C and ambient temperature of 16.275°C the mean cover-ambient temperature is

$$T_{am} = 0.5\left(T_a + T_c\right) = 0.5\times\left(16.275 + 17.622\right) = 16.95\,°\text{C or } 290.10\,\text{K}.$$

For this temperature, the thermophysical properties of air [98KR1] are

Air density	$\rho_{ca} = \dfrac{p_a}{287.08\times T_{am}} = \dfrac{100066}{287.08\times 290.10} = 1.2015\ \text{kg/m}^3$
Specific heat capacity of air	$c_{pca} = 1006.64\ \text{J/kg.K}$
Air conductivity	$k_{ca} = 0.025451\ \text{W/m.K}$
Dynamic viscosity of air	$\mu_{ca} = 1.80108\ \text{x}10^{-5}\ \text{N/s.m}^2$

The above thermophysical properties give a Prandtl number of

$$Pr_{ca} = \frac{\mu_{ca}\,c_{pca}}{k_{ca}} = \frac{1.80108\,\text{x}10^{-5}\,\text{x}\,1006.64}{0.025451} = 0.7124.$$

The effective length for a square cover is the side length, L_c, of the cover (see Appendix A). The dimensionless Grashof number is thus

$$Gr_{ca} = \frac{2\left(T_c - T_a\right) g\,L_c^3\,\rho_{ca}^2}{\left(T_c + T_a\right)\mu_{ca}^2} = \frac{2\times\left(290.772 - 289.425\right)\text{x}\,9.8\,\text{x}\,1.0^3\,\text{x}\,1.2015^2}{\left(290.772 + 289.425\right)\text{x}\left(1.80108\,\text{x}10^{-5}\right)^2} = 202.7088\ \text{x}10^6$$

and the corresponding Reynolds number is

$$Re_{ca} = \frac{\rho_{ca}\,v_w\,L_c}{\mu_{ca}} = \frac{1.2015\,\text{x}\,0.4\,\text{x}\,1.0}{1.80108\,\text{x}10^{-5}} = 26684$$

Using equation (2.25) the respective length averaged cover-air, $\bar{h}_c$, and film-air, $\bar{h}_f$, heat transfer coefficients are determined. Respective values of

$$\bar{h}_c = 4.6187 \text{ W/m}^2\text{K}$$

and

$$\bar{h}_f = 4.6588 \text{ W/m}^2\text{K}$$

are obtained.

Substitute the applicable dimensionless numbers into equation (M.1), and find

$$5.67\times10^{-8}\left[\frac{1}{0.88}+\frac{1}{0.8}-1\right]^{-1}\left(T_w^4-T_c^4\right)=4.6187\left(T_c-\bar{T}\right)+$$
$$+\left[\left(202.7085\times10^6\times0.7124\right)^{1/3}\left(0.227+1.406\times10^{-6}\times26684\right)\right]\frac{0.025451}{1.0}\left(T_c-289.425\right)$$
$$+0.88\times5.67\times10^{-8}\left[T_c^4-\left(0.0552\times289.425^{1.5}\right)^4\right]$$

This equation simplifies to

$$40.898\times10^{-9}\left(T_w^4-T_c^4\right)=4.6187\left(T_c-\bar{T}\right)+$$
$$+3.535\left(T_c-289.425\right)+49.896\times10^{-9}\left(T_c^4-271.796^4\right) \qquad \text{(M.4)}$$

At a water temperature of 38.391°C (311.541 K), the thermophysical properties of the water, according to Kröger [98KR1], are

Water density	$\rho_w = 992.933 \text{ kg/m}^3$
Specific heat capacity of water	$c_{pw} = 4176.8 \text{ J/kg.K}$

Upon substitution of these properties into equation (M.2) as well as the predicted water temperature for 00h22:02 (see Table M.1), the water energy equation becomes

$$-4.6588\left(T_w-\overline{T}\right)-5.67\times10^{-8}\times\left[\frac{1}{0.88}+\frac{1}{0.8}-1\right]^{-1}\left(T_w^4-T_c^4\right)$$
$$=992.933\times0.19\times4176.8\times\frac{T_w-311.5558}{60}$$

which subsequently reduces to

$$-4.6588\left(T_w-\overline{T}\right)+40.898\times10^{-9}\times\left(T_w^4-T_c^4\right)$$
$$=13.1331\times10^{3}\times\left(T_w-315.5821\right) \qquad \text{(M.5)}$$

The specific heat capacity for the air at a temperature of 16.8116 °C (289.961 K), according to Kröger [98KR1], is

Specific heat capacity of air $c_p = 1006.64$ J / kg.K

Using the previously determined values, the conservation of energy equation for the air becomes

$$0.09656\times1006.64\times289.425+1.0\times4.6588\times\left(T_w-\overline{T}\right)+1.0\times4.6187\times\left(T_c-\overline{T}\right)$$
$$=0.09656\times1006.64\times\left(2\overline{T}-289.425\right)$$

The above equation simplifies to

$$28.1324\times10^{3}+4.6588\times\left(T_w-\overline{T}\right)+4.6187\times\left(T_c-\overline{T}\right)=92.2012\times\left(2\overline{T}-289.425\right) \qquad \text{(M.6)}$$

Solving equations (M.4), (M.5) and (M.6) simultaneously, the cover, water tank and air temperatures are predicted as 17.662 °C (290.772 K), 38.391 °C (311.541 K) and 16.811 °C (289.961 K) respectively. These predicted values show good agreement with the experimentally measured cover temperature of 17.795°C and the experimental mean weighted water temperature of 39.166°C.